Fats, tumours and survival: Investigating the prognostic association of fatty acid oxidation in breast cancer

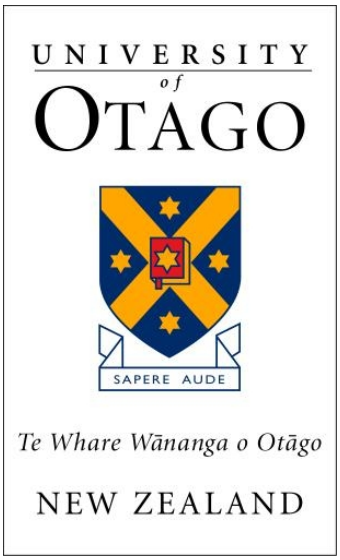

Abdul Aziz Bin Aiderus

A thesis submitted for the degree of

Doctor of Philosophy

University of Otago, Dunedin, New Zealand

Abstract

Over the past 15 years, a number of prognostic and treatment predictive signatures for breast cancer have been reported and utilised in the clinic. These signatures, for most part, are dominated by genes that reflect tumour proliferation, and provide limited insight into the biological pathways that drive tumour growth. Large gene expression datasets from primary tumours and well annotated clinical follow-up data have the potential to identify pathways correlated with treatment response and outcome. Rewiring of cellular metabolism is vital to meet the proliferative demands of tumours. To date, very little is known about how tumour metabolism influences patient outcome. This study sought to identify and characterise the metabolic features of tumours which associate with survival in breast cancer patients.

Cox regression and gene set enrichment analyses were performed on gene expression data from 973 breast cancer patients. High expression of a signature comprised of 19 genes involved in fatty acid oxidation (FAO) was correlated with better disease-specific survival. The prognostic performance of this signature was validated using independent datasets from breast and several other cancer types. Analysis of the FAO signature in tumour-normal gene expression data revealed decreased expression in tumours compared to normal counterparts, which was exacerbated in advanced disease, compared to primary tumour tissues. The FAO signature was downregulated in various models of EMT induction in cell and organoid systems, independently of proliferation. Additionally, activation of MAPK and Wnt signalling pathways were observed to downregulate

expression of the FAO signature in gene expression datasets from *in vitro* and *in vivo* systems.

Overexpression of *CPT1A* in MDA-MB231 breast cancer cells decreased the proliferation and wound healing rates. No significant differences were observed in transwell migration rates, or colony formation in soft agar between basal and *CPT1A* overexpressing cells. MCF7 breast cancer cells with *CPT1A* knockdown did not alter proliferation rates or colony formation in soft agar, compared to basal expression control. Modulation of *CPT1A* expression did not alter oxygen consumption in response to exogenous palmitate. Transcriptome analysis suggested that transcriptional activity of EMT, MAPK and Wnt pathways was increased in MCF7 cells with *CPT1A* knockdown suggests a trend towards increased transcriptional activity of these pathways in this cell system.

In summary, this work suggests that cancer cell proliferation and migration processes decreases the FAO signature expression, which is associated with poor patient prognosis. Alterations in the rate-limiting enzyme of this pathway alters proliferation and migration rates in MDA-MB231 cells, and increases expression of genes corresponding to key oncogenic pathways in MCF7 cells. These findings warrant further investigation of this pathway in breast and other cancer cell types. Understanding of how FAO affects tumour biology could help advance therapies that modulate this pathway.

Acknowledgements

It took me *ten* years to complete this thesis. Not the actual time on the labour of this project, but from when I made the decision a decade ago to pursue this degree to where I am now typing this section. Admittedly, I could not have undertaken this colossal project on my own, and have had the great fortune to receive support from many people that I wish to thank.

I owe a lifelong debt to my family: Habsah, Aiderus, Amin, Hamid and Shakilah. I can never repay your sacrifices and faith in me, and the tremendous moral (and financial) support you have extended through these years, *terima kasih semua*. We've come a long way as a family, and the completion of this degree is another milestone for us. I hope this inspires Shareef and Sadiq to pursue their dreams and achieve great things in life.

I am grateful to Dr Anita Dunbier for the opportunity to join her group and her advisory role on this project. I am appreciative of the freedom granted through most of this project, and the feedback provided for the final form of this thesis. Thank you for allowing me to co-author research grants to fund experiments (albeit unsuccessfully), supporting multiple external funding applications required for travel during my PhD study, and taking the trouble to arrange and drive to Christchurch for the Seahorse analysis. Your supervision style not only developed me academically, but also instilled a strong sense of independence and resourcefulness, which I am certain will be vital in future. I would also like to extend my gratitude to Associate Professor Mik Black as a co-supervisor, for input on all things statistical and helping me through some serious crises with R programming.

My mental state would have been in shambles if it weren't for Jody Hazlett. Heartfelt thanks for being a great listener of all my scientific, and more importantly, non-scientific

rants. Thank you for being generous with your time in the lab, always watching out and helping with the smallest things, which means the most during very frantic days in the lab. Kudos for taking up the inhumane task of chief editor of this thesis, and braving through multiple drafts of chapters, striving to make sense of things that even I couldn't comprehend at times!

A special thank you to Dr Augustine Chen - a dear mentor, colleague and friend throughout my time in this lab. I am indebted to you for being selfless and generous with your expertise, and being a sounding board for my ideas and stimulating scientific discussions. On a personal note, thanks for being there through some dark abyss during the course of my thesis.

A lot of the initial cloning experiments were expertly coached by Dr Sofie van Huffel. Thanks for your guidance and patience with my foray into molecular biology, and imbuing scientific rigour in experimental planning and data interpretation.

I have had the pleasure of making remarkable friends along the way, which I hope continues to be life long. Anna Bundock and Adelaide Hopkins, thanks for being there through some very difficult moments in my thesis. Anna: Sunday morning coffee will always be a highlight. Adelaide, thanks for being a great listener, and someone that shares many similar interests, as different a people we are (Go West Brom FC!). Chris Haakaart and Henry Beetham, thanks for being great mates through this journey, and lending a listening ear when experiments weren't going as planned (or they did, but I wanted a smaller p-value). Shout out to Chris Haakaart and Tyler McInnes for your generous and patient guidance when I was freshly minted into the treacherous world of R programming - perhaps I could write a loop to convey my gratitude for your help? Much thanks to Kimberley Dainty - a one-stop, walking and talking LaTeX user guide,

for assistance to get this document together in the end.

Monsieur/Professeur Parry Guilford, thanks for the encouraging, wise words through my thesis, particularly so towards the end of my study. I very much enjoyed the memorable runs up Signal Hill, and that less memorable one up the Pineapple Track. I am certain your advise will serve me well in my future endeavours.

To the past and present members of the Cancer Genetics Lab: thanks for being a great host during my time here. In particular, Tanis Godwin - thanks for making sure the lab runs smoothly and the constant (but futile) reminders to empty the Frosty Boy(s) after use.

A lot of the analysis in this thesis were based on tumour material from cancer patients - *human beings* that I have never, and probably never meet. Reflecting on the data from analysis of these samples transcends abstraction, and is a constant reminder of the significance of what I'm doing everyday. I am immensely grateful to all of you for your selflessness during, presumably, your most vulnerable moment to further cancer research; and I hope my humble effort in this thesis has done some justice to your contributions.

The support from Professor Mark Hampton's group in Christchurch, in particular Drs Andree Pearson and Karina O'Connor for the Seahorse analysis is much appreciated. Much thanks to Marcel and Mel Brew for their unconditional, generous hospitality during my short stay in Christchurch.

Part of my training involve attending conferences and a workshop around the world, which could not have been possible without the generosity of various funding bodies. Thanks to the Department of Biochemistry for the Marjorie MacCallum Travel Grant;

Genesis Oncology Trust for a Professional Development Award; and the Wellcome Trust-Sanger Institute for a bursary - all of which were vital in funding my attendance of a workshop at the Sanger Institute. I am also grateful to the Division of Health Sciences and the Centre for Translational Cancer Research for funding for my conference travel towards the end of my study.

Contents

Abstract **i**

Acknowledgements **iii**

List of Figures **xx**

List of Tables **xxiv**

List of Abbreviations **xxv**

1 Introduction **1**
1.1 Clinically significant prognostic and predictive markers in breast cancer 1
1.1.1 Prognostic factors 1
1.1.1.1 *Axillary lymph node status* 2
1.1.1.2 *Tumour size* 2
1.1.1.3 *Histologic and nuclear grade* 3
1.1.2 Predictive factors 4
1.1.2.1 *Oestrogen receptor as a prognostic and treatment predictive marker* 4
1.2 Pharmacotherapy of ER-positive breast tumours 5
1.2.1 Tamoxifen 6
1.2.2 Aromatase inhibitor (AI) 7
1.2.2.1 *Efficacy of AIs versus tamoxifen* 8
1.2.2.2 *Treatment outcome and survival* 9
1.3 Molecular risk stratification of breast cancer 10
1.3.1 Genomic technologies and data analysis methods 10
1.3.1.1 Molecular intrinsic subtyping of breast tumours 11
1.3.1.1.1 *Luminal A* 11
1.3.1.1.2 *Luminal B* 12
1.3.1.1.3 *HER2-enriched* 12
1.3.1.1.4 *Basal-like* 13
1.3.1.2 Integrative clustering based molecular stratification of breast cancer 13

1.3.2 Commercially-available prognostic signatures 15
1.3.2.1 *Oncotype DX* 15
1.3.2.2 *PAM50-based Prosigna* 16
1.3.2.3 *MammaPrint* 16
1.3.3 Limitations of first-generation molecular signatures 17
1.3.3.1 *Performance of first-generation molecular signatures* . . 17
1.3.3.2 *Proliferation as a key hallmark of prognostic signatures* 17
1.3.3.3 *Biology-driven signatures* 18
1.4 Metabolic reprogramming as a key feature in cancer biology 19
1.4.1 A brief history of cancer metabolism 20
1.4.2 *Why do cancer cells have a sweet tooth?* 22
1.4.2.1 *Glycolysis is not the main source of ATP during proliferation* 22
1.4.2.2 *Glycolytic intermediates are important building blocks of macromolecules* 23
1.4.3 Glutamine metabolism 25
1.4.3.1 *Contribution of glutamine to cancer cell physiology* . . . 26
1.4.4 Fatty acid metabolism 27
1.4.4.1 *What is the role of fatty acid synthesis in cancer cells?* 27
1.4.4.2 *Fatty acid oxidation in cancer* 29
1.4.4.2.1 Fatty acid uptake and activation 29
1.4.4.2.2 Carnitine shuttle 30
1.4.4.2.3 Beta oxidation of acyl-CoA 31
1.4.4.3 Fatty acid oxidation in cancer 31
1.4.5 Oncogene and tumour suppressor activity, signalling pathways and cancer metabolism 33
1.4.5.1 *Oncogenes and tumour suppressors associated with cancer metabolism* 33
1.4.5.2 *Wnt and MAPK signalling pathways and cancer metabolism* 34
1.4.6 Metabolic features associated with epithelial-to-mesenchymal transition and cellular differentiation 37
1.4.6.1 EMT and metabolism 37
1.4.6.1.1 *Glycolysis and EMT* 37
1.4.6.1.2 *Fatty acid metabolism and EMT* 38
1.4.6.2 Stem cell differentiation and metabolism 40
1.4.6.2.1 Link between EMT-associated factors and mammary stem cell differentiation 41
1.4.7 Tumour microenvironment and metabolism 41
1.4.8 Prognostic association of cancer metabolic pathways 42
1.5 Aim 44
1.5.1 Thesis outline 44

2 Materials and Methods **46**
2.1 *Cell lines and complete media* 46
2.1.1 Cell culture maintenance 47

2.2 Expression plasmids and primers . . . 47
2.3 Preparation of RNA samples . . . 50
2.3.1 *Reverse transcription* . . . 50
2.4 Polymerase chain reaction of CPT1A cDNA . . . 51
2.5 Preparation and ligation of DNA fragments . . . 52
2.5.1 *Heat shock transformation of competent bacteria with ligated products* . . . 52
2.5.2 *PCR screen for positive transformants* . . . 53
2.6 Generation of double-stable, inducible MDA-MB231 cell line . . . 54
2.6.1 *Transfection of pTetOn plasmid into MDA-MB231 cell line* . . . 54
2.6.2 *Selection and isolation of stable pTetOn transfectants* . . . 54
2.6.3 *Preparation of doxycycline hydrochloride and puromycin stock solutions* . . . 55
2.6.4 *Luciferase-based screening of single transfectant clones* . . . 55
2.6.5 *Co-transfection of pTetOn single transfectant cell line with pTRE and pBabe puro* . . . 56
2.6.6 *Assessing CPT1A mRNA induction in putative overexpression clones* . . . 57
2.7 Establishing stable MCF7 and MCF10A cell lines for *CPT1A* knockdown 58
2.7.1 Cloning of shRNA constructs into pTRIPZ vector . . . 58
2.7.1.1 *Assessing knockdown efficiency of shRNA constructs* . . . 61
2.7.1.2 *Lentivirus particle production* . . . 61
2.7.1.3 Determining viral transducing unit . . . 62
2.7.1.4 *Lentiviral shRNA infection of MCF7 and MCF10A cells* 62
2.7.1.5 *Screening for stable shRNA knockdown clones in MCF7 and MCF10A* . . . 63
2.7.1.6 *Immunoblot analysis of inducible cell systems* . . . 63
2.7.1.6.1 Induction of CPT1A transgene in MDA-MB231 pTRE-CPT1A cell lines . . . 63
2.7.1.6.2 Induction of *CPT1A* shRNA expression in MCF10A and MCF7 cells . . . 64
2.7.1.6.3 Immmunoblot procedure . . . 64
2.7.1.6.4 Soft agar assay . . . 65
2.7.1.6.5 Boyden chamber assay . . . 66
2.7.2 Real time FAO flux analysis using the Seahorse XF extracellular flux technology . . . 67
2.7.2.1 Induction of CPT1A expression and knockdown in cell systems . . . 68
2.7.2.2 *Optimisation of FCCP required to achieve maximal OCR in cell systems* . . . 69
2.7.2.3 *FAO assay set up* . . . 69
2.8 Bioinformatics analysis methods . . . 70
2.8.1 *Cox proportional hazards regression to identify features significantly associated with outcome* . . . 70
2.8.2 *Collapsing multiple probesets to unique genes* . . . 71

2.8.3 *Gene set enrichment analysis* . . . 71
2.8.4 *Kaplan-Meier survival analysis* . . . 71
2.8.5 *Accessing publicly available gene expression datasets* . . . 72
2.8.6 *RNA-Seq analysis of CPT1A overexpressing and knockdown cell lines* . . . 72

3 Identification of pathways associated with breast cancer treatment response and prognosis 74
3.1 Background . . . 74
3.2 Objectives . . . 75
3.3 Results . . . 75
3.3.1 *Gene signatures significantly associated with breast cancer disease-specific survival* . . . 75
3.3.2 *High FAO signature expression is associated with better disease-specific survival in training dataset* . . . 80
3.3.3 *FAO signature expression is prognostic in independent breast cancer cohorts* . . . 82
3.3.4 *Low FAO signature expression is correlated with clinical factors associated with poor prognosis* . . . 84
3.3.5 *FAO signature expression is prognostic independently of standard histopathological features in breast cancer* . . . 86
3.3.6 *FAO signature expression is inversely correlated with proliferation gene signature* . . . 86
3.3.7 *High FAO signature expression is associated with good response to neoadjuvant aromatase-inhibitor treatment* . . . 87
3.3.7.1 *ESR1 knockdown in MCF7 decreases FAO signature expression relative to basal expression control* . . . 87
3.3.8 *Low FAO signature expression is correlated with better neoadjuvant chemotherapy response* . . . 89
3.3.9 *CPT1A* is likely to be co-amplified with *CCND1* in multiple cancers 90
3.3.10 *FAO signature is prognostic in multiple cancers* . . . 92
3.3.11 *FAO signature expression is down-regulated in tumour compared to normal tissues* . . . 96
3.3.11.1 *Androgen-deprivation increases FAO signature expression in prostate cancer* . . . 97
3.4 Discussion . . . 98
3.4.1 *FAO signature expression is prognostic independently of standard histopathological features in breast cancer* . . . 98
3.4.1.1 *ESR1 knockdown decreases FAO signature expression in MCF7 cell line* . . . 100
3.4.2 *CPT1A is co-amplified with CCND1 in multiple cancers* . . . 101
3.4.3 *FAO signature expression is lower in tumours, compared to normal tissues; and is prognostic in several cancer types* . . . 103
3.4.3.1 *Gastric cancer* . . . 103
3.4.3.2 *Lung cancer* . . . 104

3.4.3.3 *Clear cell renal cell cancer* . . . 104
3.4.3.4 *Colorectal cancer* . . . 105
3.4.3.5 *Prostate cancer* . . . 106
3.5 Summary, strengths and limitations . . . 107

4 Epithelial-to-mesenchymal transition and cellular differentiation alters the FAO signature expression 109
4.1 Background . . . 109
4.2 Objectives . . . 110
4.3 Results . . . 111
4.3.1 FAO signature expression and EMT in cell systems . . . 111
4.3.1.1 *Transforming growth factor beta-induced EMT decreases FAO signature expression in cell systems* . . . 111
4.3.1.2 *TGFβ-mediated downregulation of FAO signature observed in other cell types* . . . 113
4.3.1.3 *2-hydroxyglutarate-induced EMT decreases FAO signature expression* . . . 115
4.3.1.4 *EMT associated transcription factors and FAO signature expression in cell systems* . . . 116
4.3.1.5 *FAO signature expression and EMT in organoid systems* 121
4.3.1.6 *FAO signature expression not correlated with EMT signature in primary breast tumours* . . . 123
4.4 FAO signature expression and cellular differentiation . . . 123
4.4.1 *FAO signature expression increases during mammary epithelial cell differentiation* . . . 123
4.4.2 *Correlation analysis between FAO, MKS and mammary luminal/stem gene signatures* . . . 124
4.4.3 *FAO signature expression and confluence-induced differentiation* 126
4.4.4 *FAO signature increased in butyrate-induced colorectal cancer cell differentiation* . . . 127
4.5 Discussion . . . 130
4.5.1 What is known about FAO and EMT? . . . 130
4.5.2 Association of EMT and FAO signatures in cell and organoid systems 131
4.5.2.1 *TGFβ-treatment and transgenic expression of EMT transcription factors* . . . 131
4.5.2.2 *Mutations in IDH1/2* . . . 132
4.5.3 EMT and FAO in primary breast tumours . . . 132
4.5.4 Can activating FAO rescind EMT? . . . 133
4.5.5 Cellular differentiation and FAO signature expression . . . 134
4.6 Summary, strengths and limitations . . . 136

5 Activation of key oncogenic signalling pathways alters FAO signature expression 137
5.1 Background . . . 137
5.2 Objectives . . . 138

5.3 Results . . . 138
5.3.1 Alteration of Wnt signalling members *in vivo* alters FAO signature expression . . . 138
5.3.1.1 *Knockout, knockdown or single allele inactivation of APC decreases FAO signature expression* . . . 138
5.3.1.2 *Knockout of Bcl9 increases FAO signature expression* . 141
5.3.1.3 *Altering Wnt signalling components in vitro influences FAO signature expression* . . . 143
5.3.1.4 *Constitutive Wnt signalling in mouse mammary glands decreases FAO signature expression* . . . 146
5.3.1.5 *FAO signature expression is not associated with prognosis in colorectal cancer* . . . 146
5.4 FAO signature expression is associated with MAPK pathway and MITF status in melanoma . . . 148
5.4.1 *Pharmacological inhibition of mutant BRAF increases FAO signature expression* . . . 148
5.4.2 *BRAF mutant expression alters FAO signature expression* . . . 150
5.4.3 *RAS mutant expression alters FAO signature expression* . . . 152
5.4.4 *BRAF or MEK inhibition in other cancer types increases FAO signature expression* . . . 154
5.4.5 MITF expression is associated with FAO signature expression . . 156
5.5 Discussion . . . 159
5.5.1 Wnt signalling and FAO signature expression . . . 159
5.5.2 MAPK pathway activity and FAO signature expression . . . 160
5.5.2.1 *BRAF activity and FAO signature expression* . . . 160
5.5.2.2 *MAPK pathway modulation and FAO signature expression* 162
5.5.3 Extreme ends of MITF expression decreases proliferation and upregulates FAO signature . . . 162
5.6 Summary, strenghts and limitations . . . 164

6 Analysis of *CPT1A* modulation in *in vitro* breast cancer cell systems 166
6.1 Background . . . 166
6.2 Objectives . . . 167
6.3 *CPT1A* expression higher in ER-positive compared to ER-negative breast tumours and cell lines . . . 168
6.4 Generation of CPT1A overexpression in MDA-MB231 cell line . . . 172
6.4.1 *Luciferase assay for Tet induction in MDA-MB231 single, stable transfectant clones* . . . 172
6.4.2 *Generation of double, stable transfectant clones overexpressing CPT1A* 173
6.4.3 *Dose- and time course optimisation of CPT1A induction in MDA-MB231 double transfectants* . . . 175
6.5 Generation of *CPT1A* knockdown system in MCF7 cell line . . . 176
6.6 Generation of *CPT1A* knockdown system in MCF10A cell line . . . 177
6.7 Characterisation of stable cell systems modulating *CPT1A* expression . 181
6.7.1 Real time growth assay in response to *CPT1A* modulation . . . 181

6.7.1.1 *CPT1A overexpression decreases growth rate of MDA-MB231 cells* . . . 181
6.7.1.2 *CPT1A overexpression decreases wound closure rate of MDA-MB231 cells* . . . 183
6.7.1.3 *CPT1A overexpression does not affect transwell migration rate of MBA-MB231 cells* . . . 183
6.7.1.4 *CPT1A overexpression does not affect anchorage-independent growth of MDA-MB231 cells* . . . 185
6.7.1.5 *CPT1A knockdown does not affect proliferation rate of MCF7 cells* . . . 186
6.7.1.6 *CPT1A knockdown does not affect anchorage-independent growth rate of MCF7 cells* . . . 189
6.8 FAO flux analysis of breast normal and cancer cell lines with CPT1A modulation . . . 190
6.8.1 *Real time FAO flux in MDA-MB231 cells with CPT1A overexpression* . . . 190
6.8.2 *Real time FAO flux in MCF7 cells with CPT1A knockdown* . . . 192
6.8.3 *Real time FAO flux in MCF10A cells with CPT1A knockdown* . . . 192
6.9 Discussion . . . 192
6.9.1 CPT1A modulation decreases growth and wound closure rates in MDA-MB231, but not MCF7 cells . . . 195
6.9.1.1 *Culture media constituents and concentrations are key in metabolism experiments* . . . 197
6.9.2 CPT1A modulation does not affect anchorage-independent growth 198
6.9.2.1 *Varied roles of metabolic pathways during anchorage-independent growth* . . . 200
6.9.3 Seahorse XF analysis of transgenic lines . . . 200
6.10 Summary, strengths and limitations . . . 202

7 Transcriptome analysis of breast cancer cell systems in response to CPT1A modulation 204
7.1 Background . . . 204
7.2 Results . . . 205
7.2.1 Differential expression analysis in MDA-MB231 cells with *CPT1A* overexpression . . . 205
7.2.1.1 *Gene set enrichment analysis* . . . 208
7.2.2 Differential expression analysis in MCF7 cells with *CPT1A* knockdown . . . 215
7.2.2.1 *Gene set enrichment analysis* . . . 217
7.2.3 Targeted pathway analysis . . . 225
7.2.3.1 *Wnt, MAPK and EMT signature expression in MDA-MB231 transgenic systems* . . . 225
7.2.3.1.1 *Wnt signature expression* . . . 225
7.2.3.1.2 *MAPK signature expression* . . . 225
7.2.3.1.3 *EMT signature expression* . . . 226

7.2.3.2 *Wnt, MAPK and EMT signature expression in MCF7 transgenic systems* . . . 228
7.2.3.2.1 *Wnt signature expression* . . . 228
7.2.3.2.2 *MAPK signature expression* . . . 228
7.2.3.2.3 *EMT signature expression* . . . 228
7.2.4 Analysis of publicly available datasets that modulate FAO in different cell systems . . . 229
7.2.4.1 *Wnt, MAPK and EMT signature expression in PC3 cells with PGC1A overexpression and NCI-H2347 cells treated with pioglitazone* . . . 229
7.2.4.2 *Differential expression analysis of transcriptome data from PC3 cells with PCG1A overexpression* . . . 231
7.2.4.3 *Differential expression analysis of transcriptome data from NCI-H2347 cells treated with pioglitazone* . . . 233
7.3 Discussion . . . 233
7.3.1 Differential and gene set enrichment analysis . . . 234
7.3.1.1 MDA-MB231 *CPT1A* overexpression . . . 234
7.3.1.2 MCF7 *CPT1A* knockdown . . . 235
7.3.1.3 Public datasets . . . 235
7.3.2 Targeted analysis . . . 236
7.3.2.1 MDA-MB231 *CPT1A* overexpression . . . 236
7.3.2.2 MCF7 *CPT1A* knockdown . . . 237
7.3.2.3 Public datasets . . . 238
7.3.3 Conclusions and limitations . . . 239

8 Conclusions and future directions 241
8.1 General discussion . . . 241
8.1.1 Conclusion . . . 243
8.1.2 Overall strengths and limitations . . . 244
8.2 Future directions . . . 244
8.2.1 *siRNA knockdown of CPT1A in ER-positive breast cancer cell lines* 244
8.2.2 *Pharmacologic activation or inhibition of FAO in cancer cell lines* 245
8.2.3 *Analysis of other platforms to identify novel regulators and correlates of FAO* . . . 246
8.2.4 *How does hypoxia affect FAO flux?* . . . 247
8.2.5 *Targeting co-dependencies in tumours with low FAO* . . . 248
8.2.6 *Elucidating the interaction between tumour metabolism and microenvironment* . . . 250
8.2.7 *Xenopus laevis appendage regeneration as a model system to understand metabolic correlates of cancer initiation and progression* 251
8.3 Potential translational relevance of FAO in oncology . . . 252
8.3.1 *Radiolabelled fatty acid to image tumours* . . . 252
8.3.1.1 *PET imaging of FAO in cancer* . . . 253
8.3.2 *Using genomic correlates of tumour metabolism to actively target metabolic dependencies* . . . 253

A Supplementary Figures **255**

B Supplementary Tables **275**

C Supplementary Figures **348**

References **350**

List of Figures

1.1 Tamoxifen and aromatase inhibitor inhibit oestrogen signalling by different mechanisms. . . . 6
1.2 Multi-platform molecular risk stratification of breast cancer patients. . . 14
1.3 Brief schematic of glycolysis, glutamine oxidation and fatty acid synthesis pathways. . . . 24
1.4 Key steps in the fatty acid beta oxidation pathway. . . . 30

3.1 Enrichment plot of KEGG Fatty Acid Metabolism pathway. . . . 77
3.2 FAO genes in the KEGG Fatty Acid Degradation/Metabolism pathway. 78
3.3 Cluster analysis of genes in the FAO signature in the METABRIC training cohort. . . . 81
3.4 FAO signature is significantly associated with DSS of METABRIC training data. . . . 82
3.5 FAO signature expression higher in ER-positive, Grade 1 and luminal A molecular subtype. . . . 85
3.6 High FAO signature expression is associated with good response to short-term neoadjuvant AI treatment . . . 88
3.7 *ESR1* knockdown decreases FAO signature expression in MCF7 cell line. 89
3.8 Low FAO signature expression is associated with neoadjuvant chemotherapy pCR. . . . 90
3.9 Cytogenetic locations of *CCND1* and *CPT1A* in 11q13. . . . 91
3.10 *CPT1A* is likely to be co-amplified with *CCND1* in breast cancer. . . . 92
3.11 FAO signature expression is associated with overall survival in different cancers. . . . 94
3.12 FAO signature expression is associated with melanoma survival in different datasets. . . . 95
3.14 FAO signature is downregulated in tumours compared to normal tissues. 96
3.13 FAO signature is downregulated in tumours compared to normal tissues. 97
3.15 FAO signature expression is altered in castrated or androgen-independent prostate xenografts in mice. . . . 99

4.1 TGFβ treatment of MCF10A or NMuMG mammary epithelial cells induces alterations in FAO and EMT signature expression. 112
4.2 TGFβ treatment of A549 lung cancer, Panc1 pancreatic cancer, or M-BE bronchoepithelial cells induce alterations in FAO and EMT signature expression. 114
4.3 Alterations in FAO and EMT signature expression upon TGFβ-induced EMT in a panel of lung cancer cells. 115
4.4 IDH1/2 mutations or 2-HG treatment induces alterations in FAO and EMT signature expression. 117
4.5 Overexpression of EMT transcription factors in mammary epithelial or breast cancer cells alter FAO and EMT signature expression. 119
4.6 SNAI1 overexpression decreases FAO signature expression in three lung cancer cell lines. 120
4.7 SNAI1 overexpression in II-18 lung cancer cell line decreases FAO signature expression. 121
4.8 TGFβ treatment of mouse normal intestinal, colon or tubular adenocarcinoma organoids alter expression of FAO and EMT signatures. 122
4.9 FAO signature expression increases from mammary stem to differentiated ductal cell. 124
4.10 FAO signature expression increases during HMEC differentiation. 128
4.11 FAO signature expression increases upon treatment with sodium butyrate. 129
4.12 FAO signature expression increases in CC-531 rat colon carcinoma cells at earlier time points of sodium butyrate treatment. 130

5.1 APC knockout, knockdown, or single allele inactivation decreases FAO signature expression. 140
5.2 Bcl9 knockout increases FAO signature expression. 142
5.3 APC or DKK-1 overexpression, or β-catenin knockdown increases FAO signature expression. 144
5.4 β-catenin knockdown or dnTCF4 expression alters FAO signature expression in Ls174T cells. 145
5.5 Constitutive Wnt signalling decreases FAO signature expression across different stages of mammary tumour development. 147
5.6 Vemurafenib treatment of BRAF mutant melanoma cell lines decreases FAO signature expression. 149
5.7 BRAF inhibition increases FAO signature expression in a panel of melanoma cell lines. 150
5.8 Transgenic mutant BRAF expression in melanocytes decreases FAO signature expression. 151
5.9 Mutant RAS expression in melanocyte or melanoma cell lines influences FAO signature expression. 153
5.10 BRAF or MEK inhibition in colorectal cancer cell lines increases FAO signature expression. 155
5.11 MEK inhibition increases FAO signature expression in a panel of pancreatic cancer cell lines. 156

5.12 MITF overexpression or knockdown increases FAO signature expression. 158

6.1 ER-positive tumours have higher *CPT1A* mRNA expression compared to ER-negative tumours. 168
6.2 ER-positive cell lines have higher *CPT1A* mRNA expression compared to ER-negative cell lines (Neve *et.al.* dataset) 170
6.3 ER-positive cell lines have higher *CPT1A* mRNA expression compared to ER-negative cell lines (Astra Zeneca dataset). 171
6.4 Luciferase assay to measure rtTA inducibility in MDA-MB231 TetOn clones. 174
6.5 *CPT1A* mRNA overexpression screen after 48 hr induction in putative MDA-MB231 pTRE-CPT1A clones. 175
6.6 CPT1A overexpression screen after 48 hr induction in selected MDA-MB231 pTRE-CPT1A clones. 176
6.7 Dose response and time course characterisation of CPT1A overexpression in MDA-MB231 cells. 177
6.8 *CPT1A* mRNA knockdown screen after 5 days induction in putative MCF7 shRNA clones. 178
6.9 Characterising CPT1A knockdown in MCF7 cells. 178
6.10 *CPT1A* mRNA knockdown screen in MCF10A shRNA polyclones. . . . 179
6.11 Characterising CPT1A knockdown in MCF10A cells. 180
6.12 Characterising CPT1A knockdown in MCF10A cells. 180
6.13 CPT1A overexpression in MDA-MB231 decreases proliferation rate, compared to Tet parental. 182
6.14 CPT1A overexpression in MDA-MB231 decreases wound healing rate, compared to Tet parental. 184
6.15 CPT1A overexpression does not affect transwell migration rate of MDA-MB231 cells. 185
6.16 CPT1A overexpression does not affect anchorage-independent growth in MDA-MB231 cells. 186
6.17 CPT1A knockdown does not affect proliferation in MCF7 cells. 188
6.18 CPT1A knockdown does not affect anchorage-independent growth in MCF7 cells. 189
6.19 Real time oxygen consumption analysis in CPT1A overexpressing MDA-MB231 cells. 191
6.20 Real time oxygen consumption analysis in MCF7 cells after CPT1A knockdown. 193
6.21 Real time oxygen consumption analysis in MCF10A cells after CPT1A knockdown. 194

7.1 Genesets enriched in pTRE-CPT1A clone 3 overexpressing *CPT1A*, relative to basal expression. 210
7.2 Genesets enriched in pTRE-CPT1A clone 17 overexpressing *CPT1A*, relative to basal expression. 212
7.3 Genesets enriched in pTRE-CPT1A clones 3 and 17 overexpressing *CPT1A*, relative to basal expression. 214

7.4 Processes enriched in MCF7 shRNA1 clone compared to non-silencing basal expression. . . . 218
7.5 Processes enriched in MCF7 shRNA2 clone compared to non-silencing basal expression. . . . 219
7.6 Genesets enriched in MCF7 shRNA1 *CPT1A* knockdown, relative to basal non-silencing cells. . . . 221
7.7 Genesets enriched in MCF7 shRNA2 *CPT1A* knockdown, relative to basal non-silencing cells. . . . 222
7.8 Genesets enriched in MCF7 shRNA1 and shRNA2 combined *CPT1A* knockdown, relative to basal non-silencing cells. . . . 224
7.9 Wnt, MAPK and EMT signature expression analysis in MDA-MB231 TetOn and pTRE-CPT1A clones. . . . 227
7.10 Wnt, MAPK and EMT signature expression analysis in MCF7 non-silencing and *CPT1A* shRNA1 and shRNA2 clones. . . . 230
7.11 Wnt, MAPK and EMT signature expression analysis in PC3 cells with PGC1A overexpression or NCI-H2347 cells treated with pioglitazone. . . 232

A.1 FAO signature is expressed higher in lung adenocarcinoma compared to squamous cell carcinoma. . . . 255
A.2 FAO signature is expressed lower in laser capture microdissected (LCM) tissue compared to bulk biopsy colon tumours and normal colon tissue. 256
A.3 ER-positive cell lines have higher *CPT1A* mRNA expression compared to ER-negative cell lines (GSE41313 dataset). . . . 257
A.4 ER-positive cell lines have higher *CPT1A* mRNA expression compared to ER-negative cell lines (Cancer Cell Line Encyclopedia dataset). . . . 258
A.5 Leaky CPT1A expression in pTRE-CPT1A clone 5 in the absence of Dox induction. . . . 259
A.6 Growth curves of pTRE-CPT1A clone 3 with basal and CPT1A overexpression. . . . 260
A.7 Growth curves of pTRE-CPT1A clone 17 with basal and CPT1A overexpression. . . . 261
A.8 Would healing rate of pTRE-CPT1A clone 3 with basal and CPT1A overexpression. . . . 262
A.9 Would healing rate of pTRE-CPT1A clone 17 with basal and CPT1A overexpression. . . . 263
A.10 Growth curves of MCF7 non-silencing, shRNA clones 1 and 2. . . . 264
A.11 Geneset enrichment analysis of TetOn cells with Dox treatment. . . . 265
A.12 Geneset enrichment analysis of TetOn cells with Dox treatment. . . . 266
A.13 Geneset enrichment analysis of PC3 cells with basal or PGC1A overexpression. . . . 267
A.14 Geneset enrichment analysis of PC3 cells with basal or PGC1A overexpression. . . . 268
A.15 Genesets enriched in NCI-H2347 cells 12 hrs after pioglitazone treatment. 269
A.16 Genesets enriched in NCI-H2347 cells 24 hrs after pioglitazone treatment. 270
A.17 Genesets enriched in NCI-H2347 cells 48 hrs after pioglitazone treatment. 271

A.18 Genesets enriched in NCI-H2347 cells 12 hrs after pioglitazone treatment. 272
A.19 Genesets enriched in NCI-H2347 cells 24 hrs after pioglitazone treatment. 273
A.20 Genesets enriched in NCI-H2347 cells 48 hrs after pioglitazone treatment. 274

List of Tables

2.1 Cell lines used in this study. 46
2.2 Plasmids used in this study. 48
2.3 Primers used in this study. 49
2.4 Reverse transcription mix components per reaction. 51
2.5 PCR protocol for *CPT1A* cDNA amplification. 52
2.6 qPCR cycling protocol. 58
2.7 Ultramer sequences for amplifying shRNA sequence against *CPT1A*. . . 59
2.8 PCR protocol for shRNA ultramers amplification. 60
2.9 Mitochondrial inhibitors utilised in real time FAO flux analysis. 68
2.10 XF24 Fatty oxidation instrument run protocol. 70

3.1 KEGG genesets associated with disease-specific survival of the METABRIC training cohort. 77
3.2 19-gene signature involved in FAO associated with disease-specific survival in METABRIC training cohort. 79
3.3 FAO signature expression is associated with survival in multiple breast cancer datasets. 83
3.4 FAO gene signature is an independent prognostic factor in breast cancer. 86
3.5 FAO signature expression is negatively correlated with the MKS proliferation signature in breast cancer datasets. 87
3.6 *CPT1A* is likely to be co-amplified with *CCND1* in multiple cancers. . . 93

4.1 Spearman correlation analysis of FAO and EMT signatures on breast cancer datasets. 123
4.2 Spearman's correlation matrix of indicated signatures on GSE47376 (mouse). 125
4.3 Spearman's correlation matrix of indicated signatures on GSE19446 (mouse). 125
4.4 Spearman's correlation matrix of indicated signatures on mouse mammary stem and luminal progenitor enriched cell populations (GSE20402). 126
4.5 Spearman's correlation matrix of indicated signatures on human mammary stem and luminal progenitor enriched cell populations (GSE16997). 126

5.1 FAO signature expression is not associated with survival in colorectal cancer cohorts. 147

7.1 Top 20 genes differentially expressed in CPT1A overexpression clone 3. . 207
7.2 Top 20 genes differentially expressed in CPT1A overexpression clone 17. 208
7.3 Top 20 genes differentially expressed in shRNA clone 1. 215
7.4 Top 20 genes differentially expressed in shRNA clone 2. 216

B.1 Clinical information of METABRIC training data. 276
B.2 Cell lines with *CCND1* and *CPT1A* co-amplification. 277
B.3 Upregulated KEGG genesets in pTRE-CPT1A clone 3 in response to *CPT1A* overexpression. 278
B.4 Upregulated Reactome genesets in pTRE-CPT1A clone 3 in response to *CPT1A* overexpression. 280
B.5 Upregulated WikiPathways genesets in pTRE-CPT1A clone 3 in response to *CPT1A* overexpression. 281
B.6 Upregulated Panther genesets in pTRE-CPT1A clone 3 in response to *CPT1A* overexpression. 282
B.7 Downregulated KEGG genesets in pTRE-CPT1A clone 3 in response to *CPT1A* overexpression. 283
B.8 Downregulated Reactome genesets in pTRE-CPT1A clone 3 in response to *CPT1A* overexpression. 284
B.9 Downregulated WikiPathways genesets in pTRE-CPT1A clone 3 in response to *CPT1A* overexpression. 285
B.10 Downregulated Panther genesets in pTRE-CPT1A clone 3 in response to *CPT1A* overexpression. 286
B.11 Upregulated KEGG genesets in combined pTRE-CPT1A clones 3 and 17 in response to *CPT1A* overexpression. 287
B.12 Upregulated Reactome genesets in combined pTRE-CPT1A clones 3 and 17 in response to *CPT1A* overexpression. 288
B.13 Upregulated WikiPathways genesets in combined pTRE-CPT1A clones 3 and 17 in response to *CPT1A* overexpression. 289
B.14 Upregulated Panther genesets in combined pTRE-CPT1A clones 3 and 17 in response to *CPT1A* overexpression. 290
B.15 Downregulated KEGG genesets in combined pTRE-CPT1A clones 3 and 17 in response to *CPT1A* overexpression. 291
B.16 Downregulated Reactome genesets in combined pTRE-CPT1A clones 3 and 17 in response to *CPT1A* overexpression. 292
B.17 Downregulated WikiPathways genesets in combined pTRE-CPT1A clones 3 and 17 in response to *CPT1A* overexpression. 293
B.18 Downregulated Panther genesets in combined pTRE-CPT1A clones 3 and 17 in response to *CPT1A* overexpression. 294
B.19 Upregulated KEGG genesets in TetOn parental cells in response to Dox treatment. 295
B.20 Upregulated Reactome genesets in TetOn parental cells in response to Dox treatment. 297

B.21 Upregulated WikiPathways genesets in TetOn parental cells in response to Dox treatment. 298
B.22 Upregulated WikiPathways genesets in TetOn parental cells in response to Dox treatment. 299
B.23 Downregulated KEGG genesets in TetOn parental cells in response to Dox treatment. 300
B.24 Downregulated Reactome genesets in TetOn parental cells in response to Dox treatment. 302
B.25 Downregulated WikiPathways genesets in TetOn parental cells in response to Dox treatment. 303
B.26 Downregulated Panther genesets in TetOn parental cells in response to Dox treatment. 304
B.27 Upregulated KEGG genesets in pTRE-CPT1A clone 17 in response to *CPT1A* overexpression. 305
B.28 Upregulated Reactome genesets in pTRE-CPT1A clone 17 in response to *CPT1A* overexpression. 307
B.29 Upregulated WikiPathways genesets in pTRE-CPT1A clone 17 in response to *CPT1A* overexpression. 308
B.30 Upregulated Panther genesets in pTRE-CPT1A clone 17 in response to *CPT1A* overexpression. 309
B.31 Downregulated KEGG genesets in pTRE-CPT1A clone 17 in response to *CPT1A* overexpression. 310
B.32 Downregulated Reactome genesets in pTRE-CPT1A clone 17 in response to *CPT1A* overexpression. 312
B.33 Downregulated WikiPathways genesets in pTRE-CPT1A clone 17 in response to *CPT1A* overexpression. 313
B.34 Downregulated Panther genesets in pTRE-CPT1A clone 17 in response to *CPT1A* overexpression. 314
B.35 Upregulated KEGG genesets in MCF7 shRNA1 clone in response to *CPT1A* knockdown, compared to non-silencing control. 315
B.36 Upregulated Reactome genesets in MCF7 shRNA1 clone in response to *CPT1A* knockdown, compared to non-silencing control. 316
B.37 Upregulated WikiPathways genesets in MCF7 shRNA1 clone in response to *CPT1A* knockdown, compared to non-silencing control. 317
B.38 Upregulated Panther genesets in MCF7 shRNA1 clone in response to *CPT1A* knockdown, compared to non-silencing control. 318
B.39 Downregulated KEGG genesets in MCF7 shRNA1 clone in response to *CPT1A* knockdown, compared to non-silencing control. 319
B.40 Downregulated Reactome genesets in MCF7 shRNA1 clone in response to *CPT1A* knockdown, compared to non-silencing control. 320
B.41 Downregulated WikiPathways genesets in MCF7 shRNA1 clone in response to *CPT1A* knockdown, compared to non-silencing control. 321
B.42 Downregulated Panther genesets in MCF7 shRNA1 clone in response to *CPT1A* knockdown, compared to non-silencing control. 322

B.43 Upregulated KEGG genesets in MCF7 shRNA2 clone in response to *CPT1A* knockdown, compared to non-silencing control. 323
B.44 Upregulated Reactome genesets in MCF7 shRNA2 clone in response to *CPT1A* knockdown, compared to non-silencing control. 325
B.45 Upregulated WikiPathways genesets in MCF7 shRNA2 clone in response to *CPT1A* knockdown, compared to non-silencing control. 326
B.46 Upregulated Panther genesets in MCF7 shRNA2 clone in response to *CPT1A* knockdown, compared to non-silencing control. 327
B.47 Downregulated KEGG genesets in MCF7 shRNA2 clone in response to *CPT1A* knockdown, compared to non-silencing control. 328
B.48 Downregulated Reactome genesets in MCF7 shRNA2 clone in response to *CPT1A* knockdown, compared to non-silencing control. 329
B.49 Downregulated WikiPathways genesets in MCF7 shRNA2 clone in response to *CPT1A* knockdown, compared to non-silencing control. 330
B.50 Downregulated Panther genesets in MCF7 shRNA2 clone in response to *CPT1A* knockdown, compared to non-silencing control. 331
B.51 Upregulated KEGG genesets in combined MCF7 shRNA1/2 clones in response to *CPT1A* knockdown, compared to non-silencing control. . . . 332
B.52 Upregulated Reactome genesets in combined MCF7 shRNA1/2 clones in response to *CPT1A* knockdown, compared to non-silencing control. . . . 334
B.53 Upregulated WikiPathways genesets in combined MCF7 shRNA1/2 clones in response to *CPT1A* knockdown, compared to non-silencing control. . 335
B.54 Upregulated Panther genesets in combined MCF7 shRNA1/2 clones in response to *CPT1A* knockdown, compared to non-silencing control. . . . 336
B.55 Downregulated KEGG genesets in combined MCF7 shRNA1/2 clones in response to *CPT1A* knockdown, compared to non-silencing control. . . . 337
B.56 Downregulated Reactome genesets in combined MCF7 shRNA1/2 clones in response to *CPT1A* knockdown, compared to non-silencing control. . 339
B.57 Downregulated WikiPathways genesets in combined MCF7 shRNA1/2 clones in response to *CPT1A* knockdown, compared to non-silencing control. 340
B.58 Downregulated Panther genesets in combined MCF7 shRNA1/2 clones in response to *CPT1A* knockdown, compared to non-silencing control. . . . 341
B.59 Datasets analysed for survival analysis in different cancer types. 342
B.60 Datasets analysed for neoadjuvant treatment analysis. 343
B.61 Datasets analysed for tumour-normal analysis. 344
B.62 Datasets analysed for EMT and cell differentiation analysis. 345
B.63 Datasets analysed for Wnt and MAPK signalling analysis. 346
B.64 Datasets analysed for experimental analysis and RNA-Seq chapters. . . 347

C.1 Gene members of the MAPK, Wnt and EMT signatures analysed in this thesis. 349

List of Abbreviations

Unless listed, all abbreviations in this thesis are described in the "Instructions to Authors" of the Biochemical Journal (https://academic.oup.com/DocumentLibrary/JB/tabletwo.pdf)

% - Percent

% w/v = Weight-to-volume

μg - Microgram

μL - Microlitre

μM - Micromole

$^{\circ}$ C - Degrees celsius

AI - Aromatase inhibitor

APC - Adenomatous Polyposis Coli

ATCC - American Type Culture Collection

BRAF - B- Rapidly Accelerated Fibrosarcoma

CPT1A - Carnitine palmitoyl transferase 1A (CPT1A)

CCND1 - Cyclin D1

CTTNB - Beta-catenin

CO2 - Carbon dioxide

EMT - Epithelial-to-mesenchymal transition

ER - Oestrogen receptor

FAO - Fatty acid oxidation

FBS - Fetal bovine serum

FCCP - Carbonyl cyanide-p-trifluoromethoxyphenylhydrazone

g - Gram

HER2 - Human Epidermal Growth Factor Receptor 2 HRAS - Harvey rat sarcoma

KRAS - Kirsten rat sarcoma

mg - Milligram

MKS - Mitosis kinome score

mL - Millilitre

NRAS - Neural rat sarcoma

ng - Nanogram

nM - Nanomolar

PCR - Polymerase chain reaction

PgR - Progesterone Receptor

PGC1A - Peroxisome proliferator-activated receptor gamma coactivator 1A

PPAR - Peroxisome proliferator-activated receptor

RCC - Renal cell carcinoma

RFP - Red fluorescent protein

RPM - Revolutions per minute

RPMI - Roswell Park Memorial Institute

qPCR - Quantitative Polymerase Chain Reaction

SERM - Selective oestrogen receptor modulator

shRNA - Short hairpin ribonucleic acid

TBST - Tris-buffered saline with Tween-20

TCGA - The Cancer Genome Atlas

Tet (or rtTA) - Reverse tetracycline transactivator

TGFβ - Transforming growth factor beta TRE - Tet response element

TUBA - Alpha-tubulin

Chapter 1

Introduction

1.1 Clinically significant prognostic and predictive markers in breast cancer

1.1.1 Prognostic factors

Prognostic factors are defined as features that correlate with the *natural* course of the disease, independently of treatment. Therefore, these factors reflect the inherent characteristics of a primary tumour. In breast cancer, established prognostic factors include nodal status, tumour grade and size, histological subtype, and demographic variables such as age, menopausal status and ethnicity (Cianfrocca and Goldstein, 2004). It is worthwhile noting, however, that prognostic and predictive markers are not mutually exclusive. Some markers such as oestrogen receptor (ER), progesterone receptor (PgR), and human epidermal growth factor receptor 2 (HER2), provide both prognostic and predictive information (Taneja et al., 2010). Selected clinical prognostic factors are briefly mentioned below.

1.1.1.1 *Axillary lymph node status*

In primary breast cancer, axillary lymph node involvement is the most powerful prognostic factor (Jatoi et al., 1999). Cancer cells detected in axillary lymph nodes indicate disseminated disease. Additionally, removal of involved nodes has little impact on survival, which supports node involvement as an established surrogate of advanced disease (Jatoi et al., 1999). A strong, linear relationship exists between outcome and the number of nodes involved (Hilsenbeck et al., 1998). The disease-free- and overall survival decreases with each additional node involved. The 5-year relapse-free survival for patients with no tumour cells in the lymph node or node-negative is 80% (Hilsenbeck et al., 1998). The relapse-free survival decreases to approximately 75% when 1-3 nodes are involved; 55% with 4-9 nodes involved and 30% when 10 or more nodes are positive (Cianfrocca and Goldstein, 2004).

1.1.1.2 *Tumour size*

Tumour size is another important prognostic factor, especially in node-negative patients (Cianfrocca and Goldstein, 2004). As with node involvement, there is a direct relationship between tumour size and outcome. Patients with tumours less than 1 cm had an overall survival of nearly 99%(Rosen et al., 1993). This figure drops to 89% for tumours 1-3 cm in size, and 86% for tumour sizes between 3 to 5 cm. For node-negative patients, tumour size is the most powerful prognostic factor (Cianfrocca and Goldstein, 2004). Data from large studies have shown that tumours less than 1 cm in size in node-negative patients have a 20 year relapse-free survival of 90%, compared to approximately 72% for tumours more than 1-2 cm in size (Rosen et al., 1989). Futhermore, there is an inverse correlation between tumour size and median time to metastasis (Rosen et al., 1993; Koscielny et al., 1984; Carter, Allen, and Henson, 1989).

1.1.1.3 *Histologic and nuclear grade*

Several histological features of primary breast tumours have been associated with risk for distant relapse (Bloom and Richardson, 1957). However, histologic grading is subject to interobserver variability and lack of agreement, and therefore, has been criticised for poor reproducibility (Gilchrist et al., 1985). Additionally, several systems for determining the tumour grade exists, which may further confound the reliability of this feature as a prognostic factor. Nonetheless, when conducted in a centralised institution by experienced pathologists, the tumour grade has a strong relationship with clinical outcome (Contesso et al., 1987).

The two most common methods of tumour grading are the Scarff-Bloom-Richardson classification and Fishers nuclear grading system (Bloom and Richardson, 1957). The Scarff-Bloom-Richardson method considers three features of the tumour; (i) degree of differentiation, (ii) pleomorphism and (iii) mitotic index. Differentiation assesses the extent of similarity of the tumour to normal, differentiated features such tubular, glandular and papillary formations. Pleomorphism assesses the shape and size of the cell and nuclei. Mitotic index measures the number of mitosis per high power field, and is an indication of the proliferation rate of the tumour. Each of these components are given a score of 1-3, and finally categorised as grades 1, 2 or 3. With increasing grade, the tumours are less differentiated, have less consistent cell morphology and more distorted nuclei structures such as multi-nucleated and aneuploid chromosomes; and have higher rates of proliferation. A study by Doussal *et. al.* found a positive correlation between tumour grade as determined by the SBR method and recurrence (Le Doussal et al., 1989).

1.1.2 Predictive factors

1.1.2.1 *Oestrogen receptor as a prognostic and treatment predictive marker*

The oestrogen receptor (ER) exists as two isoforms - ER alpha (ERα) and ER beta (ERβ) - each encoded by different genes (Kumar et al., 2011). Both isoforms mediate the physiological effects of oestrogen and have different tissue-specific distribution (Gustafsson, 1999). ERα and ERβ reside mainly in the cytoplasm, where they are both sequestered in an inactive state. In this thesis, ER will be mentioned and discussed in the context of ERα.

Patients with ER-positive tumour have a better disease-free survival compared with ER-negative patients, particularly over shorter period of time post-diagnosis (Hilsenbeck et al., 1998). The prognostic advantage of ER gradually diminishes with increasing follow-up period. This time-dependent effect suggests that ER expression is associated with slower proliferation, rather than the metastatic potential of a tumour.

A large meta-analysis by the Early Breast Cancer Trialists' Collaborative Group (EBCTCG) that included approximately 70,000 women from at least 56 randomised trials conclusively proved that ER status is a significant predictor of benefit for 5 years of treatment with the anti-oestrogen tamoxifen (EBCTCGb, 2005). The annual recurrence risk and death was significantly lower for ER-positive compared to ER-negative disease. The degree of benefit from tamoxifen is directly correlated to the ER levels of the tumour. Patients with tumours with ER levels of >100 fmol/mg protein have a much-lowered recurrence rate from 5 years of tamoxifen compared to patients with lower ER levels. This is supported by the NSABP-14 biomarker trial that found quantitative measurement of ER by quantitative polymerase chain reaction to be predictive of tamoxifen benefit.

Up to 60% of ER-positive tumours respond to endocrine therapy, whereas only 10% of ER-negative benefit from the same treatment (Ellis et al., 2001). In the latter case, it is possible that assays for ER expression yielded false-negatives, or some level of heterogeneity in ER expression is present within the tumour. Additionally, the extent of benefit from endocrine therapy is positively correlated with of ER expression (Dowsett et al., 2008). Tumours with high ER expression benefit the most from treatment, whereas tumours with low ER expression have a poorer response to endocrine therapy, possibly due to the activation of alternative signalling pathways.

There is evidence to suggest that breast cancer patients with ER/PgR-positive tumours benefit less from various chemotherapy regimes (Henry and Hayes, 2007). Furthermore, studies that show benefit from chemotherapy regardless of ER status may be confounded by the ovary ablating effects of chemotherapy. For instance, in a trial that compared taxotere, adriamycin and cyclophosphamide (TAC) versus a 5-fluorouracil, adriamycin and cyclophosphamide combination, TAC was interpreted as being superior regardless of ER status (Martin et al., 2005). However, more than half of the patients were premenopausal and a greater incidence of chemotherapy-induced amenorrhea was reported in the TAC arm. Therefore, the beneficial effect observed in TAC-treated patients may be due to the indirect endocrine therapy. This effect of ER on chemotherapy response is supported by data from neoadjuvant trials. Pathological complete response, where no residual tumour can be visualised by imaging after a short course of treatment, was more commonly achieved in ER-negative (20%) compared to ER-positive (5%) tumours (Mazouni et al., 2007).

1.2 Pharmacotherapy of ER-positive breast tumours

Approximately 70-80% of breast cancers are ER-positive, and therefore depend on oestrogen for tumour growth and survival. Surgery is the main intervention to remove

the primary, localised tumour. Additionally, pre-menopausal women may have an ovariectomy while post-menopausal women may undergo adrenalectomy (Johnston and Dowsett, 2003). These procedures surgically deplete the body of oestrogen, and therefore, block the growth of the hormone-sensitive breast tumour.

Pharmacologically, the dependence of ER-positive tumours is targeted by two main mechanisms; (i) antagonism of ER and (ii) depriving ER of its ligand, oestradiol. Two common drugs utilised to achieve this are tamoxifen - a selective oestrogen receptor modulator (SERM), and aromatase inhibitors (Fig 1.1).

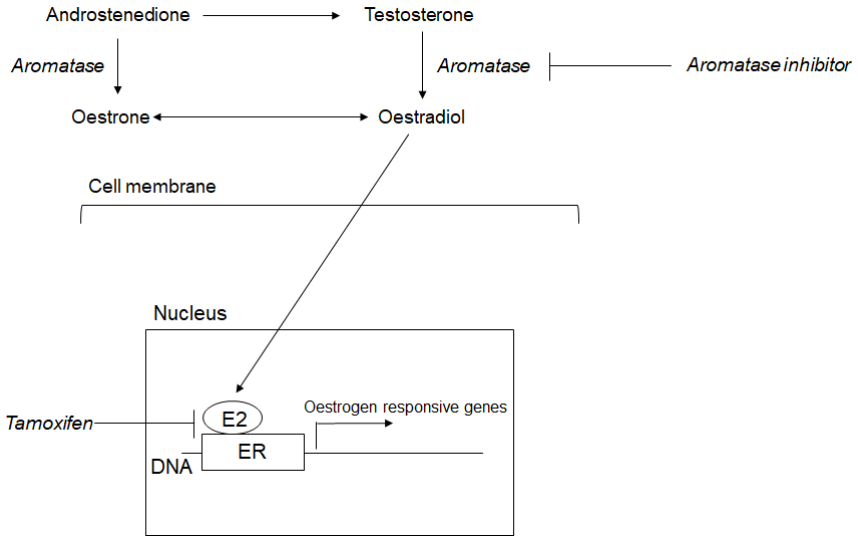

Figure 1.1: Tamoxifen and aromatase inhibitor inhibit oestrogen signalling by different mechanisms. Aromatase inhibitors block the aromatisation of testosterone or androstenedione precursor, thereby inhibiting oestrogen synthesis, while tamoxifen competitively antagonise the ER. Both mechanism result in the decreased expression of oestrogen-responsive genes, including those involved in proliferation. E2= oestradiol. Figure adapted from Johnston and Dowsett, 2003.

1.2.1 Tamoxifen

Tamoxifen functions as a SERM due to its selective agonistic and antagonistic nature that varies between cell types (Grese et al., 1997). The balance between the two func-

tions depends on molecular events that mediate ER signalling, such as recruitment of co-activators or co-repressors, and cross-talk with other signalling cascades (Dutertre and Smith, 2000). The large side chain of another SERM, raloxifene, stabilises helix 12 of ER and maintains the receptor in an inactivated state, incapable of interacting with co-activators (Brzozowski et al., 1997).

Large, randomised clinical trials have established that 5 years of adjuvant tamoxifen treatment in early stage breast cancer patients reduces the relative recurrence and mortality rates by 47% and 26% respectively (EBCTCG, 1998). Furthermore, the recurrence and mortality rates were substantially lower 10 and 15 years after diagnosis respectively (Davies et al., 2011). Therefore, 5 years of tamoxifen has a carry-over beneficial effect for at least 10 years post-diagnosis.

1.2.2 Aromatase inhibitor (AI)

To avoid the possible oestrogenic-like activity of SERMs, agents that block the *synthesis* of oestrogen were developed. Oestrogen is synthesised from the aromatisation of androgens catalysed by the rate-limiting enzyme aromatase. Aromatase - a member of the cytochrome (CYP) P450 family of enzymes - first converts androgens into oestrone, which is then reduced to oestrogen by 17-hydroxysteroid dehydrogenase I. Aromatase is expressed at high levels in the placenta and granulosa cells of the ovaries, under the temporal control of gonadotropin stimulation (Johnston and Dowsett, 2003). After menopause, non-endocrine tissues such as subcutaneous fat, liver, muscle, brain and normal breast continue to synthesise residual amounts of oestrogen (Smith and Dowsett, 2003).

AIs can be classified into steroidal or non-steroidal depending on their aromatase binding site. Steroidal AIs are androstenedione analogues that bind and are converted into

reactive intermediates that covalently associate with the aromatase active site. In contrast, the nitrogen within the triazole of non-steroidal agents bind reversibly to the heme-center of aromatase, therefore disrupting the catalytic cycle of the enzyme (Kelly and Buzdar, 2010).

Third generation AIs such as anastrozole, letrozole and exemestane were developed in the early 1990s. On average, third-generation AIs inhibit at least 97% of aromatase activity, although a small trial found letrozole to suppress aromatase more than anastrozole (Geisler et al., 2002). Several clinical trials in the neoadjuvant and adjuvant setting have been conducted to assess the efficacy of different AIs or between AIs and tamoxifen in post-menopausal women.

1.2.2.1 *Efficacy of AIs versus tamoxifen*

Two large adjuvant trials, Breast International Group (BIG) 1-98 and Arimidex, Tamoxifen and in combination (ATAC) compared the efficacy of third generation non-steroidal AIs, letrozole and anastrozole respectively, against tamoxifen (Thurlimann et al., 2005; Cuzick et al., 2010). BIG 1-98 had four treatment arms: (1) monotherapy of tamoxifen or (2) letrozole; (3) tamoxifen for 2 years followed by 3 years of letrozole; and (4) letrozole for 3 years followed by tamoxifen for 2 years. The ATAC trial had a simpler treatment stratification, 5 years of either anastrozole or tamoxifen, and a combination of both agents for a similar time span.

In BIG 1-98, patients in the letrozole-only treatment arm had a decreased risk for a disease-free survival (DFS) event as compared to tamoxifen (hazard ratio (HR) 0.82, p=0.0002). Furthermore, the hazard ratio for secondary endpoints - overall survival, distant relapse-free interval and disease-free interval - were all consistently lower in the

letrozole monotherapy group as compared to tamoxifen.

The results of the ATAC trial parallels that of BIG 1-98. Patients in the 5 year anastrozole treatment arm exhibited an absolute reduction in recurrence by 2.7% and 4.3% at 5- and 10 years respectively. Furthermore, distant-relapse was also lower in the anastrozole group, with an absolute difference of 2.6% at 10 years. As oestrogen is involved in maintaining bone health, patients on anastrozole had an increased risk for fracture (odds ratio 1.33, $p<0.0001$). Additionally, the incidence of endometrial cancer was four times lower in the anastrozole treated group (odds ratio 0.25, $p=0.001$). Taken together, the data from these trials suggest that early-stage ER-positive breast cancer patients that received AI may gain a modest improvement in remaining disease-free, as compared to patients that received tamoxifen.

1.2.2.2 *Treatment outcome and survival*

A meta-analysis by the EBCTCG provided strong evidence for the positive effect of both endocrine and chemotherapy on survival (EBCTCGb, 2005). However, currently, only a handful of clinicopathologic factors such as ER/PgR and HER2 status, tumour grade and node involvement are used to aid treatment decisions and estimate prognosis. Such factors, however, do not capture the extensive heterogeneity of tumours, which may have therapeutic implications. For instance, a common treatment regime for node-positive patients is the combination of anthracycline and taxanes, followed by an endocrine agent in the case of ER-positive tumours. However, patients that are treatment responsive may still be administered suboptimal drug doses and receive unnecessary combination of other toxic agents. As such, with current treatment guidelines, chemotherapy is administered to approximately 60% of patients with early-stage breast cancer, from which only up to 15% may derive benefit, leaving the rest at risk of toxic side effects. These figures, therefore, suggest an urgent need to identify predictors of response to hormone-

or chemotherapy that (i) improve outcome by ensuring optimal treatment for a given patient and (ii) decrease complications from unnecessary exposure of toxic treatments.

1.3 Molecular risk stratification of breast cancer

Meta-analysis of clinical trials that compared tamoxifen to AI treatment for five years suggests that approximately 20% of women have a recurrence based on 8 year follow-up data (Dowsett et al., 2010). This suggests a need to identify patients that are likely to have a poor prognosis when designing, or prior to starting, adjuvant treatment. Molecular profiling of tumours using high throughput technologies has generated a rich volume of clinically meaningful data (Cross and Burmester, 2004; Wesolowski and Ramaswamy, 2011). To date, several comprehensive genomic characterisation of tumours including gene expression-, single nucleotide polymorphism- and copy number profiling, and DNA sequencing have been performed in several large cancer genomic studies (Koboldt et al., 2012; Curtis et al., 2012; Gatza et al., 2014).

1.3.1 Genomic technologies and data analysis methods

The general objective of gene expression profiling experiments is to identify genes that are differentially expressed between different sample groups or subgroups. As this methodology measures a large number of transcripts per assay, statistical and machine learning methods have been increasingly utilised to interpret data from this technology. The more common analysis methods can be divided into unsupervised and supervised approaches. Unsupervised methods require only the microarray data to discover patterns based on the similarities of gene expression profile between samples. Common methods in unsupervised analysis include hierarchical clustering, k-means clustering, self-organising maps, singular value decomposition and principal component analysis. Supervised methods, on the other hand, attempts to identify patterns or relationships

in the data based on pre-defined labels applied. Most of the early microarray-based studies performed on primary breast tumours utilised either approach, and the focus of these studies were to derive treatment predictive or prognostic molecular features to facilitate assessment of disease outcome independently of traditional clinico-pathological parameters (Symmans et al., 2010; Liedtke et al., 2009; Hatzis et al., 2011; Vijver et al., 2002; Goncalves and Bose, 2013).

1.3.1.1 Molecular intrinsic subtyping of breast tumours

Perhaps the most enduring progress made from the early days of breast tumour molecular profiling is based on work by Perou *et. al.* (Perou et al., 2000). Using an array-based and hierarchical clustering approach, the authors identified four molecular subtypes of breast cancers: luminal, HER2-enriched, basal-like and normal - each with distinct prognosis. This work was then followed up by another study from the same group (Sorlie et al., 2001). Subsequently, Parker *et. al.* developed a 50-gene (PAM50) risk-of-relapse model based on the molecular subtypes defined by Perou *et. al.* (Parker et al., 2009). These intrinsic subtypes were also reproduced more recently in a comprehensive sequencing effort by The Cancer Genome Atlas (Koboldt et al., 2012), and features of the various subtypes are briefly described below.

1.3.1.1.1 ***Luminal A*** Luminal tumours can be subclassified into luminal A and luminal B. Luminal A is the most prevalent subtype, representing up to 60% of all breast cancers. Tumours of this subtype express low levels of proliferation genes and high levels of GATA3, a transcription factor involved in regulating luminal cell differentiation in the mammary gland. Using immunohistochemistry, luminal A tumours are characterised by the expression of ER, PgR, Bcl-2, and cytokeratins CK8 and CK18 (Eroles et al., 2012). Luminal A tumours also have a lower proliferation rate as compared to luminal B, which is reflected in lower levels of the cell division marker Ki67. Patients

of this subtype have a good prognosis, with a relapse rate of slightly over 25%, which is significantly lower compared to other subtypes (Kennecke et al., 2010). Furthermore, with a median survival period of 2.2 years from the time of relapse, luminal A subtype patients generally survive longer following relapse relative to other subtypes. Of clinical significance, luminal A tumours have a higher tendency (19%) to metastasise to the bones as compared to other anatomic locales such as the brain, lung and liver (2-, 7- and 8% respectively) (Kennecke et al., 2010).

1.3.1.1.2 ***Luminal B*** Luminal B tumours represent between 10 to 20% of breast cancers, and are more aggressive than luminal A. Luminal B tumours present with a higher histological grade and proliferation rate, which may explain the poor prognosis of this subtype. In addition to increased expression of proliferation genes such as cyclin B and Ki67, luminal B tumours may also express growth factor receptors such as the epidermal growth factor receptor (EGFR) and HER2. This presents alternative signalling pathways, apart from oestrogen signalling to trigger cell growth and division.

1.3.1.1.3 ***HER2-enriched*** Approximately one-fifth of breast cancer cases are positive for HER2 expression. Amplification of the gene - which codes for the HER2 protein - and overexpression of its associated amplicon are common features of this subtype (Koboldt et al., 2012). HER2-positive tumours are highly proliferative, with three-quarter of cases presenting with high histological grade and a substantial number of cases harbour mutations in *TP53*. HER2-positive patients have a bleak prognosis, but the development of anti-HER2 therapies have substantially improved the outcome of women in this subtype (Dawood et al., 2010). Additionally, due to the high proliferative nature of HER2-positive tumours, 43% of patients have a complete response to chemotherapy, which is higher than that of luminal subtype patients.

1.3.1.1.4 *Basal-like* Basal-like tumours generally do not express ER, PgR or HER2, and therefore, are referred to as triple-negative. However, three-quarters of tumour defined as basal-like by intrinsic subtyping are clinically triple-negative while the remainder comprise of other molecular subtypes. Clinical characteristics of basal-like tumours include earlier age onset, a larger tumour size and, higher grade and node positive disease (Bosch et al., 2010). Basal-like tumours display high frequency of *TP53* mutations, in agreement with pathway analysis which revealed loss of *TP53* in almost all basal-like cases. Furthermore, loss of function in other genes involved in maintaining genome integrity such as *RB1* and *BRCA1* are common features of this subtype (Herschkowitz et al., 2008; Turner and Reis-Filho, 2006). *PIK3CA*, while commonly mutated, was paradoxically observed to have the highest pathway activity among all subtypes (Koboldt et al., 2012). Some possibilities that may account for this increased PIK3CA activity include loss of function in the phosphatases PTEN and INPP4B, which negatively regulate this pathway.

1.3.1.2 Integrative clustering based molecular stratification of breast cancer

The intrinsic subtype/PAM50-based classification is based primarily on the gene expression profile of a particular tumour. Recently, a collaborative effort by the Molecular Taxonomy of Breast Cancer International Consortium (METABRIC) analysed the copy number abberations, single nucleotide variants, and gene expression profiles from over 2000 primary breast tumours, and proposed an alternative molecular classification system (Curtis et al., 2012). This study identified ten integrative clusters, based on the genomic and transcriptomic correlates of tumours. The features of each cluster are succinctly summarised by Dawson *et. al.* (Dawson et al., 2013). Clusters 2, 5 and 10 were associated with poor prognosis (Fig 1.2). These clusters had intermediate to high genomic instability, different copy number aberrations such as amplifications in 11q13/14, 8q gain, and *HER2* amplification, and patients diagnosed younger with higher grade

and large tumours, and lymph-node positive disease. Clusters with good prognosis included tumours from patients that were older at diagnosis, low grade tumours and low genomic instability, and negligible to low copy number aberrations, compared to the poor prognosis clusters.

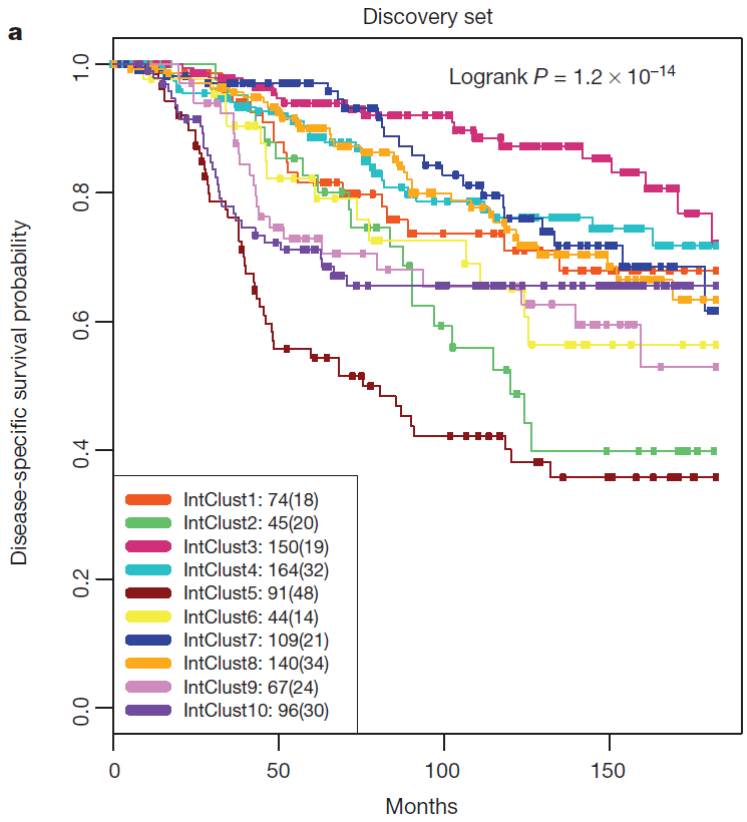

.

Figure 1.2: Multi-platform molecular risk stratification of breast cancer patients . Kaplan-Meier survival curve of patients in different integrative cluster as defined by the METABRIC investigators. Clusters 2 (green line), 5 (brown line) and 10 (dark purple line) have poorer disease-specific survival compared to other clusters. Patients in cluster 10 exhibit poor outcome at earlier time points, but otherwise remain event-free after approximately 60-70 months, which suggests time-dependency in this cluster. Figure adapted from Curtis et al., 2012

1.3.2 Commercially-available prognostic signatures

Several of the gene expression studies conducted earlier have resulted in prognostic signatures that are commercially available and utilised in the clinic to determine the prognosis and tailoring adjuvant treatment to each patient.

1.3.2.1 *Oncotype DX*

This signature comprises of 16 classifier and 5 reference genes from which a recurrence score is derived that categorises patients into three groups: low (<18), intermediate (18-30), and high (>31). This signature comprises of proliferation and invasion associated genes, as well as genes correlated with oestrogen signalling and HER2 expression. Retrospective analysis of samples from the National Surgical Adjuvant Breast and Bowel Project B-14 (NSABP-14) trial, in which ER-positive, node-negative patients were treated with tamoxifen, demonstrated a significant difference between low and high risk for distant recurrence at 10 years (6.5% vs 30.5% respectively; $p < 0.001$) (Paik et al., 2004).

This Oncotype DX signature is also predictive of benefit from adjuvant chemotherapy based on retrospective analysis of the NSABP B-20 and Southwest Oncology Group 8814 trials (Albain et al., 2010). High-risk patients derived more benefit from the combination of chemotherapy with tamoxifen, compared to low-risk patients (HR 0.26, 95% confidence interval 0.13-0.53) (Paik et al., 2006). Therefore, the Oncotype DX can identify patients that have a low risk of relapse and as such, do not require adjuvant chemotherapy.

1.3.2.2 *PAM50-based Prosigna*

The PAM50-based signature Prosigna, which has been approved by the United States Federal Drug Agency (FDA), is based on the expression levels of 50 classifier genes, and categorises patients into one of four intrinsic subtypes with associated prognostic significance (Parker et al., 2009). A sub-study from the ATAC trial found the PAM50 risk-of-relapse (ROR) score to be more prognostic than the Oncotype DX recurrence score (Dowsett et al., 2013). The ROR score could also better stratify patients with an intermediate recurrence risk as determined by the Oncotype DX assay. This was supported by the findings of Kelly *et. al.*, whom were able to classify about half of patients in the intermediate risk group by Oncotype DX into low-risk luminal A subtype using the PAM50 classifier (Kelly et al., 2012).

1.3.2.3 *MammaPrint*

Mammaprint, another FDA-approved signature, was developed at the Netherlands Cancer Institute in 2002 using tumour samples from relatively young, node-negative breast cancer patients (Veer et al., 2002). This microarray-based 70-gene assessment assigns patients as having either a high or low 5-year risk for distant relapse. A validation analysis, by the same group, was conducted on retrospectively collected samples, which included both node-negative and node-positive patients. This validation exercise, however, has been criticised for including 61 patients from the original study and 130 patients that received either adjuvant chemotherapy or hormonal therapy. Consequently, the resulting data would be inaccurate in terms of assessing the prognostic performance of this signature. Nonetheless, another independent study done in patients that did not receive systemic therapy confirmed the original findings by Veer *et. al.* (Vijver et al., 2002; Wittner et al., 2008).

1.3.3 Limitations of first-generation molecular signatures

1.3.3.1 *Performance of first-generation molecular signatures*

While many molecular signatures have been reported in the literature, there is little overlap of genes that make up these signatures (Haibe-Kains et al., 2008). Prat *et. al.* compared the concordance of six signatures in their recurrence prediction performance (Prat et al., 2012). All six signatures were strongly prognostic in node-negative patients. Furthermore, in this patient subset, all of the signatures were also able to identify patients with very favourable prognosis with 88-96% relapse-free at 5- and 8.5 years post-diagnosis. In contrast, in node-positive patients, the prognostic performance of most signatures was limited. Moreover, none of the signatures analysed could identify node-positive patients with 90% distant relapse-free survival following adjuvant tamoxifen treatment. If all six signatures had similar prognostic performance, could it be driven by a common underlying biological process?

1.3.3.2 *Proliferation as a key hallmark of prognostic signatures*

To investigate the question above, Wirapati *et. al.* conducted a meta-analysis of published prognostic signatures, and demonstrated that proliferation was the driving force of many prognostic signatures (Wirapati et al., 2008).

First, they mined a large multi-platform gene expression dataset and found 524 genes that were significantly associated with outcome. Of these, 71% were highly coexpressed with *AURKA* - a kinase involved in mitosis - while 26% were coexpressed with *ESR1* and 2% coexpressed with *HER2*. Therefore, these findings suggest that in their dataset, most genes associated with outcome were correlated with proliferation. Additionally, when analysing individual signatures, the authors found that many of the genes were also strongly correlated with proliferation, but not with *ESR1* and *HER2*. Furthermore,

when the signatures were divided into proliferative and non-proliferative constituents, overall prognostic performance was not affected using only proliferation-associated genes. In contrast, when only non-proliferation genes were applied, the prognostic performance of the signatures decreased. These findings were supported by the work of Desmedt *et. al.*, who demonstrated proliferation to be the strongest prognostic factor in ER+/HER2- tumours (Desmedt et al., 2008). Taken together, these findings suggests that most of the prognostic performance of molecular signatures are driven by genes involved in proliferation.

In a seminal study by Venet *et. al.*, the authors demonstrated that adjusting for the proliferating cell nuclear antigen (PCNA) metagene - which comprises of the top 1% of genes positively correlated with PCNA in 47 published signatures - resulted in a dramatic drop in association with outcome in multiple breast cancer datasets (Venet, Dumont, and Detours, 2011). This study also reported that several signatures of no biological significance in breast cancer, such as a signature associated with social defeat in mice, had significant prognostic performance. Taken together, the implications of the findings from Wirapati *et. al.*, Desmedt *et. al.* and Venet *et. al.* are threefold; (i) many signatures invariably contain proliferation-associated genes; (ii) established signatures may consist of genes that weaken their prognostic performance; and (iii) random signatures, by virtue of correlation with proliferation, may be significantly associated with outcome in breast cancer patients.

1.3.3.3 *Biology-driven signatures*

Another critical shortcoming of first-generation gene signatures is that they are not informative with regards to the *pathways* and *processes* driving the disease (Yao et al., 2012). As mentioned above, proliferation/cell-cycle associated genes are components of many signatures. Since proliferation is strongly prognostic in ER-positive, but not ER-

negative disease, many of these signatures are therefore prognostic only in ER-positive tumours (Weigelt and Reis-Filho, 2009). However, is it surprising that many published gene signatures from tumours identify features that are correlated with proliferation? The more pertinent question should be: can one identify pathway enrichments in these features that could be targeted clinically?

There are two implications for biology-driven signatures. Firstly, it extends the current appreciation of tumour biology by identifying clinically significant networks that have yet to be reported. Secondly, pathways corresponding to these biology-driven signatures may then be targeted for with approved drugs, or initiate the development of novel agents that could improve patient prognosis.

1.4 Metabolic reprogramming as a key feature in cancer biology

The transformation of a cell from one that complies with homeostatic decrees to a rogue entity involve alterations in cellular processes, including metabolism. Indeed, in a follow up to their first perspective, Hanahan and Weinberg considered altered cellular energetics as an emerging hallmark of cancer (Hanahan and Weinberg, 2011). The nomination of altered metabolism as a tenet of cancer biology is not unexpected, as proliferating cells require energy and biomass to synthesise DNA, proteins and lipids. Cultures of mouse fibroblast cells revealed that the energetic requirements for the genesis of a new cell is approximately 50% higher (assuming glucose as the primary substrate) than that required for homeostatic needs (Kilburn, Lilly, and Webb, 1969). What this suggests, then, is that the accumulation of biomass to synthesise an entire daughter cell - or the doubling of one cell - is more likely to be limiting than the energetic status *per se*. But how are these lofty energetic and anabolic requirements met by a proliferating cell? How

do oncogenic and tumour suppressive pathways orchestrate these metabolic rewiring to influence disease progression and prognosis? The sections below introduces the early in-roads made in cancer metabolism in the early-mid 20th century, and then review the questions above in light of the literature.

1.4.1 A brief history of cancer metabolism

Altered cellular energetics is an emerging hallmark of cancer. Tumours - a perverse, corporeal microcosm of its host - are highly dependent on internal and external sources of nutrients to fuel their rampant growth. The insatiable proliferation of cancer cells demands adequate supply of molecules to meet energetic, anabolic and redox requirements. This link between proliferation and enhanced glycolysis in cancer was first observed by a German physiologist by the name of Otto Warburg, who noticed that rat liver cancer cells do *not* take up more oxygen than normal liver tissue, but instead, produce lactic acid in the presence of oxygen (Koppenol et al., 2011). This somewhat contradicts the Pasteur effect, which states that cells stop fermenting in the presence of oxygen. The increased lactic acid generation was also observed in throat, intestine, skin, penis and nose carcinomas (Koppenol et al., 2011). Seigo Minami, an academic guest at Warburg's Kaiser Wilhelm Institute, observed that while the respiration of rat liver carcinoma cells was approximately one-fifth less than normal tissues, the cancer cells metabolised glucose an order of magnitude higher than could be accounted for by mitochondrial respiration (Minami, 1923). Warburg followed up Minami's finding by showing that cancer cells produce 100 fold more lactic acid than normal tissues (Koppenol et al., 2011).

Cori and Cori reported that *in vivo*, the levels of lactic acid produced by mouse and rat tumours were substantially lower than those reported by Warburg (Koppenol et al., 2011). Venous blood exiting a Rous sarcoma tumour implanted in one wing of a chicken had higher lactic acid and lower glucose concentrations, compared to venous blood of

the other normal wing (Koppenol et al., 2011). This is likely explained by removal of the lactic acid by fresh blood supply to the tumour. Furthermore, Warburg and colleagues also showed that in venous blood of sarcoma transplanted into the stomach, the concentration of glucose was up to 70% lower compared to arterial blood supply the tumour (Koppenol et al., 2011). In contrast, the glucose concentration from the veins of the control organs was 18% lower than the arterial blood. Additionally, lactic acid concentrations between arterial and venous blood from the tumour suggests that approximately two-thirds of glucose is metabolised to lactic acid. Taken together, these findings strongly suggests increased consumption of glucose by the tumour, compared to normal tissues.

If oxygen was not able to suppress lactic acid production and promote respiration in cancer cells, does that indicate some form of mitochondrial dysfunction in these cells? Indeed, Warburg reasoned that impaired or defective mitochondrial function *caused* the increased glycosis and lactic acid generation in tumours (Koppenol et al., 2011). This was rebutted by Sidney Weinhouse, who demonstrated, alongside work from Chance *et. al.*, that cancer had normal functioning mitochondria, and are not the root of the enhanced lactic acid generation (Weinhouse, 1956, Koppenol et al., 2011). Even if Weinhouse was right then, as we know he is to a large extent today, Weinhouse had a minor hurdle to overcome: he was up against the reputation of a Nobel Prize winner in Warburg (ironically awarded for the discovery of cytochrome *c* oxidase, an essential component of mitochondrial respiration), and some of Warburg's contemporaries, including Dean Burke, one of the duo that derived the Lineweaver-Burke equation to study enzyme kinetics.

Studies conducted over the past 50-60 years have contributed a body of knowledge of cancer cell metabolism, and the sections below will review key metabolic pathways im-

plicated in disease initiation and progression.

1.4.2 *Why do cancer cells have a sweet tooth?*

As mentioned earlier, cancer cells have high glucose consumption. However, the metabolism of glucose is an inefficient source of ATP (two molecules of ATP per molecule of glucose), compared to the complete mitochondrial oxidation of pyruvate, which generates 36 molecules of ATP. Surely, then, this would be a bottleneck for rapid cell doubling? Rather, computational modelling by Pfeiffer *et. al.* suggests that assuming the supply of glucose - the most abundant nutrient in the human circulation - is not limited, then high *rates* of glycolysis is sufficient for a thriving cellular population (Pfeiffer, Schuster, and Bonhoeffer, 2001; Hay, 2016). If this is so, what other purpose could increased glycolytic flux serve for a proliferating cell?

1.4.2.1 *Glycolysis is not the main source of ATP during proliferation*

Glycolysis is not the major producer of ATP in the majority of cancer cells - oxygen consumption (surrogate of *oxidative* ATP production) and lactate secretion (surrogate of *glycolytic* ATP production) analysis in a panel of cancer cell lines and tumour tissues indicate that on average, 17% of ATP is derived from glycolysis (Zu and Guppy, 2004). Furthermore, estimates suggest that ATP is not likely to be limiting for macromolecule synthesis to generate a new cell (Kilburn, Lilly, and Webb, 1969). In fact, ATP consumption is vital for key rate-limiting glycolytic reactions that are inhibited by a high ATP:ADP ratio (Lunt and Vander Heiden, 2011). For example, phosphofructokinase catalyses a committed step in glycolysis, and is sensitive to the ATP:ADP ratio.

1.4.2.2 *Glycolytic intermediates are important building blocks of macromolecules*

Proliferating cells require precursors to synthesise macromolecules such as nucleotides and different lipid species. An overview of this pathway is provided in Fig 1.3. Each pyrimidine and purine nucleotide comprises 9 and 10 carbon atoms respectively, half of which are derived from a downstream intermediate of ribose-5-phosphate (R5P). R5P is generated from glucose-6-phosphate through the non-oxidative arm, or through the oxidative arm via fructose-6-phosphate or glyceraldehyde-3-phosphate of the pentose phosphate pathway. In mouse lymphocytes stimulated with mitogen, an exponential increase in lactate was observed 50 hours post-stimulation, and the decrease in lactate release mirrored the decreased thymidine incorporation into DNA (Wang, Marquardt, and Foker, 1976). In support of this finding, increasing glucose concentration in rat thymocytes stimulated with mitogen also resulted in enhanced thymidine incorporation (Hume et al., 1978). Additionally, activity of glycolytic enzymes, lactate acid generation and DNA synthesis peaked during the S phase of the cell cycle (Marjanovic, Wielburski, and Nelson, 1988). Taken together, these findings suggest an important role for glycolysis is to generate nucleotides required for DNA replication.

Glycolysis also generates important precursors for various lipid species required for cellular growth (Fig 1.3). Levels of glycerol and glycerol-3-phosphate (G3P) were increased in human peripheral lymphocytes in response to mitogen stimulation (Lunt and Vander Heiden, 2011). Dihydroxyacetone phosphate (DHAP) - the product from the fourth glycolytic reaction and a precursor of glycerol-3-phosphate - is necessary for the biosynthesis of phospholipids and triacylglycerol, which are important structural lipids in cell membranes (Lunt and Vander Heiden, 2011). DHAP is also a precursor for cardiolipin, a component of mitochondrial membrane. Another glycolytic intermediate - 3-phosphoglycerate - is the precursor for sphingolipids, which serve as membrane com-

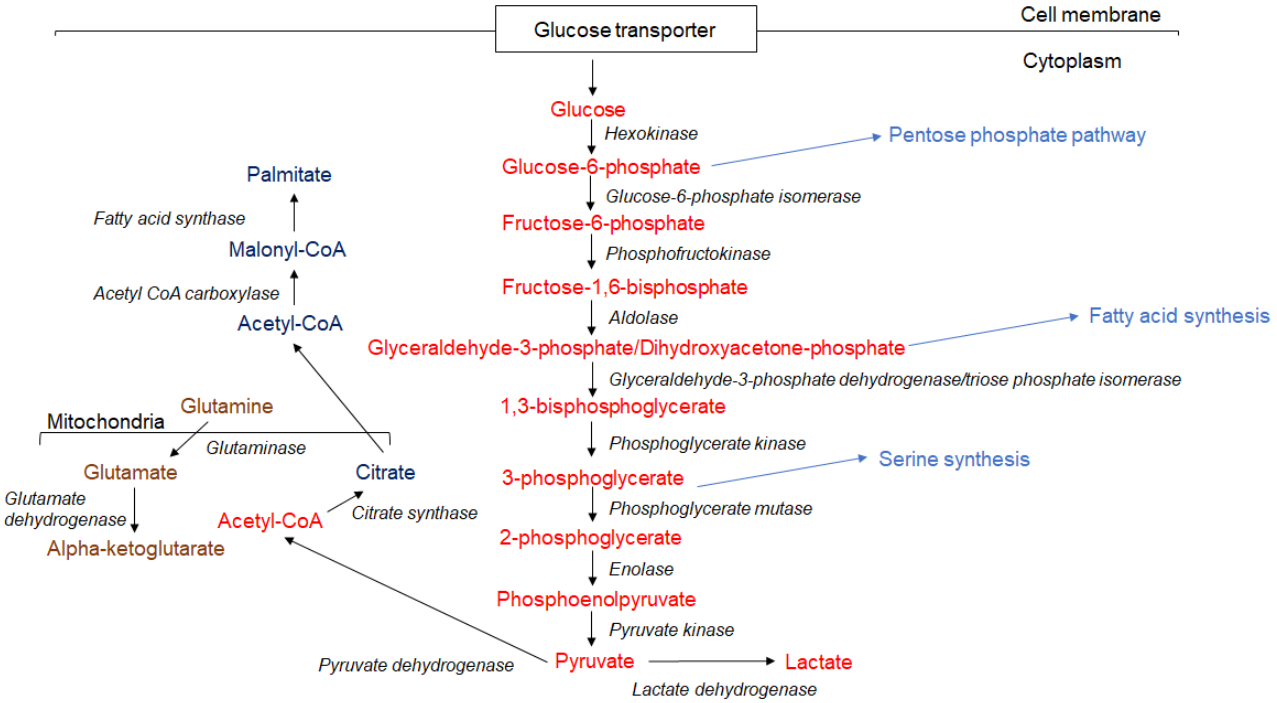

Figure 1.3: Brief schematic of glycolysis, glutamine oxidation and fatty acid synthesis pathways. Substrates for the pathways are indicated in red (glycolysis), navy blue (glutamine oxidation) and brown (fatty acid synthesis) and pathways that various intermediates can feed into are indicated in blue. Enzymes catalysing each reaction are italicised. Figure adapted from Hay, 2016,Altman, Stine, and Dang, 2016, and Rohrig and Schulze, 2016.

ponents and in cell signalling (Lunt and Vander Heiden, 2011).

Amino acids constitute a large proportion of cell mass in a proliferating cell, and therefore, would be in large demand prior to cell division (Hosios et al., 2016). Synthesis of some non-essential amino acids uses glycolytic precursors. 3-phosphoglycerate provides carbons required for cysteine, glycine and serine synthesis, while pyruvate supplies alanine synthesis. Apart from cell mass requirements, serine is also essential in folic acid metabolism, NADPH generation, phosphatidylserine synthesis and is the precursor of ethanolamine, and choline, as well as other phospholipid head group molecules (Yang and Vousden, 2016).

1.4.3 Glutamine metabolism

The second most commonly consumed substrate in proliferating cells is the amino acid glutamine (DeBerardinis and Cheng, 2010) (Fig 1.3, highlighted in brown). Glutamine is the most abundant non-essential amino acid and constitutes approximately one-fifth of free amino acids in the human circulation, and 40% in muscle (Mayers and Vander Heiden, 2015; Bergstrom et al., 1974). As such, glutamine can be a convenient source of carbon and nitrogen atoms to meet the energetics and biosynthetic needs for proliferating and cancer cells. Glutamine is transported into cells via the SLC1A5 transporter, and is converted by mitochondrial glutaminase into glutamate and an ammonium ion. There are two isoforms of glutaminase: the kidney type (GLS) and liver-type (GLS2). *GLS* is expressed in a broader range of tissues and is more relevant in several cancers, compared to *GLS2*, whose expression is restricted to the liver, brain, pituitary gland and pancreas (Ardlie et al., 2015). The *GLS* mRNA can be alternatively spliced to generate glutamine C (GAC) or kidney-type glutaminase (KGA) isoforms. The expression and activity of GAC is higher than KGA, and is increased in several cancer types, which suggests that alternative splicing may be essential in the higher glutamine metabolism

observed in cancer cells (Heuvel et al., 2012; Jacque et al., 2015).

1.4.3.1 *Contribution of glutamine to cancer cell physiology*

Why are many cancers dependent on glutamine? Several lines of evidence suggest that glutamine provides precursors for a wide variety of metabolites required for cell division (Yang, Venneti, and Nagrath, 2017). The nitrogen derived from converting glutamate to alpha-ketoglutarate can be used to synthesise amino acids such as proline, alanine and aspartate. *In vitro*, tracer analysis suggests that at least 50% of non-essential amino acids used for protein synthesis can be derived from glutamine (Alberghina and Gaglio, 2014).

Since most of the pyruvate from glycolysis is converted to lactate, this decreases the fraction of citrate generated from acetyl CoA via pyruvate dehydrogenase. Glutamine metabolism can provide an alternative source of citrate via reductive carboxylation of alpha-ketoglutarate to citrate (Metallo et al., 2011). The citrate molecule is then exported out of the mitochondria into the cytosol, where it is cleaved to generate acetyl CoA as a precursor for lipid synthesis, and oxaloacetate. This reaction is particularly prevalent in hypoxic cancer cells, or in tumours with constitutive hypoxia inducible factor (HIF) 1A activity (Gameiro et al., 2013; Wise et al., 2011; Metallo et al., 2011).

The *de novo* synthesis of nucleotides also utilises nitrogen atoms from glutamine. Cancer cells that are deprived of glutamine undergo cell cycle arrest which can be rescued by exogenous nucleotides, but not citric acid cycle intermediates such as oxaloacetate (Gaglio et al., 2009). Furthermore, aspartate derived from transamination of glutamate is an important carbon source for purine and pyrimidine synthesis, and aspartate supplementation can rescue cell cycle arrest due to glutamine deprivation (Patel et al., 2016;

Sullivan et al., 2015; Birsoy et al., 2015).

1.4.4 Fatty acid metabolism

Rapid cell division in cancer cells requires fatty acids for synthesis of organelle and cell membranes, as well as generation of lipid signalling molecules. The cell membrane is composed primarily of phospholipids such as phosphatidylethanolamine, phosphatidylcholine, and other lipids including sterols and lysophospholipid. As compared to normal cells that prefer to utilise exogenous fatty acid, tumours often engage the fatty acid synthesis pathway and generate lipids *de novo* (Rohrig and Schulze, 2016).

Fatty acid synthesis is catalysed by a series of enzymes whose expression is regulated by the sterol response element binding protein (SREBP) family of transcription factors (Horton, 2002) (brief schematic of fatty acid synthesis in Fig 1.3, highlighted in navy blue). Fatty acid synthesis is a reductive process and requires large amounts of NADPH, and SREBP regulates expression of genes that regenerate NADPH such as the oxidative arm of the pentose phosphate pathway, malic enzymes, and isocitrate dehydrogenases (Shimano et al., 1999; Shechter et al., 2003).

1.4.4.1 *What is the role of fatty acid synthesis in cancer cells?*

What are the fates of the lipids generated *de novo* by cancer cells? As mentioned earlier, proliferating cells require fatty acids for membrane assembly. The enzyme ATP-citrate lyase (ACLY), cleaves citrate to oxaloacetate and acetyl CoA; the latter being the starting point for fatty acid synthesis (Zaidi, Swinnen, and Smans, 2012). Additionally, inhibition of ACLY disrupted cell growth of immortalised haemotopoietic stem cells stimulated with growth factor (Hatzivassiliou et al., 2005).

Cardiolipins (CL) are structural phospholipids that are primarily localised to the inner mitochondrial membrane, and regulate mitochondrial respiration and signalling during apoptosis induction (Claypool and Koehler, 2012). CLs have four acyl chains that are constantly remodelled through the activity of phospholipases and acyltransferases, and hence are sensitive to alterations in cellular fatty acid composition (Chicco and Sparagna, 2007). The function of CL in the inner mitochondrial membrane, in particular, to bind cytochrome *c* - which is involved in electron transfer from complex III to complex IV - is dependent on the length and saturation of the CL acyl chains (Schug and Gottlieb, 2009). Hence, alterations in fatty acid composition can directly affect cellular bioenergetics. For example, the CL profile of mouse brain tumours were substantially different compared to normal tissue, and was correlated with impaired activity of enzymes involved in the electron transport chain (Kiebish et al., 2008).

Some signalling proteins require post-translational modification such as acylation for their function. Hence, the function of such proteins may be affected by the abundance and saturation levels of different cellular lipid species. The WNT proteins, which activate a signalling cascade that is frequently deregulated in cancer, are modified through attachment of a palmitoleoyl chain (Nile and Hannoush, 2016). Inhibition of the enzyme that catalyses this reaction - *O*-acyltransferase porcupine - effectively blocked growth of cancers that are dependent on WNT (Proffitt et al., 2013; Liu et al., 2013).

Fatty acids are also precursors of lipid signalling molecules, such as sphingosine-1-phosphate (S1P) and lysophosphatidic acid (LPA), which regulate inflammation, migration and survival (Wymann and Schneiter, 2008; Pyne and Pyne, 2010). LPA can induce proliferation, migration, inflammation and angiogenesis via autocrine and paracine signalling that involves endothelial, immune and cancer cells (Park et al., 2012). Fatty acids also have a role in synthesis of lipid second messengers such as inositol-1,4,5-triphosphate and phospatidylinositol triphosphate (Griner and Kazanietz, 2007). These

signalling lipids are derived from membrane phospholipids, which are actively remodelled and synthesised, and hence their composition is strongly correlated with cellular fatty acid availability.

Activation of *de novo* fatty acid synthesis shifts the saturation levels of membrane lipids towards saturated and monounsaturated species, and a reduction of dietary polyunsaturated species (Hilvo et al., 2011). This serves to protect cells from peroxidation of polyunsaturated lipids due to ROS generation (Rysman et al., 2010). Nonetheless lipid peroxidation has a role in the synthesis of eicosanoids such as prostaglandins, leukotrienes, and thromboxanes, which are derived from polyunsaturated fatty acids. Eicosanoids have diverse roles in tumourigenesis from modulating inflammation and immune response to remodelling the tumour microenvironment (Wang and Dubois, 2010).

1.4.4.2 *Fatty acid oxidation in cancer*

Compared to other metabolic pathways such as glycolysis and glutamine metabolism, the relevance of fatty acid oxidation in cancer is less understood (Carracedo, Cantley, and Pandolfi, 2013). However, in the past few years, several reports have began to unravel the role of fatty acid oxidation in different cancers. The subsections below will briefly introduce the fatty acid oxidation pathway, before mentioning key literature regarding this metabolic pathway in cancer.

1.4.4.2.1 Fatty acid uptake and activation Fatty acid oxidation occurs primarily in the mitochondria, although other it can also occur in the peroxisomes and microsomes. Several transport and modification of fatty acids are required prior to being oxidised in the mitochondrial matrix. A brief schematic of this pathway is provided in Fig 1.4. Cellular uptake of long- and very long chain fatty acids is facilitated by fatty acid transport proteins (FATP). Long chain acyl-CoA synthetase (ACSL) or FATP, which also

has acyl-CoA synthetase activity, converts fatty acids in acyl-CoA, thereby activating the fatty acid molecule for oxidation.

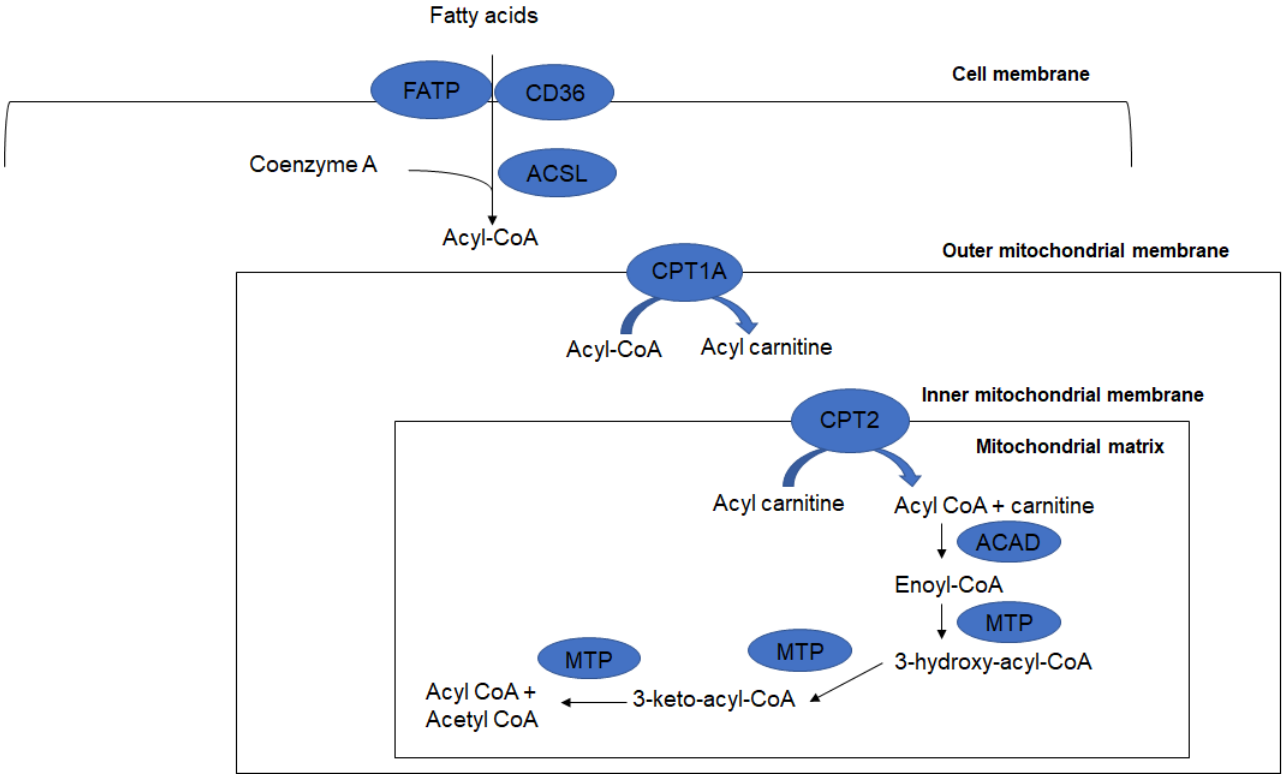

Figure 1.4: Key steps in the fatty acid beta oxidation pathway. Upon uptake into the cell via CD36/FATP, fatty acids are activated to form acyl-CoA in the cytosol. CPT1 then attaches a carnitine group to acyl-CoA to generate acyl-carnitine, which is then transported through the intermembrane space into the mitochondrial matrix, where it is dissociated into acyl-CoA and carnitine by CPT2. Acyl-CoAs are first metabolised by ACAD with different length specificities (very long chain ACAD (VLCAD) C14-C18; medium chain ACAD (MCAD) C6-C12; and short chain ACAD (SCAD) C4). The next step is catalysed by the mitochondrial trifunction protein (MTP) which has hydratase, hydroxyacyl-CoA-dehydrogenase, and thiolase activity, which generates an acetyl-CoA molecule and acyl-CoA two carbons shorter after each oxidation cycle. Figure adapted from Houten and Wanders, 2010.

1.4.4.2.2 Carnitine shuttle While fatty acid oxidation occurs in the mitochondrial matrix, the mitochondrial membrane, however, is impermeable to acyl-CoAs. The import of acyl-CoA into the mitochondria is facilitated by the carnitine shuttle. Acyl-CoA

is first converted to acylcarnitine by carnitine palmitoyl transferase 1 (CPT1), located on the outer mitochondrial membrane. The acylcarnitine molecule is then transported into the mitochondrial matrix through the mitochondrial intermembrane space. In the mitochondrial matrix, CPT2 - located in the inner mitochondrial membrane - dissociates acylcarnitine to acyl-CoA and carnitine molecules again.

1.4.4.2.3 Beta oxidation of acyl-CoA In the mitochondrial matrix, acyl-CoA is oxidised through a cycle of four reactions to generate acetyl-CoA and the reducing equivalents FADH and NADH. Briefly, in the first reaction, the acyl CoA is dehydrogenated by acyl CoA dehydrogenase (ACAD) to generate trans-2-enoyl-CoA. The resulting double bond is then hydrated by enoyl-CoA hydratase, generating 3-hydroxyacyl-CoA, before it dehydrogenation to yield 3-keto-acyl-CoA. In the final step, thiolytic cleavage of 3-keto-acyl-CoA generates an acyl-CoA that is shortened by two carbons, and an acetyl-CoA molecule. The acetyl-CoA then enters the citric acid cycle where it is oxidised further to generate reducing equivalents, which is eventually oxidised in the electron transport chain to generate ATP.

1.4.4.3 Fatty acid oxidation in cancer

At the time this thesis was written, analysis of the literature suggests a contentious role of fatty acid oxidation in cancer (Carracedo, Cantley, and Pandolfi, 2013). In two different studies, fatty acid oxidation was found to be important for cancer cell survival, but in different contexts. Schafer *et. al.* demonstrated that loss of attachment of MCF10A mammary epithelial cells resulted in decreased ATP generation due to decreased glucose uptake, as well as generation of reactive oxygen species, which suppressed fatty acid oxidation (Schafer et al., 2009). Antioxidant supplementation activated fatty acid oxidation, which resulted in increased ATP generation, without increased glucose uptake. In breast cancer, Carracedo *et. al.* demonstrated a role for the putative tumour

suppressor promyelocytic leukemia (PML) protein in activating fatty acid oxidation via peroxisome proliferator activated receptor (PPAR) signalling and showed this prevented anoikis - cell death through loss of attachment (Carracedo et al., 2012). PML expression was expressed highly in ER-negative breast cancer, and was associated with poorer patient survival. Hence, the authors concluded that targeting both PML and fatty acid oxidation in advanced ER-negative tumours may confer clinical benefits in this disease subset. Treatment of MDA-MB231 breast cancer cell line with unsaturated fatty acid promoted its proliferation; but saturated fatty acid treatment resulted in apoptotic cell death. Additionally, cell death was exacerbated when cells were treated etomoxir - a CPT1A inhibitor - likely due to accumulation of fatty acids. Furthermore, Padanad *et. al.* show that *KRAS* mutant lung cancer promotes the activity of ACSL3, which increase synthesis of acyl-CoA for fatty acid oxidation. Blocking ACSL3 activity resulted in depletion of ATP and death of lung cancer cells (Padanad et al., 2016).

Metabolomics performed on a mouse model of inducible MYC-overexpression ER-negative breast tumour found increased levels of fatty acid oxidation intermediates, such as acylcarnitines - the product of the rate-limiting step in fatty acid oxidation, compared to basal MYC expression control (Camarda et al., 2016). Furthermore, the expression of the majority of genes from a fatty acid metabolism geneset was downregulated in ER-negative, compared to ER-positive tumours from the TCGA cohort. However, the expression of *PPARGC1A* - a key regulator of fatty acid oxidation - was upregulated in ER-negative, compared to ER-positive tumours. Based on this, the authors concluded that ER-negative tumours have higher fatty acid oxidation activity, although it was not entirely evident from their PCG1A immunoblot on a panel of breast cancer cell lines that expression of this protein correlated with ER status (Camarda et al., 2016).

On the other hand, activation of fatty acid oxidation has been shown to be detrimental in different cancer cell systems. Treatment of selected lung and breast cancer cell

lines with pioglitazone - an agonist of the nuclear receptor PPARG - increased fatty acid oxidation and induced cell cycle arrest (Srivastava et al., 2014). In conducting a bioinformatics screen, Torrano *et. al.* reported that increased expression of peroxisome proliferator gamma coactivator 1A (PGC1A) in prostate tumours was associated with good prognosis (Torrano et al., 2016). Importantly, overexpression of PGC1A in PC3 prostate cancer cell line increased fatty acid oxidation flux, and decreased the proliferation rate and colony formation of cells. Taken together, the literature suggests that the role of fatty acid oxidation in cancer is conflicting, and merits further investigation.

1.4.5 Oncogene and tumour suppressor activity, signalling pathways and cancer metabolism

Since genetic aberrations drive tumourigenesis, do these mutations also influence the metabolism necessary to meet the demand of rapidly proliferating cells?

1.4.5.1 *Oncogenes and tumour suppressors associated with cancer metabolism*

One of the earliest pieces of evidence that oncogenes regulate tumour metabolism was the observation that the transcription factor MYC activates glycolysis via upregulating the expression of *LDHA* and most glycolytic enzymes (Shim et al., 1997; Osthus et al., 2000). MYC also has a role in the transcriptional activation of genes involved in mitochondrial biogenesis and glutamine metabolism (Li et al., 2005; Wise et al., 2008). In line with its role in supporting the metabolic requirements of cell proliferation, MYC regulates the synthesis of nucleotides and lipids required for cell division (Vazquez, Markert, and Oltvai, 2011; Morrish et al., 2010).

The PI3K-Akt-mTOR signalling axis is one of the most commonly activated pathways in cancer (Liu et al., 2009). Increased AKT activity recruits glucose transporters to the

cell surface, and enhances hexokinase 2 and phosphofructokinase 1, two of the three enzymes that catalyse committed steps in glycolysis (Hay, 2016). The negative regulator of the PI3K pathway - the phosphatase PTEN - also has roles in cancer metabolism. Loss of PTEN activates glycolysis in leukemia cells, while increased PTEN expression in mice was found to shift cellular metabolism from glycolysis to mitochondrial respiration (Tandon et al., 2011; Garcia-Cao et al., 2012). The mammalian target of rapamycin (mTOR) protein - a serine/threonine kinase downstream component of PI3K signalling - activates anabolic pathways. mTOR regulates HIF1A and SREBP1 to activate glycolysis and the pentose phosphate, and lipid synthesis pathway (Duvel et al., 2010).

The HIF1 and HIF2 complexes are transcription factors that facilitate the molecular response to low oxygen conditions (Nakazawa, Keith, and Simon, 2016; Schofield and Ratcliffe, 2004). These complexes consist of HIFα and HIF1β subunits, which are stabilised during hypoxia. Under normal oxygen tension, the HIFα subunits are hydroxylated in an oxygen-dependent manner, which is recognised by the E3 ligase von Hippel-Lindau (VHL) for proteosomal degradation (Schofield and Ratcliffe, 2004). In cancer, the HIF complex can be activated by hypoxia, mutations in VHL, succinate dehydrogenase, fumarate hydratase, and PI3K signalling (Nakazawa, Keith, and Simon, 2016). Upon stabilisation, HIF1 transcriptionally activates a retinue of genes, including glucose transporters and the majority of glycolytic enzymes (Schofield and Ratcliffe, 2004). HIF1 also activates the pyruvate dehydrogenase kinase, which phosphorylates and inactivates the pyruvate dehydrogenase complex, thereby uncoupling glycolysis from mitochondrial metabolism (Nakazawa, Keith, and Simon, 2016).

1.4.5.2 *Wnt and MAPK signalling pathways and cancer metabolism*

Two of the most frequently activated oncogenic signalling pathways in cancer are the mitogen activated protein kinase (MAPK) and the Wnt signalling cascades (Burotto

et al., 2014; Polakis, 2012).

Adenomatous polyposis coli (*APC*) inactivation occurs in approximately 80% of colorectal tumours (Muzny et al., 2012a). *APC* is a cardinal regulator of the Wnt signalling pathway by forming a multi-protein complex with Axin, casein kinase 1 and glycogen synthase kinase-3β to sequentially phosphorylate and ubiquitinate β-catenin for proteosomal degradation (Duchartre, Kim, and Kahn, 2016). Furthermore, gain-of-function mutations in *CTNNB1* and *TCF4* have been reported in colorectal cancers without *APC* inactivation, which suggests a positive selection for Wnt signalling activity in this tumour type (Fukushima et al., 2001). Activation of Wnt signalling has been shown to result in the Warburg effect in colorectal cancer cells and osteoblasts (Esen et al., 2013; Pate et al., 2014). Additionally, expression of monocarboxylate transporter 1, which catalyses lactate efflux, was decreased in response to dominant-negative lymphoid enhancer binding factor 1 (LEF1) expression in two colorectal cancer cell lines (Sprowl-Tanio et al., 2016).

The RAS-RAF-MEK/ERK signalling axis is frequently activated across several cancers (Roberts and Der, 2007). This is due to abberant activation of receptor tyrosine kinases or gain-of-function mutations in downstream components of this pathway. Oncogenic mutations in the *RAS* genes are common in several cancers: *KRAS* mutations occur in colon, pancreatic and lung cancers; *NRAS* mutations in melanoma and acute lymphoblastic leukaemia; and *HRAS* mutations have been observed in bladder- and head and neck cancers (Muzny et al., 2012a; Hammerman et al., 2012; Hodis et al., 2012; Neri et al., 1988; Guo et al., 2013; Agrawal et al., 2011; Bailey et al., 2016).

Oncogenic mutations in *RAS* and *BRAF* can alter cellular metabolism (Gaglio et al., 2009; Chiaradonna et al., 2006; Ying et al., 2012; Parmenter et al., 2014; Haq et al., 2013). Mouse fibroblasts transformed with RAS exhibit enhanced glycolysis and glu-

taminolysis, and culture of the transformed fibroblasts or MDA-MB231 breast cancer cells in 1 mM glucose dramatically reduced proliferation compared to 25 mM glucose (Gaglio et al., 2009; Chiaradonna et al., 2006). In pancreatic ductal adenocarcinoma, KRAS G12D promotes glucose uptake to generate intermediates for the hexosamine biosynthesis pathway and reducing equivalents for redox homeostasis (Ying et al., 2012). *KRAS* mutation in colorectal cancer cell lines and tumour tissues was associated with increased uptake of aspartate and conversion to asparagine (Toda et al., 2016). This was achieved via increased asparagine synthetase expression, through KRAS activation of PI3K-Akt signalling. Treatment of BRAF V600E mutant melanoma cell lines with vemurafenib decreased glucose uptake and lactate production, and increased oxidative phosphorylation (Parmenter et al., 2014; Haq et al., 2013).

Staying within the theme of BRAF V600E-induced rewiring of metabolism, vemurafenib treatment of BRAF-mutant melanoma cell lines resulted in increased oxidative metabolism via activation of PGC1A (Haq et al., 2013). Expression of PGC1A, is in turn, positively regulated by the micropthalmia associated transcription factor (MITF)(Haq et al., 2013). The transcription factor MITF is pertinent in normal melanocyte development and melanomagenesis (Garraway et al., 2005). MITF protein expression is exquisitely regulated, and a rheostat model has been proposed to reconcile MITF expression and the multifarious fates associated, ranging from melanoma cell cycle arrest and senescence (low), invasiveness (low to intermediate) and proliferation (intermediate) to differentiation of melanocytes (high) (Wellbrock et al., 2008; Goding, 2011). However, the metabolic correlates of different MITF expression levels is poorly understood.

1.4.6 Metabolic features associated with epithelial-to-mesenchymal transition and cellular differentiation

Epithelial-to-mesenchymal transition (EMT) is a transdifferentiation process during which cancer cells lose cell-to-cell adhesion, adopt a mesenchymal phenotype, and acquire migratory and invasive properties to metastasise (Nieto et al., 2016). In breast and cervical tumours, acquisition of mesenchymal properties is associated with aggressiveness, and disease progression and survival (Imani et al., 2016; Rojas-Puentes et al., 2016). EMT induction in human mammary epithelial cells induced expression of stem cell markers, and culture of stem-like mammary cells formed mammospheres, a property of mammary stem cells, and expressed similar markers of mammary epithelial cells that have undergone EMT (Mani et al., 2008). Additionally, a subpopulation of CD44high/CD24low cells - markers of cancer stem cells, albeit controversially - from oral cancer cell lines not only express stem-related proteins (SOX2, NANOG, OCT4), but also exhibit EMT characteristics such as decreased expression of CDH1, and increased expression of VIM (Ghuwalewala et al., 2016).

1.4.6.1 EMT and metabolism

Because of the role of EMT in cancer dissemination, understanding its metabolic alterations during this process may help delay metastasis, and reduce distant recurrence rates.

1.4.6.1.1 ***Glycolysis and EMT*** Several enzymes in glycolysis have been implicated in EMT: breast cancer stem cells have increased HK2 expression, and treatment with 2-deoxyglucose resulted in a dose-dependent inhibition of the stem cells undergoing EMT (Bacci et al., 2016). Overexpression of phosphoglucoisomerase in breast cancer cells results in EMT via activation of nuclear factor kappa B, increased expression of several EMT transcription factors and downregulation of miR-200, resulting in

decreased E-cadherin expression (Ahmad et al., 2011). Upregulation of aldolase A in lung squamous carcinoma cells induced migration and EMT via decreased E-cadherin expression and increased vimentin and fibronectin expression, while silencing of enolase in a non-small cell lung cancer cell line disrupted EMT induction (Du et al., 2014; Fu et al., 2015). The preferred PKM2 isoform in cancer, and transforming growth factor beta-induced EMT in the SW480 colorectal cell line resulted in nuclear translocation of PKM2 to form a complex with homeobox 2, to effect epigenetic changes and down regulate E-cadherin expression (Hamabe et al., 2014).

In MCF7 cells, overexpression of the transcription factor distal-less homeobox 2 resulted in increased glycolysis, glutamine metabolism and EMT induction (Lee et al., 2015; Lee et al., 2016). Genetic or pharmacologic inhibition of *GLS1* abrogated EMT induced by Dlx2 expression, transforming growth factor beta, Wnt3 and Snail1 (Lee et al., 2016). Furthermore, knockdown of *GDH* in LoVo and SW480 cells resulted in decreased expression of ZEB1 and vimentin, while expression of E-cadherin was increased (Liu et al., 2013).

1.4.6.1.2 ***Fatty acid metabolism and EMT*** Substantial effort in characterising the role of fatty acid metabolism in EMT focused mainly on the anabolic aspect. Lipidomics performed on DU145 prostate cancer cells treated with tumour necrosis factor alpha to induce EMT revealed increased fatty acid synthase (FASN) expression and triacylglycerol synthesis (Dalmau et al., 2015). Further supporting the role of FASN in EMT, MCF7 cells treated with osthole - which suppresses FASN expression - inhibited EMT induction (Hung et al., 2011). Overexpression of acyl-CoA synthetase (ACSL) and stearoyl CoA desaturase (SCD) - enzymes that are involved in priming fatty acid synthesis and remodelling to unsaturated species, respectively - promoted EMT, while glycolysis and proliferation was not affected (Sanchez-Martinez et al., 2015a). Activation of AMPK - a master energy sensor of the cell which promotes catabolic and

represses anabolic reactions during energetic stress - reversed the EMT phenotype in response to transgenic expression of ACSL and SCD (Sanchez-Martinez et al., 2015a). It is worthwhile mentioning that in A549 lung cancer cell line, knockdown of *FASN* induced EMT, and TGFβ treatment increased respiration (Jiang et al., 2015). This suggests that metabolic adaptations during EMT may be dependent on cell type and genetic background.

What does increased fatty acid synthesis and remodelling during EMT achieve? In a panel of breast cancer cell lines with knockdown expression of *CerS6*, which encodes ceramide synthase isoform 6, affected the fluidity of the cell membrane to promote cell migration (Edmond et al., 2015). In NMuMG murine mammary gland, HCV29 bladder cancer and MCF7 cell lines, inhibition of glycosphingolipid synthesis resulted in down regulation of E-cadherin, and increased expression of N-cadherin, fibronectin and vimentin, as well as adoption of fibroblastic morphology and enhanced motility (Guan, Handa, and Hakomori, 2009). TGFβ-induced EMT of HCV29 and NMuMG cell lines also resulted in similar decreases in several glycosphingolipid species. Supplementation with ganglioside M2 and ceramide Gg4, but not GM1 or GM3 prevented the EMT induction in all three cell lines. Indeed, a recent study by Tisza *et. al.* showed that reorganisation of the cell membrane constituents, with a particular involvement of lipid raft destabilisation (Tisza et al., 2016). This destabilisation was essential to maintain a stem cell phenotype and relay EMT-related signalling from the cell membrane. Exogenous supplementation with docosahexanoic acid, an omega 3 fatty acid, stabilised the lipid raft, and reduced migration and mammosphere formation. Taken together, these data suggest that increased fatty acid anabolism may have a role in providing substrate for remodelling lipid species to effect EMT.

As compared to fatty acid synthesis, lesser is known with regards to the role of fatty acid oxidation in EMT. Very recently, metabolomic analysis of the D492 breast epithe-

lial cells and its mesenchymal derivative - D492M - found that fatty acid oxidation was *increased* in the mesenchyme line, compared to its epithelial parental (Halldorsson et al., 2017). In this study, the mesenchyme line was generated from spontaneous EMT of D492 cells co-cultured three-dimensionally with endothelial cells. Importantly, the authors show that while fatty acid oxidation was increased in the mesenchymal line, the proliferation rate was *slower* compared to the epithelial parental line. This finding is particularly crucial, given that this thesis has reported a negative correlation between a fatty acid oxidation gene signature and tumour proliferation (details in Section 3.3.6, Table 3.5). Nevertheless, how different modalities of inducing EMT such as treatment with transforming growth factor beta (Xu, Lamouille, and Derynck, 2009), mutations in isocitrate dehydrogenase and fumarate hydratase (Grassian et al., 2012; Sciacovelli et al., 2016), in different cell systems, affect fatty acid oxidation remains unclear and requires investigation.

1.4.6.2 Stem cell differentiation and metabolism

Both stem cells and EMT share an underlying theme of cellular differentiation, and cellular *de*differentiation has been proposed as one facet of cancer (Harris, 2005). Furthermore, the transcriptional program that governs stem cell renewal and maintaining an undifferentiated state has been suggested to also be exploited in cancer (He, Nakada, and Morrison, 2009). As such, one may suggest that the metabolic proclivities in cancer are not only a reflection of rapid cell proliferation, but also maintenance of an undifferentiated state, compared to the cell of origin.

Several examples warrant this point: proliferating stem cell progenitors of the tadpole *Xenopus laevis* rely heavily of glycolysis for ATP, but differentiation into neurons results in increased mitochondrial respiration (Love et al., 2014). Importantly, this was not due to limited oxygen availability or respiratory defects, which suggests a cell-intrinsic

mechanism controlling differentiation and metabolism (Fiske and Vander Heiden, 2012; Agathocleous et al., 2012). Secondly, embryonic stem cells had higher unsaturated metabolites compared to differentiated cardiomyocytes and neurons, and inhibition of eicosanoid metabolism - which involves oxidation of unsaturated metabolites - *delayed* differentiation and maintained a pluripotent state (Yanes et al., 2010). Thirdly, nuclear reprogramming of mouse embryonic fibroblasts to a pluripotent state resulted in a shift from oxidative metabolism to glycolysis (Folmes et al., 2012). Inhibiting glycolysis with 2-deoxyglucose or bromopyruvate; or promoting oxidative metabolism via dichloroacetate *decreased* the reprogramming efficiency of the mouse embryonic fibroblasts to a pluripotent state.

1.4.6.2.1 Link between EMT-associated factors and mammary stem cell differentiation Mammary epithelial cell (MEC) differentiation is a step-wise, hierarchical process, starting from mammary stem cell to a bipotent progenitor, and then leading to either myoepithelial or luminal progenitors (Visvader and Stingl, 2014). The basal cells from the mammary stem population express EMT genes such as *SNAI2* and *TWIST1*; and knockout of *SNAI2* in this basal population led to expression of differentiated luminal cell markers such as GATA3 and ER. This suggests that *SNAI2* is essential to maintain a less differentiated basal stem cell population of mammary stem cells (Nassour et al., 2012). Importantly, studying mammary stem cells also provides a system to identify molecular processes that are relevant in both cellular differentiation and EMT.

1.4.7 Tumour microenvironment and metabolism

Thus far, most of this introduction focuses on the cell autonomous role of cancer metabolism. It is important to note that tumour metabolism may also be influenced by factors external to the tumour (i.e., tumour microenvironment). Two examples from the

literature support this point. Primary cultures established from lung tumours in mice showed increased lactate secretion from glycolysis, and greater glutamine anaplerosis, compared to the primary tumours they were derived from (Davidson et al., 2016). When these cultured cells were re-implanted into mouse lungs, the tumours exhibit metabolic features similar to the original tumour. Secondly, co-culture of breast cancer cells with adipocytes promote lipolysis and drives cancer cell proliferation and invasion (Balaban et al., 2017).

1.4.8 Prognostic association of cancer metabolic pathways

In breast cancer, prognosis is determined based on clinical factors such as ER status, tumour size, grade, and lymph node involvement. Apart from the association of some of these factors such as tumour grade with proliferation, in general, little can be gleaned about the biology of a tumour from these metrics. As mentioned earlier, many molecular gene signatures in breast cancer also inevitably capture mainly the proliferative component of tumours. While the central role of metabolism in tumour initiation and progression is recognised, little is known regarding the association of metabolic pathways opted by tumours and patient survival. Nonetheless, several studies have made early attempts to understand the metabolic dysregulation in primary breast tumours and its association with disease (Haider et al., 2016; Gaude and Frezza, 2016; Leoncikas et al., 2016), and two of them will be briefly discussed below.

Haider *et. al.* analysed mutation, mRNA and copy number data from over 6000 tumour-normal samples from 10 different cancer types and identified 44 metabolism-associated genes whose mRNA expression were increased due to copy number gains or amplifications (Haider et al., 2016). These 44 genes were enriched in hypoxic tumours, which suggests a core metabolic program enrichment in response to low oxygen tumour microenvironment. Of these 44 genes, 25 of them were prognostic in several cancers, and

the authors focused on *SQLE* - which encodes squalene oxidase - an enzyme involved the cholesterol synthesis pathway. While *SQLE* was co-amplified with *MYC*, it was prognostic in the METABRIC breast cancer cohort independently of *MYC* amplification. Small molecule inhibition of SQLE resulted in a dose-dependent decrease in viability in two of three cell lines with *SQLE* amplification. Additionally, clonogenic assays performed in hypoxic conditions in seven cell lines revealed decreased number of colonies in response to SQLE inhibition, compared to non-treated controls. Taken together, this study suggests the prognostic and potential translation value of targeting SQLE in a subset of cancer patients.

More recently, Gaude *et. al.* analysed gene expression data, with a particular focus on metabolism related genesets, from 20 tumour types using data from TCGA (Gaude and Frezza, 2016). The authors found that cancers converge toward a common metabolic phenotype: the downregulation of genes involved in mitochondrial metabolism such as the citric acid cycle and oxidative phosphorylation. Importantly, this down regulation of mitochondrial metabolism was associated with *poor* patient survival. Ten out of 15 cancers exhibited a downregulation of at least one mitochondrial metabolic pathway, with 60% of tumours showing decreased expression of genes encoding subunits I and IV of the electron transport chain. Furthermore, the downregulation of mitochondrial metabolism was correlated with increased expression of genes involved in EMT, hypoxia and angiogenesis. In comparing primary and metastatic melanoma, expression of the oxidative phosphorylation geneset was decreased further in disseminated disease, compared to the primary tumour.

Taken together, these studies suggest that dysregulation of certain metabolic pathways are clinically relevant and can influence patient survival. The extensive metabolic network in tumour warrants more in-depth analysis and characterisation, and the accumulation of detailed understanding of these pathways may identify metabolic nodes or

vulnerabilities.

1.5 Aim

This thesis set out to identify features associated with prognosis in breast cancer patients, with a particular focus on metabolic pathways that were informative of patient outcome. The hypothesis of this thesis is that increased expression of an FAO gene signature is correlated with good response to endocrine therapy and is associated with favourable prognosis.

Therefore, the overall aims were to:

(i) identify the genes and pathways involved in metabolism that are associated with prognosis in breast cancer patients

(ii) explore the consequences of manipulating the fatty acid oxidation pathway on key cancer hallmarks including proliferation and migration in breast cancer cell systems

1.5.1 Thesis outline

Chapter 3 describes the generation and validation of a prognostic gene signature involved in fatty acid oxidation in breast, as well as other cancer types. The expression of this signature between tumour and normal tissues from different cancer types will also be explored. In light of findings by Gatza *et. al*, this thesis will highlight the potential co-amplification of genes encoding cyclin D1 and CPT1A, and discuss the implication of this finding based on the literature.

Chapter 4 explores how the fatty acid oxidation gene signature is associated with epithelial-to-mesenchymal transition, a key process understood for cancer cells to metastasise. Furthermore, how cellular differentiation - a component of tumour grade in breast cancer - affects expression of the fatty acid oxidation will also be analysed.

Chapter 5 highlights how activation of two key oncogenic signalling pathways - Wnt and MAPK - affects expression of the fatty acid oxidation signature expression.

Chapter 6 describes the generation and characterisation of breast cancer cell systems with stable CPT1A overexpression and knockdown. Characterisation experiments include assessing the proliferation, migration, anchorage-independent growth and oxygen consumption analysis. Findings from this chapter will be discussed in light of what is known based on current literature.

Chapter 7 assesses the global transcriptomes of the transgenic cell systems described in the previous chapter, with a particular focus on identifying pathways that are significantly altered in response to CPT1A modulation.

Finally, Chapter 8 concludes by bringing together the findings from Chapters 3 to 7. This chapter will also highlight the clinical implication of findings from this thesis, and proposes potential experiments that could be conducted for future analyses.

Chapter 2

Materials and Methods

2.1 *Cell lines and complete media*

The basic features of the cell lines utilised in this study are summarised in Table 2.1. MCF7, MDA-MB231, and MCF10A cell lines were obtained from the American Type Culture Collection (ATCC) or Sigma. MDA-MB231 and MCF7 cells were maintained in RPMI1640 media, supplemented with 10% foetal bovine serum (FBS). MCF10A cells were maintained in DMEM/F12, supplemented with 5% horse serum, 20 ng/mL epidermal growth factor, 0.5 mg/mL hydrocortisone, 100 ng/mL cholera toxin and 10 μg/mL insulin (conditions recommended by Professor Joan Brugge's lab, Department of Cell Biology, Harvard Medical School).

Table 2.1: Cell lines used in this study.

Cell line	Company	Catalog number	Tissue	Morphology
MDA-MB231	ATCC	HTB-26	Breast; metastatic pleural effusion	Epithelial
MCF7	ATCC	HTB-22	Breast; metastatic pleural effusion	Epithelial
MCF10A	Sigma	CLLS1042	Breast; fibrocyst	Epithelial

2.1.1 Cell culture maintenance

Cells were grown in complete media in a humidified incubator at 37 °C and 5 % carbon dioxide. Cells were passaged at subcultivation ratios and media replaced as recommended by the ATCC for each cell line. To trypsinise cells, media was aspirated and cells rinsed with phosphate buffered saline (PBS) once, before 1 and 3 mL of 0.05% trysin was added to T25 or T75 flasks, respectively. Flasks were incubated at 37 ° C until all cells were detached, and trypsin inactivated with complete media. Cells were collected in a 15 mL Falcon tube, and centrifuged at 500 revolutions per minute (rpm) for 5 mins. For MCF7 and MDA-MB231 cell lines, media was replaced and cells were re-seeded into new flasks at respective subcultivation ratios. For MCF10A cells 1 million cells were re-seeded into a T75 flask.

2.2 Expression plasmids and primers

The bacterial strains and expression plasmids used in this study are summarised in Table 2.2. All primers used in this thesis are provided in Table 2.3 and were purchased from Integrated DNA Technologies.

Table 2.2: Plasmids used in this study.

Plasmids	**Relevant features**
pTET-ON	CMV promoter drives rtTA expression, neomycin- and ampicillin resistance genes
pTRE	Cloning site downstream of Tet response element (TRE)
pTRE-luc	Firefly luciferase cloned downstream of TRE
pTRE-CPT1A	CPT1A cloned downstream of TRE
pBabe-puro	Empty backbone plasmid that expresses puromycin resistance gene
pTRIPZ	Lentiviral vector for expression of shRNA and RFP downstream of TRE

Table 2.3: Primers used in this study.

	Forward	**Reverse**
Transgene		
CPT1A NM_001876.3	5' ACCGCGGATGGCAGAAGCTCACCAAGC 3'	5' GCGTCTAGATTACTTTTTGGAATTAGAACTG 3'
Sequencing		
CPT1A Internal	5' CAGGCCGAAAACCCATGTTG 3'	5' AGGAGTGTTCAGCGTTGAGG 3'
Vector	5' CCACGCTGTTTTGACCTCC 3'	5' CCCTGAAAACTTTGCCCCCT 3'
Quantitative PCR		
CPT1A	5' ATCAATCGGACTCTGGAAACGG 3'	5' TCAGGGAGTAGCGCATGGT 3'
GAPDH	5' TGCACCACCAACTGCTTAGC 3'	5' GGCATGGACTGTGGTCATGAG 3'

2.3 Preparation of RNA samples

Total RNA was extracted from MCF10A cells using the Quick RNA Mini-Prep kit (Zymo) and all reagent formulations are propietary. Cells were lysed in 600 μL of Lysis Buffer and gently pipetted or vortexed intermittently for one minute. The lysate was cleared by centrifugation at 10,000 rpm for one minute. The supernatant was transferred into a Spin-Away Filter column and centrifuged at 10,000 rpm for one minute to remove excess genomic DNA. One mL of absolute ethanol was added to the flow through and transferred into a Zymo-Spin IIICG column, centrifuged for 30 seconds (sec) and flow-through discarded. To remove residual genomic DNA, in-column DNase treatment was performed. Four hundred μL of RNA Wash Buffer was added to the column, centrifuged and flow-through discarded. Eighty μL of DNase I reaction mixture was added to the column matrix and incubated for 15 min at room temperature, and then centrifuged for 30 secs. Next, 400 μL of RNA Prep buffer was added to the column, centrifuged for one minute, and flow-through discarded. The RNA was washed twice with the RNA wash buffer and centrifuged first for 30 sec, and then 2 mins to ensure complete removal of the wash buffer. Finally, total RNA was eluted in an RNase-free tube by adding 35 μL of DNase/RNase-free water to the column and centrifuged at 13,000 rpm for 30 sec. The quality and quantity of the RNA preparation was measured using the NanoDrop ND1000 spectrophotometer and stored at -80 °C.

2.3.1 *Reverse transcription*

Complementary DNA (cDNA) from total RNA prepared as described in section 2.3 was obtained by performing reverse transcription using the PrimeScript First Strand cDNA synthesis kit. Volumes and concentrations of reaction mix are summarised in Table 2.4.

Table 2.4: Reverse transcription mix components per reaction.

Reagent	**Sample (μL)**	**Standard (μL)**	**Sample no RT control (μL)**
5X Primescript buffer	2	2	2
PrimeScript RT enzyme	0.5	0.5	0
oligo dT primers	0.5	0.5	0.5
Random 6mers	0.5	0.5	0.5
RNA and milliQ water	up to 6.5 (500 ng final)	up to 6.5 (2000 ng final)	up to 6.5 (500 ng final)

Reaction mixtures were made up in PCR tubes, gently pipetted several times to mix and collected by briefly centrifuging, and placed in the Biorad C1000 Thermal Cycler. The reaction was incubated at 37 °C for reverse transcription for 15 mins, and then heated at 85 °C to inactivate the RT enzyme.

2.4 Polymerase chain reaction of CPT1A cDNA

From the resulting cDNA, *CPT1A* was selectively amplified using conventional polymerase chain reaction. Primers were designed against CPT1A RefSeq NM01876.3

A standard reaction consisted of 500 ng of cDNA (prepared as above), 0.005 units of Q5 High Fidelity polymerase (New England Biolab catalog no. M0491), 200 μM dNTPs, 0.5 μM of both forward and reverse primers and 5 μL of 5X Q5 Reaction Buffer, and topped up to 25 μL with milliQ water. Negative control was set up as the reaction mixture above but cDNA replaced with milliQ water. The PCR cycling conditions are summarised in Table 2.5.

Table 2.5: PCR protocol for *CPT1A* cDNA amplification.

Step	Temperature (°C)	Duration	Cycles
Initial denaturation	95	3 min	Hold
Denaturation	95	30 secs	35
Annealing	72	30 secs	35
Extension	72	2.5 min	35
Additional extension	72	5 min	Hold

2.5 Preparation and ligation of DNA fragments

To prepare for ligation, digested PCR products, which is approximately 2.2 kb in size, and plasmid vectors were resolved on a 0.8% agarose gel, visualised under minimal ultraviolet radiation (approximately 5-10 seconds), and the product of expected size excised. The gel fragment was then column purified (Macherey-Nagel, Norrie Biotech, NZ catalog no. 740588.10), quantitated and added to the ligation reaction mixture.

A 10 μL ligation reaction was prepared that consisted of the pTRE digested plasmid, *CPT1A* insert, T4 ligase, ligation buffer, and milliQ water, and left in the fridge overnight at approximately 4 °C. To estimate self-ligation of digested pTRE digested plasmid, a vector only ligation mix was prepared similarly, but milliQ water added instead of the *CPT1A* insert.

2.5.1 *Heat shock transformation of competent bacteria with ligated products*

DH5alpha *E.coli* competent bacteria were thawed on ice, and split into two 100 μL volumes in 2 mL tubes. Five μL of the pTRE-CPT1A or pTRE-only ligation mixes were

added to each tube, and placed on ice for 30 min. The suspensions were then placed at 42 ° C (heat shock step) for 5 mins, and then placed on ice. No positive control was performed for this transformation step. One mL of LB media without ampicillin was added to each tube and incubated with gentle shaking (200rpm) for one hour. Fifty μL of this suspension was inoculated on an LB agar plate (with 10 μg/mL ampicillin). The remainder of the suspension was spun down at 5000 rpm for 5 mins, and supernatant removed until approximately 50 μL was left, which was innoculated on an LB agar plate (with 10 μg/mL ampicillin). The agar plates were incubated at 37 ° C overnight.

2.5.2 *PCR screen for positive transformants*

The following day, colonies were picked using a sterile pipette tip, and dipped in 15 μL of milliQ water, before the tip was displaced into 2 mL of LB media with ampicillin in a 15 mL Falcon tube. The PCR tubes were topped up to 20 μL of PCR master mix (Thermo Scientific catalog no. 10342020; in a 20 μL reaction: 10X buffer 2 μL, 10 μM forward and reverse primers 0.5 μL each, DNA polymerase 0.5 μL, 200 μM dNTP 0.5μL, 50 mM magnesium chloride 0.6 μL, DNA 25 ng, top up with milliQ water to 20 μL) and PCR was performed to identify colonies that had taken up the *CPT1A* insert. Positive clones in LB/ampicillin (10 μg/mL) media were cultured at 37 ° C for approximately 16 hours. Glycerol stocks were prepared by mixing 500 μL and 500 μL of glycerol. The pTRE-CPT1A plasmids were prepared using the Qiagen Plasmid Mini Kit (BioStrategy, NZ, catalog no. 12125) and Sanger sequencing performed (Genetic Analysis Service, University of Otago) to verify that no mutations were present in the *CPT1A* transgene.

2.6 Generation of double-stable, inducible MDA-MB231 cell line

2.6.1 *Transfection of pTetOn plasmid into MDA-MB231 cell line*

To generate the first stable MDA-MB231 constitutively expressing the reverse tetracycline transactivator protein (rtTA), MDA-MB231 cells were transfected with the pTetOn plasmid (Clontech catalog no. 631018) using Lipofectamine LTX (Thermo Scientific, NZ, catalog no. A12621). Cells were plated in a 24 well plate at a density of 125,000 cells per well in a total of six wells, and left overnight to adhere. Based on optimisation experiments, 1.25 μL of Lipofectamine LTX reagent and 0.25 μL of Plus reagent were used for pTetOn transfection. The transfection mix was prepared in serum-free media and added for six hours to cells grown in serum, then media replaced and cells incubated overnight. The following day, cells were trypsinised, total cells from the six wells resuspended in 6 mL media, and plated in 10- and 15 cm dishes at three different densities (1 mL of cells into each of two 15 cm dishes, 1 mL of cells into each of two 10 cm dishes, 0.5 mL of cells into each of two 15 cm dishes, and 0.5 mL of cells each into 10 cm dishes. Media was made up to 8 mL in the 10 cm dish, and 15 mL in the 15 cm dish.

2.6.2 *Selection and isolation of stable pTetOn transfectants*

Selection of stable clones was commenced at 24 hours post-seeding into dishes using 800 μg/mL of G418. Media was replaced every two days with G418-containing conditioned media. Once single colonies were observed, media replacement was performed every four days, until colonies of approximately 50 cells were observed. To isolate these individual clones, media was removed and cells were rinsed with PBS. Sterile, punch-holed Whatman papers dipped in trypsin were placed over individual colonies, and left

for two minutes. Upon completion of trypsinisation, each colony was transferred to a well of a 24-well plate. The Whatman papers were left for up to 72 hours and cells were cultured in conditioned, selective media until sufficient cell numbers were available to be frozen. MDA-MB231 cells were frozen in complete media (RPMI + 10% serum) in 5% dimethyl sulfoxide in cryotubes (approximately 1 million cells in 1 mL of media per tube). Cryotubes were then transferred into Mr Frosty and placed in -80 °C overnight, before being transferred to liquid nitrogen container for long term storage.

2.6.3 *Preparation of doxycycline hydrochloride and puromycin stock solutions*

Doxycycline hydrochloride (Dox) (Sigma-Aldrich, catalogue no. D3447) was prepared as a 2 mg/mL stock in sterile milliQ water, filter sterilised through a 0.2 micron membrane, aliquoted into Eppendorf tubes and stored at -20 °C. Once thawed, stocks were used for no more than two weeks.

Puromycin dihydrochloride (Sigma-Aldrich, catalogue no. P8833) was prepared as a 10mg/mL stock in sterile milliQ water. This stock solution was added at required volume to the RPMI1640 culture media achieve the working concentration, which was then sterile filtered as above.

2.6.4 *Luciferase-based screening of single transfectant clones*

Putative single stable transfectant clones were plated in duplicates in a 24-well plate and transiently transfected with pTRE-luciferase. Transfection was set up similar to that described in Section 2.6.1. One well was induced with 2 μg/mL of Dox, and the same volume of milliQ water added to the uninduced well, for 48 hrs. Cells were lysed in 50 μL of cell culture lysis buffer (Promega catalogue no. PME1500), vortexed, and

whole cell lysates frozen at -20 °C until assayed. Prior to conducting the assay, whole cell lysates were centrifuged at 4 °C for five mins and 10 μL of supernatant added to 100 μL of substrate reagent solution in a white-walled, flat bottom 96-well plate. The plate was then placed in the ClarioStar plate reader (BMG LabTech, Thermo Fisher Scientific), and luminescence measured for 10 secs. Clones with at least 20-fold induction were independently screened again, and the clone with the highest inducibility taken for further downstream analysis.

2.6.5 *Co-transfection of pTetOn single transfectant cell line with pTRE and pBabe puro*

Upon generation of a single, stable pTetOn MDA-MB231 cell line, a second round of co-transfection was performed with 450 ng of a doxycycline-inducible plasmid carrying the *CPT1A* transgene, and 50 ng of a plasmid conferring puromycin resistance. Briefly, 125,000 cells were plated in a 24-well plate and left overnight to adhere. The following day, each well was transfected with 450 ng of pTRE-CPT1A and 50 ng of pBabe puro using 1.25 μL Lipofectamine LTX per well. A total of six wells were transfected. Twenty four hours post transfection, cells were trypsinised and plated into 10 cm dishes. Puromycin selection (1 μg/mL) was commenced the following day, and cells were maintained in 80% complete media with 400 μg/mL G418 and 20% conditioned media obtained from pTetOn MDA-MB231 cells every 24 hours. Once colonies were observed, colony lifts were performed as described in section 2.6.2. A PCR screen was performed to determine if the puromycin-resistant colonies had stably integrated the pTRE plasmid. Positive colonies were further expanded to conduct experiments measuring the inducibility of *CPT1A*.

2.6.6 *Assessing CPT1A mRNA induction in putative overexpression clones*

To measure the inducibility of *CPT1A*, 250,000 cells per colony were plated in duplicate in a six well plate and left overnight to adhere. One of the wells was induced with 2 μg/mL of Dox for 48 hours and total RNA extracted as described in section 2.3. Expression of *CPT1A* in the putative overexpression clones were assayed by quantitative PCR (qPCR). A 10.2 μL reaction consisted of 5 μL of KAPA SYBR FAST qPCR Master Mix Universal (Kapa Biosystems, catalogue no. KK4601), 20 ng of cDNA, 0.2 μL of forward and reverse primers, 0.2 μL ROX High reagent. No reverse transcriptase control samples from cDNA synthesis were assayed for genomic DNA contamination during RNA preparation, and no template control assayed to ensure no contamination of assay reagents. As this is a screen, only one reference gene - *GAPDH* - was assayed to normalise *CPT1A* expression. Each condition was plated in three technical replicates, and only one biological replicate was conducted for screening. Reactions were plated into a 384-well plate, sealed, spun and placed in the 7900HT Fast Real-Time PCR system (Applied Biosystems). Melt curves were also performed to verify a specific product. The reaction cycling protocol summarised in Table 2.6. Standards were derived from cDNA prepared from 2 μg of total RNA from MCF7 breast cancer cells, and diluted in milliQ water to achieve concentrations of 100-, 20-, 2-, 0.2- and 0.02 ng in 4.5 μL per well. These standards were assayed in three technical triplicates. The qPCR assay data was analysed using the SDS 2.4 software (Applied Biosystems) and quantifying the amount of *CPT1A* mRNA based on the standard curve performed.

Table 2.6: qPCR cycling protocol.

Step	Temperature (°C)	Duration	Cycles
Enzyme activation	95	3 mins	Hold
Denaturation	95	5 secs	40
Annealing/extension	60	30 secs	40

2.7 Establishing stable MCF7 and MCF10A cell lines for *CPT1A* knockdown

2.7.1 Cloning of shRNA constructs into pTRIPZ vector

The pTRIPZ (GE Healthcare, Dharmacon) plasmid is an inducible, lentiviral vector that expresses shRNA against a target gene in response to Dox treatment. The mature antisense shRNA sequence was obtained from the Dharmacon website and reverse engineered to generate the coding sequence of four shRNA constructs against *CPT1A*. PCR was performed using ultramers that prime off each other to generate a fragment encoding each shRNA (Rangasamy, Tremethick, and Greaves, 2008). Four unique pairs of ultramers were amplified, giving rise to four shRNA constructs, and the sequence is provided in Table 2.7. The cycling conditions are summarised in Table 2.8.

Table 2.7: Ultramer sequences for amplifying shRNA sequence against *CPT1A*.

CPT1A shRNA ultramer	**Forward**	**Reverse**
Construct 1	5' gct cga gaa ggt ata ttg ctg ttg aca gtg agc g CA AAG AAG TTC ATC AGA TTC AA tag tga agc cac aga tgt a T TGA ATC TGA TGA ACT TCT TTT tgc cta ctg cct cgg aat tcg 3'	3' cga gct ctt cca tat aac gac aac tgt cac tcg c GT TTC TTC AAG TAG TCT AAG TT atc act tcg gtg tct aca t A ACT TAG ACT ACT TGA AGA AAA acg gat gac gga gcc tta agc 5'
Construct 2	5' gct cga gaa ggt ata ttg ctg ttg aca gtg agc g CG CCA TGA AGC TCT TAG ACA AA tag tga agc cac aga tgt a T TTG TCT AAG AGC TTC ATG GCT tgc cta ctg cct cgg aat tcg 3'	3' cga gct ctt cca tat aac gac aac tgt cac tcg c GC GGT ACT TCG AGA ATC TGT TT atc act tcg gtg tct aca t A AAC AGA TTC TCG AAG TAC CGA acg gat gac gga gcc tta agc 5'
Construct 3	5' gct cga gaa ggt ata ttg ctg ttg aca gtg agc g GT ACA GTG GTA TTT GAA GTT AA tag tga agc cac aga tgt a T TAA CTT CAA ATA CCA CTG TAA tgc cta ctg cct cgg aat tcg 3'	3' cga gct ctt cca tat aac gac aac tgt cac tcg c CA TGT CAC CAT AAA CTT CAA TT atc act tcg gtg tct aca t A ATT GAA GTT TAT GGT GAC ATT acg gat gac gga gcc tta agc 5'
Construct 4	5' gct cga gaa ggt ata ttg ctg ttg aca gtg agc g GC TGG ACT TCA TTC CTG GAA AA tag tga agc cac aga tgt a T TTT CCA GGA ATG AAG TCC AGA tgc cta ctg cct cgg aat tcg 3'	3' cga gct ctt cca tat aac gac aac tgt cac tcg c CG ACC TGA AGT AAG GAC CTT TT atc act tcg gtg tct aca t A AAA GGT CCT TAC TTC AGG TCT acg gat gac gga gcc tta agc 5'

Table 2.8: PCR protocol for shRNA ultramers amplification.

Step	Temperature (°C)	Duration	Cycles
Initial denaturation	94	2 min	Hold
Denaturation	94	30 secs	29
Annealing	50	30 secs	29
Extension	72	2.5 min	29
Additional extension	72	5 min	Hold

Digested plasmid (13 kilobase) and PCR products (150 base pairs) were resolved on a 1.2% agarose gel for 25 min at 100V. Gels were visualised under a UV lamp and bands corresponding to purified, digested plasmid and PCR products were excised. DNA from gel extracts was eluted using a column (NucleoSpin Gel and PCR Clean-up). Ligation was performed as per section 2.5 overnight at 4 °C using a 1:2 vector-to-insert ratio. This translates into 100 ng of plasmid and 8 ng of insert. To estimate background re-ligation of vector without insert, a vector only control ligation of identical setup was performed, with water used in place of purified shRNA construct. The following day, 5 μL of the ligation reaction was transformed into STBL3 *E.Coli* strain using the heat shock method (42 °C, 5 mins) , and recovered in LB for one hour at 37 °C. No positive control was performed for this transformation step. The culture was then pelleted and 50 μL inoculated on an ampicillin-containing (10 μg/mL) agar plate, and incubated overnight at 37 °C.

The following day, colonies were picked and PCR screened for uptake of shRNA constructs using construct specific primers. Positive colonies were grown for approximately 16 hours in 3 mL of LB/ampicillin (10 μg/mL) media and plasmids prepared. All shRNA constructs were sequence verified by Sanger sequencing (Genetic Analysis Service, University of Otago).

2.7.1.1 *Assessing knockdown efficiency of shRNA constructs*

To compare knockdown efficiencies of the different constructs, a transient knockdown experiment was performed using MCF7 cells. Two hundred thousand cells were plated in triplicates in a six well plate for each construct, including a non-silencing construct control and left to adhere overnight. Cells were transfected with 2 μg of respective constructs using FuGENE HD (Promega) according to manufacturers recommendation. The transfection mix was prepared in serum-free media, and transfection performed on cells grown in serum. Six hours post-transfection, 2 μg/mL Dox was added to induce shRNA expression. The following day, cells were visualised for RFP expression to estimate transfection efficiency, which was approximately 40-60%. Cells were then selected with 2 μg/mL of puromycin for 72 hours. After 72 hours, total RNA was prepared and expression of *CPT1A* was determined using qPCR based on a standard curve, as described in section 2.6.6. Expression of *CPT1A* was normalised to the *GAPDH* expression as reference.

2.7.1.2 *Lentivirus particle production*

Lentivirus particles were produced using the second generation system (Wang and McManus, 2009). This is achieved by transfecting HEK293FT cells with three plasmids that consist of the transfer plasmid pTRIPZ carrying the shRNA of interest, the psPAX2 packaging plasmid and the VSV-G envelope plasmid.

Cells were seeded at a density of 5.6 million cells/mL in a T75 flask and allowed to adhere overnight. The following day, a transfection mix of 18.6 μg of pTRIPZ, 9.6 μg of psPAX2, and 4.8 μg of VSVG plasmid was prepared in serum-free RPMI 1640 media to a final volume of 1 mL, and filtered into another 15 mL Falcon tube containing 55.7 μL of Lipofectamine 2000 in 944.3 μL of RPMI 1640. This mix was incubated for 20 min at room temperature, and added drop-wise into the flask while gently tilting to facili-

tate equal distribution of the mix. Transfection was done in cells grown in serum. The flasks were incubated overnight and replaced with complete media the following day. Fourty-eight hours post-transfection, supernatants from the flasks were recovered, and centrifuged at 3,000 rpm for 15 min. The supernatant containing the lentiviral particles were filtered through a 0.45 μm PVDF filter to remove debris and frozen at -80 °C as 500 μL aliquots.

2.7.1.3 Determining viral transducing unit

Both MCF7 and MCF10A cells were plated in triplicates in a clear bottom, black-walled 96 well plate at a density of 4,000 cells/well. The following day, serial dilutions of the viral stock were prepared from ranging from 2 to 64 fold, together with 2μg/mL of doxycycline. Media was replaced with 100μL of respective dilutions, and left for 48 hours. To determine the transducing units, cells were fixed in PBS with 0.25% (v/v) paraformaldehyde and 0.075% (v/v) saponin and stained with 2 μg/mL DAPI, and plates wrapped in tin-foil for at least one hour and imaged using the Cytell imaging system using the DAPI and TRITC filters. Images were imported in CellProfiler and ratios of DAPI-to-RFP cells determined.

2.7.1.4 *Lentiviral shRNA infection of MCF7 and MCF10A cells*

MCF7 and MCF10A cells were plated at a density of 150,000 cells/well in a six well plate and left overnight to adhere. While tittering of the viral stock was conducted as above, this method proved to yield unrealiable viral concentrations. The following day post-seeding, cells were transduced with 50- or 100 μL of viral supernatants carrying the shRNA constructs. Six hours post-transduction, 2μg/mL Dox was added to each well to induce RFP expression to estimate transduction efficiency. Fourty eight hours post-transduction, approximately 20-30% of the transduced wells expressed RFP. MCF10A and MCF7 cells were selected with 1.5- and 1 μg/mL of puromycin respectively to gen-

erate stable polyclonal populations.

2.7.1.5 *Screening for stable shRNA knockdown clones in MCF7 and MCF10A*

To select for clones that show the best knockdown of *CPT1A*, total RNA was prepared from the polyclonal populations of MCF10A and MCF7 cells and qPCR performed. MCF10A cells (20,000 cells/well) and MCF7 cells (80,000 cells/well) were plated in six well plates and induced with 2- or 4μg/mL of doxycycline for 5 days, with fresh media replaced on day 3.

qPCR analysis was performed to determine the expression of *CPT1A*, and clones that showed at least 50% mRNA decreased expression after 5 days of knockdown were taken forward for immunoblotting.

2.7.1.6 *Immunoblot analysis of inducible cell systems*

2.7.1.6.1 Induction of CPT1A transgene in MDA-MB231 pTRE-CPT1A cell lines For CPT1A induction analysis of putative overexpression clones, 150,000 cells were seeded for each clone in duplicate in six well plates, and one of the wells induced with 2 μg/mL Dox for 48 hours. Cells were lysed and scraped in ice cold radio immunoprecipitation assay buffer (50 mM Tris pH8.0, 150 mM NaCl, 0.1% sodium dodecyl sulfate, 1% w/v sodium deoxycholate, 0.01% NP40), transferred into 1.5 mL Eppendorf tubes, and placed on ice for at least 15 mins with intermittent vortexing. Whole lysates were frozen at -80 °C until analysed. For time course experiments, 100,000 cells were seeded into 10 mm dishes and induced with 2 μg/mL Dox for up to 120 hours. For 96- and 120 hr time points, media was replaced at 72 hours. Lysates were prepared as above.

2.7.1.6.2 Induction of *CPT1A* shRNA expression in MCF10A and MCF7 cells To determine CPT1A knockdown in MCF7 and MCF10A cell lines, 50,000- and 25,000 cells, respectively, were seeded in six-well plates and induced with 2 μg/mL Dox for one week, and lysates prepared.

2.7.1.6.3 Immmunoblot procedure Cell lysates were thawed and spun at 13,000 rpm for 10 mins at 4 °C. The bicinchoninic acid assay was performed to quantitate the amount of protein in each sample. Samples were diluted 10 fold in RIPA buffer, and a 2 mg/mL stock solution of bovine serum albumin was diluted to give a range from 0.025- to 2 mg/mL to generate a standard curve. Twenty-five μL of standards and samples were plated in triplicates, 200 μL of working reagent added and incubated at 37 °C, and absorbance at 562nm measured. Protein quantity were measured using the standard curve, taking into account the dilution factor.

Ten % sodium dodecyl sulfate (SDS) polyacrylamide gels were poured and set in the fridge overnight. The resolving gel consisted of 6.6 mL 30% acrylamide, 5 mL 1 M Tris-hydrochloride (pH 8.8), 200 μL 10% SDS, 100 μL 10% APS, 20 μL TEMED and 8.9 mL milliQ water. The resolving gel was poured into the Bio-Rad Mini Protean 3 system (Bio-Rad Laboratories) gel cast, layered with isopropanol, and allowed to set. Stacking gel consisted of 1.16 mL 30% acrylamide, 1.26 mL Tris-hydrochloride (pH 6.8), 50 μL SDS, 5 μL TEMED, 25 μL 10% APS, and 3 mL milliQ water.

For all immunoblot analysis, 20 μg of proteins were resolved at 100V for approximately 2 hours. Proteins were transferred onto a PVDF membrane at 90V for 90 minutes, and blocked with 5% (w/v) milk for one hour at room temperature. Blots were then rinsed in Tris-buffered saline with 0.1% Tween 20 (TBST) and incubated with anti-CPT1A (88kDa, 1:1000, or 1 μg/mL from 1 mg/mL stock, Abcam catalogue 128568 mouse

monoclonal) overnight at 4 °C. Blots were washed with TBST thrice for 10 minutes per wash, and incubated with sheep anti-mouse secondary antibody linked to horseradish peroxidase (1:10,000, Amersham catalogue NA931) for 1 hour. Blots were washed as previously described, and enhanced chemiluminescence reagent (Pierce ECL Plus Western Blotting Substrate, catalog no. 32132) added for 1 minute and imaged using the LiCor Odyssey under the 'Chemi' channel for 2 mins. Since CPT1A and alpha-tubulin of different sizes, blots were not stripped, but rinsed and re-probed with alpha-tubulin (50 kDa, 1:5000, Sigma catalogue TA6199 mouse monoclonal) , and subsequent washes, secondary antibody incubation, and development performed as previous.

2.7.1.6.4 Soft agar assay For the base agar, a 1.2 % agarose solution was prepared using sterile milliQ water. The agar was left to cool on a heat block to approximately 55 °C, before equal volumes of the agarose solution and 2 x RPMI/20% FBS mixture was prepared. Two mL of this final 0.6% agarose solution in 1x RPMI/10% FBS was added to six well plates and left to cool at room temperature, before leaving at 4 °C overnight. The following day, a 0.6% agarose solution was prepared and incubated on a 37 °C heat block. Cells were prepared at a density of 300,000- (MDA-MB231) and 120,000 cells (MCF7) in 3 mL of 2 x RPMI/20% FBS, and added to 3 mL of 0.6% agarose. Two mL of this solution was plated above the base agar, to give a final concentration of 50,000- (MDA-MB231) or 10,000 (MCF7) cells in 0.3% agar. This mixture was allowed to set, and complete media added the following day, with or without 2 μg/mL Dox. One mL of fresh media was replaced every 2-3 days. After three weeks, the agar was fixed and stained with 20% methanol at room temperature and 0.05% crystal violet (which binds to protein and DNA, thereby indicating colonies) solution for 30 mins and plates wrapped in tin-foil. Stains were washed several times with milliQ water and colonies from 9 random fields (4x magnification) counted using a phase-contrast microscope.

2.7.1.6.5 Boyden chamber assay MDA-MB231 TetOn or pTRE-CPT1A clone 3 cells were induced with 2 μg/mL Dox for 5 days. Cells were resuspended to a final concentration of 1 million cells/mL in serum-free media, and 200 μL of this suspension was added to the transwell insert overlaying 600 μL of complete media in the bottom well, careful to avoid bubble formation between the media in the bottom well and insert. Cells seeded in the transwell were supplemented with 175 μM of BSA-palmitate and 0.5 mM carnitine. Carnitine (50 mM stock) was prepared diluting 0.15 g of carnitine (Sigma catalog. C0283) in 15 mL of milliQ water, filter sterilised (0.2 micron filter), aliquoted into 1 mL volume in sterile Eppendorf tubes, and frozen at -80 °C until required. BSA-palmitate was prepared according to protocol provided by Seahorse Biocsciences. Briefly, 1g of fatty acid-free BSA (Sigma catalog no. A8806) was dissolved in 44 mL of milliQ water in a 250 mL beaker and stirred. This BSA solution was then placed in a 600 mL beaker with pre-warmed (37-40 °C) distilled water, and continued to stir until all the BSA dissolved. From this solution, 22 mL was removed in the tissue culture flow hood, and diluted with 22 mL of 150 mM sodium chloride to generate 44 mL of 0.17 mM BSA stock solution. The remainder 22 mL of undiluted BSA solution was used to conjugate to sodium palmitate (Sigma catalog no. P9767). Palmitate solution was prepared by adding 30.6 mg of sodium palmitate to 44 mL of 150 mM sodium chloride solution in a 100 mL beaker. This beaker containing the palmitate solution was then placed in a one litre beaker containing distilled water, and the temperature slowly raised to 70 °C on a stir plate, and the palmitate continuously stirred until a clear solution was obtained. From this solution, 17.6 mL was transferred into the 22 mL of undiluted BSA solution and continued to stir not beyond 40 °C, for approximately two hours, until a clear solution was obtained. A further 4.4 mL of 150 mM sodium chloride was added to this solution to generate 44 mL of 1 mM conjugated palmitate stock solution, before adjusting the pH to 7.4 with 1 M sodium hydroxide. The 0.17 mM BSA and BSA-palmitate conjugate solution was then aliquoted (4mL volume) into

sterile universal glass vials, wrapped with tin foil, and stored at -20 °C until use.

Migration experiment was conducted for 48 hours, following which cells that had migrated and adhered to the bottom well were fixed in PBS with 0.25% (v/v) paraformaldehyde and 0.075% (v/v) saponin and stained with 2 μg/mL DAPI, and plates wrapped in tin-foil for at least one hour, and nuclei count performed using the Cytation 3 imaging system (Biotek Instruments).

2.7.2 Real time FAO flux analysis using the Seahorse XF extracellular flux technology

The Seahorse XF analyser measures the oxygen consumption rate (OCR) and extracellular acidification rate (ECAR) as a proxy for mitochondrial respiration and glycolysis, respectively. Changes in concentrations of dissolved oxygen due to mitochondrial respiration and free protons due to lactate secretion can be measured using solid state sensor probes. These probes are suspended 200 microns above a cell monolayer and measure the OCR in pmol/min and ECAR at mpH/min at 2-5 min intervals. Baseline OCR/ECAR measurements are measured up to five times before cells are treated with inhibitors, substrates, or other small molecules through an injection port.

In these series of experiments, three mitochondrial inhibitors, which are provided as part of the MitoStress test assay kit (In Vitro Technologies, NZ catalog no. SEA103015100): oligomycin, carbonyl cyanide-4-(trifluoromethoxy)phenylhydrazone (FCCP) and antimycin A, that bind to different components of the electron transport chain (ETC), were utilised. These compounds were reconstituted according to manufacturer's instructions.

Oligomycin binds to the oligomycin-sensitive conferring protein on ATP synthase, thereby inhibiting ATP synthesis. Hence, the cells require an alternative source of ATP, which

is primarily achieved from increased glycolysis.

FCCP is a lipid soluble, weak acid that facilitates proton permeability across the mitochondrial matrix and intermembrane space, thereby abolishing the obligatory proton gradient required for oxidative phosphorylation. This results in decreased ATP production, thereby increasing citric cycle activity and generation of reducing equivalents such as NADH and FADH2. Oxygen is the terminal electron acceptor from oxidation of these reducing equivalents, hence explaining the marked increase in oxygen consumption in the presence of a mitochondrial uncoupler.

Antimycin A inhibits cytochrome *c* oxidoreductase and prevents the oxidation of ubiquinone. This prevents the transfer of electrons from NADH and succinate to oxygen, thereby resulting in decreased demand and consumption of oxygen. The compounds, their targets and effects on OCR are summarised in Table 2.9.

Table 2.9: Mitochondrial inhibitors utilised in real time FAO flux analysis.

Compound	**Target**	**Effect on OCR**
Oligomycin	ATP synthase	Decrease
FCCP	Inner mitochondrial membrane	Increase
Antimycin A	Complex III	Decrease

2.7.2.1 Induction of CPT1A expression and knockdown in cell systems

MDA-MB231 TetOn and pTRE-CPT1A overexpressing clones were seeded at a density of 200,000 cells/well in a six well plate. Three wells were induced with 2μg/mL Dox for 5 days. Media was replaced on day 3. MCF10A cells were seeded at 20,000 cells/well and MCF7 cells were seeded at 50,000 cells/well in a six well plate and induced with 2μg/mL Dox for 7 days.

2.7.2.2 *Optimisation of FCCP required to achieve maximal OCR in cell systems*

The FAO assay workflow uses BSA, which can bind to FCCP and thereby decrease the effective concentration available to cells. As such, the concentration of this compound requires optimisation to achieve maximal OCR in the presence of BSA for each cell line.

MDA-MB231 TetOn and pTRE-CPT1A overexpression clones were plated at a density of 60,000 cells/well in 100 μL of substrate-limited media and left at room temperature for 30 mins to allow even dispersion prior to a 4 hr incubation at 37 °C to allow adherence. A further 150 μL of substrate-limited media was added to each well and cells incubated overnight. The same setup was performed for MCF7 and MCF10A knockdown systems, with cells seeded at a density of 40,000 cells/well. These cell densities were selected to achieve approximately 80-90% confluence post-seeding and also within the manufacturer's recommended baseline range for ECAR (20-120 mpH/min) and OCR (50-400 pmol/min). A standard MitoStress assay was carried out, with FCCP concentrations ranging from 0.5- to 4 μM and assayed for maximal OCR.

2.7.2.3 *FAO assay set up*

MDA-MB231 TetOn and pTRE-CPT1A overexpression clones were plated at a density of 60,000 cells/well in 100 μL of media and left at room temperature for 30 mins for even dispersion prior to a 4 hr incubation at 37 °C to allow adherence. A further 150 μL of substrate-limited media was added to each well and incubated overnight. The same setup was performed for MCF7 and MCF10A knockdown systems, with cells seeded at a density of 40,000 cells/mL. These cell densities were selected to achieve approximately 80% confluency post-seeding and also within the manufacturer's recommended baseline range for ECAR (20-120 mpH/min) and OCR (50-400 pmol/min).

The following day, cells were rinsed once, and media replaced with 375 μL of FAO assay media and incubated at 37 °C without carbon dioxide for 30 min. Mitochondrial inhibitors oligomycin, FCCP and antimycin A were prepared for injection into respective ports. The concentrations of compounds used in each cell line are summarised in Table 2.10. Unused, free ports were filled with assay media. Fifteen minutes prior to the start of assay, 37.5 μL of 400 μM etomoxir (approximately 40 μM final) was added into designated wells. Prior to loading of the plate to be assayed, 87.5 μL of BSA- or BSA-palmitate was added into designated wells.

Table 2.10: XF24 Fatty oxidation instrument run protocol.

Command	**Number of loops**	**Time (mins)**
Calibrate: Mix, wait, measure	5	3, 2, 3
Inject oligomycin (1 μM) : Mix, wait, measure	3	3, 2, 3
Inject FCCP (1-2 μM): Mix, wait, measure	3	3, 2, 3
Inject antimycin A (10 μM): Mix, wait, measure	3	3, 2, 3

2.8 Bioinformatics analysis methods

2.8.1 *Cox proportional hazards regression to identify features significantly associated with outcome*

To identify genes that were significantly associated with disease specific survival (DSS), univariate Cox regression was performed using the gene expression as the dependent variable. This analysis was performed on the gene expression data from the METABRIC

training cohort *coxph*() function from the 'survival' package in RStudio (RStudio Team, 2015). To account for multiple comparison tests, p-values from the Cox regression were adjusted using the false-discovery rate method using the *p.adjust* function. Multivariate Cox regression analysis was performed using the *coxph*() function, and including other co-variates for respective analysis.

2.8.2 *Collapsing multiple probesets to unique genes*

In many microarray platforms, a gene can be represented by multiple probesets and may have different sensitivities to measure expression levels of a particular transcript. Therefore, prior to performing Cox regression analysis, the expression matrix was collapsed so that each probeset represented a unique gene using the collapseRows package (Miller et al., 2011). Collapsing the matrix also ensures that the adjusted p-values are not confounded by multiple probesets to represent each gene.

2.8.3 *Gene set enrichment analysis*

To identify pathways that were enriched from the Cox regression, gene set enrichment analysis (GSEA) was performed using the GSEA software (versions 2.2.0 and 2.2.3) available from the Broad Institute. Genes were pre-ranked based on their adjusted p-value in ascending order. The gene set database was obtained from Kyoto Encyclopaedia of Genes and Genomes (KEGG) or Reactome.

2.8.4 *Kaplan-Meier survival analysis*

Kaplan-Meier survival curves were plotted to determine the association of a gene expression signature or clinico-pathologic variable with outcome. This analysis was performed using the *survplot*() function, and statistical significance between curves was calculated

using the log-rank test using the *survdiff*() function from the 'survival' package.

All signature expression scores were generated based on *mean* expression value of genes comprising the signature. Unless stated otherwise, the dichotomous cut-off for gene expression signatures are based on being below (Low group) or above (High group) *median* signature expression score of the cohort.

2.8.5 *Accessing publicly available gene expression datasets*

Publicly available gene expression datasets were accessed from the Gene Expression Omnibus or ArrayExpress repositories. Datasets were normalised by contributing authors prior to submission. Normalisation procedures aim to balance hybridisation intensities to ensure meaningful biological comparisons can be made between arrays (Quackenbush, 2002). Potential sources of variability that normalisation serves to reduce include differences in starting RNA amount, differences in the labelling or detection efficiencies with regards to the fluorescent dye utilised, and systematic biases of gene expression measurements. All datasets from The Cancer Genome Atlas were accessed from the Cancer Browser hosted by University of California Santa Cruz. Of note, where survival analyses were performed, many A summary of the datasets analysed in this thesis is provided in Table B.59-B.64.

2.8.6 *RNA-Seq analysis of CPT1A overexpressing and knockdown cell lines*

To investigate for genes and pathways that were differentially expressed in response to overexpression of CPT1A in MDA-MB231 and knockdown in MCF7 cells, RNA-sequencing transcriptome analysis on the Illumina HiSeq platform using the services of New Zealand Genomics Limited. TetOn and CPT1A overxpression clones 3 and 17 were

seeded in six well plates and induced for 5 days with 2μg/mL Dox. MCF7 non-silencing and *CPT1A* shRNA1 and shRNA2 lines were seeded in six well plates and induced with 2μg/mL Dox for 7 days. Total RNA was extracted as described in section 2.2. Two biological replicates from the overexpression and knockdown experiments were prepared for transcriptome analysis. The services of New Zealand Genomics Limited was employed for RNA sequencing and alignment.

Differential analysis expression was performed using the 'limma' package in RStudio, and codes were adapted from the package user manual (Ritchie et al., 2015; Phipson et al., 2016; Liu et al., 2015). Geneset enrichment analysis was performed using the Enrichr online software (Chen et al., 2013; Kuleshov et al., 2016). For targeted analysis, the Wnt target signature was derived from Van der Flier *et. al.* (Flier et al., 2007). The MAPK signature was derived from the Reactome database (ERK_MAPK_TARGETS), and the EMT signature was obtained from Groger *et. al.* (Fabregat et al., 2016; Croft et al., 2014; Groger et al., 2012). Gene members in these signatures are provided in Supplementary C.1.

Chapter 3

Identification of pathways associated with breast cancer treatment response and prognosis

3.1 Background

A multitude of prognostic gene expression signatures have been identified through the application of transcriptomic technologies to breast tumour tissues and clinical data (Gyorffy et al., 2015). While there is little overlap in the genes that make up these different signatures, most of them quantify two key processes in breast cancer: ER signalling and proliferation (Venet, Dumont, and Detours, 2011; Wirapati et al., 2008; Weigelt and Reis-Filho, 2009). This leaves the potential for substantial gains to be made in utilising data from gene expression studies to identify the *biological* processes that sustain tumour growth during treatment. Furthermore, potential molecular processes identified can also be analysed in other tumour types, which may facilitate a broader understanding of how the particular pathway contributes to tumourigenesis or disease progression. Therefore, the aim of this chapter is to identify the molecular processes associated with survival in ER-positive breast cancer patients that received adjuvant

hormone- and/or radiotherapy.

The METABRIC study, conducted in the United Kingdom, Canada and Norway, analysed gene expression and copy number aberrations from over 2000 primary breast tumours (Curtis et al., 2012). When this section of this thesis was undertaken, this study was the best resource for gene expression analysis with regards to sample size and completeness of clinical data. Importantly, the size of the METABRIC study allows for subgroup analysis (e.g., ER-positive patients, adjuvant treatment). The clinicopathologic information of patients in the METABRIC training cohort for analysis in this chapter is summarised in Supplementary Table B.1.

3.2 Objectives

The objectives of this chapter are to:

(i) identify pathways that are associated with prognosis in a breast cancer training cohort of patients that received radiation and/or endocrine therapy
(ii) select and validate one pathway of interest in independent breast cancer datasets
(iii) explore the association of the selected pathway with prognosis in other cancer types
(iv) investigate whether the expression of the selected pathway differs between normal and cancer tissues of different anatomical origins.

3.3 Results

3.3.1 *Gene signatures significantly associated with breast cancer disease-specific survival*

To identify genes and pathways that were associated with disease-specific survival (DSS) in the METABRIC training data (n=973), Cox regression was performed on gene ex-

pression data from patients that received either adjuvant endocrine therapy only, or a combination of endocrine- and radiation therapy. Genes were pre-ranked from most to least significantly associated with DSS based on their FDR adjusted p-value, and geneset enrichment analysis was then performed using the KEGG database to identify pathways that were enriched from the Cox regression analysis.

Table 3.1 summarises the KEGG pathways that are significantly associated with DSS in the METABRIC training cohort. Several of these genesets including base excision repair, DNA replication, pyrimidine metabolism and meiosis include genes that are involved in proliferation, which is known to be highly prognostic in breast cancer (Bianchini et al., 2013; Diest, Wall, and Baak, 2004). Therefore, these genesets provide assurance that the analysis is sound, and warrants further investigation of previously unreported prognostic genesets.

A 19-gene signature associated with fatty acid oxidation (FAO) was amongst the enriched candidate genesets (nominal $p = 0.002$, FDR adjusted p=0.038) (Fig 3.1, Table 3.1). Furthemore, the key genes in this pathway is highlighted (red circles) from the KEGG 'Fatty Acid Degradation' pathway, which was previously known as the 'Fatty Acid Metabolism' before the software was updated (Fig 3.2). Examination of the literature suggests that while fatty acid *synthesis* in cancer is well-defined, the role of fatty acid *oxidation* is unclear, and may be context-dependent (Carracedo et al., 2012; Currie et al., 2013). Since altered cellular energetics is a hallmark of cancer, metabolic pathways such as FAO could therapeutically targeted in cancer. Based on this reasoning, the 19-gene FAO signature was selected for further investigation (Table 3.2).

Table 3.1: KEGG genesets associated with disease-specific survival in the METABRIC training cohort.

Name	Enrichment score	Normalised enrichment score	Nominal p-value	FDR p-value
KEGG_VALINE_LEUCINE_AND_ ISOLEUCINE_ DEGRADATION	0.53	1.74	0	0.032
KEGG_BASE_EXCISION_REPAIR	0.55	1.71	0	0.03
KEGG_PYRIMIDINE_METABOLISM	0.48	1.68	0	0.03
KEGG_DNA_REPLICATION	0.52	1.66	0	0.03
KEGG_GLYOXYLATE_AND_ DICARBOXYLATE_ METABOLISM	0.58	1.64	0.002	0.03
KEGG_OOCYTE_MEIOSIS	0.45	1.62	0	0.03
KEGG_GLYCINE_SERINE_AND_ THREONINE_ METABOLISM	0.51	1.61	0.002	0.03
KEGG_PROTEASOME	0.48	1.58	0.002	0.04
KEGG_FATTY_ACID_METABOLISM	0.48	1.59	0.002	0.04

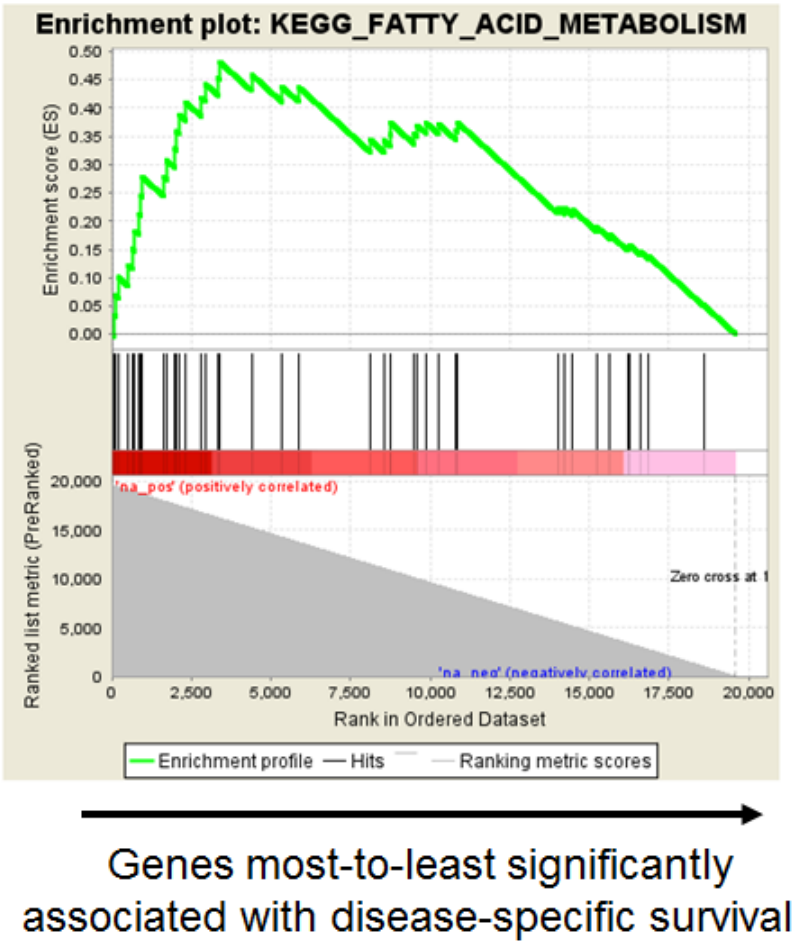

Figure 3.1: Enrichment plot of KEGG Fatty Acid Metabolism pathway. Black lines in the middle of the plot indicate genes in the KEGG Fatty Acid Metabolism geneset. Genes from left to right indicate the position of each gene in the pre-ranked list after Cox regression was performed on the training data. While the geneset had a total of 42 genes, only 19 were defined as core-enriched in the analysis.

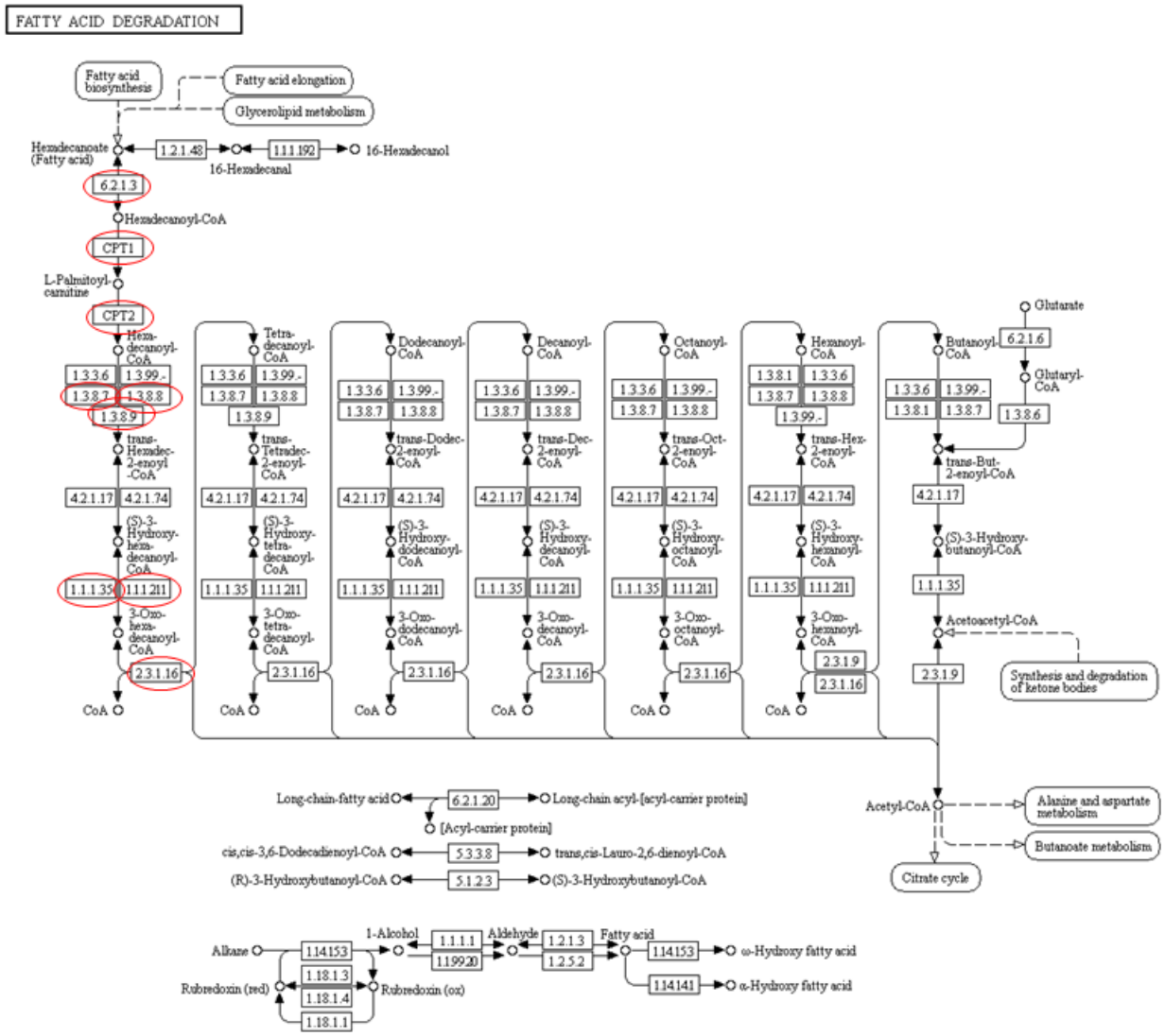

Figure 3.2: FAO genes in the KEGG Fatty Acid Degradation/Metabolism pathway. Circled in red are some genes such as *ACSL5*, *CPT1A*, *ACAD*, *HADH* and *ACAA*, all key genes in the FAO pathway.

Table 3.2: 19-gene signature involved in FAO associated with disease-specific survival in METABRIC training cohort. Genes are sorted according to their adjusted p-values.

Gene symbol	Gene name
ACAA1	acetyl-CoA acyltransferase 1
CPT1A	carnitinepalmitoyl transferase 1A
ACADM	acyl-CoA dehydrogenase, C-4 to C-12 straight chain
GCDH	glutaryl-CoA dehydrogenase
ACADS	acyl-CoA dehydrogenase, C-2 to C-3 short chain
ACAT2	acetyl-CoA acetyltransferase 2
ECI2	enoyl-CoA delta isomerase 2
ACAT1	acetyl-CoA acetyltransferase 1
ACADSB	acyl-CoA dehydrogenase, short/branched chain
CYP4A11	cytochrome P450 family 4 subfamily A member 11
ACADVL	acyl-CoA dehydrogenase, very long chain
ADH1A	alcohol dehydrogenase 1A (class I), alpha polypeptide
CPT2	carnitine palmitoyl transferase 2
HADHB	hydroxyacyl-CoA dehydrogenase/3-ketoacyl-CoA thiolase/ enoyl-CoA hydratase (trifunctional protein), beta subunit
ADH1B	alcohol dehydrogenase 1B (class I), beta polypeptide
ALDH9A1	aldehyde dehydrogenase 9 family member A1
ACSL5	acyl-CoA synthetase long-chain family member 5
ADH4	alcohol dehydrogenase 4 (class II), pi polypeptide
ALDH3A2	aldehyde dehydrogenase 3 family member A2

3.3.2 *High FAO signature expression is associated with better disease-specific survival in training dataset*

To visualise the FAO signature expression distribution in the METABRIC training cohort, a cluster analysis was performed. As shown in Fig 3.3, approximately three clusters could be *visually* determined from the heatmap: patients in cluster 1 have higher expression of the FAO signature compared to patients in cluster 3; while patients in cluster 2 exhibit more heterogenous expression of the FAO signature.

Expression of *ADH1A* and *ADH1B* genes contributed a large extent to the high FAO signature expression in cluster 1 (orange arrows). Both *ADH1A* and *ADH1B* are located next to each other on chromosome 4q23, encode enzymes that oxidise alcohol into aldehyde. At the moment, there is no evidence in the literature that ADH1A or ADH1B is involved in regulation of FAO. Additionally, cBioPortal analysis revealed no significant copy number alterations in ADH1A and ADH1B using the METABRIC and TCGA breast cancer cohorts.

Tumours from patients in cluster 3 were observed to have increased *CPT1A* and *ACAT2* expression (black arrows), although the remainder 17 genes were generally expressed lower relative to cluster 1 tumours. Of note, the emphasis in this analysis is to show that constructing a metagene from the average expression of the 19 genes is a reasonable measure of the FAO pathway in the tumour from each patient. This is important for the survival analyses that is described in the sections below.

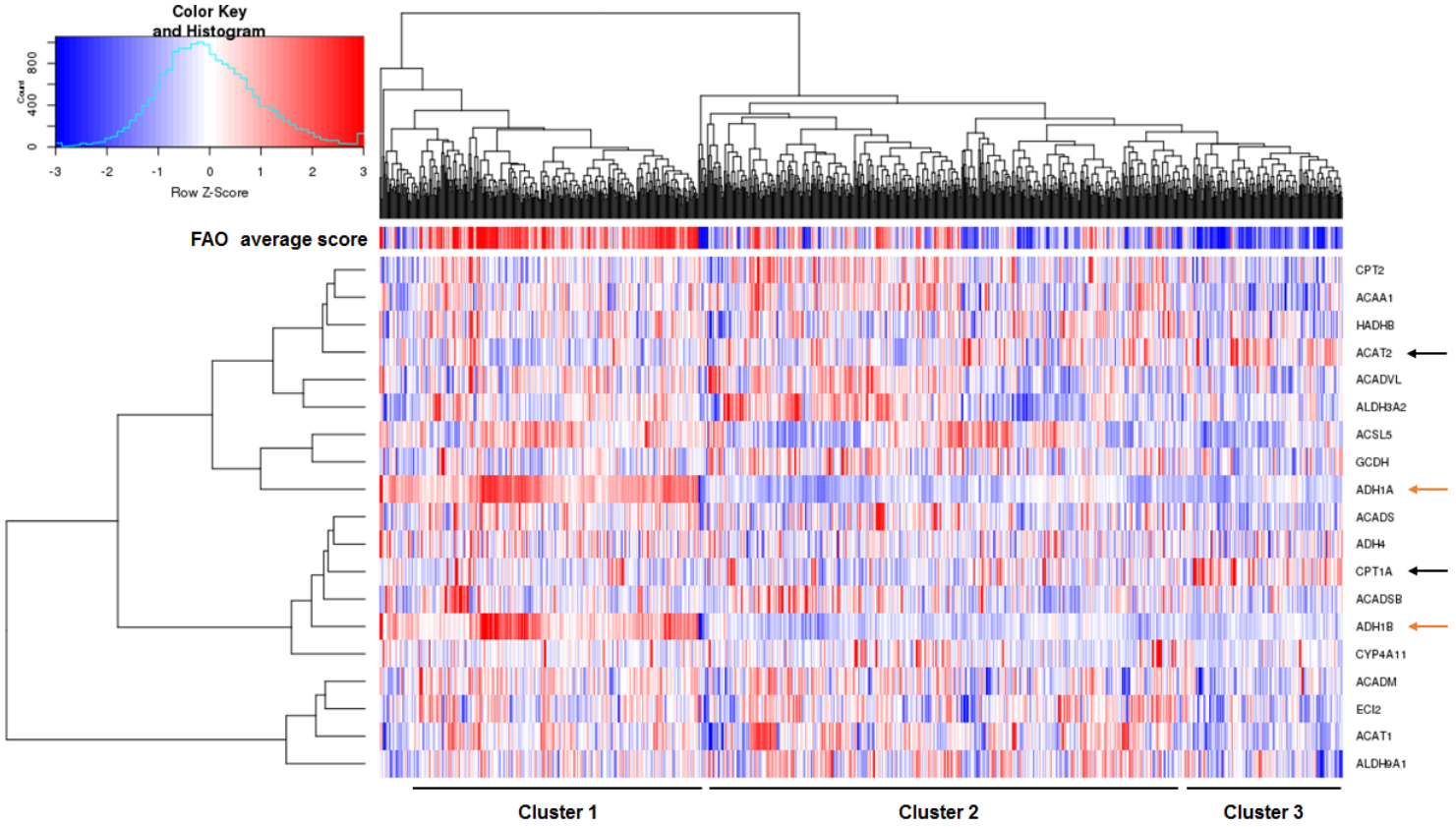

Figure 3.3: Cluster analysis of genes in the FAO signature in the METABRIC training cohort. The distribution of expression of the FAO signature in the METABRIC training cohort was visualised by cluster analysis. The distance metric was Euclidean, and complete linkage was selected as the clustering method. Red indicates higher relative expression, while blue indicates lower relative expression of genes. Columns represent each patient (n=973), while rows represent each gene as indicated on the right. The average FAO signature score is denoted on top of the heatmap, with a similar colour scale used for the cluster analysis. Black arrows indicate genes expressed higher in cluster 3, while orange arrows indicate genes expressed higher in cluster 1.

To assess how the FAO signature expression is correlated with DSS, a Kaplan-Meier survival curve was plotted using the METABRIC training data. Patients were stratified into two groups - low (below median cut-off) and high (above median cut-off), based on their average expression of the 19-gene signature. Statistical significance between curves was assessed using the log-rank test (Bland and Altman, 2004). As shown in Fig 3.4, patients with high expression of the FAO signature had better survival compared to those in the low group (log-rank test p=4.4-e06).

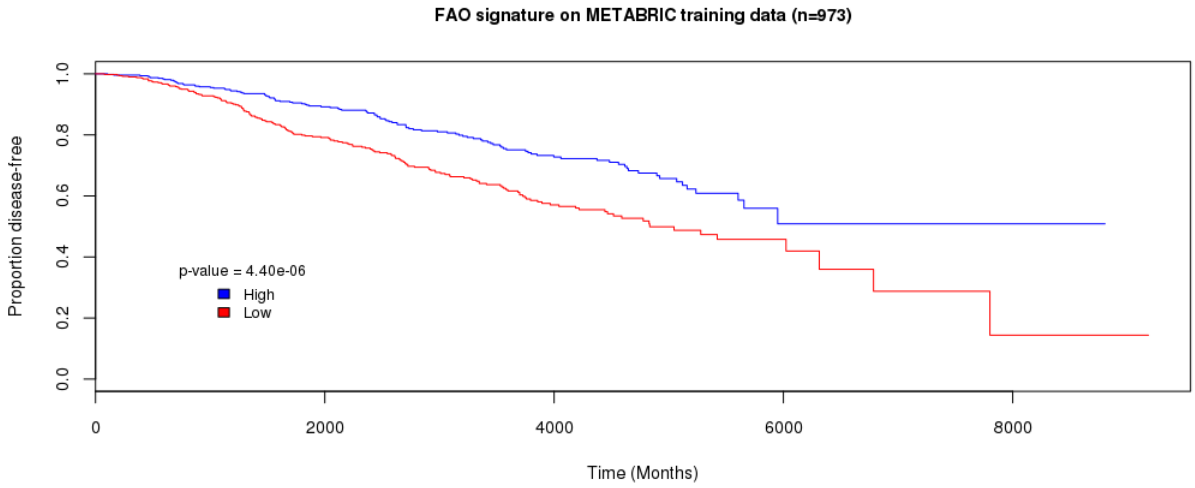

Figure 3.4: FAO signature is significantly associated with DSS of METABRIC training data. Average expression level of the signature was calculated for each patient. Based on their signature score, patients were stratified into two groups - low (below median) and high (above median cut-off). Statistical significance between curves was determined using the log-rank test.

3.3.3 *FAO signature expression is prognostic in independent breast cancer cohorts*

To investigate whether the prognostic performance of the FAO signature expression was reproducible in independent datasets, survival analysis was performed on seven independent, publicly available datasets. Of note, these datasets included those generated on different platforms (e.g. Agilent, Affymetrix, Illumina HiSeq), in addition to the Illu-

Table 3.3: FAO signature expression is associated with survival in multiple breast cancer datasets. RFS, relapse-free survival; DRFS, distant relapse-free survival; OS, overall survival. More information on the datasets is provided in Supplementary Table B59.

Dataset	n	Log rank p (survival metric)	Hazard ratio (Low vs High)	Hazard ratio 95% CI	FDR adjusted p value
GSE42568	104	0.00562 (RFS)	2.24	1.25 - 4.03	0.007
	104	9.58E-05 (OS)	4.05	1.84 - 8.66	0.000311
GSE20685	327	0.0118 (DMFS)	1.98	1.26 - 3.11	0.003
		0.00243 (OS)	1.75	1.12 - 2.27	0.013
GSE46563	94	0.000543 (DMFS)	5.46	1.86 - 16.1	0.002
GSE25066	508	5.98E-06 (DRFS)	2.43	1.64 - 3.62	1.17E-05
TCGA breast cancer cohort	776	0.00387 (RFS)	2.08	1.25 - 3.47	0.0047
	1096	0.097 (OS)	1.31	0.95 - 1.81	0.097
GSE22219	216	0.00753 (DRFS)	1.82	1.17 - 2.85	0.0085
BRCA2116	672	6.51E-05 (DRFS)	2.02	1.42 - 2.88	9.10E-05

mina BeadChip used to derive the training data. As summarised in Table 3.3, the FAO signature expression was significantly associated with distant relapse-free survival and overall survival in several breast cancer datasets. Notably, in all datasets analysed, the hazard ratio for the 'Low' group were all > 1, which suggests increased risk for an event for this group, compared to the 'High' group. Taken together, this analysis supports the concept that downregulation of genes involved in fatty acid oxidation is associated with poor survival outcomes in breast cancer. Of note, the BRCA2116 dataset - which was previously compiled and published by Associate Professor Michael Black (Nagalla et al., 2013) - was used to specifically validate the findings in the training data. In this dataset, only patients that were ER-positive and received endocrine therapy (n=672) was used to validate the performance of the FAO signature.

3.3.4 *Low FAO signature expression is correlated with clinical factors associated with poor prognosis*

To determine the correlation of the FAO signature expression with established prognostic factors, boxplots of the FAO signature expression compared to tumour grade and molecular subtype was performed. As shown in Figure 3.5a and b, the FAO signature expression was lower in ER-negative, compared to ER-positive tumours. In two independent datasets, grade 1 had higher expression of the FAO signature compared to grade 3 tumours. (Fig 3.5c,d). Furthermore, the FAO signature was expressed higher in luminal A, compared to basal/HER2-enriched molecular subtypes (Fig 3.5e-g). Therefore, the data suggests that the FAO signature expression is significantly correlated with clinical features associated with poor prognosis.

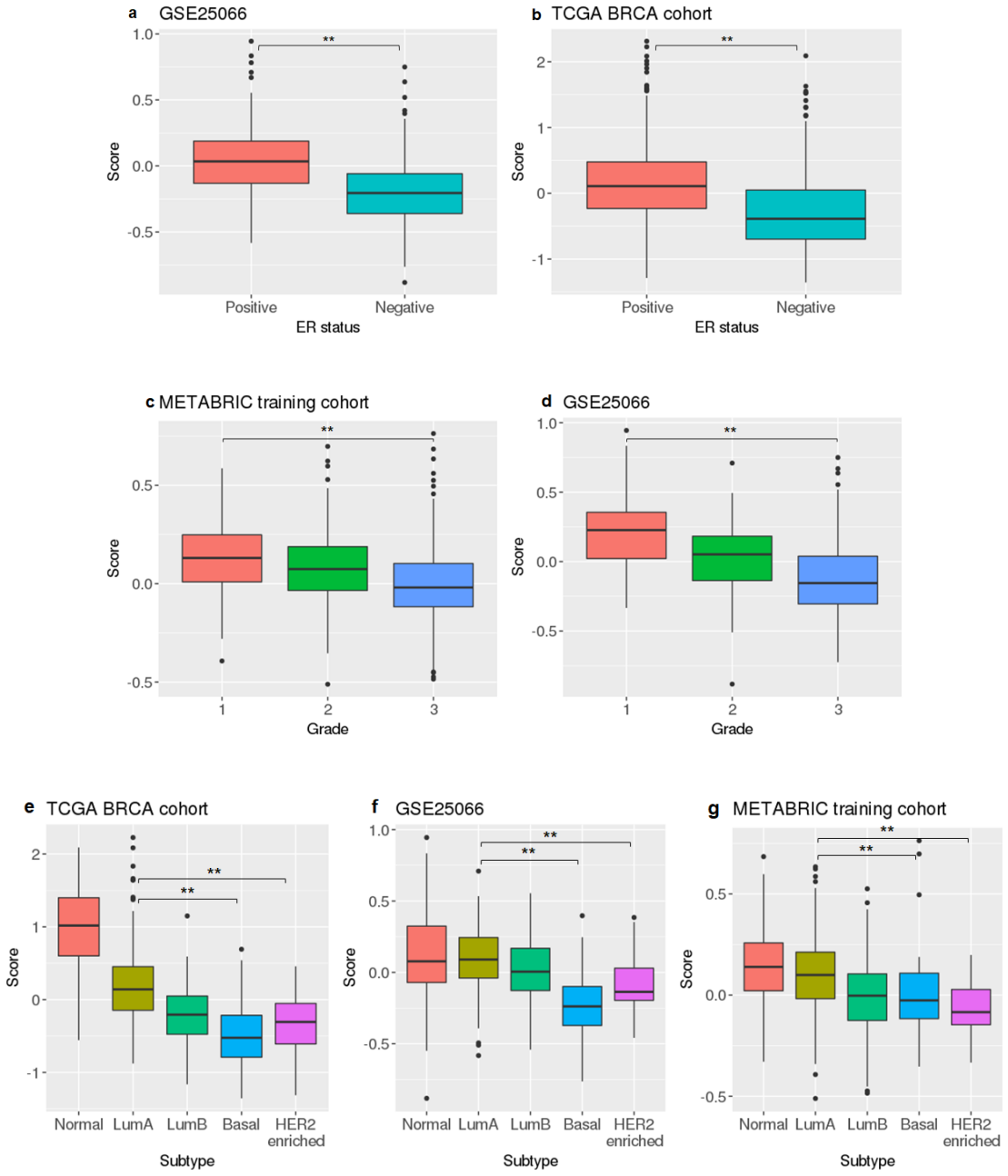

Figure 3.5: FAO signature expression higher in ER-positive, Grade 1 and luminal molecular subtype. FAO signature expression higher in (a, b) ER-positive compared to ER-negative tumours; (c,d) grade 1 compared to grade 3 tumours and (e, f, g) Luminal A compared to basal molecular subtype tumours. Wilcoxon-rank sum test $p^{**} \leq 0.01$.

Table 3.4: FAO gene signature is an independent prognostic factor in breast cancer. RFS = relapse-free survival, DRFS = distant relapse-free survival.

Dataset	Covariates	Hazard ratio (Low vs High)	FDR adjusted p-value
GSE25066 (n=466) (DRFS)	Grade, ER status	1.62	0.0592
BRCA2116 (n=660) (DRFS)	Grade, size, lymph node status	1.5	0.09
GSE42568 (n=104) (RFS)	Grade, size, lymph node status	2.55	0.009
GSE22219 (n=216) (RFS)	ER status, age, size, lymph node status	1.91	0.014
GSE46563 (n=94) (DRFS)	Grade, ER status, size	5.54	0.009
GSE20685 (n=327) (DRFS)	Age	1.7	0.009
TCGA breast cancer (RFS)	ER status	1.61	0.09

3.3.5 *FAO signature expression is prognostic independently of standard histopathological features in breast cancer*

To determine whether the FAO signature is an independent prognostic factor, multivariable Cox regression was performed by including other established clinical prognostic covariates in the model. This analysis was conducted on eight datasets and is summarised in Table 3.4. After adjustment for available clinical factors, in most datasets, the FAO signature was a significant, or trended towards an independent prognostic factor, with hazard ratios ranging from 1.3 to 5.5.

3.3.6 *FAO signature expression is inversely correlated with proliferation gene signature*

High expression of the FAO signature is associated with better survival, and low tumour proliferation is also associated with good prognosis. Therefore, the assocation between the FAO signature and proliferation was explored. An 12-gene proliferation signature known as the mitosis kinome score (MKS) was used as a molecular readout of cell proliferation (Bianchini et al., 2013). As summarised in Table 3.5, the FAO signature has a significant negative correlation with proliferation in all datasets analysed.

Table 3.5: FAO signature expression is negatively correlated with the MKS proliferation signature in breast cancer datasets. All p values are FDR adjusted.

Dataset	n	Spearman's rho	p
GSE42568	104	-0.27	5.174E-03
GSE20685	327	-0.44	<3.85E-16
GSE46563	94	-0.403	7.70E-05
GSE25066	508	-0.45	<3.85E-16
GSE22219	216	-0.6	<3.85E-16
TCGA breast cancer	1215	-0.59	<3.85E-16

3.3.7 *High FAO signature expression is associated with good response to neoadjuvant aromatase-inhibitor treatment*

In the METABRIC and BRCA2116 datasets, tamoxifen was the main anti-oestrogen administered to patients who received endocrine therapy. To investigate whether the FAO signature is also correlated with clinical response to aromatase inhibitors (AI), gene expression datasets from the FAIMoS neoadjuvant AI trial was analysed.

Tumours with *higher* FAO signature expression pre- two-week AI treatment were correlated with complete or partial response as determined by the RECIST guideline (Fig 3.6). In contrast, tumours from patients with stable or progressive disease had lower FAO signature expression before treatment.

3.3.7.1 *ESR1 knockdown in MCF7 decreases FAO signature expression relative to basal expression control*

Two lines of evidence suggest an association between oestrogen signalling and the FAO signature: (i) the signature expression was higher in ER-positive compared to ER-negative tumours and (ii) patients with good response neoadjuvant AI treatment had increased FAO signature expression.

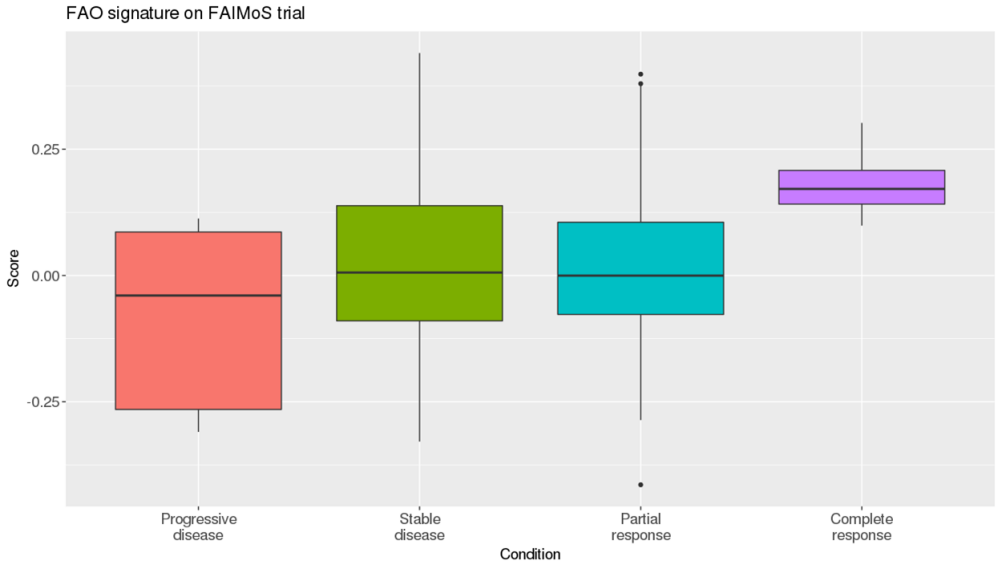

Figure 3.6: High FAO signature expression is associated with good response to short-term neoadjuvant AI treatment. FAO signature expression in 102 pre-treatment breast tumour samples with different responses to short term oestrogen withdrawal treatment (Progress n=7; complete response n=7; stable disease n=41; partial response=47). Disease progression vs complete response t-test $p = 0.039$.

To investigate how alterations in oestrogen signalling and proliferation affects the FAO signature expression, transcriptome data from MCF7 cells with *ESR1* knockdown and basal expression was analysed to compare the FAO signature expression between the two conditions (Al Saleh, Al Mulla, and Luq, 2011).

As shown in Fig 3.7, a trend between *ESR1* knockdown and decreased FAO signature expression was observed (t-test p=0.07), which achieved statistical significance when one outlier value (cirled in blue) from the *ESR1* knockdown triplicate was removed (t test p=0.0036). In this system, the MKS proliferation signature was increased, while the expression of an oestrogen responsive geneset was decreased, which suggests oestrogen-independence in *ESR1* knockdown, relative to their basal expression counterparts. Indeed, the authors of this dataset reported increased proliferation of this MCF7 cell system in their study (Al Saleh, Al Mulla, and Luq, 2011). Taken together, these data suggest that increased proliferation due to adaptation to decreased oestrogen signalling

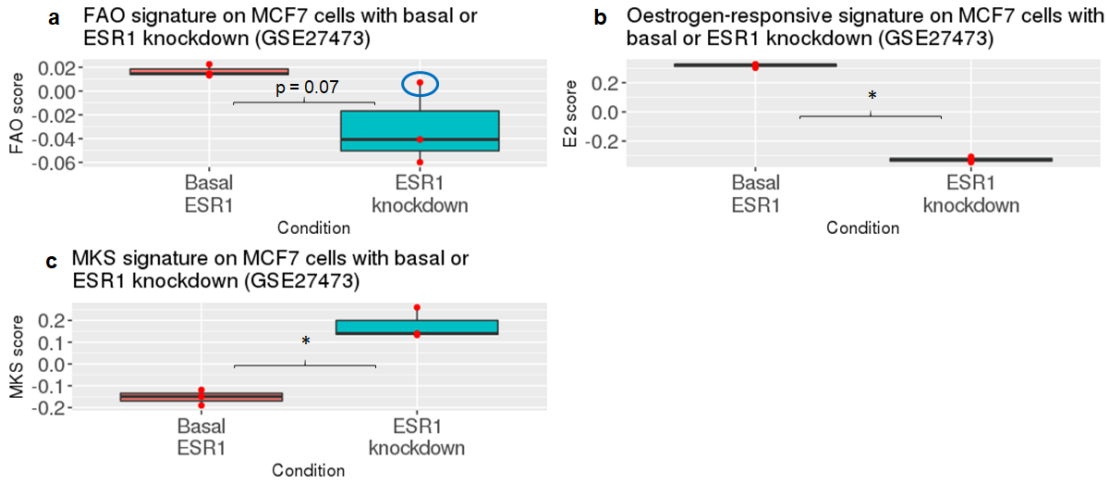

Figure 3.7: *ESR1* knockdown decreases FAO signature expression in MCF7 cell line. (a) FAO, (b) MKS and (c) oestrogen-responsive signature expression in MCF7 cells transfected with plasmid encoding *ESR1* shRNA. Control line was established from transfected cells that retained sensitivity to oestrogen and tamoxifen, most likely due to null shRNA generation. In panel (a), value circled in blue is the proposed outlier value. t-test $p^* \leq 0.05$.

decreases the FAO signature expression.

3.3.8 *Low FAO signature expression is correlated with better neoadjuvant chemotherapy response*

To determine whether the FAO signature expression was correlated with response to neoadjuvant chemotherapy, logistic regression was performed on breast tumour gene expression datasets from neoadjuvant chemotherapy clinical trials. All datasets used in this analysis are summarised in Table B.60 under 'Neoadjuvant chemotherapy'.

The average FAO signature expression score was computed for each patient, and response was defined as having achieved pathological complete response (pCR). As shown in the forest plot in Fig 3.8, *low* FAO signature score was associated with higher odds of achieving pCR. Since the signature is correlated with molecular subtypes, this finding is consistent with that of Bonnefoi *et. al.* who reported greater pCR rates for

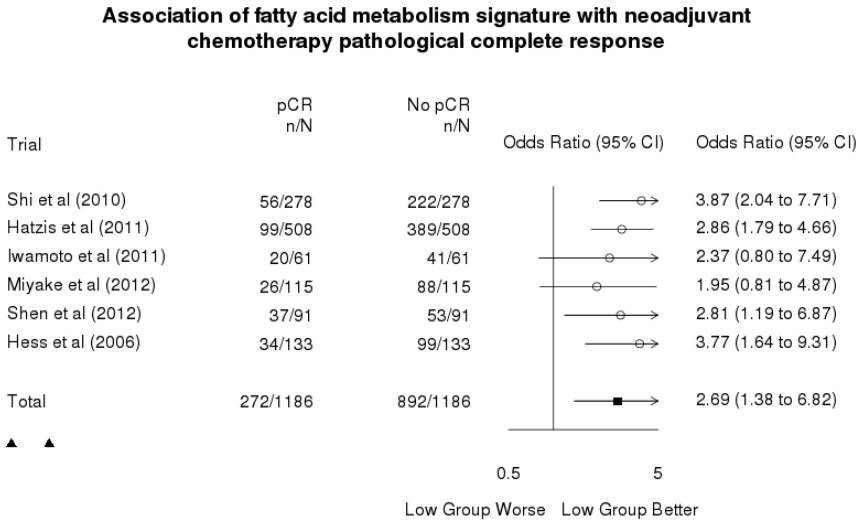

Figure 3.8: Low FAO signature expression is associated with neoadjuvant chemotherapy pCR. The n/N indicates the number of patients that achieved pCR (or not) out of the total sample size and the odds ratio gives a point estimate of the odds of achieving pCR in each trial from patients in the Low FAO signature expression group.

HER2+/non-luminal tumours, relative to luminal A tumours (Bonnefoi et al., 2014).

3.3.9 *CPT1A* is likely to be co-amplified with *CCND1* in multiple cancers

Thus far, the FAO signature expression has been shown to be correlated with good prognosis and expressed higher in tumours with favourable clinical features (e.g., ER-positive and grade 1). Gatza *et. al.* analysed the copy number and gene expression from highly proliferative breast luminal tumours and identified *CPT1A* as one of the essential genes for tumour proliferation (Gatza et al., 2014). *CPT1A* - a member of the 19-gene FAO signature - is the rate-limiting enzyme for FAO, and its amplification can be interpreted as an important feature for tumour growth. However, *CPT1A* is located in the cytogenetic band 11q13.3, which is also the cytogenetic location of *CCND1* (Fig

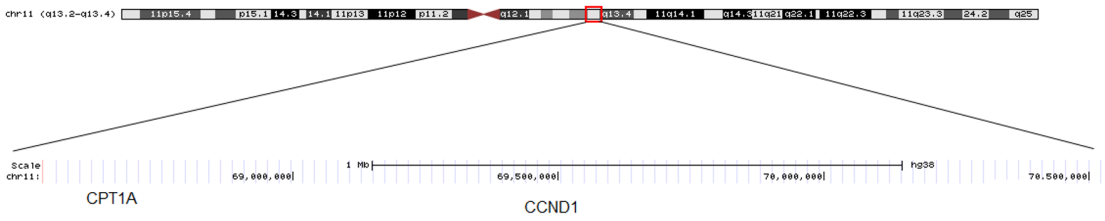

Figure 3.9: Cytogenetic locations of *CCND1* and *CPT1A* in 11q13. Genomic location of *CPT1A* relative to *CCND1* is indicated. Figure was derived from the UCSC Genome Browser.

3.9) - a key oncogene that is amplified and overexpressed in many cancers (Musgrove et al., 2011). The chromosomal proximity between these two genes begs the question: is *CPT1A* frequently co-amplified with *CCND1* in breast cancer?

To test this hypothesis, analysis of copy number data was conducted using data obtained from cBioPortal (Cerami et al., 2012; Gao et al., 2013). Three genes: *FGF3*, *FGF4*, and *CTTN* that have been shown to be co-amplified with *CCND1* were included in this analysis as 'positive' controls for 11q13 amplicon amplification (Zaharieva et al., 2003). Conversely, three genes on *other* chromosomes: *ERRB2* (chromosome 17q12), and *MELTT6* and *FGD5* (chromosome 3p25) known to be amplified at different frequencies in breast cancer were used as 'negative' controls for intra-chromosomal amplification. As observed in Fig 3.10, the amplification frequency of *CPT1A* is lower than *CCND1*. If *CCND1* is the primary amplicon driver, it is possible that genes located a substantial distance away (e.g., *CPT1A*) may not be co-amplified in some cases. Hence in most cases, when *CPT1A* is amplified, so is *CNCD1*; but the reverse is rarely true.

Using the METABRIC copy number data, 16% of the cohort had *CCND1* amplification, while 9% had a *CPT1A* amplification (Fig 3.10a). Both amplifications had a significant tendency to co-occur (odds ratio >3, Fisher's exact test p=<0.001). Similar observations were also made in the breast TCGA cohort (Fig 3.10b). Furthermore, analysis of

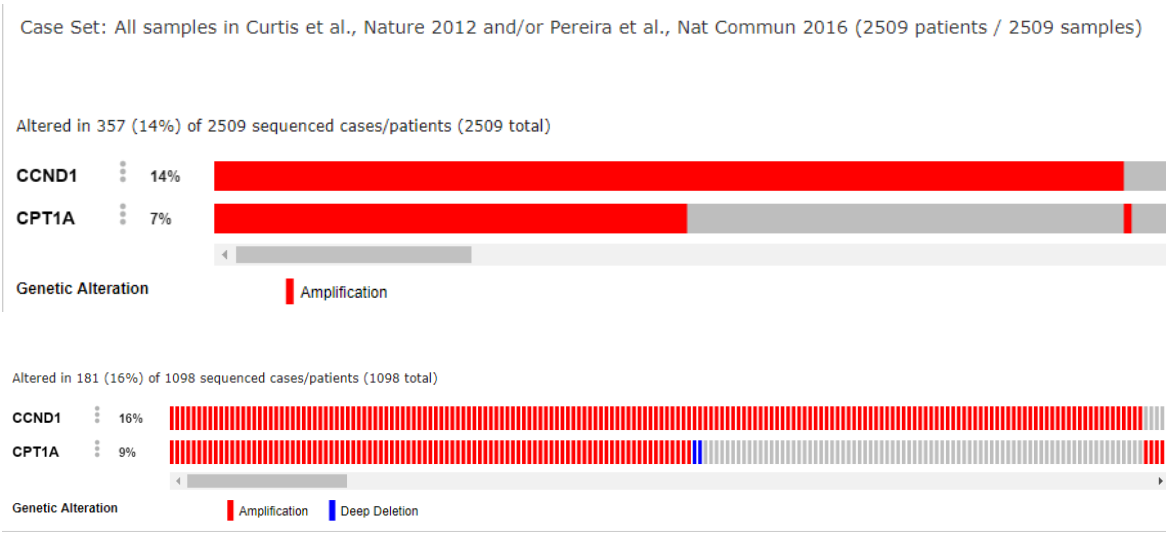

Figure 3.10: *CPT1A* is likely to be co-amplified with *CCND1* in breast cancer. cBioPortal copy number analysis of *CPT1A* and *CCND1* in (a) METABRIC and (b) TCGA cohort. In both panels, red bars indicate amplification events. In panel (b) the blue bars indicate deletion events. Of note, each column represents a single patient. This is particularly more obvious in panel (b).

other cancer types found frequent co-amplification of *CPT1A* and *CCND1*, which suggests a positive selection of this amplicon across multiple cancers (Table 3.6). Analysis performed on copy number data from the Cancer Cell Line Encyclopaedia found 73 cell lines with *CCND1* and *CPT1A* co-amplification, and is summarised in Supplementary Table B.2. Taken together, findings from these analyses suggest that *CPT1A* is likely to be co-amplified with *CCND1* within the 11q13 locus in a small subset of cancers.

3.3.10 *FAO signature is prognostic in multiple cancers*

To investigate whether the prognostic capacity of the FAO signature could be extended to other cancers, survival analysis based on the FAO signature expression was performed using datasets available from the KMplotter online software (www.kmplot.com) or accessed from public repositories. As shown in Fig 3.11, the FAO signature was associated with overall survival in lung and gastric cancers, and TCGA clear cell renal cell

Table 3.6: *CPT1A* is likely to be co-amplified with *CCND1* in multiple cancers. This table was derived from the output from cBioPortal. The log odds ratio calculates the odds of co-occurence of amplifications between *CCND1* and *CPT1A*. The statistical significance of the co-amplification was calculated using Fisher's exact test.

Cancer type (study)	**CCND1 amplification frequency (%)**	**CPT1A amplification frequency (%)**	**Log odds ratio**	**p**
Oesphageal (n=186) (TCGA, provisional)	35	20	>3	<0.001
Head and neck (n=279) (TCGA, Nature 2015)	28	15	>3	<0.001
Neuroendocrine prostate cancer (n=114) (Trento/Cornell/Broad 2016)	27	27	>3	<0.001
Lung squamous (n=504) (TCGA, provisional)	14	6	>3	<0.001
Bladder urothelial carcinoma (n=413) (TCGA, provisional)	12	7	>3	<0.001
Cholangiocarcinoma (n=36) (TCGA, provisional)	11	6	>3	<0.001
Pancreatic (n=109) (UTSW, Nature Commun 2015)	9	7	>3	<0.001
Ovarian serous (n=606) (TCGA, provisional)	7	6	>3	<0.001
Stomach adenocarcinoma (n=295) (TCGA, Nature 2014)	7	6	>3	<0.001
Cutaneous melanoma (n=479) (TCGA, provisional)	7	5	>3	<0.001
Hepatocellular carcinoma (n=442) (TCGA, provisional)	7	4	>3	<0.001

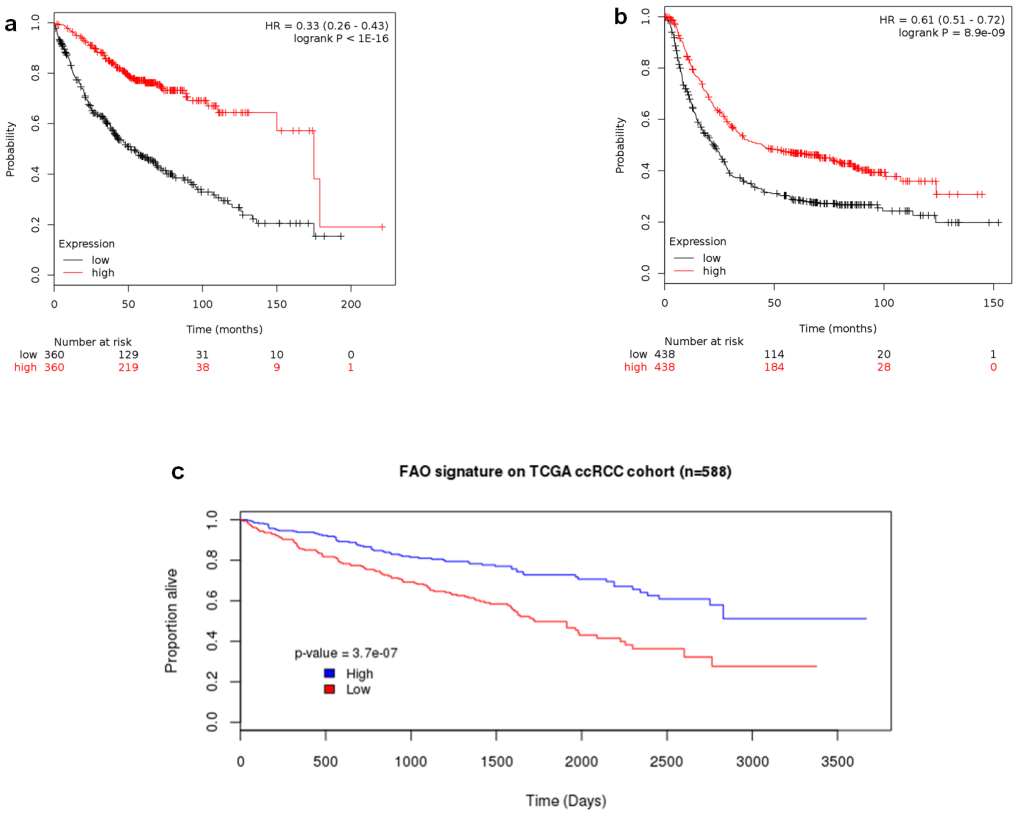

Figure 3.11: FAO signature expression is associated with overall survival in different cancers. The prognostic performance of the FAO signature was assessed in (a) lung adenocarcinoma (n=720) and (b) gastric cancer (n=876) using the KMplotter online software. (c) FAO signature expression is associated with overall survival in TCGA ccRCC cohort (n=588).

carcinoma (ccRCC) (Szasz et al., 2016; Creighton et al., 2013). Furthermore, the signature expression was a significant prognostic factor in ccRCC after adjusting for tumour size and stage (HR 1.77, p=0.0002). In melanoma, higher FAO signature expression was correlated with better survival. In the GSE65904 dataset reported by Cirenajwis *et. al.*, high FAO signature expression was associated with better disease-free survival (Fig 3.12a), while in the TCGA cohort, the FAO signature expression was significantly associated with overall survival (Fig 3.12b) (Cirenajwis et al., 2015; Akbani et al., 2015).

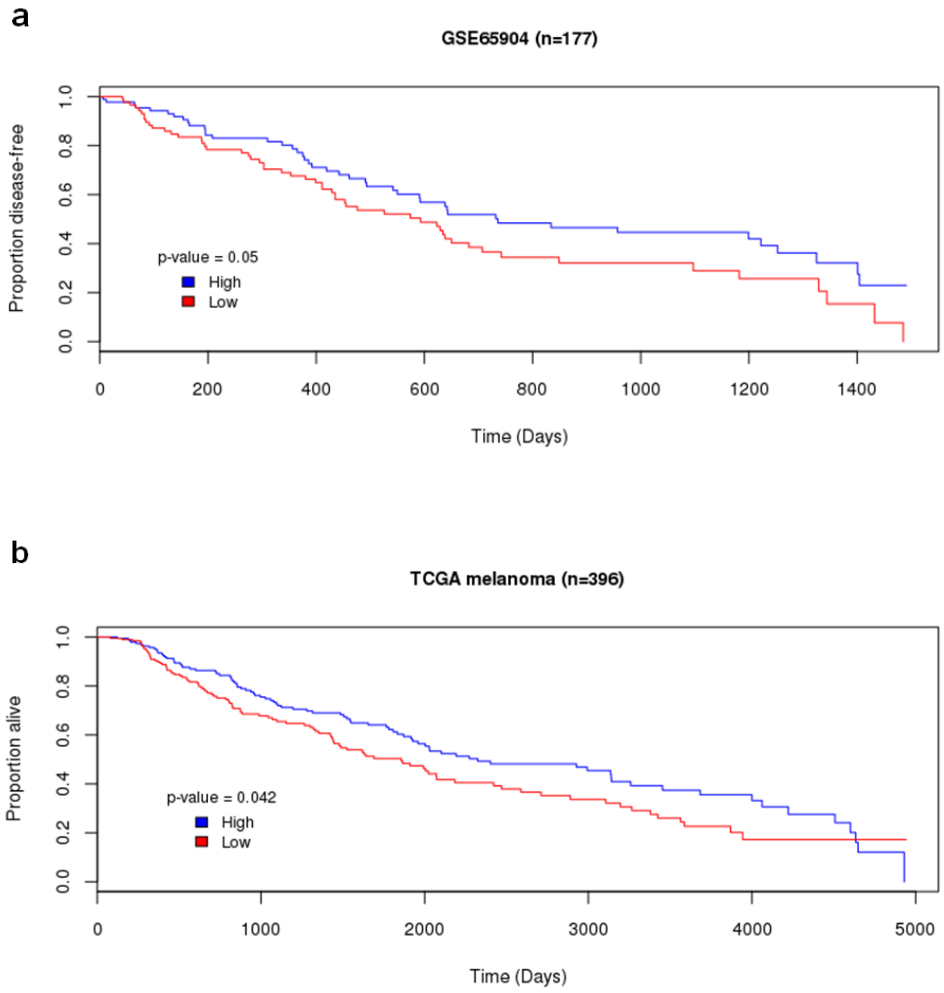

Figure 3.12: FAO signature expression is associated with melanoma survival in different datasets. The FAO signature is associated with (a) disease-specific survival (GSE65904, n=177) and (b) overall survival (TCGA cohort, n=396).

3.3.11 *FAO signature expression is down-regulated in tumour compared to normal tissues*

To investigate how the FAO signature expression compares between normal and tumour tissues, gene expression datasets from multiple cancers with associated normal tissues were analysed. As shown in Fig 3.13 and 3.14, the FAO signature was down regulated in 11 different tumour types compared to their normal counterparts. Additionally, in prostate- (Fig 3.13d), oral- (Fig 3.14d) and bladder (Fig 3.14e) cancers, there was a clear downregulation of the FAO signature expression from healthy, normal tissues to increased disease states. Of note, the scales on the y-axis vary between different datasets due to different normalisation methods (e.g., robust multichip average or MicroArray Suite 5.0) performed by authors that deposit these datasets. Regardless of this methodological difference, the trend of decreased FAO signature expression in tumour tissues was consistent across all cancer types analysed.

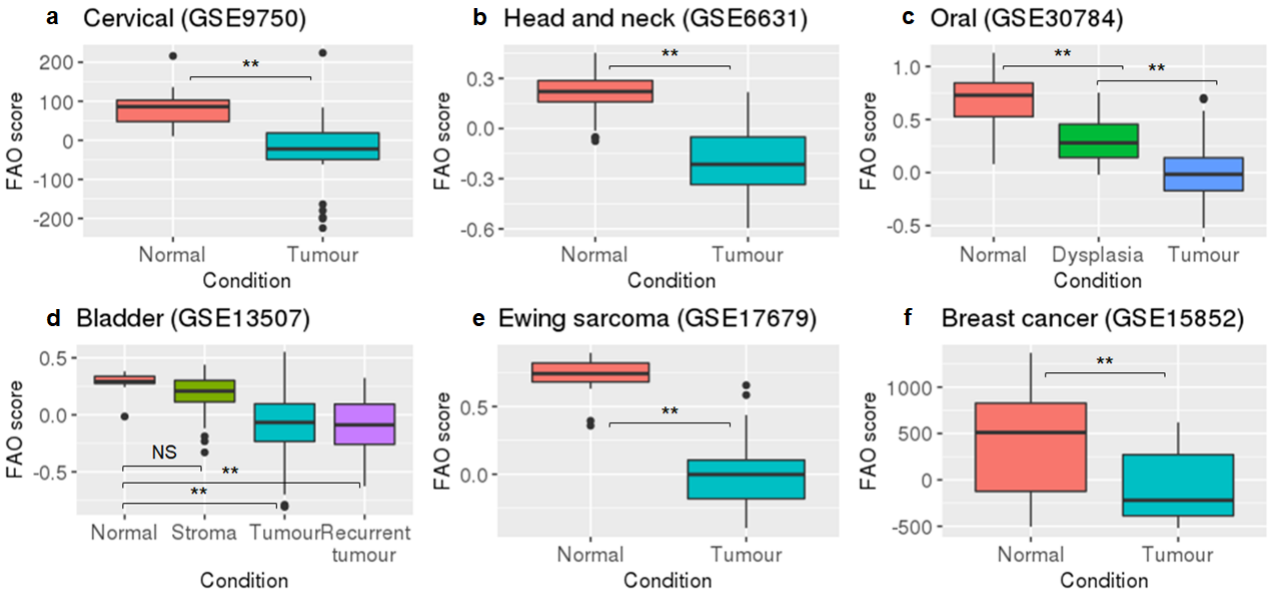

Figure 3.14: (a-e) **FAO signature is downregulated in tumours compared to normal tissues**. FDR-adjusted p **$\leq$0.01.

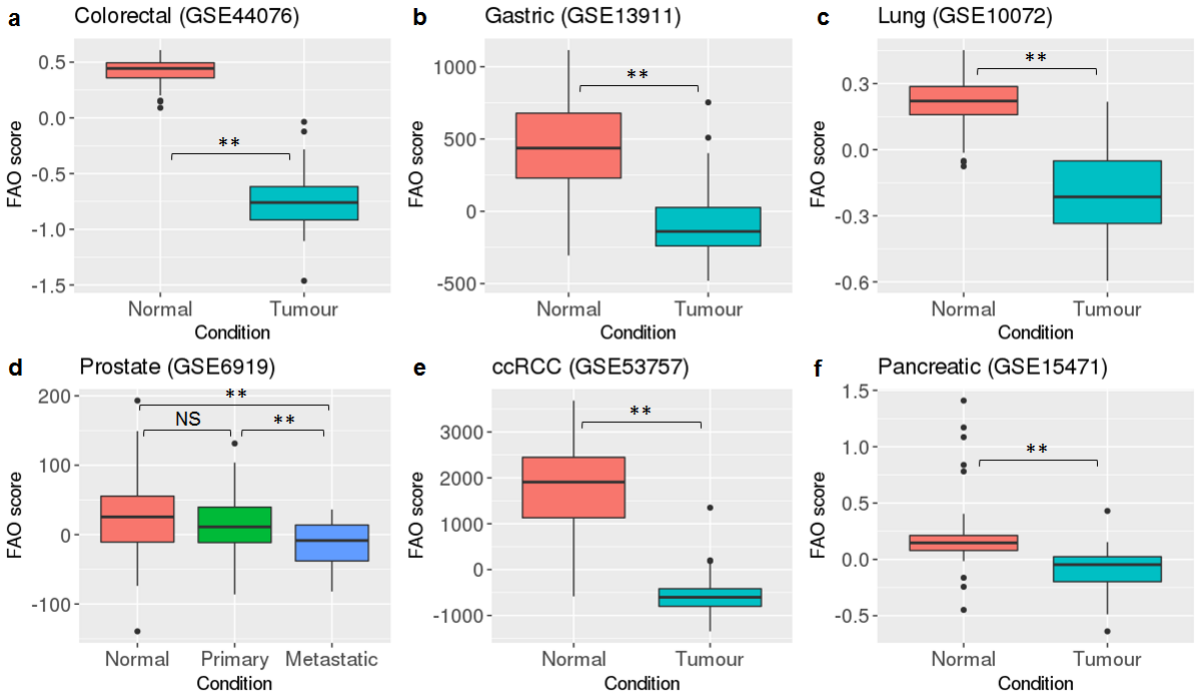

Figure 3.13: (a-f) **FAO signature is downregulated in tumours compared to normal tissues**. FDR-adjusted p **$\leq$0.01; NS = non-significant.

3.3.11.1 *Androgen-deprivation increases FAO signature expression in prostate cancer*

Apart from breast cancer, prostate cancer is another hormone-driven malignancy: over 95% of prostate tumours express the androgen receptor (Leav et al., 2001). Castration - a means of depriving prostate cancer cells of androgen - is the first line treatment for androgen-dependent tumours, analogous to oestrogen-withdrawal treatment in ER-positive breast cancer. To investigate whether the findings observed between the association of the FAO signature and inhibition of oestrogen signalling demonstrated earlier could also be extended to prostate cancer, gene expression datasets from mouse tumour xenografts post-castration were analysed.

In the GSE33316 dataset generated by Sun *et. al.* (Sun et al., 2014), surgical castration of mice with LuCaP35 xenografts resulted in the decreased expression of an androgen-

responsive geneset, which indicates decreased androgen signalling (Fig 3.15c). Consequently, proliferation was lowered in castrated mice, compared to the sham-treated counterparts (Fig 3.15b). Notably, the FAO signature expression was significantly increased in castrated, compared to sham-treated mice (Fig 3.15a). In an independent dataset using tissue from KuCaP2 xenograft (Terada et al., 2010), castrate-resistant tumours reacquired their androgen signalling and proliferation to levels similar to androgen-dependent tissue (Fig 3.15f). The FAO signature was significantly down regulated in the castrate-resistant, compared to androgen-dependent tissue (Fig 3.15d).

3.4 Discussion

3.4.1 *FAO signature expression is prognostic independently of standard histopathological features in breast cancer*

The FAO signature is one of several genesets that are associated with adjuvant endocrine treatment resistance. However, the signature expression was also found to be correlated with outcome in the adjuvant or neoadjuvant settings in several breast cancer cohorts, of which some were from chemotherapy clinical trials. In the endocrine- or chemotherapy treated adjuvant setting, *high* FAO signature expression was observed to correlate with *better* recurrence-free or overall survival in multiple breast cancer datasets. After adjusting for prognostic clinical factors, the signature expression remained significantly associated with survival.

In the neoadjuvant setting, the FAO signature expression was *higher* in post-, compared to pre-treatment biopsies of patients that had *good* response to short term AI treatment. In contrast, no significant difference in the FAO signature expression was observed in poor responders when comparing the pre- and post-treatment biopsies. In neoadjuvant chemotherapy trials, *low* signature expression in the primary biopsies was observed

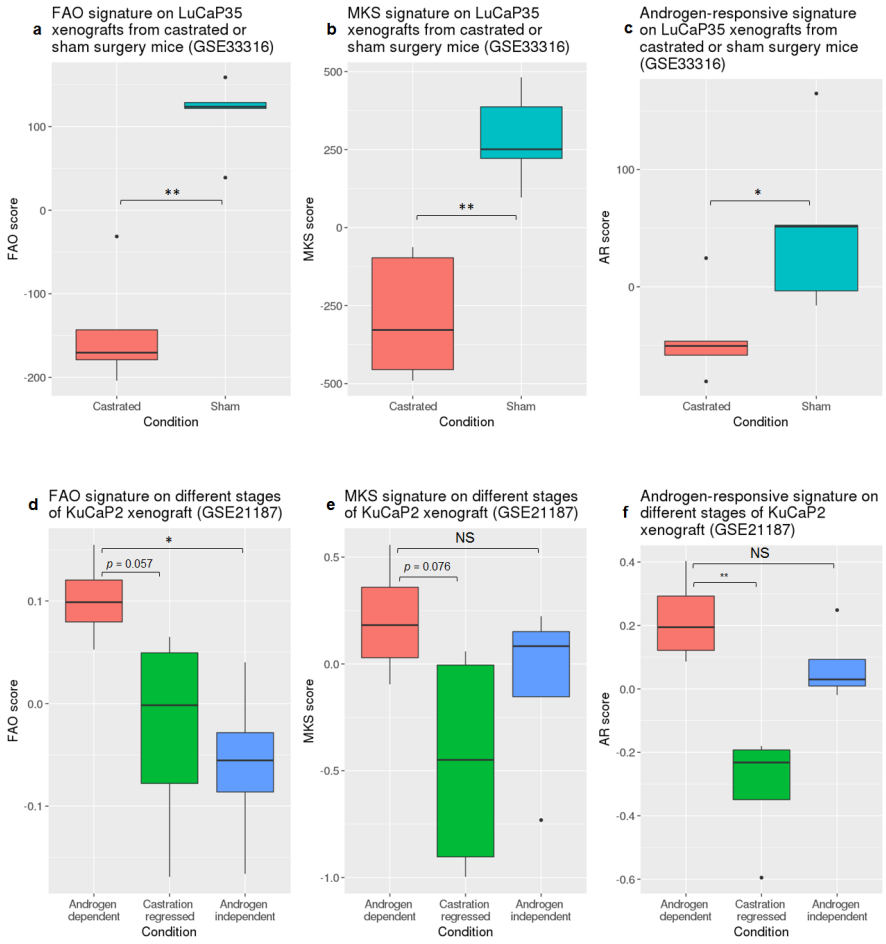

Figure 3.15: FAO signature expression is altered in castrated or androgen-independent prostate xenografts in mice. (**a-c**)(a) FAO, (b) MKS and (c) androgen-responsive signature expression in LuCaP35 xenografts inoculated subcutaneously for one month, and then tumours harvested one month post castration or sham surgery. n=5 for both conditions. (**d-f**) (d) FAO, (e) MKS and (f) androgen-responsive signature expression in KuCaP2 xenografts established in mice and tissues harvested at various stages pre- (androgen-dependent) and post-castration (regressed, androgen-independent). n=4 for all conditions.

to be significantly associated with achieving a complete pathological response. Given that the FAO signature was negatively correlated with the MKS proliferation signature, these findings suggest an association between proliferation and FAO in primary tumours.

The FAO signature expression was higher in ER-positive and grade 1, compared to ER-negative, grade 3 breast tumours. What evidence is available currently that could possibly explain the inverse relationship between tumour ER status and the FAO signature expression? Using isotope-labelling and mass spectrometry metabolome analysis, Louie *et. al.* demonstrated the different fates of exogenous palmitate in a panel of cancer cell lines, including breast cancer (Louie et al., 2013). The ER-negative, highly invasive MDA MB231 cell line incorporated exogenous palmitate into structural and signalling lipid molecules, while the ER-positive, poorly invasive MCF7 cell line directed exogenous fatty acids to generate acylcarnitine, a precursor of β-oxidation. As such, the different fates of palmitate between these two cell lines could explain why the FAO signature expression differs between ER-positive and negative tumours. Additionally, since FAO occurs in the mitochondria, one cannot discount a general decreased mitochondrial respiration in cancer cells. Indeed, oxygen consumption analysis on a panel of breast cancer cells indicate that MDA-MB231 cells have a higher extracellular acidification rate (ECAR)-to-oxygen consumption rate (OCR), which suggests higher aerobic glycolysis in MDA MB231, relative to MCF7 cells (Pelicano et al., 2014). In contrast, MCF7 cells have a higher OCR:ECAR ratio, which suggests more active mitochondrial oxidative metabolism.

3.4.1.1 *ESR1 knockdown decreases FAO signature expression in MCF7 cell line*

Based on the observation that patients with good response to AI treatment - which blocks oestrogen signalling - had increased FAO signature expression, the relationship

between *ESR1* expression and FAO signature expression was explored. It should be noted that the increased expression of the FAO signature expression in patients that respond or achieved complete response to short term oestrogen withdrawal therapy is likely due to decreased tumour proliferation.

In MCF7 cells, knockdown of *ESR1* *decreased* the FAO signature expression, while expression of the MKS proliferation signature was increased. One possibility for the increased proliferation is that this particular population of cells could have engaged alternative signalling pathways to bypass decreased oestrogen signalling, and therefore, phenocopies endocrine-treatment resistance. As such, the *decreased* FAO signature expression observed in *oestrogen-independent* MCF7 cells complements the finding of increased signature expression in patients with good response to neoadjuvant anti-oestrogen treatment. These results do not imply that genes involved in FAO are directly regulated by ER. More likely, these findings suggest the decrease in the FAO pathway in proliferating cells. Instead, these findings suggests that the alterations in other pathways brought about by oestrogen dependence (or independence) may indirectly rewire expression of genes involved in FAO.

3.4.2 *CPT1A is co-amplified with CCND1 in multiple cancers*

An unexpected, but intriguing finding in this chapter is the observation that *CPT1A* is co-amplified with *CCND1* in several cancers. This analysis was motivated the findings of Gatza *et. al.*, who reported *CPT1A* as an essential gene in a subset of highly proliferative breast luminal tumours (Gatza et al., 2014). *CCND1* is located within the same cytoband as *CPT1A*, and is more commonly amplified in ER-positive, compared to ER-negative breast tumours (Elsheikh et al., 2008). Analysis of copy number data in multiple cancers suggests *CPT1A* is most likely co-amplified with *CCND1*. This may explain why tumours with *CPT1A* amplification were highly proliferative. Furthermore,

FGF3 and *FGF4* were amplified at similar frequency as *CCDN1*. The FGF family is associated with tumour initiation and progression, and phase I/II trials that inhibit FGF receptor signalling was shown to exhibit antitumour response (Dieci et al., 2013; Turner and Reis-Filho, 2006; Jing et al., 2016).

Of all the amplified genes that were associated with high proliferation identified by Gatza *et. al.* (Gatza et al., 2014), only *CPT1A* expression was not associated with survival in two independent datasets. However, several reports have interpreted the increased expression or amplification of *CPT1A per se* as an important oncogenic event. Using the cBioPortal database, Balaban *et. al.* found ER-positive tumours with *CPT1A* alterations to have worse overall survival than what was defined as 'normal' expression (Balaban et al., 2017). It was not clear how the cut-offs were defined, and this finding was not reproduced in an independent dataset. It is tempting to speculate that patients with 'alterations' in *CPT1A* may also have *CCND1* amplification. In their review, Deep *et. al.* mentioned 22% of patients from a cohort of neuroendocrine prostate tumours (Trento/Cornell/Broad dataset) that were resistant to anti-androgens had amplifications in *CPT1A*, which were likely to *drive* the resistance phenotype (Deep and Schlaepfer, 2016). Based on this, the authors proposed inhibiting FAO as a second-line treatment in these androgen-independent tumours. As shown in Table 3.6, in this dataset, *CCND1* and *CPT1A* were co-amplified at a frequency of 27%. It was not apparent whether Deep *et. al.* were aware of *CCND1* and *CPT1A* co-amplification in these tumours.

Experimental evidence is required to demonstrate that amplification of *CPT1A* is indeed oncogenic, and not a passenger event of *CCND1* amplification. If *CPT1A* amplification is a selected trait, this should make the cancer cells more sensitive to CPT1A small molecule inhibition such as etomoxir, compared to cells that are not amplified at that locus. Similarly, cells with *CCND1* amplification would be more sensitive to CDK4/6 inhibition (e.g., palbociclib), relative to non-amplified cells. If the latter, but not for-

mer, is true, then a case with experimental evidence can be made against *CPT1A* as an oncogene in subset of cancers with 11q13 amplification.

3.4.3 *FAO signature expression is lower in tumours, compared to normal tissues; and is prognostic in several cancer types*

Even though the FAO signature was generated using gene expression data from breast cancer, the prognostic association of this signature was also observed in gastric, lung and kidney cancers, and melanoma. The subsections below provide a discourse of the FAO signature in terms of its prognostic capacity and expression between tumour and normal tissues, taking the literature into consideration.

3.4.3.1 *Gastric cancer*

In gastric cancer, the survival curves for both high and low FAO signature expression groups showed a steep initial decline, which is characteristic of advanced disease due to late diagnosis. Nonetheless, the signature significantly risk-stratified patients. In addition, the FAO signature was found to be down regulated in tumour, compared to normal tissues. This finding is in agreement with a pilot study by Enjoji *et.al*, who reported decreased expression of genes involved in fatty acid β-oxidation in gastric tumours, compared to normal tissues (Enjoji et al., 2016). On the other hand, the authors observed increased expression of genes involved in lipid synthesis (e.g., *ACC1, FAS, SREBP1C*) in cancer relative to normal gastric tissues. These findings are consistent with the known mutually exclusive activity between fatty acid catabolic and anabolic reactions.

3.4.3.2 *Lung cancer*

The lung cancer dataset used in the KMplotter analysis comprised both squamous and adenocarcinoma cases. Analysis of both histological subtypes combined showed a substantial separation of the Kaplan-Meier curves. When analysed as individual histological subtypes, the signature was strongly prognostic in the adenocarcinoma only cohort, but no significant difference in survival was observed in the squamous cell only cohort. This could be due to squamous cell lung cancer having very low fatty acid oxidation activity, such that it is not feasible to stratify patients further based on this pathway. This is supported by the lower FAO signature expression in squamous, compared to adenocarcinoma of the lung (Supp Fig A.1).

Treatment of lung adenocarcinoma cell lines with pioglitazone - an agonist of the nuclear receptor PPAR agonist - resulted in increased fatty acid oxidation (Srivastava et al., 2014). The increased oxidative metabolism resulted in the generation of reactive oxygen species, leading to the activation of the retinoblastoma tumour suppresor protein and cell cycle arrest. Furthermore, the increased FAO in response to pioglitazone treatment resulted in decreased glutamine oxidation, a key anaplerotic pathway utilised by cancer cells. Therefore, the Srivastava *et. al.* study suggests that pharmacologically induced increase in FAO can halt the cell cycle of lung cancer cells, and rewire the metabolic state toward a less proliferative state.

3.4.3.3 *Clear cell renal cell cancer*

In ccRCC, inactivation of *VHL* occurs in approximately 90% of tumours, which consequently stabilises the transcription factor HIF1A (Nickerson et al., 2008). This results in the transcriptional activation of genes involved in glycolysis and lactate efflux such as *GLUT1, LDHA* and *MCFT4*, and anaplerotic pathways (Pinthus et al., 2011). However, the role FAO in this extensive metabolic rewiring observed in this disease remains

poorly characterised.

The FAO signature was expressed higher in normal kidney, compared to ccRCC tumours. This finding is a more relevant extension of that reported by La Gory *et. al*, whom observed a decreased expression of a geneset involved in FAO in 786-O ccRCC cell line compared to normal kidney cells (LaGory et al., 2015).

Survival analysis using the ccRCC TCGA cohort found that patients with high FAO signature expression had better overall survival, compared to patients in the low group. Notably, the FAO signature expression was an independent prognostic factor after adjusting for tumour grade and stage. ccRCC can be classified into two molecular subtypes: ccA and ccB (Brannon et al., 2014). The ccA subtype had increased expression of genes involved in FAO, angiogenesis, and decreased expression of cell cycle and EMT-related genes, relative to the ccB subtype. Importantly, patients assigned the ccA subtype had *better* disease- and overall survival, compared to the ccB subtype. In another study, combined proteomics and metabolomics of ccRCC tissues revealed decreased abundance and activity of enzymes involved in the FAO pathway with increasing tumour grade. Taken together, findings in this chapter corroborate and extend those in the literature (Brannon et al., 2014; LaGory et al., 2015), and show for the first time, a prognostic association between FAO and survival in ccRCC.

3.4.3.4 *Colorectal cancer*

In colorectal tumour-normal analysis, the FAO signature was down regulated as the disease progressed from normal tissue to benign adenoma to adenocarcinoma, which suggests the reprogramming of FAO during disease progression. Laser capture microdissected tumours had lower FAO signature expression compared to bulk tumour sections, which suggests the alteration is mainly from tumour, rather than stromal cells (Supp

Fig A.2). These findings are in agreement with that of Wisnieswki *et. al.*, who reported decreased protein abundance of most of the enzymes involved in FAO, including CPT1A, CPT2 and ACAD (Wisniewski et al., 2015).

3.4.3.5 *Prostate cancer*

In prostate tumours, the signature expression was lower in tumours, relative to normal prostate tissues. Furthermore, castrate-resistant tumours had lower signature expression compared to benign and local disease. Analysis of xenograft studies showed that the FAO signature was increased upon castration, and castrate-resistant tumours had decreased signature expression relative to androgen-dependent tissues. Furthermore, the MKS and FAO signatures were inversely expressed in these prostate cancer studies, which supports the negative correlation between both signatures observed in breast cancer.

The findings from the analysis above corroborates several recent studies reported in the literature regarding the role of FAO in prostate cancer. By performing a bioinformatics screeen on several prostate tumour datasets, Torrano *et. al.* identified low peroxisome proliferator gamma co-activator 1 alpha (PGC1A) - a key oxidative metabolism transcriptional co-regulator - expression to be associated with poor prognosis (Torrano et al., 2016). Overexpression of PGC1A in DU145, PC3 and LNCaP prostate cancer cell lines promoted beta-oxidation, decreased growth rates of all three cell lines; and lowered anchorage-independent growth and bromodeoxyuridine incorporation in PC3 cells. In another study, FAO flux analysis using the Seahorse XF system in syngeneic RWPE-1 normal prostate epithelial cells with increasing degree of invasiveness found highly invasive clones to have *decreased* FAO flux, relative to the parental epithelial and pre-malignant counterparts (Vayalil and Landar, 2015). Additionally, Dueregger *et. al.* showed that RWPE-l cells were more capable of utilising exogenous lipid for energetic

purposes, compared to prostate cancer cell lines (Dueregger et al., 2015).

3.5 Summary, strengths and limitations

To summarise, the 19-gene FAO signature expression is:

1. prognostic in breast and several other cancer types
2. associated with response to neoadjuvant endocrine or chemotherapy in breast cancer
3. expressed lower in tumour, compared to normal tissues in 11 different cancers

An overarching finding in this chapter is the inverse correlation between the FAO and MKS proliferation signatures. This raises two questions: (i) why is FAO decreased in proliferating cells, and (ii) what is the effect of modulating FAO on cancer cell proliferation? Answering these questions in experimental systems might shed new insights on how an important metabolic pathway intersects with proliferation, and may reveal potential therapeutic opportunities.

The strength of this chapter is that the validation exercise robustly reproduced the prognostic performance of the FAO signature in seven independent breast cancer datasets, as well as on datasets from other cancer types. Furthermore, tumour-normal analysis of the FAO signature expression was also performed across a panel of cancer types. In short, the comprehensive analyses in term of sample size and range of tumour type undertaken and described in this chapter provides strong statistical support for observations made.

There are also limitations to this analyses presented in this chapter. Firstly, all of the analyses conducted were based on mRNA expression. Establishing a correlation between gene and protein expression of metabolic enzymes in tumour tissues is not trivial, given that many factors, including tissue type, contexts such as hypoxia and locale of a particular biopsy relative to the whole tumour, need to be considered. Furthermore, metabolic

pathway flux is regulated by a minority of rate-limiting enzymes, relative to all enzymes involved in the pathway. Therefore, deriving a pathway surrogate from the average score of all 19 genes from the FAO signature may not fully represent its *activity* level. However, proteogenomic correlation analysis of TCGA colorectal and breast cancer cohorts found a correlation between mRNA and protein expression levels (Spearman's rho = 0.47 for colorectal cohort, FDR p= 9.42e-5 for colorectal, rho = 0.5-0.75 for breast cohort, p=0.009), supporting studies such as this as a 'first-pass' to evaluate pathway activity (Mertins et al., 2016; Zhang et al., 2014). Furthermore, proteome analysis of metabolic enzymes between normal colon, adenoma and laser microdissected tumours found a decreased expression of enzymes involved in beta-oxidation in tumours, relative to healthy colon tissue (Wisniewski et al., 2015). Therefore, these data suggest that, in colorectal and breast cancer at least, there is some correlation between mRNA and protein expression of genes involved in FAO. However, proteome analysis of other tumours would be required to further substantiate the mRNA-protein correlation in other tumour types.

Secondly, it is possible that other mechanisms (e.g., post-translational phosphorylation, acetylation, epigenetic) could affect the activity of a particular metabolic enzyme regulation, which would not be observed at the mRNA level. Thirdly, metabolic pathways do not occur in silos, but rather, as highly organised networks. Therefore, changes in FAO may also inevitably alter the flux through other pathways. Since no other key pathways involved in central carbon metabolism (e.g., glycolysis, oxidative phosphorylation) were significantly enriched from the Cox regression analysis on breast tumours, it is not clear to what extent alterations in FAO alter *global* cancer cell metabolism.

Chapter 4

Epithelial-to-mesenchymal transition and cellular differentiation alters the FAO signature expression

4.1 Background

Epithelial-to-mesenchymal transition (EMT) is a transdifferentiation process during which cancer cells lose cell-to-cell adhesion, adopt a mesenchymal phenotype, and acquire migratory and invasive properties to metastasise (Nieto et al., 2016).

Both stem cells and EMT share an underlying theme of cellular differentiation. For instance,and as mentioned in the Introduction, basal population of mammary stem cells (MaSC) expresses key EMT effectors such as *SNAI2* and *TWIST1*; and knockout of *SNAI2* in the basal population of MaSC led to expression of luminal markers such as GATA3 and ER, which suggests that *SNAI2* is essential to maintain the less differentiated basal stem cell population (Nassour et al., 2012). With regards to metabolism,

Folmes *et. al.* show that as stem cell differentiates, oxidative metabolism increases (Folmes et al., 2012). However, how FAO contributes to cell fate acquisition remains unclear. This chapter will explore how changes in the morphological and differentiation cell states affect the FAO signature expression.

This chapter aims to address two related question:
(i) Since low expression of the FAO signature is associated with prognosis in certain cancers, and EMT is understood to be important for tumour metastasis; is there an association between these two processes?
(ii) As mentioned above, EMT is associated with loss of an epithelial phenotype. Since cancer cells typically lose their differentiation status (Jogi et al., 2012), what is the relationship between cellular differentiation and the FAO signature expression?

4.2 Objectives

The two overarching objectives of this chapter are to use published gene expression datasets to:

(i) investigate the association between the FAO signature expression and EMT induced by different methods such as TGFβ treatment, 2-hydroxyglutarate accumulation, and transgenic expression of key EMT transcription factors;

(ii) gain insight into how cellular differentiation from a mammary stem cell to mature luminal cell, and treatment of colorectal cancer cells with butyrate influence the FAO signature expression

4.3 Results

4.3.1 FAO signature expression and EMT in cell systems

4.3.1.1 *Transforming growth factor beta-induced EMT decreases FAO signature expression in cell systems*

Treatment of selected cell lines with transforming growth factor beta (TGFβ) is an established model to study EMT (Xu, Lamouille, and Derynck, 2009). To explore an association between the FAO signature and EMT, microarray datasets of human and mouse mammary epithelial cells treated with TGFβ were accessed. In these studies, MCF10A or mouse NMuMG mouse mammary glands cells were treated with TGFβ at different concentrations and time points to study EMT (Deshiere et al., 2013; Shao et al., 2016; Chang et al., 2013). The EMT signature comprises of 65 genes that were upregulated during EMT, and was derived from Groger *et. al.* (Groger et al., 2012).

As shown in Fig 4.1a and 4.1d, treatment of MCF10A cells with TGFβ significantly down regulated the FAO signature expression, relative to untreated control. As expected, an EMT geneset was up regulated in the TGFβ treated cells, relative to untreated cells (Fig 1b,e). Similar results were observed in mouse mammary gland cells treated with TGFβ to induce EMT (Fig 1g,h). Notably, TGFβ treatment followed by a 13 day withdrawal resulted in the recovery of the FAO signature expression, which suggests that TGFβ signalling *suppresses* expression of genes involved in FAO. TGFβ treatment either had no significant influence (Fig 4.1c,f) or decreased proliferation (Fig 4.1i) based on the MKS proliferation signature expression.

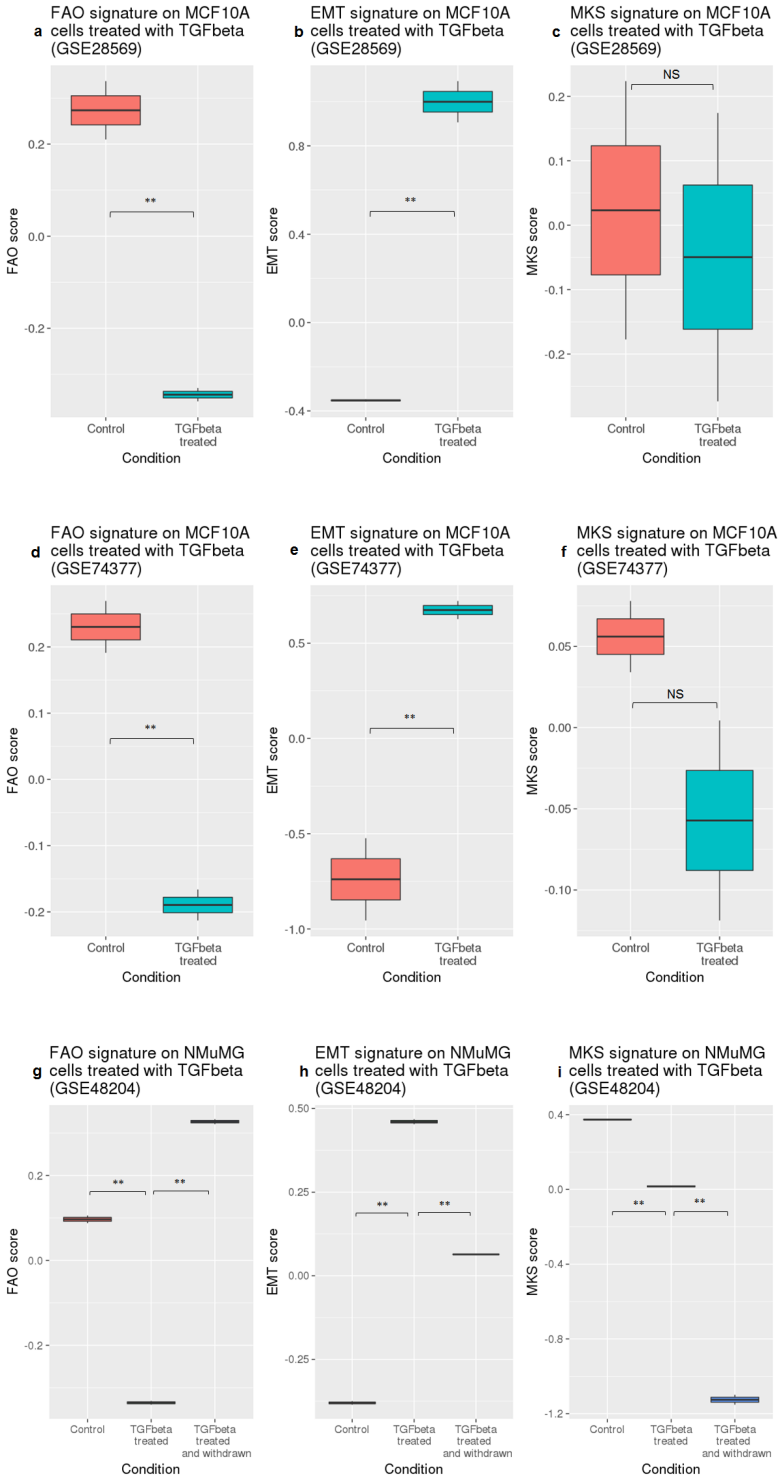

Figure 4.1: TGFβ treatment of MCF10A or NMuMG mammary epithelial cells induces alterations in FAO and EMT signature expression. (**a,b,c**) FAO (a), EMT (b) and MKS (c) signature expression in cells treated with 4ng/mL of TGFβ for three days. n=2 for both conditions. (**d,e,f**) FAO (d), EMT (e) and MKS (f) signature expression in cells treated with 5ng/mL of TGFβ for three days. n=2 for both conditions. (**g,h,i**) FAO (g), EMT (h) and MKS (i) signature expression in cells treated with 4ng/mL of TGFβ for 11 days, or treated and then withdrawn for 13 days. n=2 for all conditions. FDR-adjusted p **$\leq$0.01.

4.3.1.2 *TGFβ-mediated downregulation of FAO signature observed in other cell types*

To investigate whether the association between EMT and FAO could be extended to other cell types, gene expression datasets from lung- and pancreatic cancer and melanoma cell lines treated with TGFβ to induce EMT were analysed. All cell lines featured in this analysis were treated with 5ng/mL TGFβ for various times, and transcriptome analysis performed (Sartor et al., 2010; Maupin et al., 2010).

Consistent with the findings from mammary epithelial cells, TGFβ-induced EMT in all three cell lines resulted in significant down regulation of the FAO signature, compared to controls (Fig4.2a,d,g). No significant difference in the MKS signature expression was observed in these cell lines in response to TGFβ treatment (Fig 4.2c,d,f,i). Furthermore, in another dataset that analysed the transcriptome of three lung cancer cell lines after TGFβ treatment, the FAO signature expression was down regulated in all cell lines (Fig 4.3) (Sun et al., 2014).

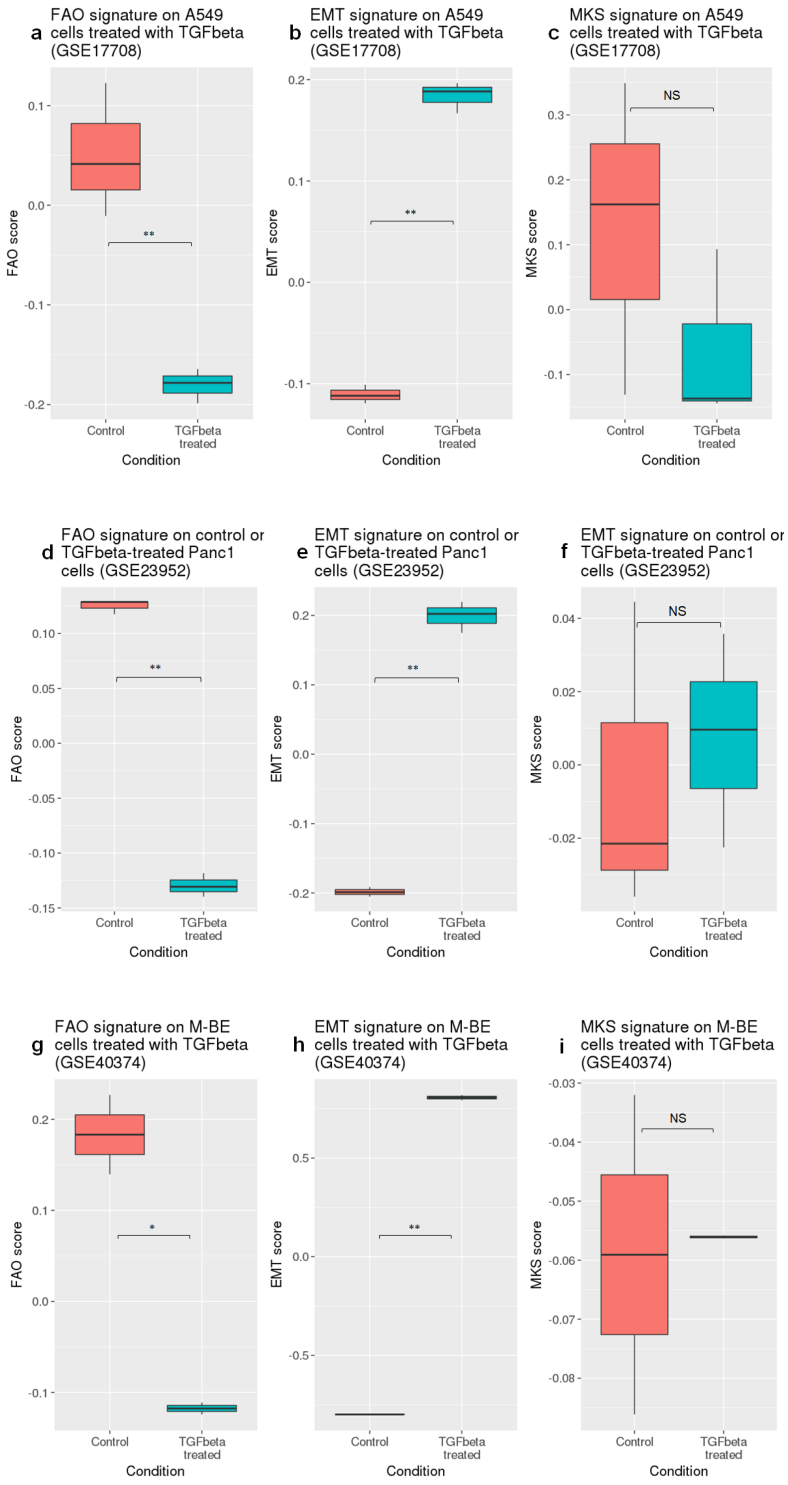

Figure 4.2: TGFβ treatment of A549 lung cancer, Panc1 pacreatic cancer or M-BE bronchoepithelial cells induces alterations in FAO and EMT signature expression. (**a,b,c**) FAO (a), EMT (b) and MKS (c) signature expression in A549 cells that were serum-starved for 24 hours and then treated with 5ng/mL of TGFβ for three days. n=3 for both conditions. (**d,e,f**) FAO (d), EMT (e) and MKS (f) signature expression in Panc1 cells treated with 5ng/mL of TGFβ for two days. n=3 for both conditions. (**g,h,i**) FAO (g), EMT (h) and MKS (i) signature expression in M-BE cells treated with 5ng/mL TGFβ for six days. n=3 for all conditions. FDR-adjusted p **$\leq$0.01, *$\leq$0.05.

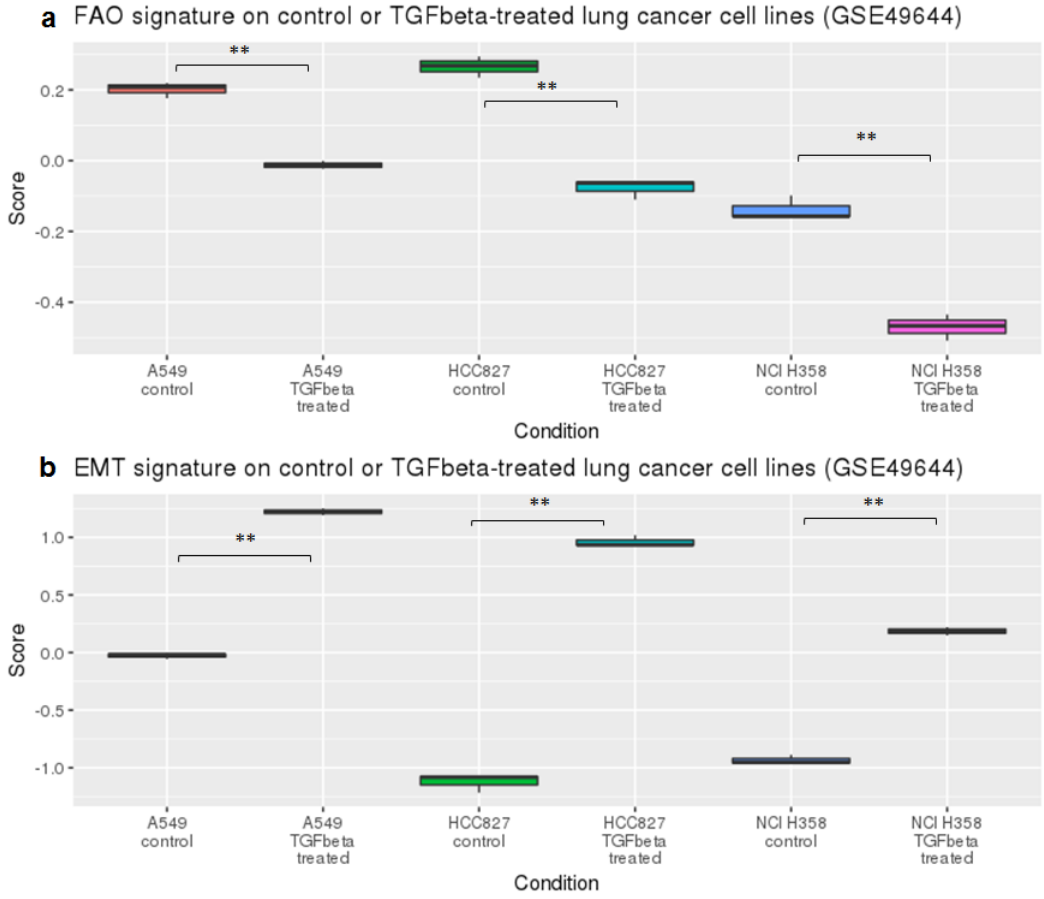

Figure 4.3: Alterations in FAO and EMT signature expression upon TGFβ-induced EMT in a panel of lung cancer cells. FAO (a) and EMT (b) signature expression in cells treated with or without 2ng/mL of TGFβ for 3 weeks. n=3 for all conditions. FDR-adjusted p **$\leq$0.01.

4.3.1.3 *2-hydroxyglutarate-induced EMT decreases FAO signature expression*

Accumulation of metabolites due to altered activity levels of the citric cycle enzymes isocitrate dehydrogenase (IDH) and fumarate hydratase have been shown to induce EMT (Grassian et al., 2012; Sciacovelli et al., 2016). Introducing heterozygous mutations in *IDH1*, but not *IDH2*, by genome editing in HCT116 colorectal cancer cells induced EMT via the transcription factor ZEB1 and miR-200 microRNA family (Grassian et al., 2012). Of note, mutations in *IDH1/2* result in a gain-of-function neomorphic activity

that results in the accumulation of 2-hydroxyglutarate (2-HG). To explore whether EMT induced by accumulation of 2-HG alters the FAO signature expression, gene expression data generated from HCT116 cells with IDH1 R123H and IDH1 R132C mutations and mouse bone marrow cells transduced with IDH1 mutants or treated with 2-HG were analysed (Grassian et al., 2012; Chaturvedi et al., 2016).

As shown in Fig 4.4a, the FAO signature was decreased in IDH1 R123H and IDH1 R132C clones, compared to parental or non-targeting controls (blue bars). As expected, the EMT geneset was upregulated in the IDH1 mutants, relative to controls (orange bars). This finding was also observed in mouse bone marrow cells transduced with wild type or mutant IDH1, or treated with 2-HG (Fig 4.4b). Taken together, these findings indicate that the FAO signature is down regulated in response to the oncometabolite 2-HG induced EMT.

4.3.1.4 *EMT associated transcription factors and FAO signature expression in cell systems*

Activity of transcription factors such as SNAI1 and SNAI2 are key to effect EMT (De Craene and Berx, 2013). To gain insight on how modulating such transcription factors affects the association between EMT and FAO signature expression, gene expression datasets from studies that transgenically expressed these factors in MCF7 and human mammary epithelial (HMEC) cell lines were analysed (Tam et al., 2013; Gras et al., 2014; Dhasarathy et al., 2011). As shown in Fig (4.5a-c), increased *SNAI1*, *SNAI2* and *TWIST1* expression in mammary epithelial cells down regulated expression of the FAO signature. Of note, upregulation of *SNAI1* potently induced EMT and decreased expression of the FAO signature, compared to *SNAI2* and *TWIST1*.

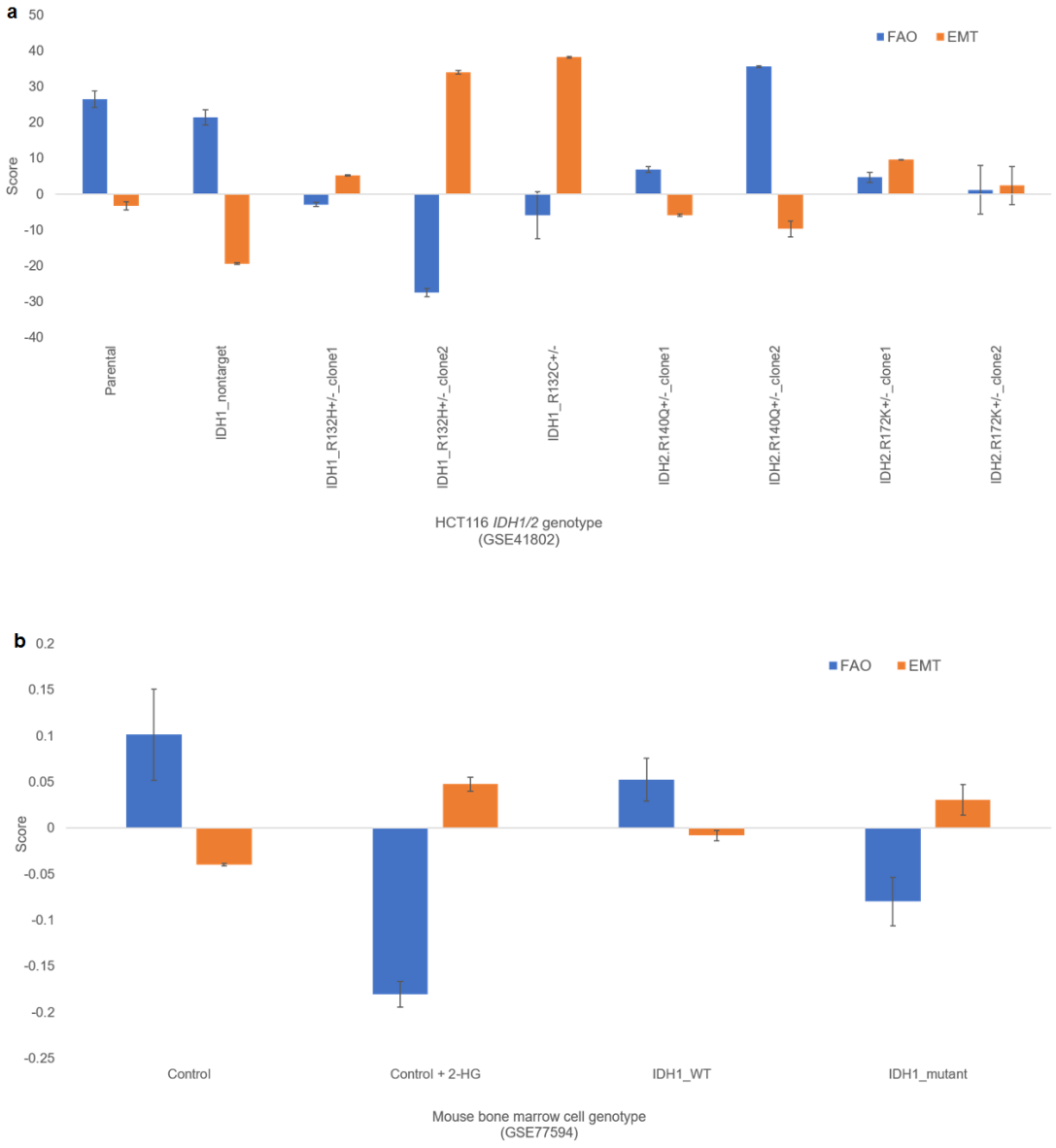

Figure 4.4: IDH1/2 mutations or 2-HG treatment induces alterations in FAO and EMT signature expression. (a) Parental and stable isogenic clones of non-edited and different *IDH1/2* were grown for 6 days before RNA was harvested. n=2 for all conditions (GSE41802). (b) Immortalised bone marrow cells from C57BJ/6 were retrovirally transduced with empty vector, *IDH1* wildtype or mutant constructs, and then transplated into mouse bone marrow. Half of the recipients of bone marrow cells transduced with empty vector were treated with R-2HG (1mg/day) for four weeks. Four weeks post transplantation, cells from bone marrow were flow sorted based on GFP expression, and RNA harvested. n=3 for all conditions (GSE77594). Error bars = SEM.

This finding was supported by analysis of an independent dataset that overexpressed *SNAI1*, *SNAI2* and *SNAI3* (Fig 4.5d-f). In this instance, *SNAI1* overexpression decreased FAO signature expression the most compared to the other two factors (Fig 5d). This is consistent with the findings reported by the authors that generated this dataset who reported weaker EMT induction by SNAI2 and SNAI3, compared to SNAI1. Importantly, this finding was also observed in a breast cancer cell system when overexpression of *SNAI1* in MCF7 cells decreased the FAO signature expression (Fig 4.5g). In all instances, the MKS signature was either significantly lower when SNAI1/2 was overexpressed (Fig 4.5i) or showed no difference, compared to control.

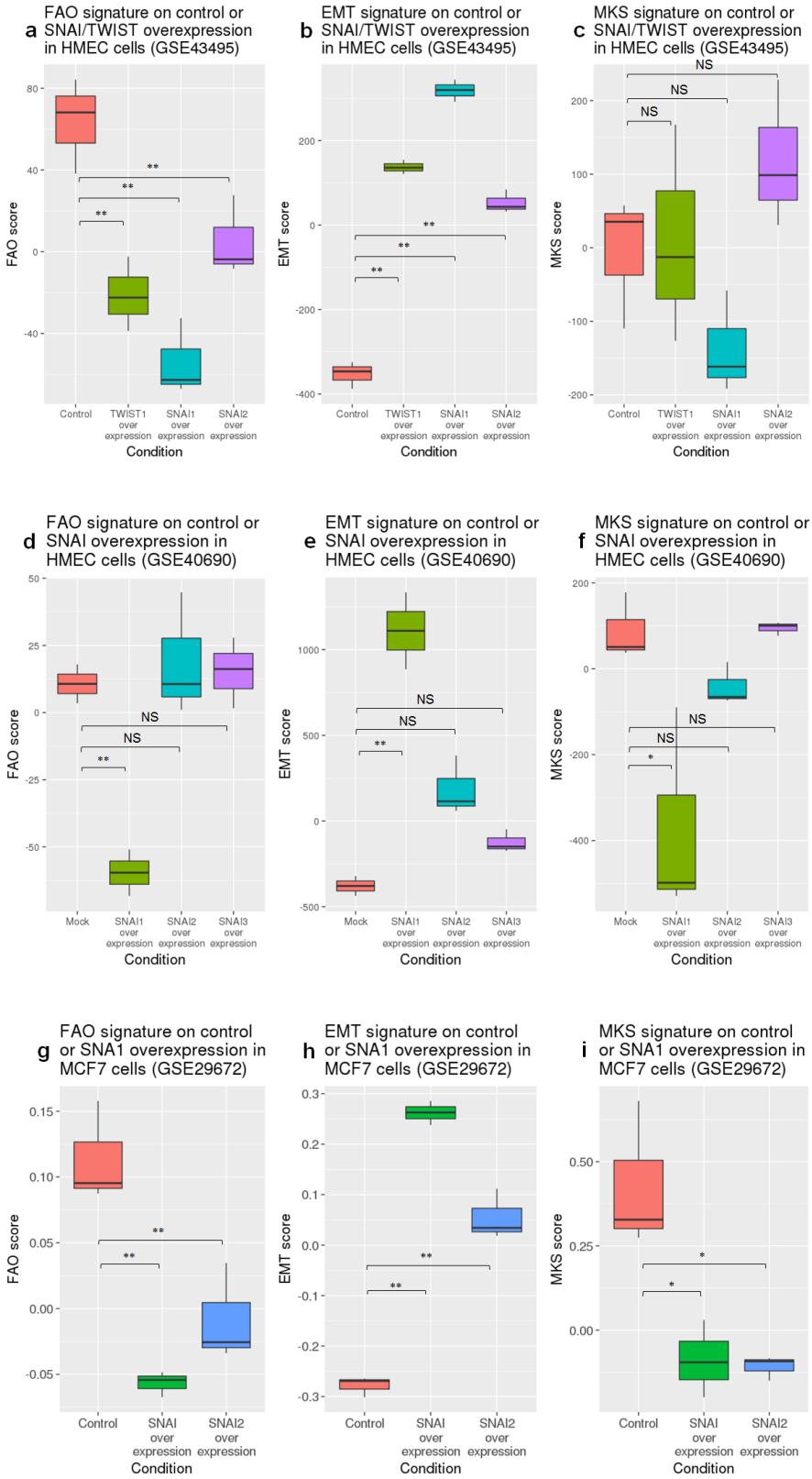

Figure 4.5: Overexpression of EMT transcription factors in mammary epithelial or breast cancer cells alter FAO and EMT signature expression. (**a,b,c**) FAO (a), EMT (b) and MKS (c) signature expression in cells stably transduced with control or *TWIST*, *SNAI1*, *SNAI2* overexpression vectors. n=3 for all conditions. (**d,e,f**) FAO (d), EMT (e) and MKS (f) signature expression in cells stably transduced with control, *SNAI1*, *SNAI2*, *SNAI3* overexpression vectors. n=2 for control and SNA1, n=3 for SNAI2 and SNAI3. (**g,h,i**) FAO (g), EMT (h) and MKS (i) signature expression in cells transduced with control, *SNAI1* or *SNAI2* overexpression adenoviral vectors for four days. n=3 for both conditions. FDR-adjusted p **$\leq$0.01; NS = non-significant.

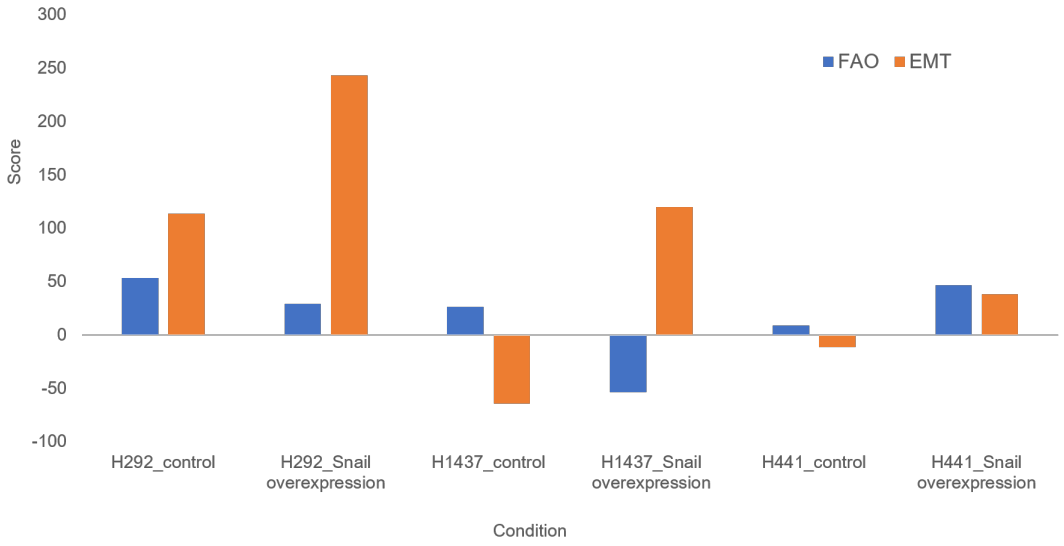

Figure 4.6: SNAI1 overexpression decreases FAO signature expression in three lung cancer cell lines. H292, H1437 and H441 non-small cell lung cancer cell lines were stably transduced with control or *SNAI1* overexpression retroviral vectors (GSE16194, Yanagawa et al., 2009). n=1 for all conditions.

To investigate whether this finding could also be observed in other cancer cell type, gene expression datasets from two independent studies that overexpressed *SNAI1* in several lung cancer cell lines were analysed (Shirogane et al., 2010; Yanagawa et al., 2009). Consistent with the findings in MCF7 and HMEC cell lines, *SNAI1* overexpression resulted in the down regulation of the FAO signature expression in most of the lung cancer cell lines (Figs 4.6 and 4.7, blue bars). Taken together, these findings provide robust evidence for alteration in the FAO signature expression in response to manipulating various EMT associated transcription factors in different cell systems.

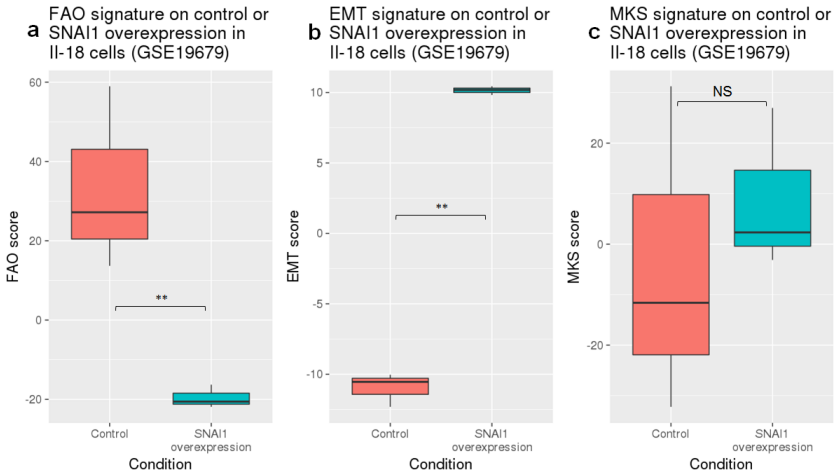

Figure 4.7: SNAI1 overexpression in II-18 lung cancer cell line decreases FAO signature expression. (a) FAO and (b) EMT signature expression in cells transduced with control or *SNAI1* overexpression retroviral vectors for 5 days. n=3 for both conditions. FDR-adjusted p **$\leq$0.01.

4.3.1.5 *FAO signature expression and EMT in organoid systems*

To investigate whether the association between the FAO signature and EMT in cell systems could be extended to organoid cultures, gene expression datasets from studies that analysed the transcriptome of normal mouse colon or adenoma with or without TGFβ treatment were analysed (Fischer et al., 2016; Fessler et al., 2016). The FAO signature expression was decreased in mouse intestinal organoids treated with TGFβ for 5 days, compared to control and TGFβ inhibitor treated organoids (Fig 4.8a). The MKS proliferation signature expression was similar between control and TGFβ-treated organoids. Similarly, in patient-derived colorectal tubular adenoma organoids treated with TGFβ, the FAO signature was down regulated compared to untreated control (Fig 4.8d), while the MKS signature expression was higher in the treated, compared to control. Taken together, data from this analyses suggests that FAO is downregulated in response to TGFβ-induced EMT in different cell types and culture systems.

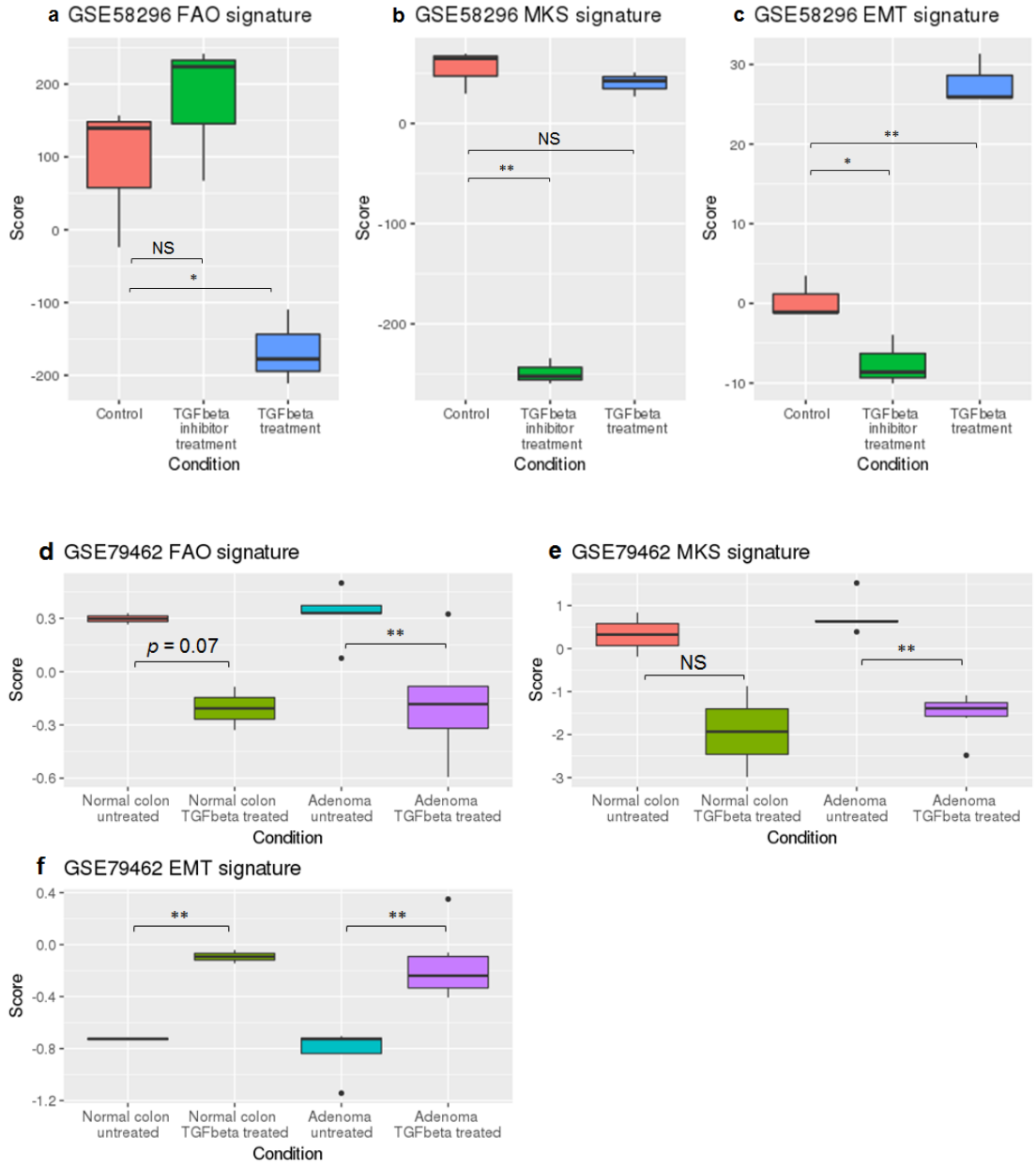

Figure 4.8: TGFβ treatment of mouse normal intestinal, colon or tubular adenocarcinoma organoids alter expression of FAO and EMT signatures. (**a-c**) FAO (a), MKS (b) and EMT (c) gene signature expression in mouse intestinal organoids treated with 0.04 ng/mL TGFβ, 20 μM of LY2109761 TGFβ inhibitor, or untreated control for 5 days. n=3 for all conditions. (**d-f**) FAO (d), MKS (e), and EMT (f) gene signature expression in human patient derived normal colon or adenoma organoids treated with A83-01 (TGFβ inhibitor) or 5 ng/mL TGFβ inhibitor for 5 days. Normal colon untreated n=2, normal colon treated n=2, adenoma untreated n=6, adenoma treated n=6. FDR-adjusted p **$\leq$0.01; NS = non-significant.

4.3.1.6 *FAO signature expression not correlated with EMT signature in primary breast tumours*

In light of the correlation between the FAO signature expression and TGFβ-induced EMT, this association was investigated in primary breast tumour datasets. As shown in Table 1, analysis of three independent datasets found no evidence of an inverse relationship between the FAO and EMT gene signatures.

Table 4.1: Spearman correlation analysis of FAO and EMT signatures on breast cancer datasets.

Dataset	n	Spearman rho	p
METABRIC (training)	973	-0.02	0.53
METABRIC (complete)	1981	-0.05	0.03
GSE25066	508	0.06	0.21
BC2116	2116	0.08	0.0004

4.4 FAO signature expression and cellular differentiation

4.4.1 *FAO signature expression increases during mammary epithelial cell differentiation*

The degree of cellular differentiation is one component of tumour grade, and patients with poorly differentiated tumours have a worse prognosis. Since high tumour grade in breast cancer was observed to have low FAO signature expression, one may ask: how does the FAO signature expression tracks, across different stages of *normal* mammary epithelial cell differentiation?

To investigate this, gene expression datasets of different stages of MEC differentiation (stem cell, luminal progenitor, and mature ductal luminal cells) were accessed. Of note,

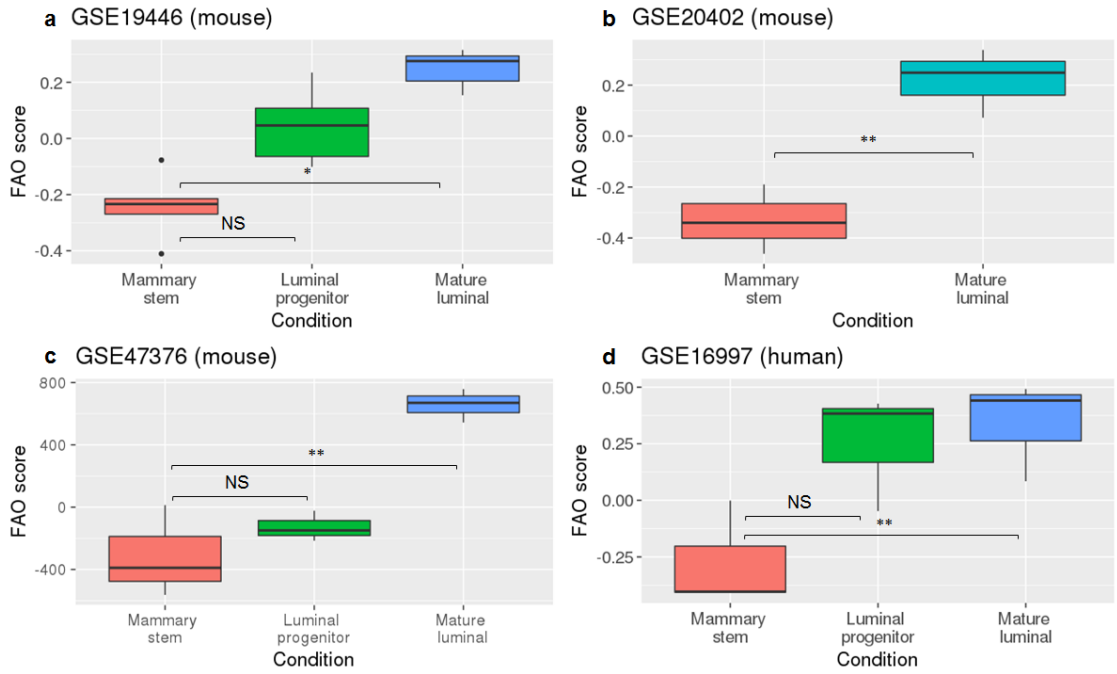

Figure 4.9: FAO signature expression increases from mammary stem to differentiated ductal cell.(**a-d**). GSE19446 n=5 for all conditions; GSE20402 n=4 for all conditions; GSE47376 n=3 for all conditions; GSE16997 n=3 for all conditions. FDR-adjusted p **$\leq$0.01; *$\leq$0.05; NS = non-significant.

in all datasets used in this analysis, the different sub-populations of cells were sorted based on established cell surface markers (e.g., CD49f, EPCAM) by flow cytometry.

As shown in Fig 4.9, in four independent datasets, the FAO signature was expressed higher in the mature luminal ductal cells, relative to the undifferentiated mammary stem cells. This observation was consistent in both mouse and human mammary cells.

4.4.2 *Correlation analysis between FAO, MKS and mammary luminal/stem gene signatures*

Molecular signatures have been established for the different cell populations during MEC differentiation (Lim et al., 2010). In support of Figure 4.9, correlation analysis found a strong positive association between the FAO and differentiated mammary luminal cell

signatures, and a negative correlation with a mammary stem cell signature (Tables 4.2 to 4.5). Importantly, the association between FAO and stem or mature luminal cells in all four datasets analysed was independent of proliferation. Taken together, these findings provide evidence that genes involved in FAO are differentially expressed during different stages of mammary cell differentiation.

Table 4.2: Spearman's correlation matrix of indicated signatures on GSE47376 (mouse). FDR-adjusted p-values are in parenthesis. n=3 for all conditions.

Signature	FAO	MKS	Luminal	Mammary stem
FAO	1 (0)	-	-	-
MKS	0.47 (0.21)	1 (0)	-	-
Luminal	**0.80 (0.01)**	0.18 (0.64)	1 (0)	-
Mammary stem	**-0.83 (0.01)**	-0.52 (0.15)	**-0.72 (0.03)**	1 (0)

Table 4.3: Spearman's correlation matrix of indicated signatures on GSE19446 (mouse). FDR-adjusted p-values are in parenthesis. n=5 for all conditions.

Signature	FAO	MKS	Luminal	Mammary stem
FAO	1 (0)	-	-	-
MKS	0.25 (0.37)	1 (0)	-	-
Luminal	**0.94 (0)**	0.12 (0.67)	1 (0)	-
Mammary stem	**-0.82 (0)**	-0.34 (0.22)	**-0.85 (0)**	1 (0)

Table 4.4: Spearman's correlation matrix of indicated signatures on mouse mammary stem and luminal progenitor enriched cell populations (GSE20402). FDR-adjusted p-values are in parenthesis. n=4 for all conditions.

Signature	FAO	MKS	Luminal	Mammary stem
FAO	1 (0)	-	-	-
MKS	0.03 (0.96)	1 (0)	-	-
Luminal	**1 (0)**	0.03 (0.96)	1 (0)	-
Mammary stem	**-0.77 (0.07)**	-0.09 (0.87)	**-0.77 (0.07)**	1 (0)

Table 4.5: Spearman's correlation matrix of indicated signatures on human mammary stem and luminal progenitor enriched cell populations (GSE16997). FDR-adjusted p-values are in parenthesis. n=3 for all conditions.

Signature	FAO	MKS	Luminal	Mammary stem
FAO	1 (0)	-	-	-
MKS	0.27 (0.49)	1 (0)	-	-
Luminal	**0.73 (0.02)**	0.33 (0.38)	1 (0)	-
Mammary stem	**-0.78 (0.01)**	-0.48 (0.19)	**-0.82 (0.01)**	1 (0)

4.4.3 *FAO signature expression and confluence-induced differentiation*

The relationship between FAO signature expression and mammary stem cell differentiation is supported from analysis of a dataset with a different experimental design: two independent human mammary epithelial cell lines (HMT 3552-S1 and HMEC 184) were cultured in three-dimensional, laminin-rich extracellular matrix to study the temporal molecular changes over 7 days of differentiation (Fournier et al., 2006).

Analysis of transcriptome data from this study found that the FAO signature was increased at later time points when cells are differentiated, compared to less differentiated

cells at earlier time points (Fig 4.10). In this instance, however, the increase in the FAO signature expression was negatively correlated with proliferation (Spearman's rho = -0.61, p=0.03).

4.4.4 *FAO signature increased in butyrate-induced colorectal cancer cell differentiation*

Treatment of colorectal cancer cells with the short-chain fatty acid butyrate has been shown to induce cellular differentiation (Orchel et al., 2005; Tanaka et al., 1989). To determine whether the relationship between differentiation and FAO observed in mammary epithelial cell could be extended to other cell types and mechanisms of differentiation, gene expression datasets from colorectal cancer cells treated with butyrate were analysed (Tabuchi et al., 2006, GSE41113 not published).

Dose response and time course treatments of HCT116 colorectal cancer cell line (Fig 4.11a,b) and mouse colon epithelial MCE301 cell line with butyrate (Fig 4.11c,d) resulted in increased expression of the FAO signature. In these datasets however, the MKS signature expression was decreased in the presence of butyrate, which is consistent with the reported anti-proliferative effect of this molecule (Siavoshian et al., 2000). In CC531 colon cancer cells treated with butyrate over a 24 hour time course, the inverse expression levels of FAO and MKS signature expression was stronger at 2- to 16 hour post treatment, but both signatures were decreased at 24 hours (Fig 4.12) (Germann et al., 2003).

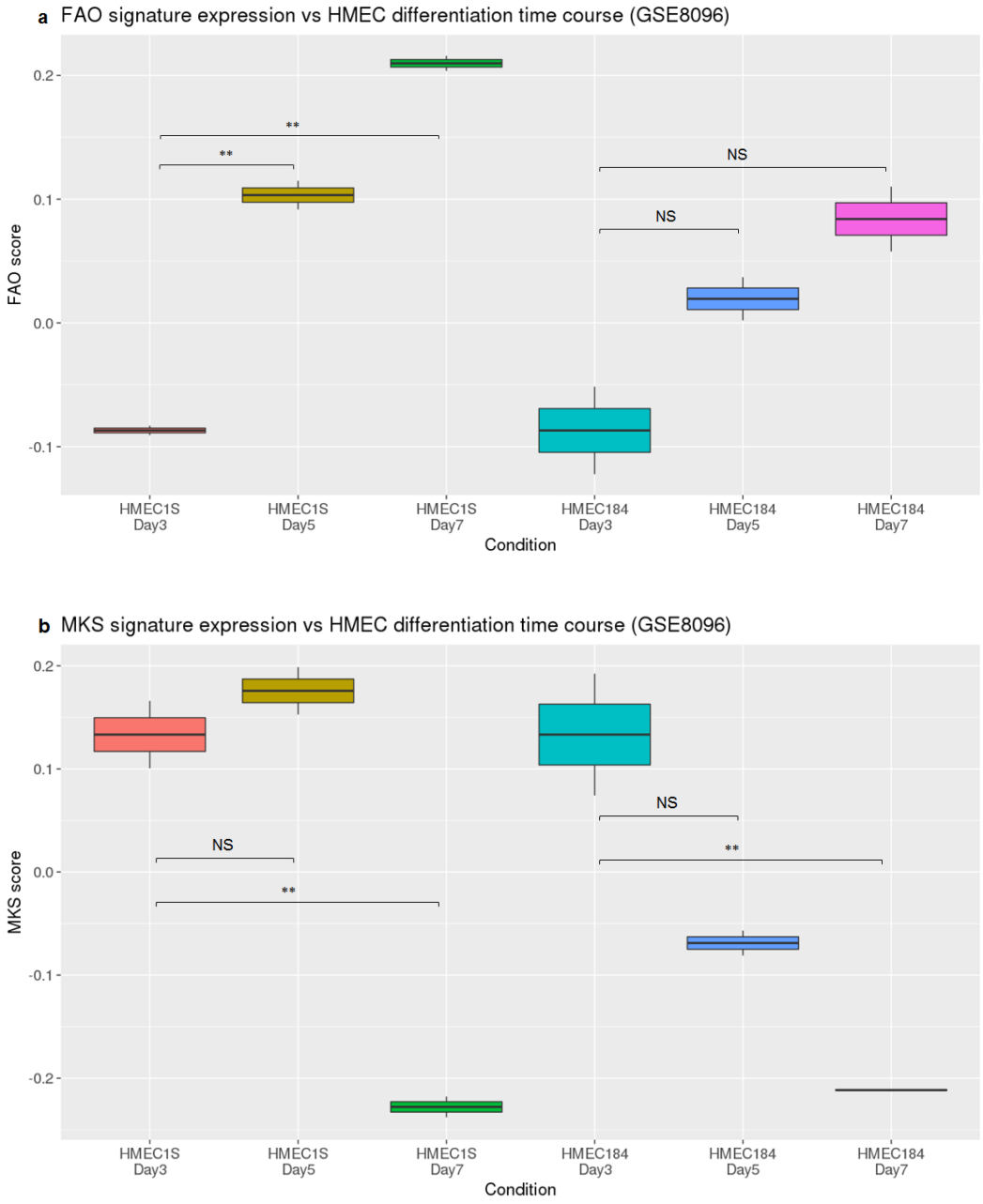

Figure 4.10: FAO signature expression increases during HMEC differentiation. HMEC1S and HMEC184 cells were seeded in laminin-rich extracellular matrix and gene expression analysed at days 3, 5, and 7 post-seeding. (a) FAO and (b) MKS signature expression over differentiation time course. FDR-adjusted p **$\leq$0.01; *$\leq$0.05; NS = non-significant. n=2 for all time points.

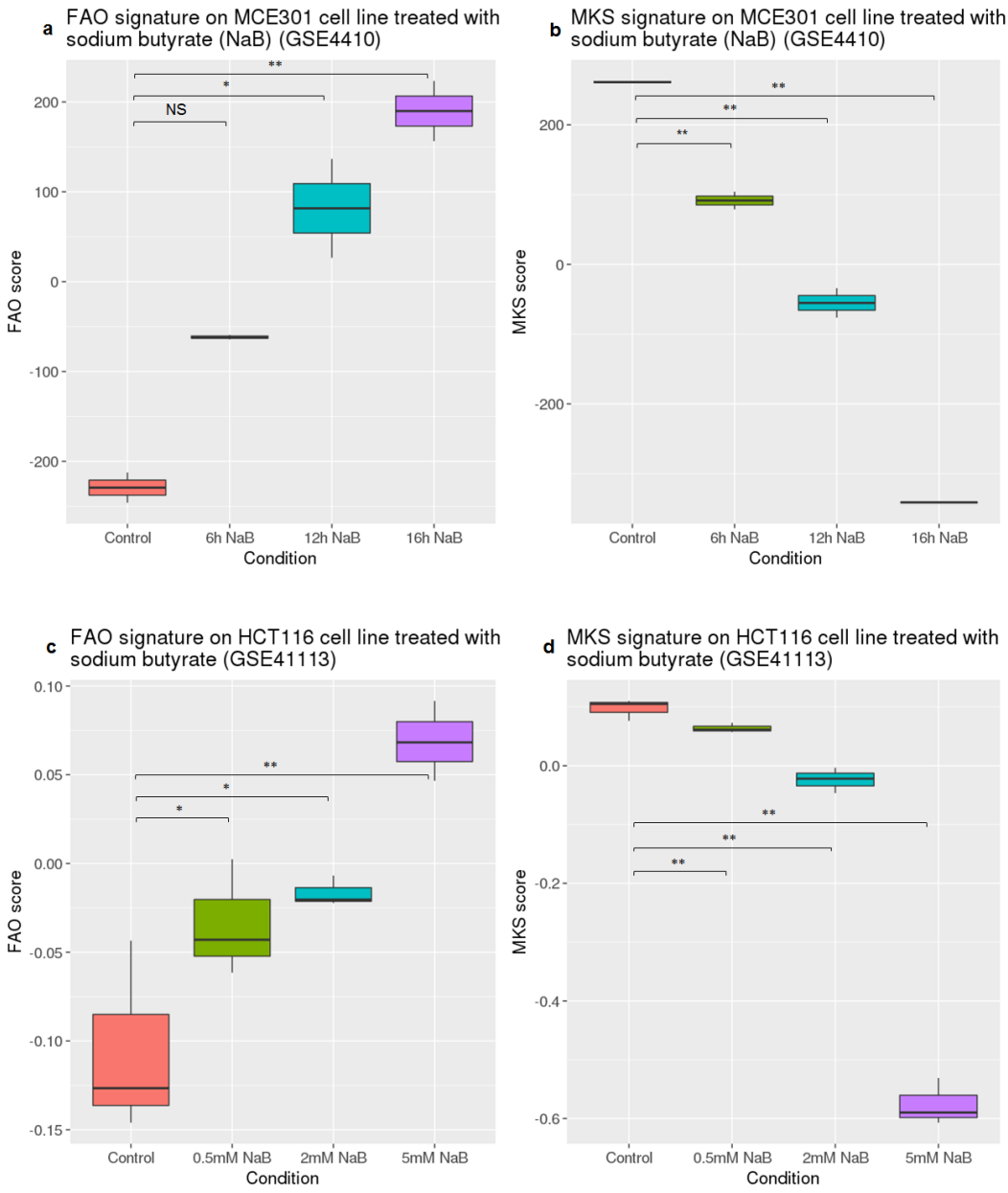

Figure 4.11: FAO signature expression increases upon treatment with sodium butyrate. (**a,b**) FAO (a) and MKS (b) signature expression in MCE301 cells treated with 2 mM sodium butyrate over a time course. n=2 for all concentrations. (**c,d**) FAO (c) and MKS (d) signature expression in HCT116 cells treated with increasing concentration of sodium butyrate over a 24 hour time course. n=3 for all time points. FDR-adjusted p **$\leq$0.01; *$\leq$0.05; NS = non-significant.

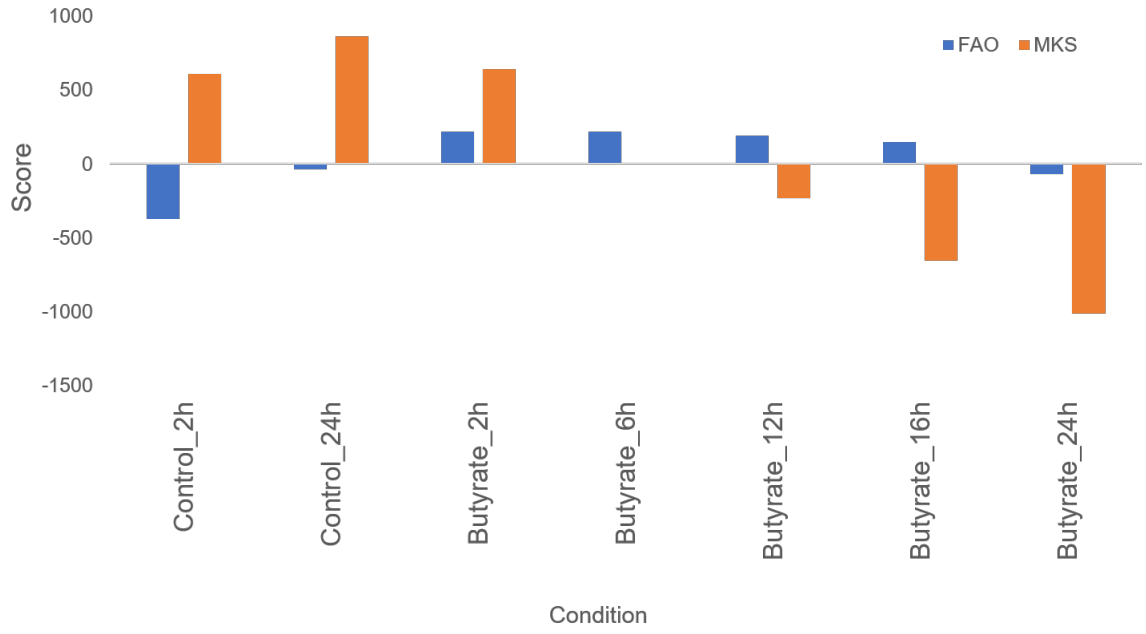

Figure 4.12: FAO signature expression increases in CC-531 rat colon carcinoma cells at earlier time points of sodium butyrate treatment. Cells treated with 4.5mM sodium butyrate for up to 24 hours (GSE424). n=1 for all time points.

4.5 Discussion

4.5.1 What is known about FAO and EMT?

EMT is an extensive process that facilitates tumour metastasis, and TGFβ signalling and transcription factors such as SNAI1 and SNAI2 regulate this process (Moustakas and Heldin, 2007; Nieto et al., 2016; Ye and Weinberg, 2015). Recently, Gaude *et.al.* analysed gene expression data from 20 cancers available from TCGA and observed that decreased expression of genes involved in mitochondrial metabolism was associated with poor prognosis (Gaude and Frezza, 2016). Intriguingly, this general decrease in mitochondrial metabolism genesets was inversely correlated with expression of genes involved in TGFβ signalling and EMT induction. A study by Marro *et. al.* compared the transcriptome of MCF10A cells cultured under sparse and confluent densities (Marro et al., 2014). MCF10A cells exhibit an epithelial or mesenchymal morphology when cultured

at confluent or sparse densities, respectively. Gene set enrichment analysis found genes involved in fatty acid metabolism to be upregulated in the confluent compared to sparse densities. As expected, genesets involved in EMT were downregulated in the confluent density. While these studies suggest some indication between epithelial-mesenchymal cellular states and genes involved in mitochondrial metabolism, whether genes involved in FAO are altered in response to *deliberate* induction of EMT by pharmacologic or genetic mechanisms remains unclear.

4.5.2 Association of EMT and FAO signatures in cell and organoid systems

4.5.2.1 *TGFβ-treatment and transgenic expression of EMT transcription factors*

TGFβ-treatment or overexpression of EMT transcription factors lead to a consistent down regulation in the FAO signature expression, as compared to respective controls. This observation was not limited to mammary epithelial, but also lung, pancreatic and colorectal cell or organoid systems. TGFβ is a pleiotropic cytokine: some of its functions include context-dependent induction or repression of cell proliferation (Massague, 2012). Analyses in this chapter found that EMT induced by either TGFβ or EMT transcription factor expression resulted in either decreased or, for most part, no significant differences in the MKS proliferation signature expression. This suggests that metabolic rewiring in cells undergoing the morphological transition is independent of proliferation. In this context, it is not unreasonable to posit that most of the cellular resources would be channelled to effect the epithelial-mesenchymal transition rather than proliferate, and thus, may explain the decreased expression of the MKS signature in some instances.

4.5.2.2 *Mutations in IDH1/2*

Loss-of-function mutations in IDH and fumarate hydratase lead to the accumulation of metabolites that are substrates of these enzymes, or generation of other metabolites due to gain-of-function neomorphic activity. Fumarate, for example, accumulates when *FH* is inactivated, and downregulates the anti-metastatic *miR-200ba429* by epigenetic mechanisms (Sciacovelli et al., 2016). Heterozygous mutations in *IDH1* generates 2-hydroxyglutarate, and induces EMT in SW480 colorectal cancer and MCF10A mammary cell lines (Grassian et al., 2012). Similar to findings from the analysis of TGFβ treatment and transgenic expression of EMT-associated transcription factor datasets, the FAO signature was also down regulated in 2HG-induced EMT. The differences in EMT and FAO signature expression were stronger in *IDH1* mutants, compared to *IDH2*. Since IDH3 is the *primary* enzyme that catalyses the conversion of isocitrate to alpha-ketoglutarate in the citric acid cycle, it is possible that *IDH1/2* mutations associated with a decrease in FAO signature expression are due to aberrant accumulation of 2-HG and consequent EMT induction, rather than alterations in mitochondrial metabolism resulting in negative feedback to lower FAO. Taken together, the analyses presented in this chapter suggest that regardless of how EMT is triggered, the FAO signature expression is down regulated when cells undergo a morphological transition from an epithelial to a mesenchymal state.

4.5.3 EMT and FAO in primary breast tumours

In breast cancer, EMT is associated with clinical factors associated with poor prognosis. Since the FAO signature expression is prognostic in breast cancer; why, then, was there no correlation observed between the FAO and EMT signatures in primary breast tumours? EMT is not a one-step, binary process, but rather, occurs in discrete, stepwise stages (Zhang et al., 2013). While the FAO signature is correlated with epithelial or mesenchymal states, it is not clear what the relationship is like during the *intermediate*

stages of EMT. In other words, genes involved in FAO could be downregulated early, in the midst, or after completion of EMT.

Secondly, it is likely that at any one time, most tumour cells in a primary tumour are *not* undergoing EMT. Should most tumour cells undergo EMT and metastasise, then the prognosis of a patient cohort would be particularly dismal. This was not apparent in the datasets used for survival analysis in this chapter. Additionally, if there were indeed a small number of cells undergoing EMT, their gene expression profile could be 'diluted' by other epithelial and stromal cells from the biopsy. Ergo, the focal and innately low EMT activity exhibited by tumour cells, together with the discrete stages involved, may account for its lack of association with the FAO signature. This admixture of cell types, however, is less pervasive in cell and organoid culture systems. As such, the relative homogeneity of these systems allows the relationship between the FAO and MKS to be gleaned with greater clarity.

The lack of correlation between EMT and FAO signature expression in primary breast tumours can also be explained from another perspective. While EMT induction decreases the FAO signature expression, the inverse (i.e. decrease in FAO results in EMT) is not necessarily true. Given the protean nature of EMT, it is unlikely that alterations in a single process alone is sufficient to facilitate morphological transitions.

4.5.4 Can activating FAO rescind EMT?

Since EMT is an important process for cells to metastasise, and the FAO signature was observed to decrease during this process, can increasing FAO abate EMT? This question was partly answered, albeit in a different context and system, by Kang *et. al.* (Kang et al., 2015). EMT has a role in fibrosis; and treatment of primary tubular renal epithelial cells (TEC) with TGFβ induced a profibrotic phenotype, with increased expression of

mesenchymal markers such as *VIM* and *FN1*. Furthermore, TGFβ treatment decreased mRNA expression of key oxidative metabolism regulators *PPARA*, *PPARGC1A*, as well as its targets *CPT1A* and *CPT2*. Oxygen consumption analysis of TGFβ-treated TEC revealed decreased baseline OCR, and reduced OCR elevation in response to exogenous palmitate, compared to untreated control. Importantly, overexpression of *PPARGC1A* or treatment with fenofibrate (PPARA agonist) - both inducers of FAO - *suppressed* the expression of mesenchymal markers in response to TGFβ treatment. The clinical significance of this study is that pharmacologic activation of FAO can negate this process; and further investigation of such agents in *in vivo* cancer models may identify a promising anti-metastasis treatment.

4.5.5 Cellular differentiation and FAO signature expression

Characterising the metabolic adaptation during differentiation has been an ongoing effort, and much of this has been focused on stem cells (Zheng et al., 2016; Yanes et al., 2010; Zhang et al., 2011). The inner cell mass of pluripotent blastocysts have lower mitochondrial membrane potential, which suggests reduced mitochondrial potential (Van Blerkom, 2009). Furthermore, cells reprogrammed from a differentiated to a pluripotent state were associated with a metabolic switch from mitochondrial respiration to glycolysis (Folmes et al., 2011). While oxidative metabolism has been shown to be upregulated in differentiated cells, it is not clear which pathways, and to what extent, they contribute to the increased citric acid cycle activity in mature cells (Teslaa and Teitell, 2015). Since pertubations in cellular differentiation is a common phenomena in cancer cells and is a component of tumour grade assessment, it may serve well to understand the metabolic idiosyncrasies associated with the differentiation status of a cell. This knowledge may identify potentially druggable pathways to supplement standard adjuvant treatment regimes.

Analyses in this chapter present evidence for increased expression of genes involved in FAO with cellular differentiation. This finding was observed in normal human and mice mammary cells at different stages of differentiation, as well as in normal colon and colorectal cancer cells treated with sodium butyrate. This observation agrees, to an extent, with increased expression of genes involved in oxidative metabolism, and fatty acid oxidation in particular, and decreased expression of glycolytic genes during cardiomyocyte stem cell differentiation. A study by Doria *et.al.* found an enrichment of genes involved in lipid metabolic processes as mice MEC matures from the stem, or basal, state to a differentiated ductal cell (Doria et al., 2014). Notably, a geneset involved in fatty acid beta oxidation that increased as the MEC matures was observed to be prognostic in breast cancer. However, how the signature cut-off for stratifying patients into 'low' or 'high' groups was not clearly indicated, and was not reproduced in an independent dataset.

In mouse mammary stem and progenitor cells, there was no correlation between the MKS proliferation and the FAO signature expression. In contrast, mammary epithelial cells grown three dimensionally in extracellular matrix, and normal colon or cancerous colorectal cells treated with sodium butyrate were observed to have a negative correlation between the two signatures. What could account for these inconsistencies? A salient explanation is that the context of studying differentiation varies between the studies. All three datasets from the human and mouse mammary cell differentiation isolated stem, luminal progenitor and ductal cells from mammary glands by flow cytometry based on specific lineage marker expression. The differentiation course *in vivo* starts from a *single* mammary stem cell to luminal progenitor and ends with a *single* mature ductal cell, and thus, no cell division occur (Visvader and Stingl, 2014). In contrast, in the confluence-induced differentiation model, *in vitro* cultured cells seeded at low density proliferate and mature, and tend to stop growing due to contact inhibition. Cells seeded at low confluency have been described to acquire a less differentiated or

mesenchymal features, and regain their epithelial status after several days of culture or increased confluency (Marro et al., 2014; Fournier et al., 2006). As such, it is possible that the confluence-induced lowered proliferation may have a role in the increased expression of the FAO signature. Taken together, the findings from this chapter suggests that differentiated cells have higher expression of genes involved in FAO as compared to their less differentiated counterparts.

4.6 Summary, strengths and limitations

This chapter has presented evidence that the FAO signature is:
(i) down regulated in response to various forms of EMT induction in *in vitro* and *in vivo* systems
(ii) up regulated during mammary stem cell differentiation, as well as during confluence-induced differentiation in breast cancer cells, and butyrate treatment of colorectal cancer cells.

The strength of this chapter is that the analyses presented have endeavoured to provide several independent lines of evidence for the relationship between FAO, EMT and cellular differentiation. However, short of experimental validation, the association demonstrated in this chapter is limited only a *correlation*. Experiments to delineate this association may identify potential therapeutic opportunity to limit EMT, and possibly metastasis, or promote tumour cell differentiation.

Chapter 5

Activation of key oncogenic signalling pathways alters FAO signature expression

5.1 Background

Genetic abberations in oncogenes or tumour suppressor genes have a profound impact on cellular metabolism. For instance, activation of *MYC* and *RAS* oncogenes, and PI3K signalling pathway, as well as loss of *TP53* function and LKB1-AMPK pathway all affect glucose and glutamine metabolism (Boroughs and DeBerardinis, 2015). Two of the most frequently activated pathways in cancer are the mitogen activated protein kinase (MAPK) and the Wnt signalling cascades (Burotto et al., 2014; Polakis, 2012).

Hitherto, the known metabolic consequence of activation of the Wnt and MAPK pathways largely revolve around glycolysis, and very little is known how these pathways affect FAO (Thompson, 2014; Munoz-Pinedo, El Mjiyad, and Ricci, 2012). This chapter explores how the FAO signature is affected by genetic or pharmacologic manipulation

of the MAPK and Wnt signalling pathways.

5.2 Objectives

The objectives of this chapter are to use published gene expression datasets to:

i. investigate how modulation of different Wnt signalling in cell and mouse models affect FAO signature expression
ii. explore whether the FAO signature is altered in response to BRAF inhibition or modulation of other MAPK pathway components
iii. gain insight on how modulating microphthalmia-associated transcription factor (MITF) expression affects expression of the FAO signature

5.3 Results

5.3.1 Alteration of Wnt signalling members *in vivo* alters FAO signature expression

5.3.1.1 *Knockout, knockdown or single allele inactivation of APC decreases FAO signature expression*

To investigate how alterations in adenomatous polyposis coli (APC) activity influences the FAO signature expression, gene expression datasets from studies that knockdown or knockout *APC* expression were analysed (Reed et al., 2015; Dow et al., 2015; Gaspar et al., 2008).

As shown in Fig 5.1, *Apc* deletion in mouse small intestine or colon polyps with *Apc* knock down decreased FAO signature expression, compared to respective controls. A similar observation was made in mice with Apc+/1638N genotype (neomycin gene intro-

duced into codon 1638 in a transcriptionally opposite orientation to Apc). The expression of the MKS signature was increased when wild type Apc expression was abrogated, or in Apc+/1638N mice. This is consistent with the role of β-catenin transcriptionally activating genes involved in proliferation, such as *CCND1* and *MYCN* (He, Nakada, and Morrison, 2009; Tetsu and McCormick, 1999; Shtutman et al., 1999).

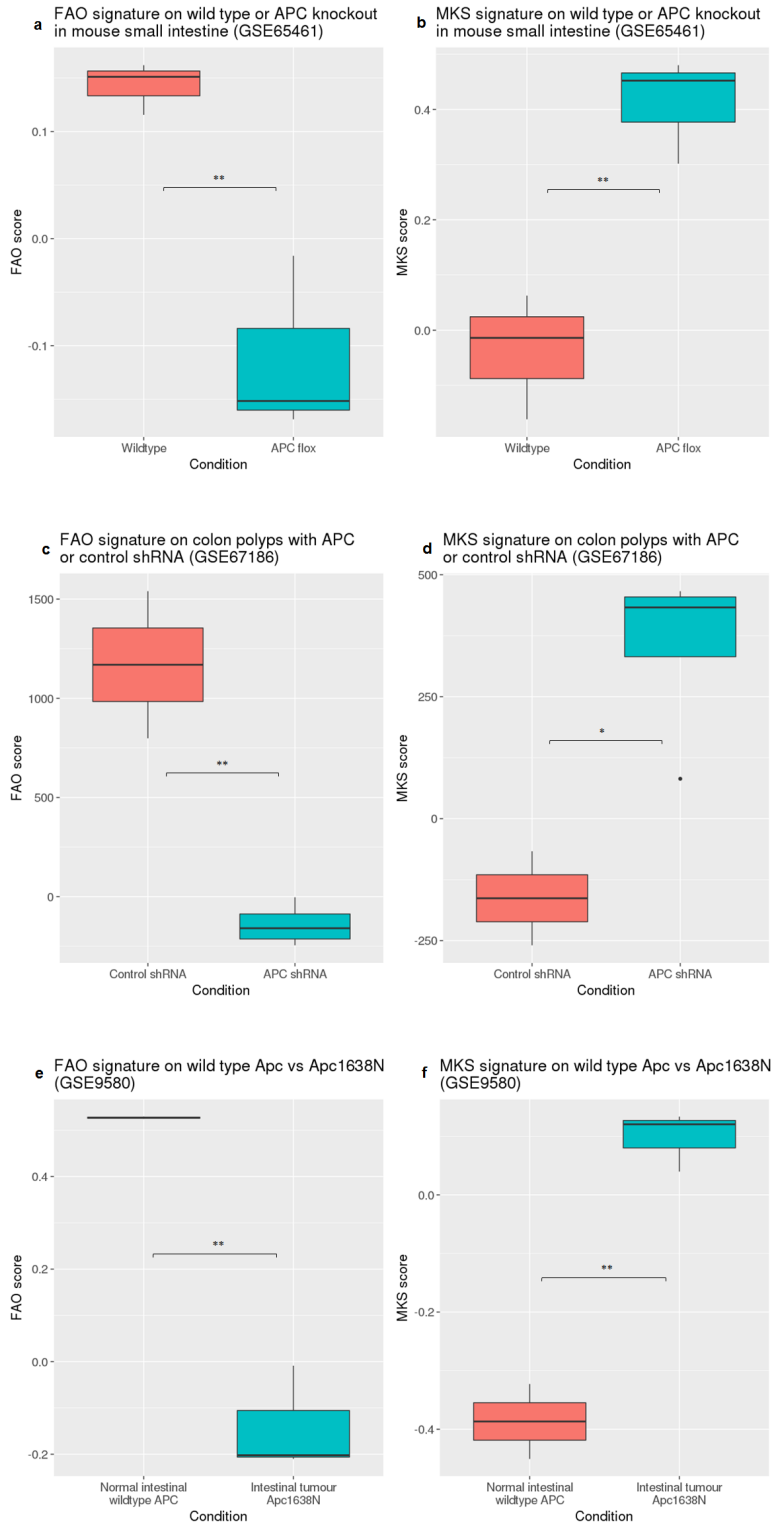

Figure 5.1: APC knockout, knockdown, or single allele inactivation decreases FAO signature expression. (**a,b**) FAO (a) and MKS (b) signature expression in mouse small intestine after *Apc* deletion for 5 days. n=3 for both conditions. (**c,d**) FAO (c) and MKS (d) signature expression in colon polyps of six week old mice fed chow containing doxycycline to induce shRNA expression against *Apc* or *Renilla* (control) and polyps isolated 4-6 weeks later. n=4 for *APC* shRNA, n=2 for Renilla control. (**e,f**) FAO (e) and MKS (f) signature expression in eight month old C57/Bl6/J mice were kept *ad libitium* under specific pathogen-free condition until sacrificed for analysis. n=2 for control, n=4 for Apc+/1638N. FDR-adjusted p **$\leq$0.01; *$\leq$0.05.

5.3.1.2 *Knockout of Bcl9 increases FAO signature expression*

The Wnt signalling pathway is also positively regulated by Bcl9 (Moor et al., 2015; Takada et al., 2012; Roche, Worm, and Bienz, 2008). To understand whether modulation of this gene alters the FAO signature expression, transcriptome data from a study that assessed the effect of *Bcl9* knockout in healthy and tumour colon tissues was analysed (Moor et al., 2015).

Knockout of *Bcl9* - a key positive regulator of β-catenin activity (Takada et al., 2012) - in mouse tumour resulted in *increased* expression of the FAO signature (Fig 5.2a,c). However, no significant difference was observed in the signature expression in normal colon tissues with Bcl9 knockout. Notably, no statistically significant difference in expression of the MKS proliferation signature was observed between endogenous and Bcl9 knockout tissues, which is consistent with the finding from the study that generated this dataset (Fig5.2b,d) (Moor et al., 2015).

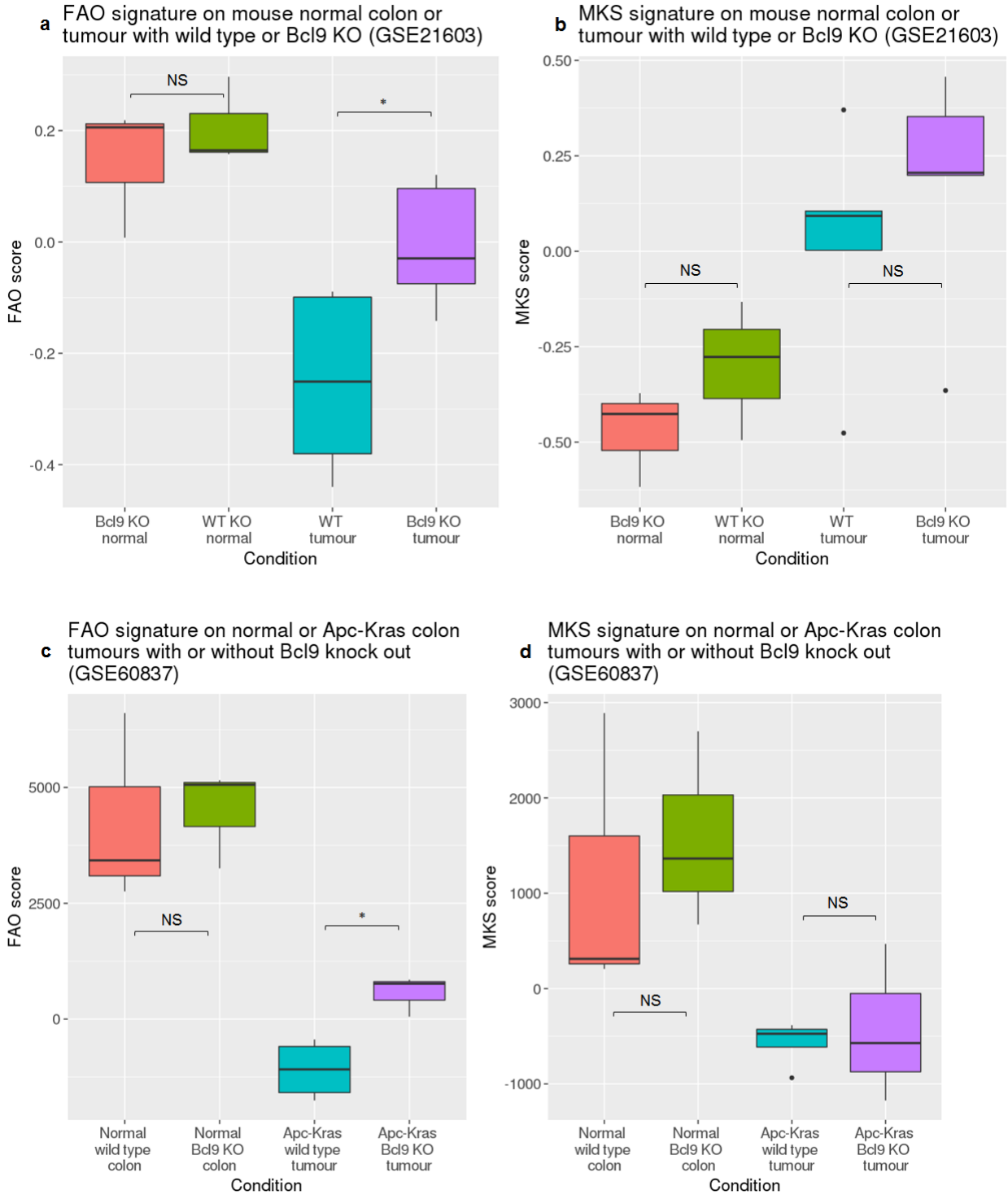

Figure 5.2: Bcl9 knockout increases FAO signature expression. (**a,b**) FAO (a) and MKS (b) signature expression in normal colon tissue (EDTA-dissociated) or tumours (laser microdissected) obtained from 129SvEv/C57BL/6/DBA/2 mice with or without Bcl9 knock out. n=5 for all conditions. (**c,d**) FAO (c) or MKS (d) signature expression in wildtype or knockout Bcl9 normal or colon tumour tissues obtained from Apc-Kras or mice treated with azoxymethane and dextran sulphate sodium to chemically-induce Wnt-driven colorectal tumours. n=4-6. FDR-adjusted p *$\leq$0.05; NS = non-significant.

5.3.1.3 *Altering Wnt signalling components in vitro influences FAO signature expression*

The effect of modulating different Wnt signalling components on the FAO signature expression in cells systems was also explored using published datasets (Azzolin et al., 2012; Herbst et al., 2014; Mokry et al., 2012, GSE35272 and GSE28467 not published).

In the SW480 colorectal cancer cell line, reintroduction of *APC* increased the expression of the FAO signature (Fig 5.3a). Furthermore, knockdown of *CTNNB1* - the gene encoding β-catenin - also increased the FAO signature expression in SW480, DLD-1 and Ls174T colorectal cancer cells (Figs 5.3a, 5.3c and 5.4a).

In the Ls174T cell line, transgenic expression of dominant negative (dn) T cell factor 4 (TCF4) - which antagonises endogenous TCF4 function - increased the expression of the FAO signature (Figs 5.4a and 5.4c). In DLD1 cells, overexpression of Dickkopf-related protein 1 (DKK1) - a negative regulator of Wnt signalling - increased expression of the FAO signature (Fig 5.4e). In all but one experiment (Fig 4B, SW480 β-catenin siRNA), the FAO signature expression in response to alterations of the Wnt signalling pathway was inversely correlated with the MKS proliferation signature.

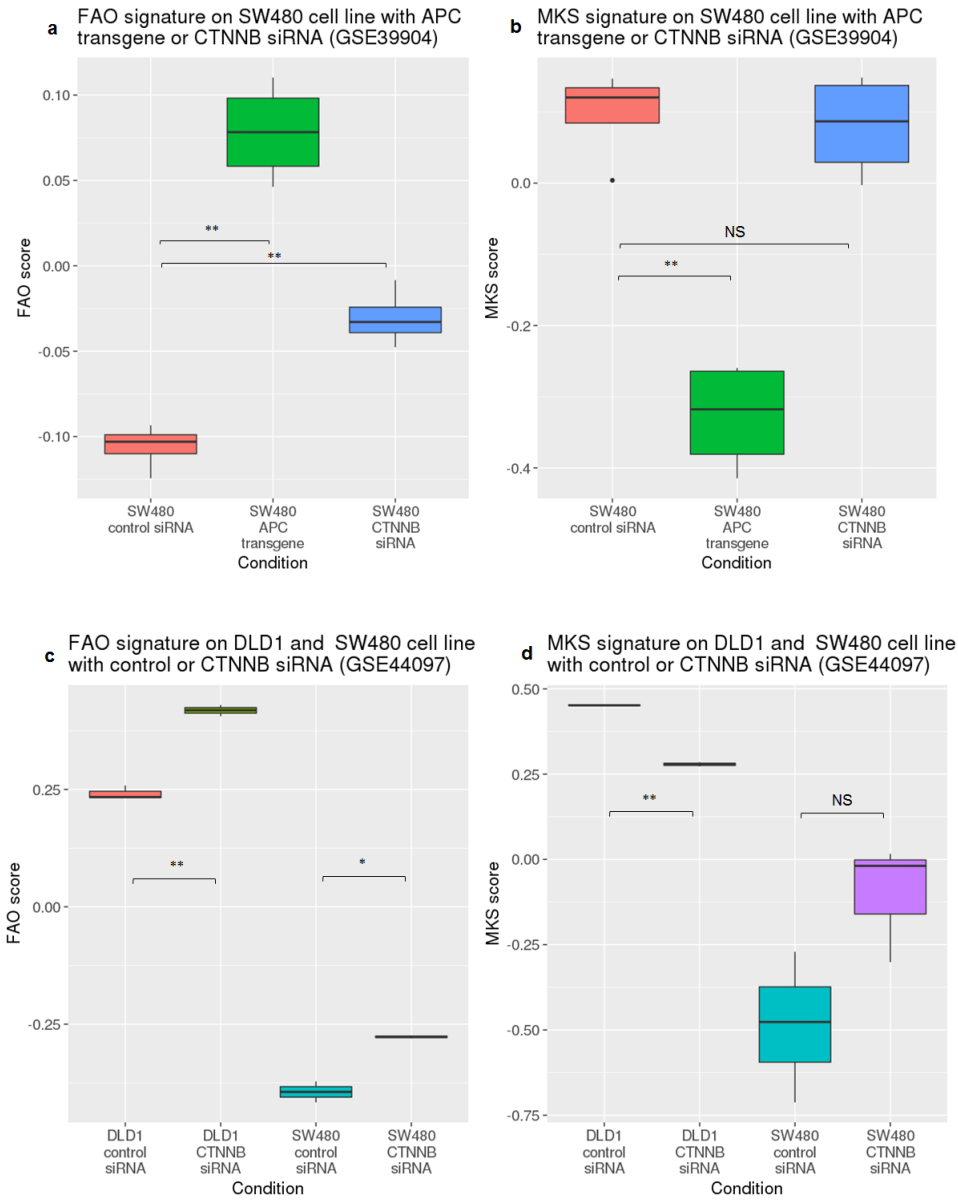

Figure 5.3: APC or DKK-1 overexpression, or β-catenin knockdown increases FAO signature expression. (a) SW480 cells were transfected with siRNA against β-catenin or a construct with APC transgene. n=4 for all conditions. (b) Cells were transfected with siRNA against β-catenin in SW480 or DLD-1 cells for 48 hrs. n=2-3. FDR-adjusted p * $\leq$0.05, **$\leq$0.01, NS = non-significant.

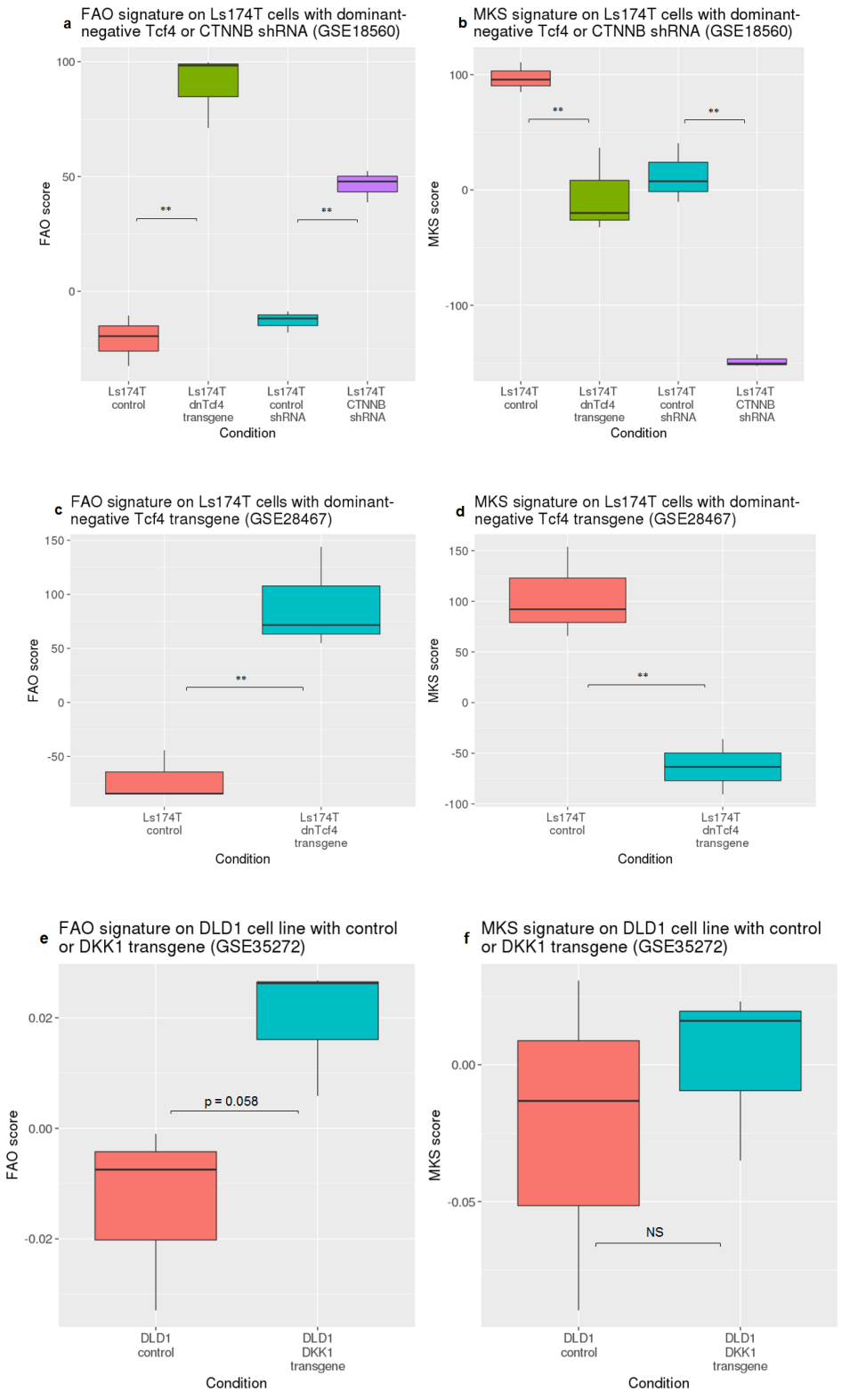

Figure 5.4: β-catenin knockdown or dnTCF4 expression alters FAO signature expression in Ls174T cells. (**a,b**) FAO (a) and MKS (b) signature expression in cells induced with 1 μg/mL doxycycline for 24 hours to induce dnTCF4 expression, or 72 hours for β-catenin knockdown. n=3 for all conditions. (**c,d**) FAO (c) and MKS (d) signature expression in cells induced with 1 μg/mL doxycycline for 20 hours to induce dnTCF4 expression. n=3 for both conditions. (**e,f**) FAO (e) and MKS (f) signature expression in DLD-1 cells lentivirally transduced with control or DKK-1 transgene and induced with 10 μg/mLdoxycycline for 24 hrs. FDR-adjusted p **$\leq$0.01, NS = non-significant.

5.3.1.4 *Constitutive Wnt signalling in mouse mammary glands decreases FAO signature expression*

Activation of Wnt signalling has been observed in basal-like breast cancers and is associated with metastasis and poor prognosis (Khramtsov et al., 2010; Dey et al., 2013). To explore the relationship between constitutive Wnt signalling in mammary glands and the FAO signature expression, transcriptome data from mice with healthy mammary glands expressing wild type β-catenin, and mammary neoplasia or tumours with constitutively active N-terminal truncated β-catenin expression was analysed (Moumen et al., 2013).

As shown in Fig 5.5a, the FAO signature expression was gradually decreased from normal mammary gland to hyperplasia, and was lowest in tumours. Conversely, the MKS proliferation signature was highest in tumours, while no difference was observed between small and large neoplasia (Fig 5b).

Taken together, these analyses provide strong *in vivo* and *in vitro* evidence that the FAO signature expression is altered in response to altering different components of the Wnt signalling pathway.

5.3.1.5 *FAO signature expression is not associated with prognosis in colorectal cancer*

Given the association between Wnt signalling and FAO signature expression in different experimental systems, the relationship between the FAO signature expression and prognosis in colorectal cancer was explored. As shown in Table 5.1, in two independent datasets, there was no association observed between FAO signature expression and outcome.

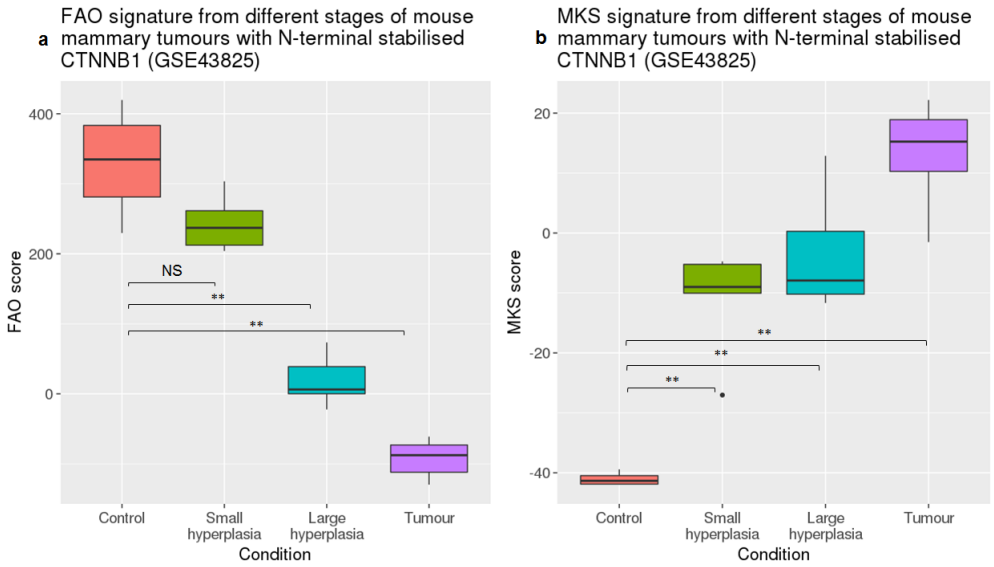

Figure 5.5: Constitutive Wnt signalling decreases FAO signature expression across different stages of mammary tumour development. FAO (a) and MKS (b) signature expression in C57BL6 mice with transgenic N-terminal truncation in β-catenin in mammary basal/myoepithelial cells sacrificed at different stages of tumour development. n=4-11. FDR-adjusted p **$\leq$0.01, NS = non-significant.

Table 5.1: FAO signature expression is not associated with survival in colorectal cancer cohorts. DFS, disease-free survival; RFS, relapse-free survival; DSS, disease-specific survival; OS, overall survival

Dataset	n	Log rank p (survival metric)	Hazard ratio	p
GSE39582	557	0.878 (RFS)	0.98	0.88
GSE39582	562	0.501 (OS)	1.1	0.5
GSE17536	177	0.242 (DFS)	1.48	0.245
GSE17536	177	0.169 (DSS)	1.45	0.17
GSE17536	177	0.749 (OS)	1.08	0.75

5.4 FAO signature expression is associated with MAPK pathway and MITF status in melanoma

5.4.1 *Pharmacological inhibition of mutant BRAF increases FAO signature expression*

BRAF is the most commonly mutated oncogene in melanoma (Hodis et al., 2012; Davies et al., 2011). To investigate whether the FAO signature expression is altered in response to BRAF V600E inhibition, gene expression datasets from three studies that performed transcriptome analysis on two melanoma cell lines treated with vemurafenib were analysed (Parmenter et al., 2014; Hoeflich et al., 2009; Seip et al., 2016). As shown in Fig 5.6 in three independent datasets, treatment of A375 and Melmet5 cells with vemurafenib increased the FAO signature expression, compared to controls (5.6a,c,e). Conversely, the MKS proliferation signature expression was down regulated as compared to untreated controls (Fig 5.6b,d,f). Furthermore, as shown in Fig 5.7, treatment of a melanoma cell line panel with PLX4032 (BRAF inhibitor) increased expression of the FAO signature, consistent with the observation in Fig 5.6 (Joseph et al., 2010).

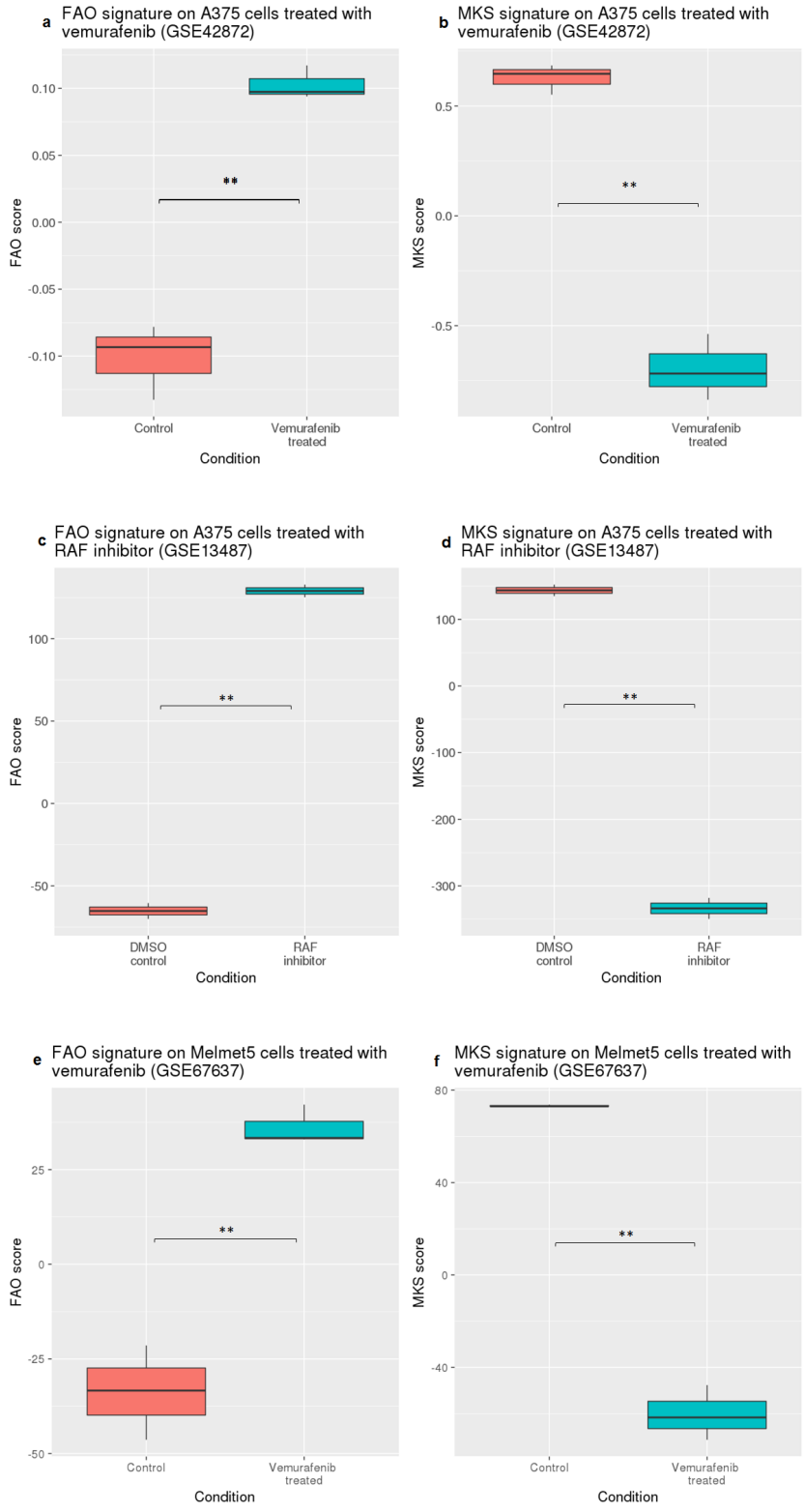

Figure 5.6: Vemurafenib treatment of BRAF mutant melanoma cell lines decreases FAO signature expression. (**a,b**) FAO (a) and MKS (b) signature expression in A375 cells treated with DMSO or 1 μM vemurafenib for 24 hours. n=3 both for conditions. (**c,d**) FAO (c) and MKS (d) signature expression in A375 cells treated with DMSO or 10 μM vemurafenib for 24 hours. (**e,f**) FAO (e) and MKS (f) signature expression Melmet15 cells were treated with DMSO or 1 μM vemurafenib for 24 hours. n=3 both for conditions. FDR-adjusted p **$\leq$0.01.

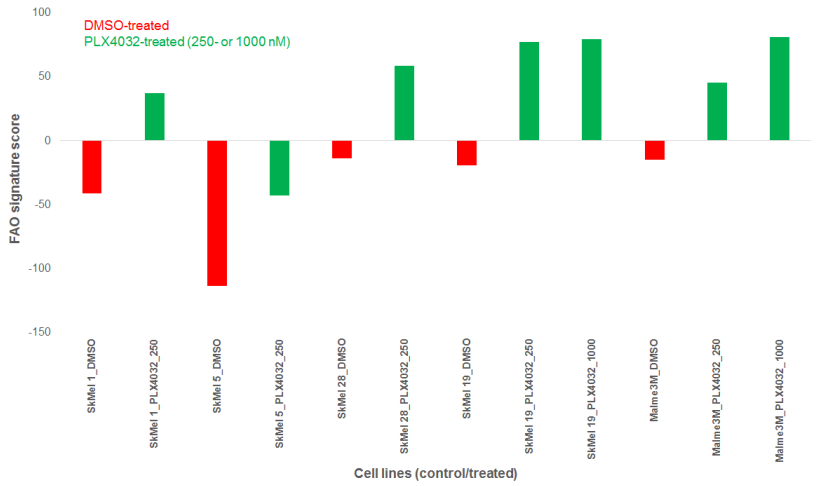

.

Figure 5.7: BRAF inhibition increases FAO signature expression in a panel of melanoma cell lines. Indicated melanoma cell lines were treated with DMSO or 250- or 1000 nM PLX4032 for 8 hrs (GSE20051). n=1 for all measurements

5.4.2 *BRAF mutant expression alters FAO signature expression*

To understand how modulation of mutant *BRAF* expression affects the FAO signature expression, gene expression datasets from studies that either overexpress or knockdown mutant *BRAF* expression in different cell systems were analysed (Capell et al., 2016; Hoeflich et al., 2009). Overexpression of BRAF in neonatal epidermal melanocytes decreased expression of the FAO signature, and a similar trend was observed in primary human melanocytes with transgenic BRAF expression (Figs 5.8a,b). Interestingly, the MKS proliferation signature was down regulated when BRAF V600E was overexpressed in melanocytes (Fig 5.8b). In the second dataset (Fig 5.8b,c), statistical significance was not achieved for either signature, which is most likely due to small sample size (n=2). Furthermore, similar to vemurafenib treatment, shRNA knockdown of mutant *BRAF* in A375 melanoma cells increased expression of the FAO signature (Fig 5.8d,e). Taken together, these findings suggest that modulation of BRAF V600E expression levels affects proliferation and alters expression of genes involved in FAO.

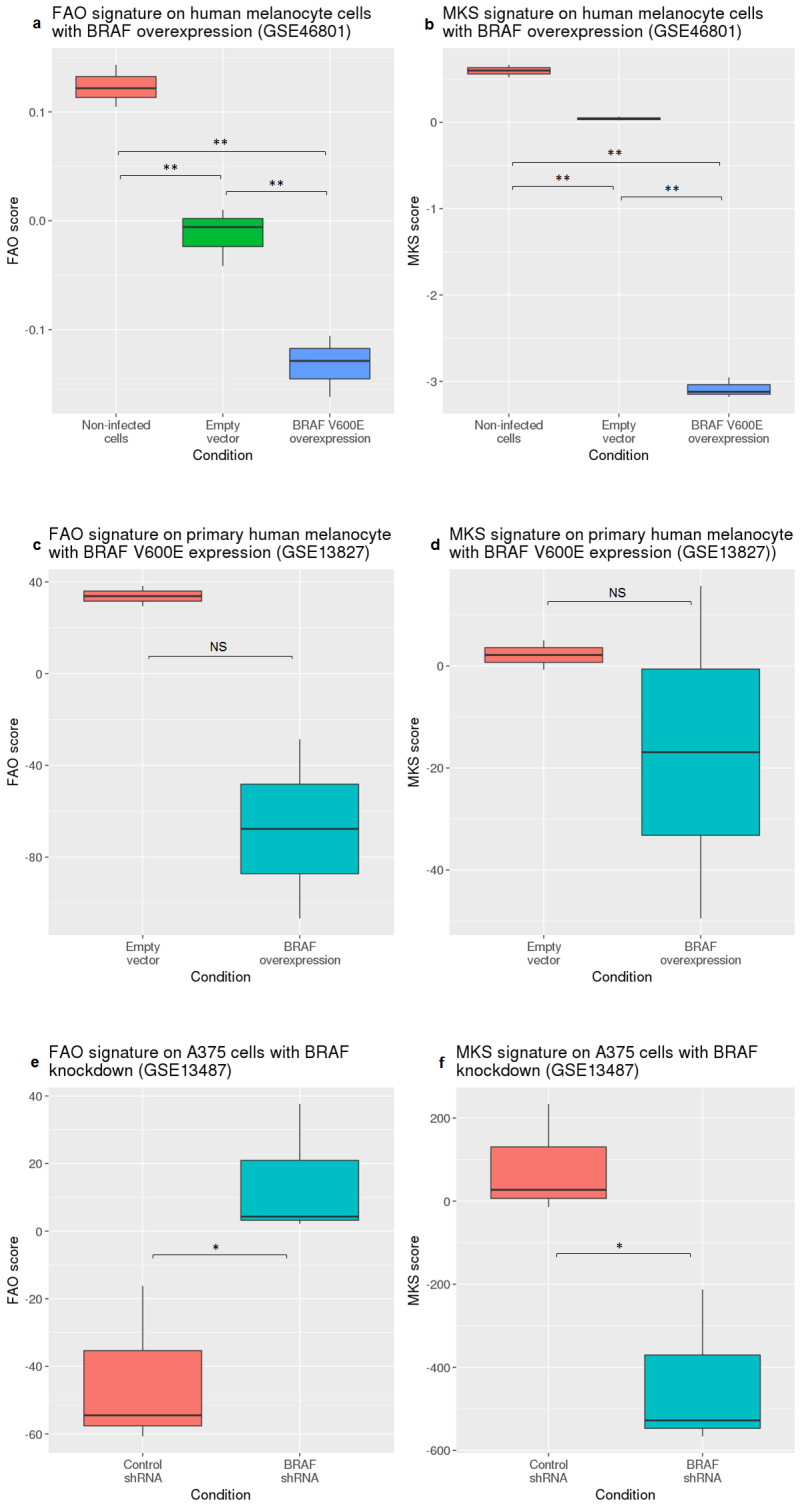

Figure 5.8: Transgenic mutant BRAF expression in melanocytes decreases FAO signature expression. (**a,b**) FAO (a) and MKS (b) signature expression in primary human melanocytes that were lentivirally transduced with control or BRAF V600E transgene for two weeks. n=3 for all conditions. (**c,d**) FAO (c) and MKS (d) signature expression in low passage primary human melanocytes that were lentivirally transduced with GFP as control or BRAF V600E transgene for 5 days. (**e,f**) FAO (e) and MKS (f) signature expression in A375 cells treated with 1 μg/mL doxycycline for 48 hours to induce shRNA expression against GFP control or BRAF. FDR-adjusted p * $\leq$0.05; **$\leq$0.01; NS = non-significant.

5.4.3 *RAS mutant expression alters FAO signature expression*

Next, whether different *RAS* mutants affect the FAO signature to different degree was investigated. To achieve this, gene expression datasets that overexpress different *RAS* mutants in primary human melanocytes, or a mouse model injected with doxycycline-inducible melanoma cells with NRAS Q61K were analysed (Gupta et al., 2016; Eskandarpour et al., 2009; Kwong et al., 2012).

Immortalised human melanocytes stably expressing NRAS Q61K, HRAS V12 or KRAS V12 mutants resulted in decreased expression of the FAO signature (Fig 5.9a). Of all RAS mutants, NRAS Q61K expression induced the largest decrease in the FAO signature. Furthermore, knockdown of NRAS in two independent melanoma cell lines increased the FAO signature expression (Fig 5.9c). However, the MKS proliferation was only significantly down regulated in 224, but not BL cells (Fig 5.9d).

Additionally, in an inducible NRAS Q61K melanoma cell line grown in mice, removal of doxycycline from the diet resulted in the up regulation of the FAO signature, compared to control (continued NRAS Q61K induction) (Fig 5.9e). Treatment with MEK inhibitor also increased expression of the FAO signature expression, albeit to a weaker extent compared to mutant RAS depletion (Fig 5.9e, blue bar). As expected, the MKS proliferation signature was significantly decreased when mutant RAS expression was depleted (Fig 5.9f). MEK inhibition did not decrease the MKS signature expression, which is consistent with the findings from the authors that generated this dataset, who showed poor anti-proliferative response of the NRAS Q61K allograft to MEK inhibitor (Kwong et al., 2012).

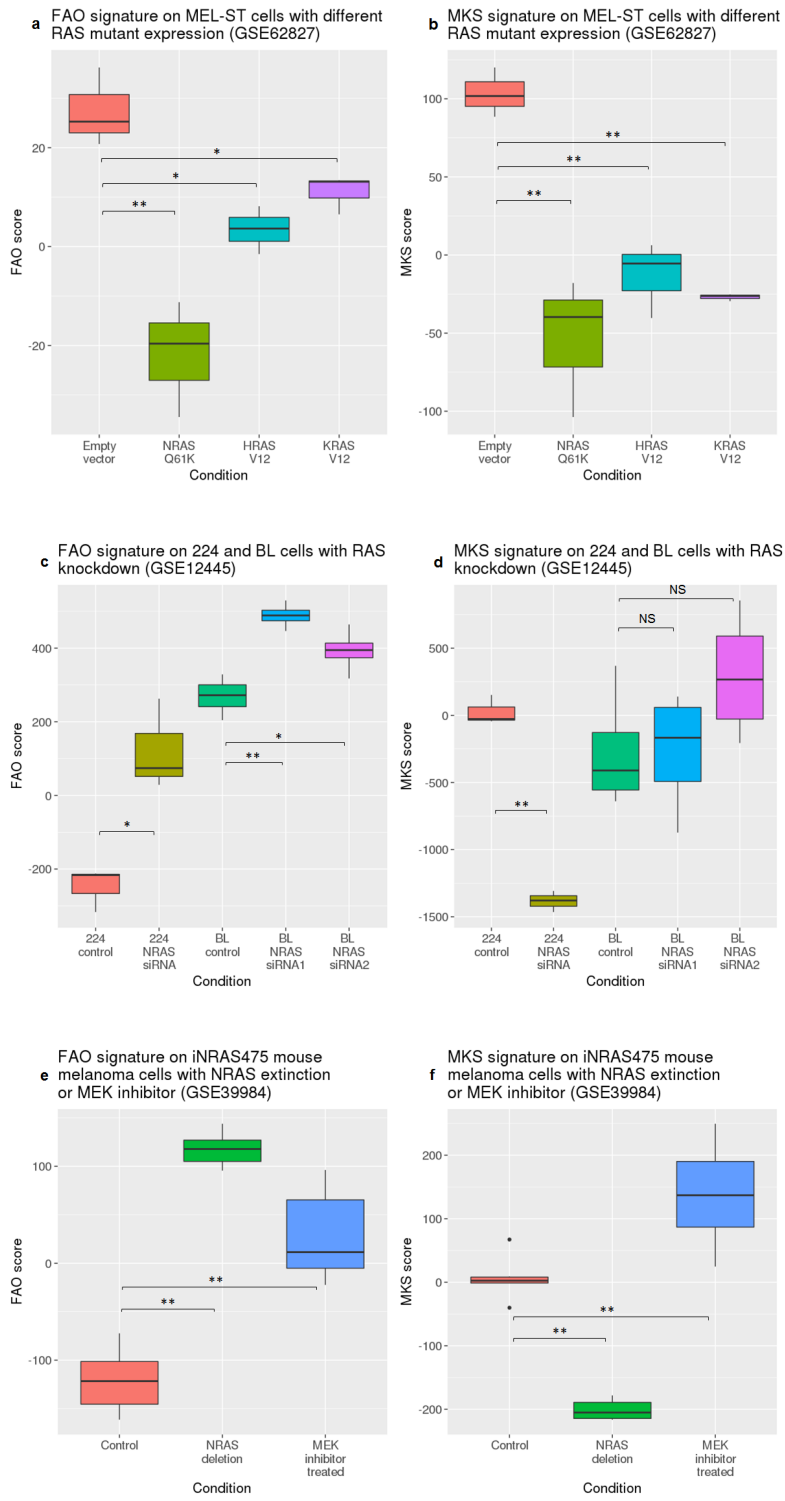

Figure 5.9: Mutant RAS expression in melanocyte or melanoma cell lines influences FAO signature expression. (**a,b**) FAO (a) and MKS (b) signature expression in primary human melanocytes transduced with control or BRAF V600E transgene lentiviruses for two weeks. n=3 for all conditions. (**c,d**) FAO (c) and MKS (d) signature expression in 224 or BL melanoma cell lines transfected with siRNAs against RAS or scramble control for up to 72 hours. n=4 for all conditions. (**e,f**) FAO (e) and MKS (f) signature expression in melanona cells injected into mice and tumours grown for 6 weeks. Mice were then treated with vehicle control, MEK inhibitor AZD6244 (100mg/kg) or doxycycline withdrawn to deplete mutant NRAS expression for four days. FDR-adjusted p *$\leq$0.05, **$\leq$0.01; NS = non-significant.

5.4.4 *BRAF or MEK inhibition in other cancer types increases FAO signature expression*

To investigate whether the previous findings can be extended to BRAF mutant colorectal cancer, as well as upon MEK inhibition, gene expression datasets of HT29 colorectal cancer cells treated with a BRAF inhibitor, wildtype BRAF SW480 colorectal cancer and a panel of pancreatic cancer cell lines treated with a MEK inhibitor, were analysed (Herr et al., 2015; Schoumacher et al., 2014; Gysin, Paquette, and McMahon, 2012).

Consistent with findings from melanoma cell lines, BRAF inhibition in HT29 cells resulted in increased expression of the FAO signature (Fig 5.10a). Inhibition of MEK - a kinase downstream of RAF - in SW480 colorectal cancer cell line and pancreatic cancer cell lines consistently increased the expression of the FAO signature, compared to untreated controls (Figs 5.10c and 5.11).

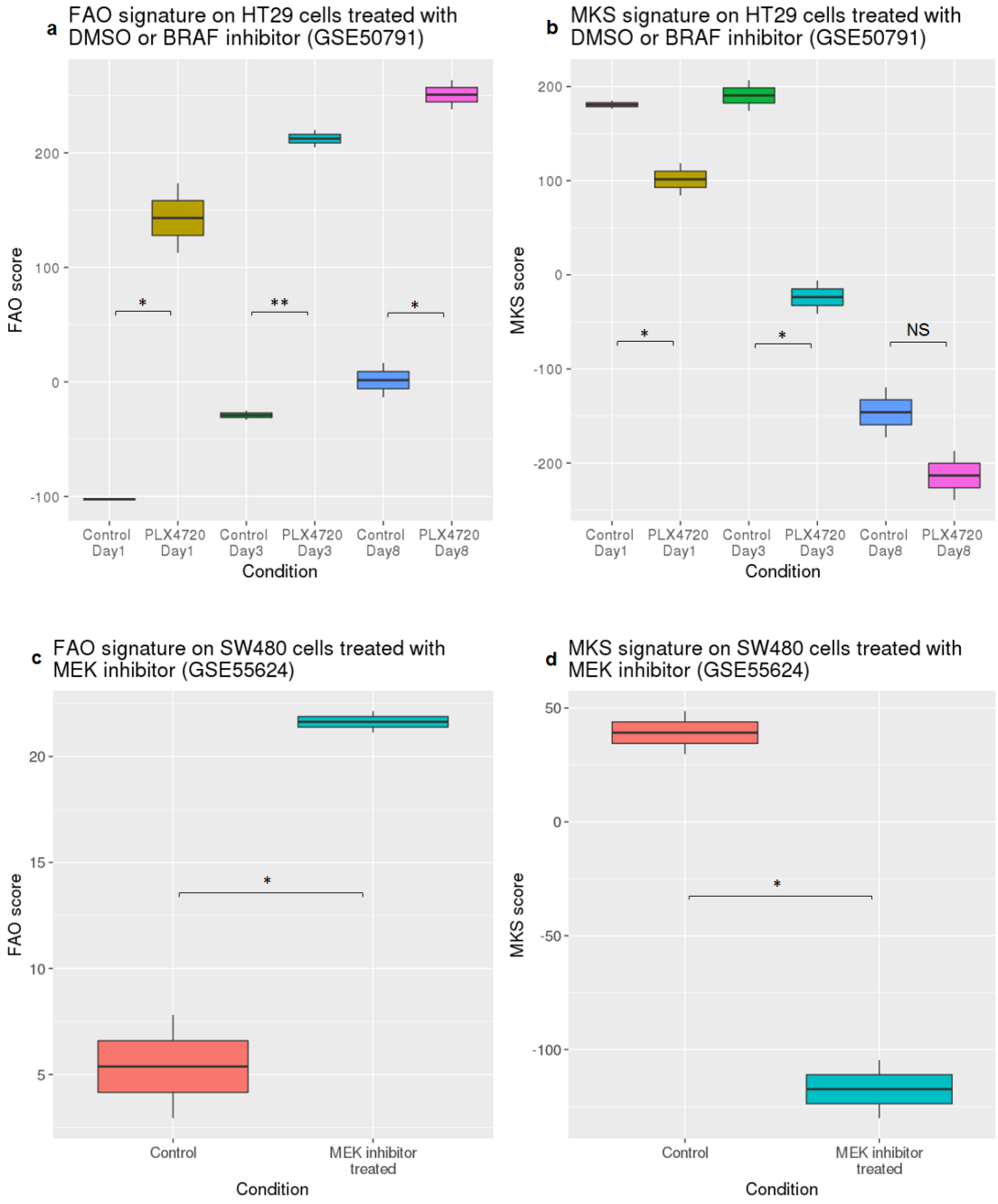

Figure 5.10: BRAF or MEK inhibition in colorectal cancer cell lines increases FAO signature expression. (**a,b**) FAO (a) and MKS (b) signature expression in cells seeded into Matrigel matrix and treated with either 3 μM PLX4720 (BRAF inhibitor) or DMSO for indicated time points. n=2 for all conditions. (**c,d**) FAO (c) and MKS (d) signature expression in cells treated with 1 μM AZD6244 (MEK inhibitor) or DMSO for 16 hours. n=2 for both conditions. FDR-adjusted p *$\leq$0.05, **$\leq$0.01; NS = non-significant.

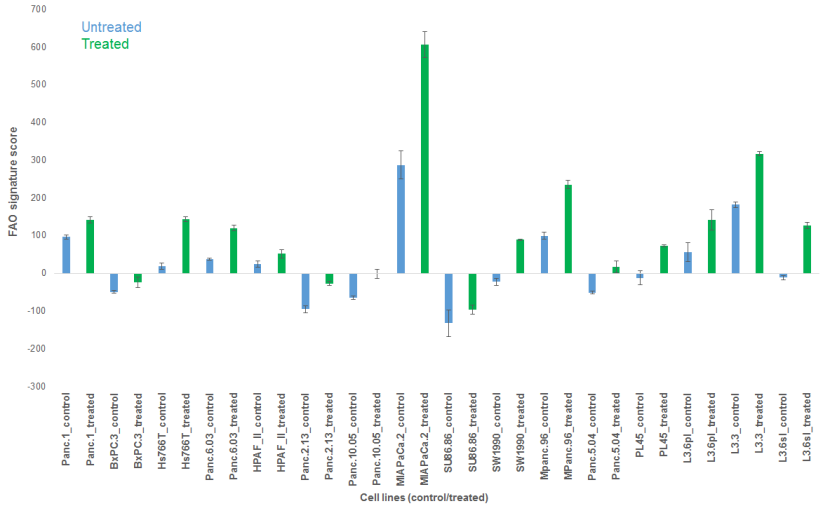

Figure 5.11: MEK inhibition increases FAO signature expression in a panel of pancreatic cancer cell lines. Indicated pancreatic cancer cell lines were treated with 2 mM CI-1040 (MEK inhibitor) for 24 hours (GSE45757). n=3, error bars = standard error of mean.

5.4.5 MITF expression is associated with FAO signature expression

As mentioned earlier, the transcription factor MITF has varied functions depending on its expression level, and has been shown to promote oxidative metabolism in response to BRAF V600E inhibition (Haq et al., 2013). However, how FAO is affected by MITF expression status remains to be determined. To explore for an association between MITF expression and FAO signature expression, gene expression datasets from different cell systems that genetically modulate MITF levels were analysed (Haq et al., 2013; Scholer et al., 2015).

As shown in Fig 5.12a, the FAO signature expression was upregulated in primary melanocytes overexpressing both BRAF V600E and MITF, compared to BRAF V600E alone. MITF overexpression also resulted in decreased proliferation, evident from decreased expression of the MKS signature (Fig 5.12b). In another dataset, siRNA against MITF in Malmet15 melanoma cell line decreased expression of the MKS proliferation signature (Fig 5.12d) and showed a trend towards increased FAO signature expression

(Fig 5.12c). The slight deviation from statistical significance could be explained by the small sample size in this experiment (n=2). Lastly, overexpression of MITF in BS149 glioblastoma cell line was observed to increase the FAO signature expression (Fig 5.12e), in agreement with the finding in the melanocyte system. Taken together, these findings reveal an hitherto unrecognised association between MITF expression and expression of genes involved in FAO.

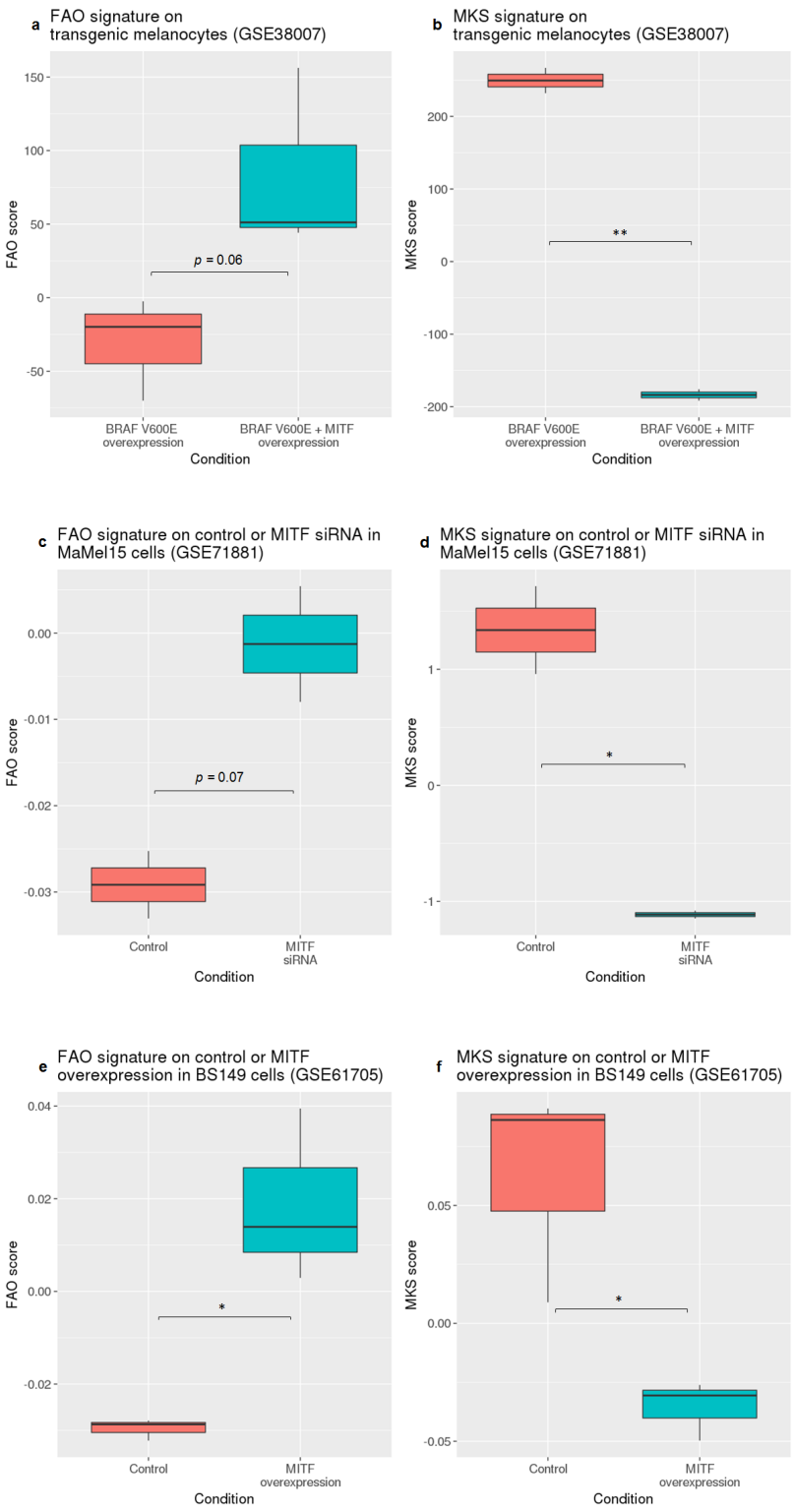

Figure 5.12: MITF overexpression or knockdown increases FAO signature expression. (**a,b**) FAO (a) and MKS (b) signature expression in immortalised, isogenic melanocytes overexpressing either BRAF V600E or BRAF V600E and MITF. n=3 for both lines. (**c,d**) FAO (c) and MKS (d) signature expression in MaMel15 cells transfected with control or MITF siRNA for 48 hours. n=2 for both lines. (**e,f**) FAO (e) and MKS (f) signature expression in BS149 cells transfected with plasmid expressing the HA tag as control or MITF for 24 hours. FDR-adjusted p *$\leq$0.05, **$\leq$0.01.

5.5 Discussion

5.5.1 Wnt signalling and FAO signature expression

The Wnt signalling pathway is dysregulated in approximately 80% of colorectal cancers (Muzny et al., 2012b). While alterations in glycolysis in response to modulation of Wnt signalling have been reported (Pate et al., 2014), the analysis presented in this chapter is the first to demonstrate that FAO is down regulated when Wnt signalling is active. Analysis of gene expression data from *in vivo* or *in vitro* systems that studied the alterations in various Wnt signalling effectors or regulators (e.g., APC, β-catenin, DKK-1, Bcl9) found a significant association between this pathway and expression of the FAO signature. It should be emphasised here that for most of these analyses, the FAO and MKS proliferation signature expression were inversely correlated. However, while knock out of *Bcl9* (wildtype Bcl9 activates Wnt signalling) in mouse colon resulted in increased FAO signature, no significant difference in MKS proliferation signature expression was observed, compared to wild type Bcl9 expression. This suggests that the FAO regulation can be uncoupled from proliferation, depending on which member of the Wnt signalling pathway is altered. Notably, the association between Wnt signalling and FAO signature expression was not limited to colon tissues or tumours, but also observed in mammary tissues across different stages of tumourigenesis.

A gene signature derived from Bcl9 knock out mouse colon was observed to be associated with *better* survival in multiple colorectal cancer datasets (Moor et al., 2015). Therefore, it is not unreasonable to expect the FAO signature to be prognostic in colorectal cancer. However, this assumption was not true: survival analysis of two colorectal cohorts found no association between the FAO signature and survival outcomes. Since the FAO signature was observed to be prognostic in multiple cancers previously, why was this not observed in colorectal cancer? A plausible explanation is that the FAO activity

in colorectal cancer is very low, and therefore, survival risk stratification based on this pathway is not practicable.

5.5.2 MAPK pathway activity and FAO signature expression

Metabolic flux analysis in a panel of melanoma cell lines found that the majority of glucose is converted to lactate, which is consistent with the Warburg effect, as well as anaplerotic contribution of glutamine to fatty acid synthesis, compared to normal melanocyte lines (Scott et al., 2011). In another study, Seahorse extracellular flux analysis found that normal melanocytes had lower basal oxygen consumption compared to melanoma cell lines (Hall et al., 2013). However, the coupling of ATP synthesis efficiency to oxygen consumption was significantly higher in melanocytes, compared to melanoma cell lines. Furthermore, mitochodrial proton leak was higher in melanoma cell lines, compared to normal melanocytes (Hall et al., 2013). This is indicative of mitochondrial metabolism dysfunction in melanoma cell lines. Despite the efforts in characterising the metabolic correlates associated with the MAPK signalling pathway, very little is known as to how alterations in this pathway alters FAO in cancer cells.

5.5.2.1 *BRAF activity and FAO signature expression*

Treatment of melanoma cell lines with vemurafenib was shown to increase the expression of genes involved in citric acid cycle and oxidative phosphorylation (Haq et al., 2013), but how this intervention affects FAO is unclear. In this chapter, analysis of gene expression datasets from BRAF mutant melanoma cell lines treated with vemurafenib found an increase in the expression of the FAO signature. This increase in FAO would be expected to result in increased acetyl-CoA generation, which is then further metabolised in the mitochondria. As such, this pathway could contribute to the increased mitochondrial respiration reported in melanoma cells in response to BRAF inhibition (Parmenter

et al., 2014).

To gain insight on the role of BRAF expression on FAO signature expression, gene expression datasets from melanocytes with transgenic BRAF expression were analysed. This analysis found that the FAO signature was down regulated upon transgenic BRAF V600E expression in melanocytes. Interestingly, the MKS proliferation signature was not increased in cells with constitutive BRAF activity. This is most likely attributed to oncogene-induced senescence, a tumour suppressive mechanism that prevents progression of benign growths (Dhomen et al., 2009). Indeed, one of the datasets analysed (GSE46801) was generated from a study that focused on elucidating the role between BRAF-induced senescence and Wnt signalling (Pawlikowski et al., 2013). Assuming that the melanocytes do not carry additional mutations, these findings suggest that constitutive BRAF activation *per se* is sufficient to alter expression of genes involved in FAO, independently of proliferation.

The association between the FAO signature and BRAF inhibition described in this chapter complement the findings by Hall *et. al.*, who reported that genetic or pharmacologic inhibition of BRAF V600E in two melanoma cell lines decreased expression of genes involved in glycolysis such as *PGAM1*, *GAPDH*, and *LDHA*, while oxygen consumption was increased 72-96 hours post-BRAF inhibition (Hall et al., 2013). Importantly, FM55-M2 and SK-MEL-28 melanoma cell lines showed 3 fold lower coupling of oxygen consumption to ATP synthesis compared to normal melanocytes. Consequently, the switch to mitochondrial respiration could not maintain sufficient ATP production to meet the energetic needs of the melanoma cells. Remarkably, overexpression of *GAPDH* in SK-MEL-28 cells was sufficient to significantly increase cell viability, and decrease the number of detached or senesced cells in response to BRAF inhibition, compared to empty vector control cells. Findings from this chapter build on the work of Hall *et.al.* (Hall et al., 2013) by presenting evidence that genes involved in FAO are significantly

altered in response to modulation of the RAS-RAF-MEK/ERK signalling pathway.

5.5.2.2 *MAPK pathway modulation and FAO signature expression*

Expression of three different RAS mutants in melanocytes significantly decreased expression of the FAO signature. This decrease was particularly stark in melanocytes with NRAS Q61K expression, which is the second most frequent oncogenic mutation in cutaneous melanoma, and occurs in a mutually exclusive manner to BRAF mutation (Hodis et al., 2012; Akbani et al., 2015). Together, this suggests that activation of upstream members of the MAPK pathway can alter expression of genes involved in FAO.

Since RAS mutations remain a challenge for small molecule inhibition, tumours with RAS-induced MAPK pathway activation can be targeted with MEK inhibitors. Pharmacological MEK inhibition in colorectal and melanoma cell lines resulted in increased expression of the FAO signature, compared to untreated control cells. Conversely, the MKS proliferation signature was decreased in the MEK inhibitor-treated cells. Furthermore, the increase in FAO signature expression was also observed in a panel of pancreatic cancer cell lines treated with a MEK inhibitor, which altogether, suggests that the association between MAPK pathway status and FAO signature expression is a feature of multiple cancers.

5.5.3 Extreme ends of MITF expression decreases proliferation and upregulates FAO signature

The regulation of MITF protein, and its functional consequence is abstruse; and as such, a rheostat model was proposed to explain various reports on MITF expression level and the associated phenotype. Adding to this complexity, Muller *et.al.* reported that increased, as well as loss of MITF expression was observed in a panel of melanoma cell

lines that acquired resistance to ERK- or BRAF inhibitor treatment (Muller et al., 2014).

The transcription factor MITF has also been implicated in regulating oxidative metabolism in melanoma (Haq et al., 2013). Analysis reported in this chapter found that melanocytes overexpressing MITF showed an increased FAO signature expression. This is consistent with the rheostat model of high MITF levels inducing differentiation and thereby, decreasing proliferation. In MaMel 15 melanoma cells, siRNA against MITF increased FAO signature expression, which is in line with low MITF levels inducing cell cycle arrest proposed by the rheostat model. In short, MITF expression at either extreme results in increased FAO signature expression.

Haq *et. al.* proposed that the MITF-induced increase in oxidative metabolism could compensate for decreased glycolysis from BRAF inhibition, and promote treatment resistance (Haq et al., 2013). However, over 75% of resistance to vemurafenib or dabrafenib treatment is due to reactivation of the MAPK pathway, which is expected to repress MITF and PGC1A expression (Rizos et al., 2014). Therefore, the proposed logic of the association between increased oxidative metabolism and BRAF inhibition resistance is somewhat dissonant. Rather, as Fig 5.12 demonstrates, overexpression of MITF in the presence of BRAF V600E decreased the expression of the MKS proliferation and increased the expression of the FAO signatures, compared to BRAF V600E overexpression alone. Since the rheostat model suggests that high expression level of MITF promotes differentiation and inhibits proliferation, one can propose an alternative notion: MITF-PGC1A mediated increase in oxidative metabolism upon BRAF inhibition is a *desirable* outcome, and therapies that promote FAO offer a mechanism of achieving this. In support of this argument to an extent, co-treatment of BRAF-mutant melanoma cell lines that are vemurafenib-resistant via an *NRAS* mutation with dichloroacetate - an inhibitor of PDK which activates PDH to oxidise pyruvate in the mitochondria - resulted in a greater degree of cell death, compared to high dose vemurafenib alone (Parmenter

et al., 2014).

5.6 Summary, strenghts and limitations

Analysis in this chapter has shown that the FAO gene signature is:

1. altered in response to transgenic expression of *Apc* or *DKK-1*, or knock down of *CTNNB1* and *Bcl9*
2. decreased in response to constitutive Wnt signalling in a mammary tumour model
3. up regulated upon pharmacologic BRAF and MEK inhibition
4. inversely correlated with activity of MAPK components
5. up regulated when MITF expression is either low or high

This chapter describe novel associations between expression of genes involved in FAO and MAPK and Wnt signalling. Importantly, the analyses conducted included datasets that modulated different components of these pathways, which was performed to demonstrate that the association observed is attributable to the activity of the pathways, rather than effects of individual genes within the MAPK or Wnt signalling cascade.

Since proliferation is a strong component of the activity of these two pathways, it is likely that expression of the FAO signature is strongly intertwined with the proliferation status of the cancer cell. These findings, however, were based only on computational analysis of published gene expression datasets. Nonetheless, they provide compelling basis for experimental characterisation in pre-clinical systems, and potential questions at hand include:

(i) can genetic or pharmacologic manipulations that promote FAO drive *BRAF* mutant melanoma cell lines, and colorectal cancer cell lines with constitutive Wnt signalling

away from glycolysis?

(ii) how do manipulations in (i) affect proliferation, invasion, migration of melanoma and colorectal cancer cells?

(iii) what are the global molecular changes that occur in response to (i)?

Addressing these questions may contribute to our understanding of the intersection between oncogenic signalling and metabolism; and may identify novel therapeutic targets to complement current standard care for patients with tumours that exhibit alterations in MAPK and Wnt signalling.

Chapter 6

Analysis of *CPT1A* modulation in *in vitro* breast cancer cell systems

6.1 Background

The previous chapters have described an association between the FAO signature expression and prognosis in certain cancers. The consistent downregulation of the signature in several different tumour types, compared to normal tissues suggests that this pathway is downregulated during disease progression. Importantly, the FAO signature is significantly negatively correlated with the MKS proliferation signature.

One mechanism of regulating metabolic pathway flux is through the activity of rate-limiting enzymes. As mentioned in the Introduction, in FAO, the rate-limiting enzyme is *CPT1A* (Bruce et al., 2009; Henique et al., 2010). Importantly, *CPT1A* is a member of the 19-gene FAO signature. Pharmacologic and genetic modulation of this enzyme has been shown to affect beta-oxidation flux (Sousa et al., 2005; Pike et al., 2011). Overexpression of *CPT1A* in haematopoietic or skeletal muscle cells resulted in increased ox-

idation of radiolabelled palmitate or oleate, while shRNA-mediated *CPT1A* knockdown of *CPT1A* in LNCaP prostate cancer cells reduced palmitate oxidation rates (Deberardinis, Lum, and Thompson, 2006; Henique et al., 2010; Schlaepfer et al., 2014). Therefore, it stands to reason that CPT1A expression level is associated with cellular FAO activity.

Two questions arise from these findings: (i) why is the FAO signature expression down-regulated in tumours, compared to normal tissues; and (ii) can, and, how does modulating FAO affect cancer cells? This chapter will attempt to answer the second question using experimental systems. Obviously, modulating the expression of all 19 genes in the FAO signature is not practical in terms of time and budget available for this project. Therefore, the second question raised above will be addressed by generating and characterising transgenic cell lines that modulate *CPT1A* expression for reasons explained above, and its effect on different cellular characteristics investigated using various functional assays.

6.2 Objectives

The objectives of this chapter are to:
(i) generate and characterise *CPT1A* overexpression and knockdown systems using normal breast and breast cancer cell lines
(ii) characterise growth rates between *CPT1A* transgenic and control lines
(iii) characterise migration rates between *CPT1A* overexpression and control line
(iv) compare anchorage-indepent growth in transgenic and control lines
(v) functionally validate transgenic lines with *CPT1A* modulation using extracellular flux technology

6.3 *CPT1A* expression higher in ER-positive compared to ER-negative breast tumours and cell lines

First, the expression of *CPT1A* was analysed using gene expression data from breast tumours. In five of six datasets with tumour ER status available analysed, *CPT1A* mRNA expression was significantly higher in ER-positive, compared to ER-negative tumours (Fig 6.1).

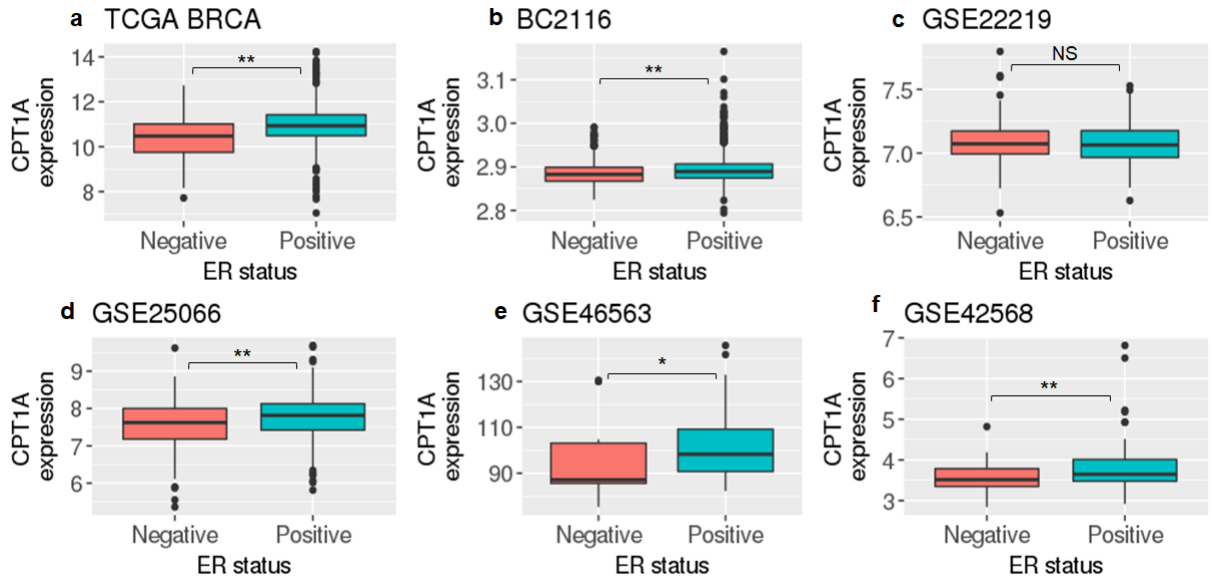

Figure 6.1: ER-positive tumours have higher *CPT1A* mRNA expression compared to ER-negative tumours. Microarray gene expression datasets from primary breast tumours with ER status were analysed for expression of *CPT1A*. Wilcox rank sum test p **$\leq$0.01; *$\leq$0.05; NS, non-significant.

To determine which cell systems to modulate CPT1A, transcriptome datasets from a panel of breast cancer cell lines were analysed for *CPT1A* mRNA expression. As shown from the waterfall plot in Fig 6.2, a striking enrichment of higher *CPT1A* expression in ER-positive, compared to ER-negative cell lines in the first dataset (Neve et al., 2006), which was also observed in two other independent datasets (Supp Figs A.3, A.4). In-

triguingly, in the second dataset, an adriamycin-resistant, oestrogen-independent variant of the MCF7 cell line previously established was observed to have lower *CPT1A* mRNA expression levels, compared to the parental line (Fig 6.3, black arrow) (Vickers et al., 1988).

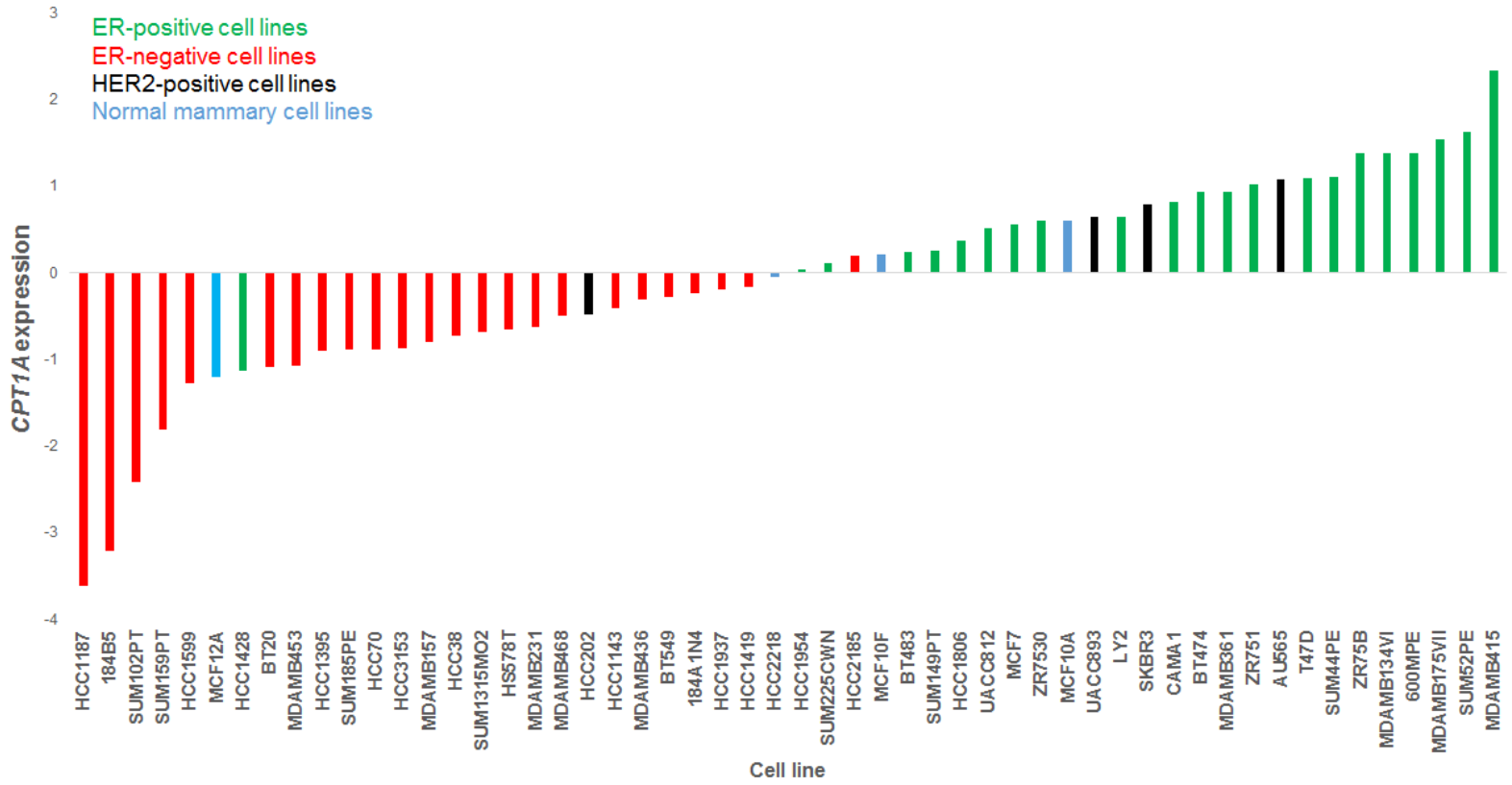

Figure 6.2: ER-positive cell lines have higher *CPT1A* mRNA expression compared to ER-negative cell lines. Neve *et.al.* dataset (n=54) (Neve et al., 2006).

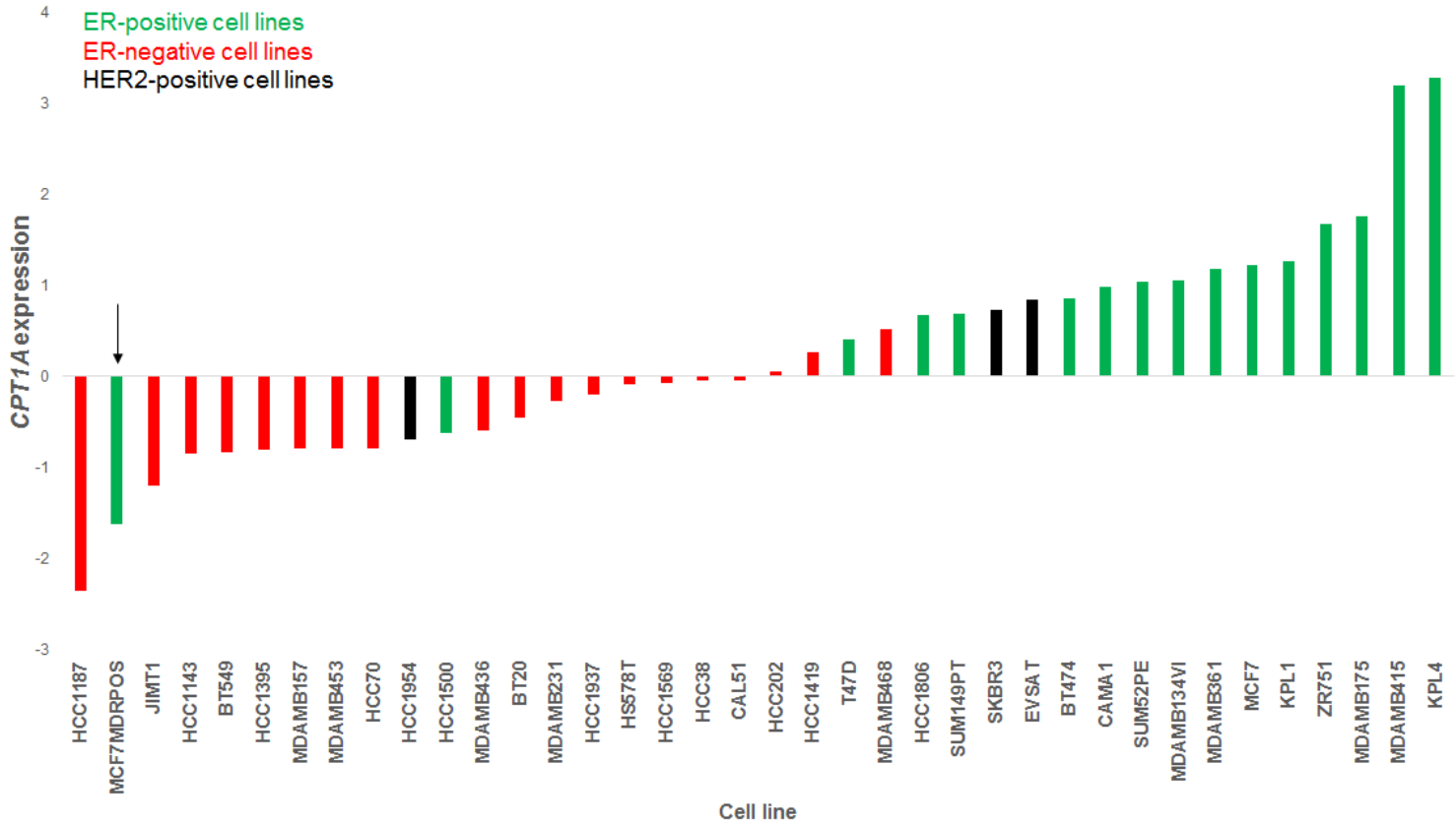

Figure 6.3: ER-positive cell lines have higher *CPT1A* mRNA expression compared to ER-negative cell lines. (AstraZeneca dataset (n=38), E-GEOD-57083).

6.4 Generation of CPT1A overexpression in MDA-MB231 cell line

To investigate the functional consequence of modulating *CPT1A* expression in cell systems, tetracycline (Tet) inducible cell lines were generated to overexpress and knockdown *CPT1A* in different cell systems.

The TetOn system is based on the transcriptional activation of a transgene downstream of a Tet response element promoter by the reverse tetracycline transactivator (rtTA) in the presence of doxycycline (Dox). The levels of induction can be optimised to achieve the optimal induction based on the dosage of Dox. In *in vitro* systems, this is achieved by transfecting cells with plasmid/s that expresses rtTA and the transgene of interest, followed by adding Dox to the culture medium. This inducible system allows the circumvention of potential cytotoxic or non-relevant effects of long-term continual expression of a transgene.

Since the MDA-MB231 cell line has low *CPT1A* expression, a double stable Tet system was generated to overexpress this gene in this cell line. Conversely, the MCF7 cell line, which has high *CPT1A* expression, was used to generate a stable shRNA-based knockdown cell system.

6.4.1 *Luciferase assay for Tet induction in MDA-MB231 single, stable transfectant clones*

To generate a double stable system using the MDA-MB231 cells, an initial transfection with pTetOn was performed. Cells were then seeded into 10- and 15 cm dishes at various densities and selected for stable transfectants with 1 mg/mL of G418. After

approximately 3 weeks of selection, colonies were lifted into 24 well plates and expanded.

To determine which G418-resistant clones demonstrated satisfactory Tet transcriptional activity in response to doxycycline treatment, clones were plated in duplicates and transfected the following day with a plasmid that expresses firefly luciferase downstream of a Tet response element (TRE). One of the two transfected wells was induced with 2 μg/mL Dox for 48 hours, and protein lysates were prepared and assayed for luciferase activity. Control wells were treated with 2 μL of milliQ water. Clones with at least 20 fold induction were taken further for repeated screens. As shown in Fig 6.4, of 29 clones screened, two clones (10 and 19) showed at least 20 fold induction of luminescence signal compared to non-induced cells (Fig 6.4a). Upon further screens, clone 10 was selected to generate the second stable, CPT1A transgenic MDA-MB231 cell line (Fig 6.4b).

6.4.2 *Generation of double, stable transfectant clones overexpressing CPT1A*

To generate a double stable cell line, pTetOn MDA-MB231 cell line was co-transfected with pTRE-CPT1A and pBabe-puro, a plasmid that confers puromycin resistance. Cells were selected for approximately 2-3 weeks with 1 μg/mL puromycin, and single clones lifted into 24 well plates. Single clones were screened for pTRE-CPT1A integration by PCR and positive clones were screened by qPCR for *CPT1A* mRNA induction upon 2 μg/mL Dox treatment (Fig 6.5).

Based on the qPCR screen, clones with $\geq$ 8-fold mRNA induction by qPCR were screened further by immunoblot analysis (Fig 6.6). Clones 3, 5 and 17 were seeded and induced for 48 hours with 2 μg/mL Dox. Total protein was harvested, resolved by SDS-PAGE and immunoblotted for CPT1A. As shown in Fig 6.6, all clones showed increased CPT1A expression after 48 hours induction. Further screens found clone 5 to

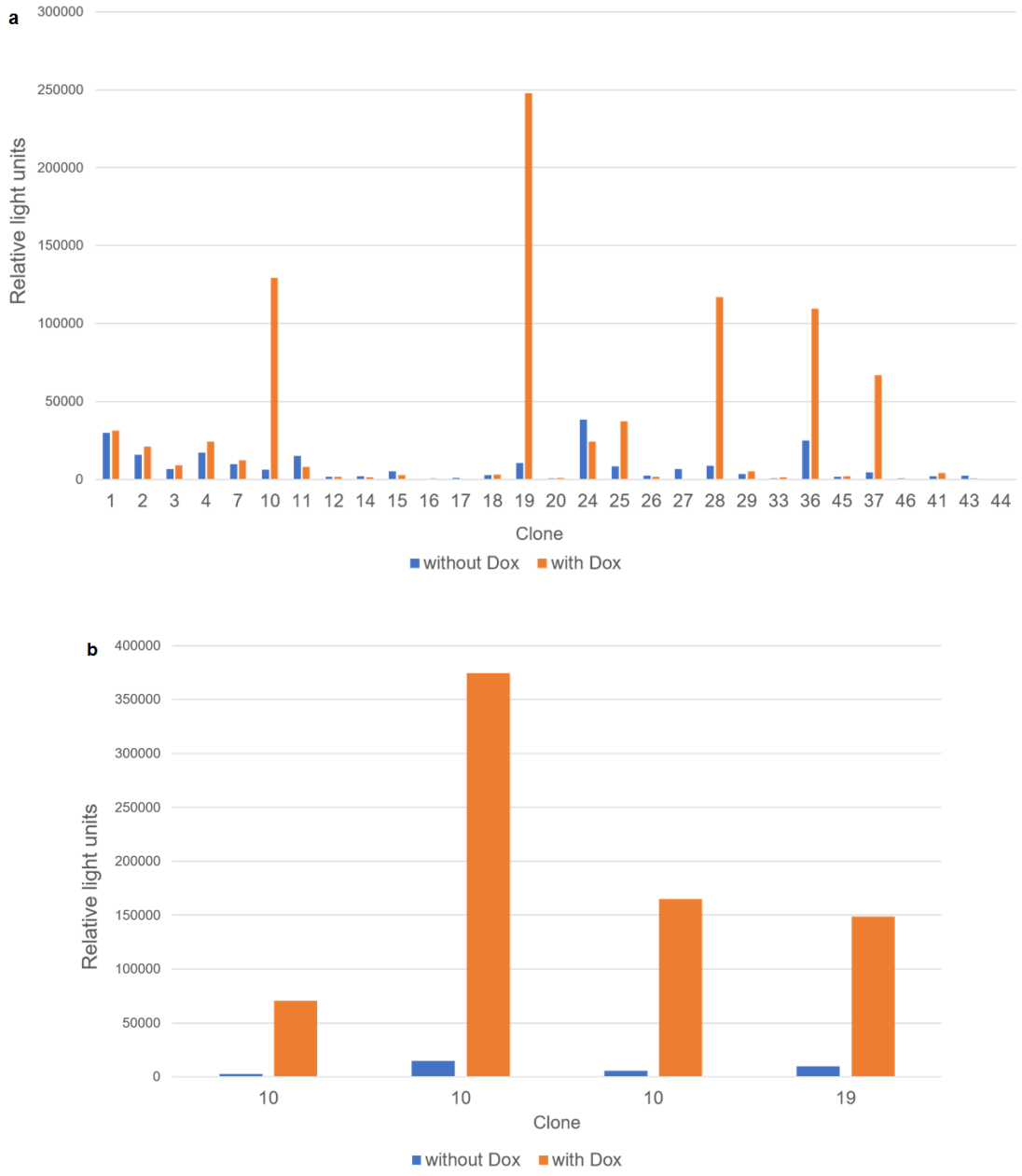

Figure 6.4: Luciferase assay to measure rtTA inducibility in MDA-MB231 TetOn clones. (a) 29 putative TetOn clones were screened and (b) clones 10 and 19 were taken further for repeated screens. n=1 for all conditions.

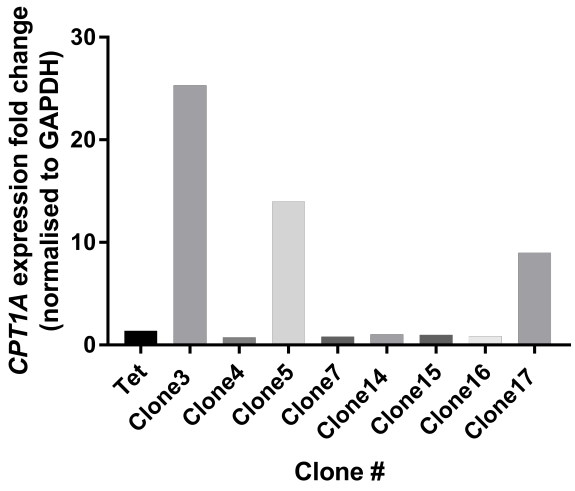

Figure 6.5: *CPT1A* mRNA overexpression screen after 48 hr induction in putative MDA-MB231 pTRE-CPT1A clones. Cells were seeded in 6 well plates in duplicates and one well induced with Dox for 48 hours. Control wells were treated with 2 μL of milliQ water. Total RNA was prepared and expression of *CPT1A* measured by qPCR, normalised to *GAPDH*. Fold changes are presented relative to -Dox. n=1 for all conditions.

express CPT1A in the absence of Dox (Supp Fig A.5.5) and hence, clones 3 and 17 were further characterised.

6.4.3 *Dose- and time course optimisation of CPT1A induction in MDA-MB231 double transfectants*

To determine the optimal induction of *CPT1A* expression, dose- and time-course experiments were performed. For Dox dose-response experiment, cells were seeded into 6 well dishes and induced with 0.5- to 5 μg/mL of Dox for 48 hours. As shown in Fig 6.7, there was a dose-dependent increase in CPT1A expression in cells induced with increasing doses of Dox. Since high Dox concentrations may have a negative impact on cells (Ahler et al., 2013), 2 μg/mL was selected as the dose for further experiments. Next, a time course analysis was performed to determine the time point at which optimal CPT1A expression occurred. Cells were seeded and induced with 2 μg/mL of Dox for

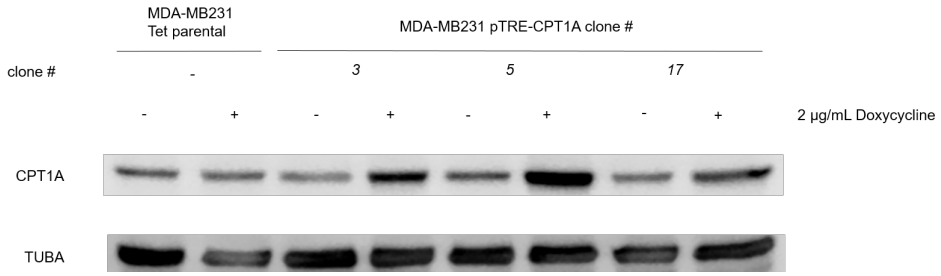

Figure 6.6: CPT1A overexpression screen after 48 hr induction in selected MDA-MB231 pTRE-CPT1A clones. Cells were seeded in 6 well plates and induced with Dox for 48 hours. Control wells were treated with 2 μL of milliQ water. Total lysates were resolved by SDS-PAGE and immunoblotted for CPT1A expression. Expression of alpha-tubulin (TUBA) was used to estimate loading accuracy. CPT1A 88 kDa; TUBA 50 kDa.

up to 96 hours. The immunoblot shown in Fig 6.7 indicates increased CPT1A expression over time, starting at 36 hours, with strong expression observed from 48 hours onwards.

6.5 Generation of *CPT1A* knockdown system in MCF7 cell line

To generate MCF7 cell lines stably expressing inducible shRNA against *CPT1A*, lentiviral particles were prepared and cells transduced, as described in Methods.

To determine extent of *CPT1A* knockdown in the single clones, cells were seeded in duplicates in 6 well dishes and induced for 5 days. qPCR was performed to compare *CPT1A* mRNA expression levels between uninduced and induced cells. Based on the normalised *CPT1A* expression depicted in Fig 6.8, clone 7 for shRNA1 (57) and clone 2 for shRNA2 (72) were selected for further analysis. Additionally, clone 6 from the non-silencing construct (green bars) was selected as the control clone for Dox-specific

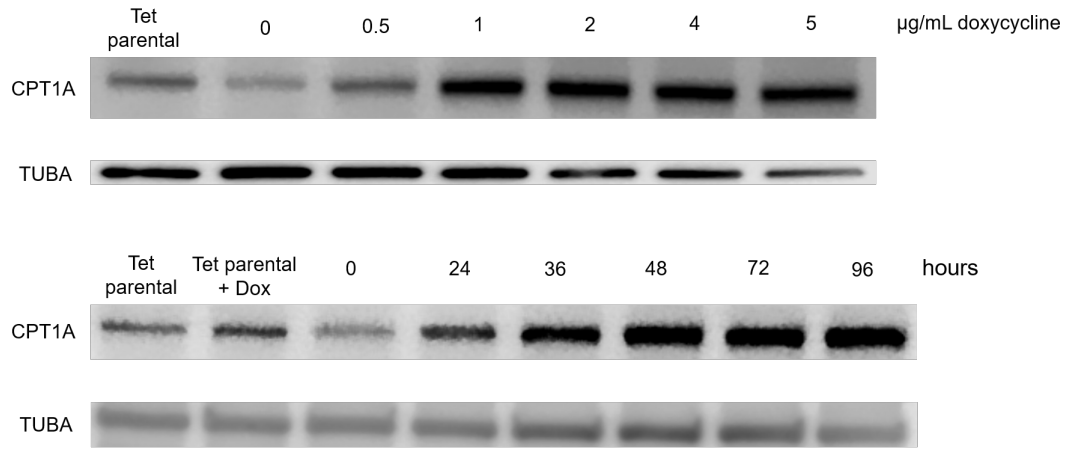

Figure 6.7: Dose response and time course characterisation of CPT1A overexpression in MDA-MB231 cells. Top panel: Cells were treated with indicated doses of Dox for 48 hours. The 0 μg/mL Dox well was treated with 2 μL of milliQ water. Bottom panel: Cells were treated with 2 μg/mL Dox for indicated times. Time 0h and Tet parental control wells were treated with 2 μL of milliQ water. CPT1A 88 kDa; TUBA 50 kDa.

effects in further analysis.

To determine Dox dose required for optimal CPT1A protein knockdown in the MCF7 clones, non-silencing and shRNA clones were treated with 0.5- to 6 μg/mL of Dox for one week. Total protein was harvested, resolved by SDS-PAGE and immunoblotted for CPT1A. As shown in Fig 6.9, one week of *CPT1A* mRNA knockdown resulted between 40- to 60% decreased expression at the protein level.

6.6 Generation of *CPT1A* knockdown system in MCF10A cell line

To generate MCF10A cell lines stably expressing inducible shRNA, cells were transduced with viral particles as described in Methods. Puromycin selection was commenced the following day, and polyclones were generated for non-silencing and the two *CPT1A* shRNAs. In this context, polyclone refers to a mixed population of cells that had stably

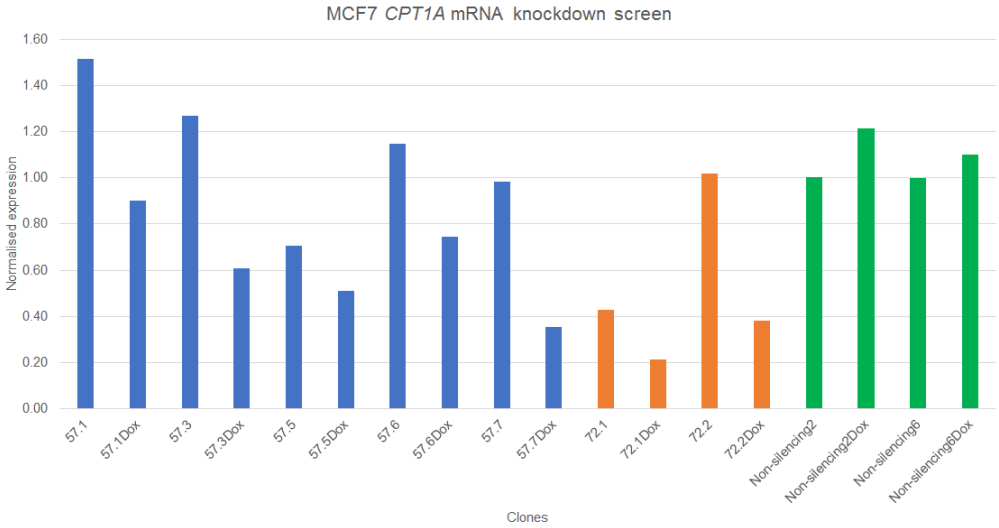

Figure 6.8: *CPT1A* mRNA knockdown screen after 5 days induction in putative MCF7 shRNA clones. MCF7 shRNA1 (blue bars) and shRNA2 (brown bars) clones were induced with Dox for 5 days. Controls were treated with milliQ water. Total RNA was prepared and expression of *CPT1A* measured by qPCR, normalised to *GAPDH*. Fold changes are presented relative to -Dox. Each clone was screened once (n=1) as a first pass, and selected clones were taken further for analysis of knockdown at protein level.

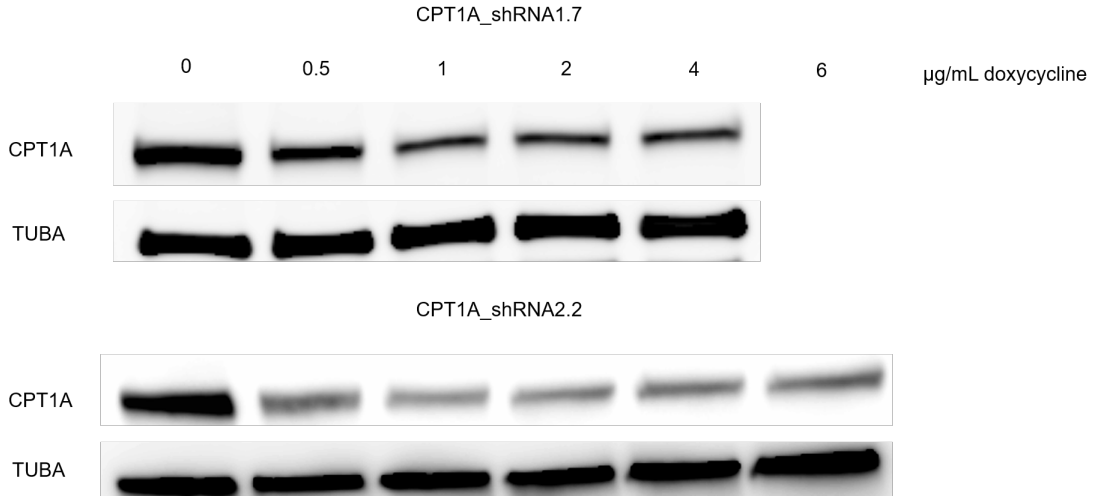

Figure 6.9: Characterising CPT1A knockdown in MCF7 cells. MCF7 shRNA1 and shRNA2 clones were induced with indicated doses of Dox for one week. Lysates were resolved by SDS-PAGE and immunoblotted for CPT1A expression. For shRNA clone 1, 6 μg/mL of Dox was observed to be toxic to the cells, and insufficient lysates precluded the analysis of this condition. The 0 μg/mL of Dox wells were treated with 2 μL of milliQ water. CPT1A 88 kDa; TUBA 50 kDa.

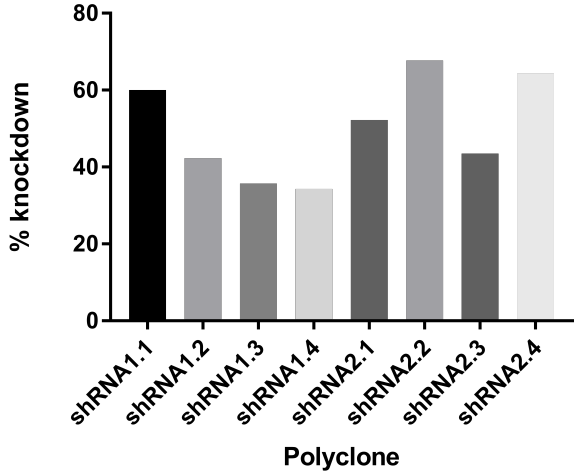

Figure 6.10: *CPT1A* mRNA knockdown screen in MCF10A shRNA polyclones. MCF10A shRNA1 and shRNA2 polyclones with 2 μg/mL Dox for 3 days and assayed *CPT1A* expression. Percentage knockdown is relative to -Dox (treated with 2 μL milliQ, normalised to *GAPDH*. n=1 for all conditions.

integrated the lentiviral construct into the genome and were viable after puromycin selection. This differs to the monoclonal system generated using MDA-MB231 and MCF7 cell lines, where cells were seeded sparsely and individual colonies picked. A mixed, polyclonal population was generated to save time that would have been required to generate monoclonal lines with stable shRNA expression.

Four polyclones from each *CPT1A* shRNAs were screened by qPCR after an initial 3 day knockdown (Fig 6.10). From the qPCR screen, selected polyclones were analysed for protein expression after 5 days of *CPT1A* knockdown. Based on the immunoblot analysis, shRNA clones 1.1 and 2.1 were selected for further experiments.

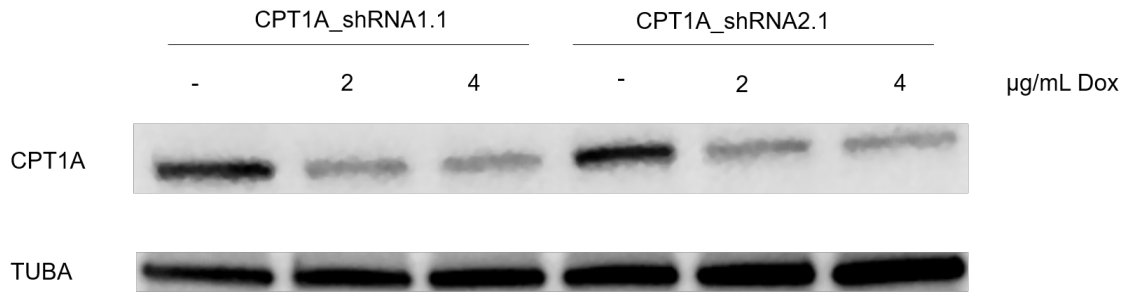

Figure 6.11: Characterising CPT1A knockdown in MCF10A cells. MCF10A shRNA clone 1.1 and shRNA clone 2.1 were induced with 2- or 4 μg/mL Dox for 5 days and 20 μg of lysates resolved by SDS-PAGE and immunoblotted for CPT1A expression. Control wells were treated with 2 μL milliQ. CPT1A 88 kDa; TUBA 50 kDa.

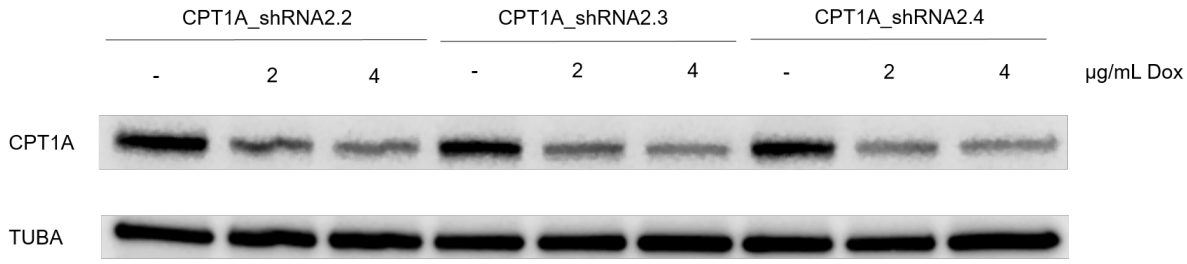

Figure 6.12: Characterising CPT1A knockdown in MCF10A cells. MCF10A shRNA clones 2.1 to 2.4 were induced with 2- or 4 μg/mL Dox for 5 days and 20 μg of lysates resolved by SDS-PAGE and immunoblotted for CPT1A expression. Control wells were treated with 2 μL milliQ. CPT1A 88 kDa; TUBA 50 kDa.

6.7 Characterisation of stable cell systems modulating *CPT1A* expression

6.7.1 Real time growth assay in response to *CPT1A* modulation

6.7.1.1 *CPT1A overexpression decreases growth rate of MDA-MB231 cells*

To determine how overexpression of *CPT1A* in the MDA-MB231 cell line affects proliferation rate, cells were pre-induced with 2 μg/mL of Dox for 48 hours prior to seeding into 96 well plates. Real time growth was monitored for one week using the Incucyte live imaging system, and phase contrast scans of confluency as a measure of proliferation were automatically generated every 2 hours. In two independent clones (3 and 17) of CPT1A overexpression, the growth rate was reduced by approximately 25-35%, as compared to the Tet parental control (Fig 6.13).

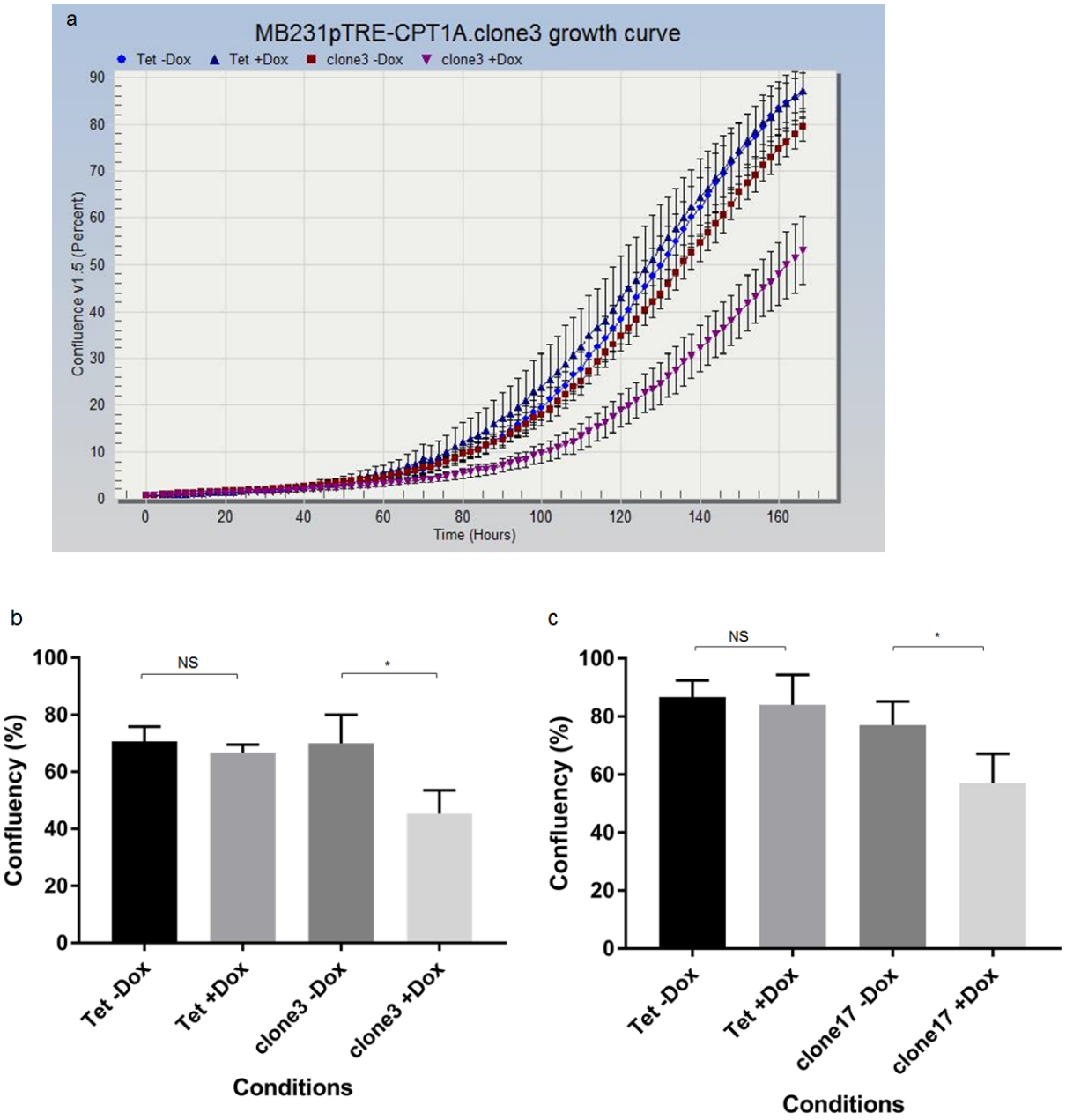

Figure 6.13: CPT1A overexpression in MDA-MB231 decreases proliferation rate, compared to Tet parental. (a) A representative growth curve of MDA-MB231 TetOn and pTRE-CPT1A clone 3. Error bars = standard deviation. Real time growth kinetics of (b) clones 3 and (c) 17 CPT1A were monitored using the Incucyte imaging system for approximately one week. Confluency at 140 hours is presented. Error bars = SEM, paired t-test p *$\leq$0.05.

6.7.1.2 *CPT1A overexpression decreases wound closure rate of MDA-MB231 cells*

Next, the effect of CPT1A overexpression in MDA-MB231 cells on the rate of wound closure as a surrogate of cell migration was investigated. CPT1A expression in MDA-MB231 cells was induced with 2 μg/mL Dox for 5 days before seeding into Essen ImageLock 96 well plate at a density to achieve full confluency the following day. A scratch through the middle of each well was performed using the Essen WoundMaker, and migration rate of the wound was monitored using the Incucyte live imaging system. A representative wound healing profile is shown in Fig 6.14a. In two independent clones, CPT1A overexpression reduced migration rate between 20-25%, compared to the Tet parental (Fig 6.14b,c).

6.7.1.3 *CPT1A overexpression does not affect transwell migration rate of MBA-MB231 cells*

To further investigate a potential role for CPT1A in migration, the migration rates between basal and CPT1A overexpression in MDA-MB231 cells were investigated using the Boyden chamber. Cells were pre-induced with 2 μg/mL Dox for 5 days and seeded into transwell inserts in serum-free media supplemented with BSA-conjugated palmitic acid and carnitine (concentrations based on conditions used for Seahorse XF flux analysis). The migration experiment was conducted for 48 hours. Cells were fixed and stained with 1 μg/mL DAPI nuclear dye in PBS with 0.25% (v/v) paraformaldehyde and 0.075% (v/v) saponin, and cells that migrated and attached to the bottom well were counted using the Cytation. As shown in Fig 6.15, no significant difference in migration rates were observed between basal and CPT1A overexpression in MDA-MB231 cells.

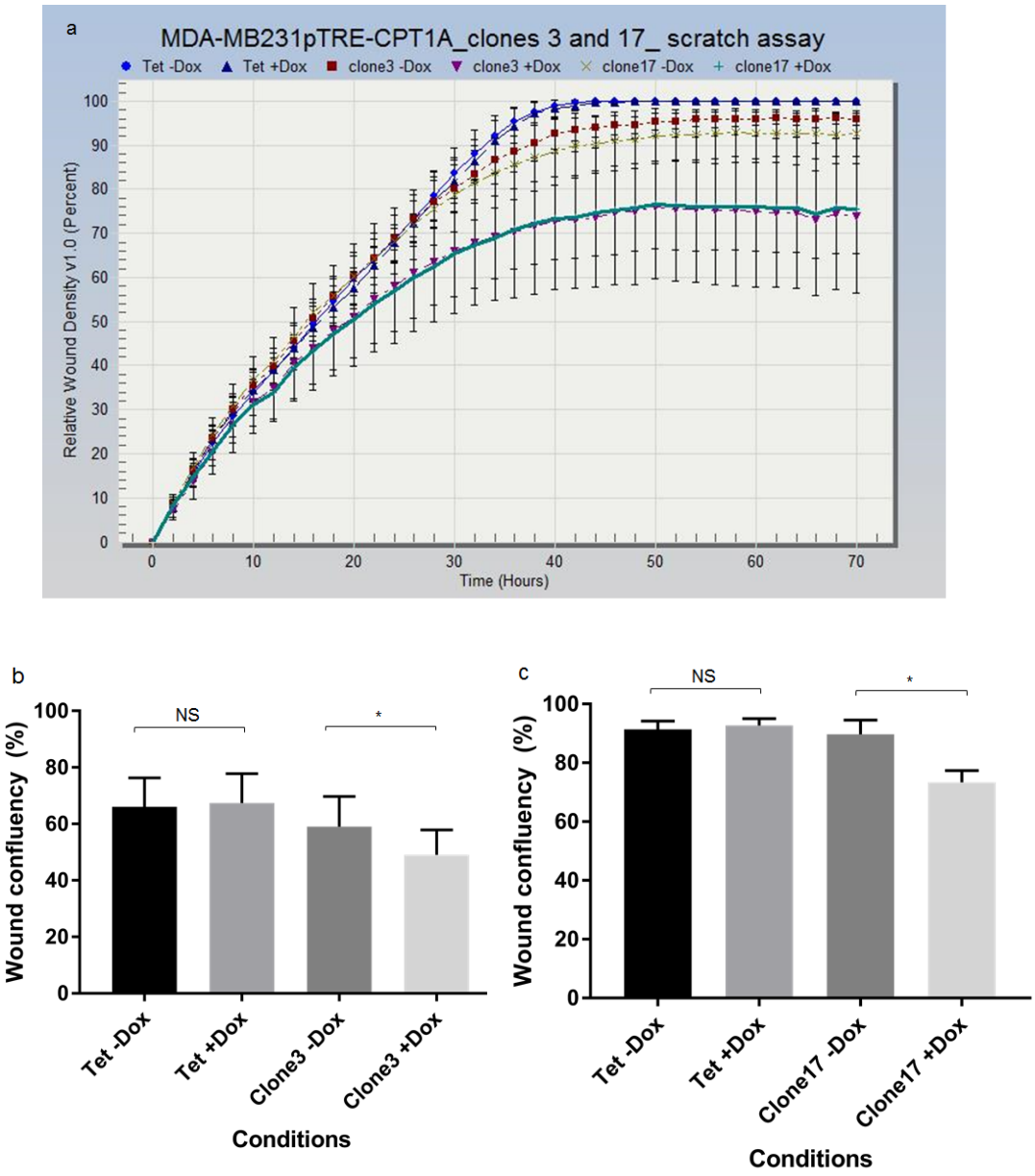

Figure 6.14: CPT1A overexpression in MDA-MB231 decreases wound healing rate, compared to Tet parental. (a) Representative real-time wound confluency profile of MDA-MB231 TetOn and pTRE-CPT1A clones. Error bars = standard deviation. Wound confluency at 30 hours of (b) clones 3 and (c) 17 CPT1A were monitored using the Incucyte imaging system for approximately one week. n=3 biological replicates. Error bars = SEM, paired t-test p *$\leq$0.05.

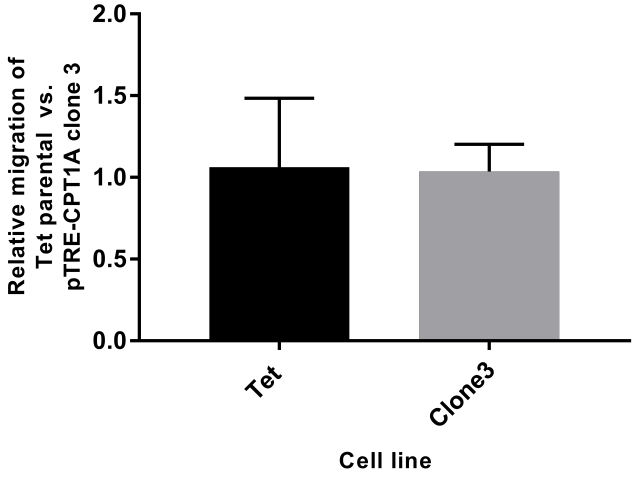

Figure 6.15: CPT1A overexpression does not affect transwell migration rate of MDA-MB231 cells. MDA-MB231 Tet parental and CPT1A overexpression clone 3 were induced for 5 days, seeded on transwell inserts and migration rates compared after 48 hours. n=3 biological replicates, with 2 technical replicates per condition per experiment. Error bars = SEM, both conditions non-statistically signficant.

6.7.1.4 *CPT1A overexpression does not affect anchorage-independent growth of MDA-MB231 cells*

Anchorage-independent growth measures the ability of cells to proliferate without attachment to a surface, and mimics the early events of metastasis. Using gas chromatography and mass spectrometry, Hunnewell *et.al* reported pathways that were active or inactive in proliferating compared to quiscent spheroid cultures of *Ras* transformed mouse embryonic fibroblast cells (Hunnewell and Forbes, 2010). Synthesis of several amino acids including alanine, glycine, and serine were found to be upregulated in proliferating, compared to quiescent spheroids. Additionally, the citric acid cycle was active in both proliferating and quiescent spheroids. However, the role of FAO in anchorage-independent growth remains poorly understood.

To investigate the effect of CPT1A overexpression in MDA-MB231 on anchorage-independent growth, soft agar assays were performed. MDA-MB231 cells were seeded in agar and

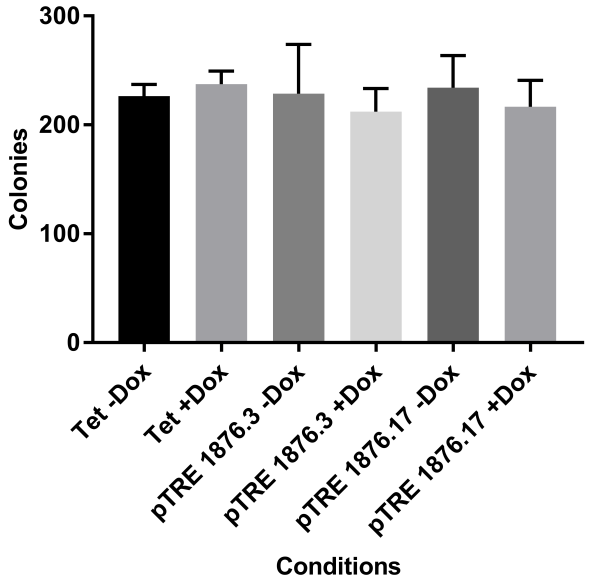

Figure 6.16: CPT1A overexpression does not affect anchorage-independent growth in MDA-MB231 cells. 50,000 MDA-MB231 Tet parental, clones 3 and 17 were seeded in 0.3% agar above a 0.6% base agar. Media was replaced every 2-3 days for 3 weeks, and colonies counted. n=3 biological replicates. Error bars = SEM, both conditions non-statistically significant.

cultured for approximately 3 weeks in 2 μg/mL Dox or milliQ as control, following which colonies were counted under a phase contrast microscope. Counts were verified by an independent observer blinded to the conditions. As shown in Fig 6.16, after 3 weeks of growth, there were no significant differences observed between basal and overexpression of CPT1A in MDA-MB231 cells.

6.7.1.5 *CPT1A knockdown does not affect proliferation rate of MCF7 cells*

If knockdown of CPT1A induces cells to engage in glycolysis, one may postulate that it could alter the cellular proliferation rate. This is possible through the generation of anabolic metabolites from glycolytic intermediates to facilitate macromolecule synthesis required for cell division (Lunt and Vander Heiden, 2011). To understand how the growth rate of MCF7 cells is affected by *CPT1A* knockdown, cells were pre-induced

with 2 μg/mL of Dox for one week, and seeded into a 96 well plate. Real-time growth rate was measured as mentioned in Section 6.7.1.1. As shown in Fig 6.17a, knockdown of CPT1A using two independent shRNA did not affect the proliferation rate of MCF7 cells. A representative growth curve is shown in Fig 6.17b. Of note, the expression of red fluorescent protein - which is driven by the same promoter with that of the shRNA - was routinely monitored to infer the shRNA expression is induced in response to Dox induction.

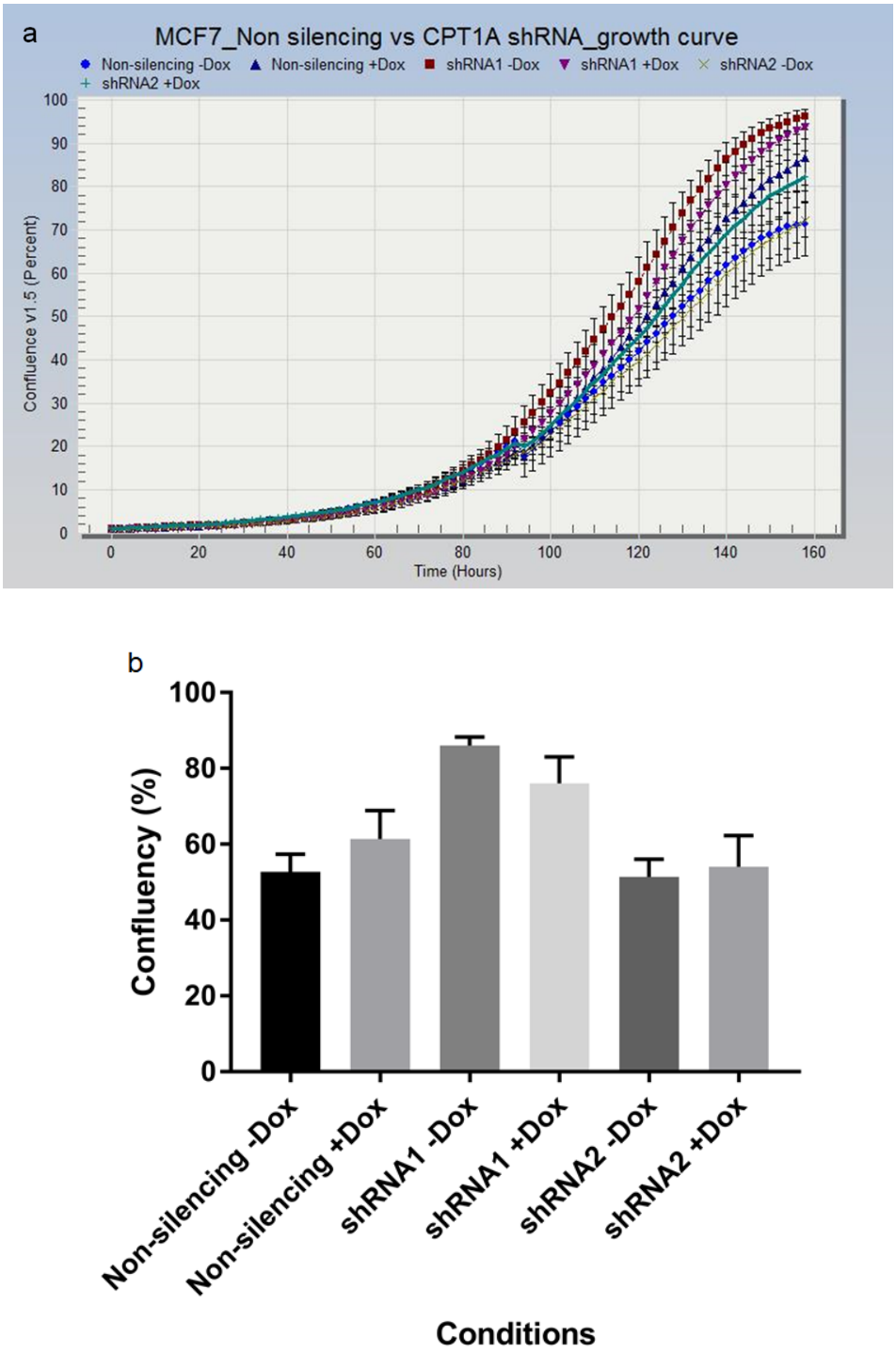

Figure 6.17: CPT1A knockdown does not affect proliferation in MCF7 cells. Cells were pre-induced for one week, before seeding into 96-well plates. Real time growth kinetics of CPT1A knockdown was using the Incucyte imaging system for approximately one week. (a) Representative growth curve profile of MCF7 non-silencing and shRNA clones. Error bars = standard deviation. (b) Confluency presented at 140 hours is presented. Error bars = SEM, differences are non-statistically signficant. n=3 biological replicates, 5 technical replicates per experiment.

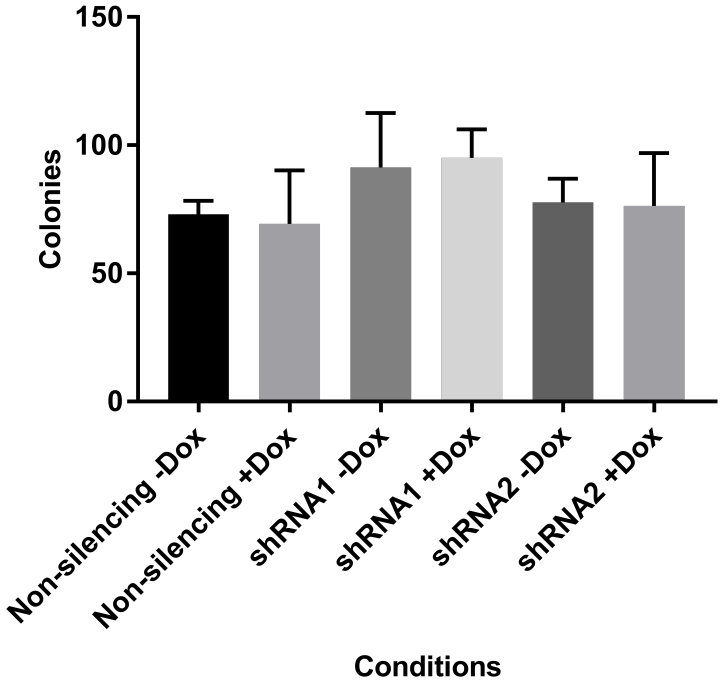

Figure 6.18: CPT1A knockdown does not affect anchorage-independent growth in MCF7 cells. 5,000 MCF7 non-silencing, and two shRNAs clones were seeded in 0.3% agar above a 0.6% base agar. Media was replaced every 2-3 days for 3 weeks, and colonies counted. No statistically significant differences were observed between the conditions. Error bars = SEM. n=3 biological replicates.

6.7.1.6 *CPT1A knockdown does not affect anchorage-independent growth rate of MCF7 cells*

To investigate whether CPT1A knockdown in MCF7 cells affects anchorage-independent growth, *CPT1A* shRNA clones were seeded in soft agar and cultured as described in methods. After 3 weeks, cells were fixed, stained, and colonies counted. As shown in Fig 6.18, there were no significant differences in the number of colonies between basal and CPT1A knockdown in MCF7 cells.

6.8 FAO flux analysis of breast normal and cancer cell lines with CPT1A modulation

To determine whether overexpression and knockdown of CPT1A in breast cell lines corresponds with FAO *flux*, the Seahorse XF extracellular flux assay was performed to determine oxygen consumption in response to exogenous palmitate. This assay is a variant of the standard MitoStress test which measures various components of mitochondrial metabolism based on oxygen consumption and extracellular acidification rate, surrogates of respiration and aerobic glycolysis, respectively (See Section 2.7.2 for method details). This assay was performed on all three transgenic cell lines generated in this study.

6.8.1 *Real time FAO flux in MDA-MB231 cells with CPT1A overexpression*

To investigate whether increased CPT1A levels are associated with increased FAO flux in MDA-MB231 cells, real-time oxygen consumption was analysed in response to exogenous palmitate. Except for CPT1A overexpression clone 17, oligomycin and antimycin treatments decreased the oxygen consumption rate (OCR) in MDA-MB231. In response to carbonyl cyanide-4-(trifluoromethoxy)phenylhydrazone (FCCPO treatment, presence or absence of Dox in the Tet parental control line did not alter OCR when treated with either BSA-only (blue and orange lines), or BSA-palmitate (yellow and grey lines). Surprisingly, in CPT1A overexpression clone 3, there was no apparent difference in OCR observed in Dox treated cells with exogenous palmitate (orange line), compared to control (yellow line) (Fig 6.19b). Furthermore, at time=0, there were no differences in OCR observed, which suggests that there was no difference in *endogenous* mitochondrial respiration between the conditions.

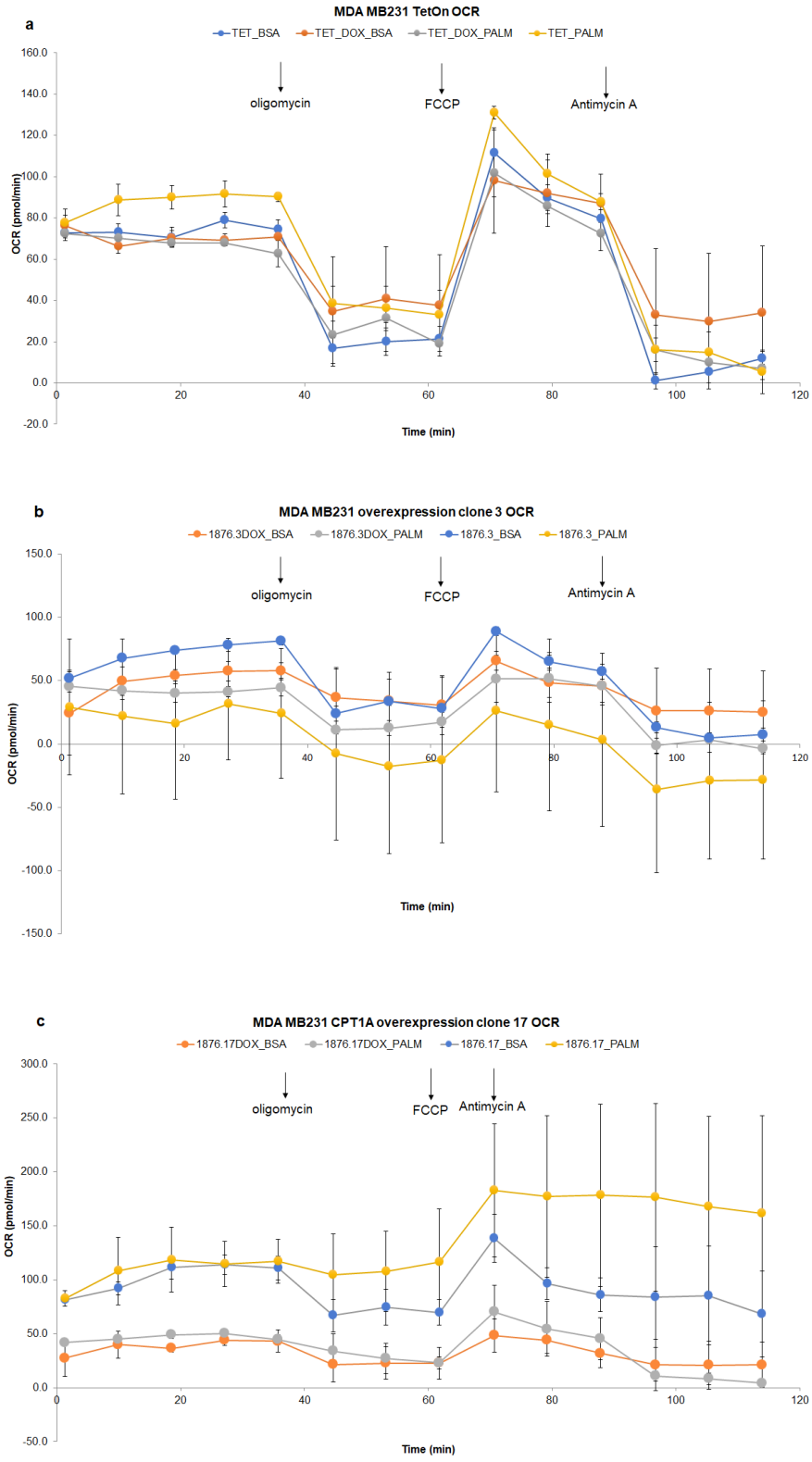

Figure 6.19: Real time oxygen consumption analysis in CPT1A overexpressing MDA-MB231 cells. Cells were pre-induced for 5 days, before seeding into XF24 well plates in substrate-limited media overnight. Error bars = standard deviation from 2 technical replicates from one experiment. Oxygen consumption analysis in (a) TetOn parental, (b) pTRE-CPT1A clone 3 and (c) pTRE-CPT1A clone 17. Arrows indicate when mitochondrial inhibitors (oligomycin, FCCP and antimycin A) were introduced into the assay.

Next, the effect of CPT1A knockdown on palmitate metabolism was analysed in MCF7 cells. Cells were induced for one week prior to oxygen consumption analysis. As expected, in the non-silencing and *CPT1A* shRNA clones, oligomycin and antimycin A treatments decreased oxygen consumption. Interestingly, addition of exogenous palmitate resulted in a more marked increase in OCR in the non-silencing (blue line, 6.20a; yellow line, 6.20b), compared to CPT1A knockdown (grey line, 6.20a; orange line, 6.20b) when treated with FCCP. This suggests that *decreased* CPT1A expression associated with *decreased* oxygen consumption. However, it should be noted that some variation was observed in the basal, endogenous OCR at time=0.

6.8.2 *Real time FAO flux in MCF7 cells with CPT1A knockdown*

The effect of CPT1A knockdown was also analysed in MCF10A cells. Cells were induced for one week prior to oxygen consumption analysis. Overall, the oxygen consumption profile in response to different ETC inhibitors were as expected, with decreased OCR in response to oligomycin and antimycin A, and maximal OCR observed with FCCP treatment. However, in these polyclonal non-silencing and *CPT1A* shRNA lines, no differences in OCR was observed in response to exogenous palmitate, compared to BSA-only control, upon treatment with FCCP.

6.8.3 *Real time FAO flux in MCF10A cells with CPT1A knockdown*

6.9 Discussion

This chapter sought to investigate the functional consequences of CPT1A modulation in breast normal and cancer cell lines. While extracellular flux rates have been reported on a panel of breast cancer cell lines measuring the glycolytic and mitochondrial respiration rates, very little is known about the FAO rate in cancer cells (Pelicano et

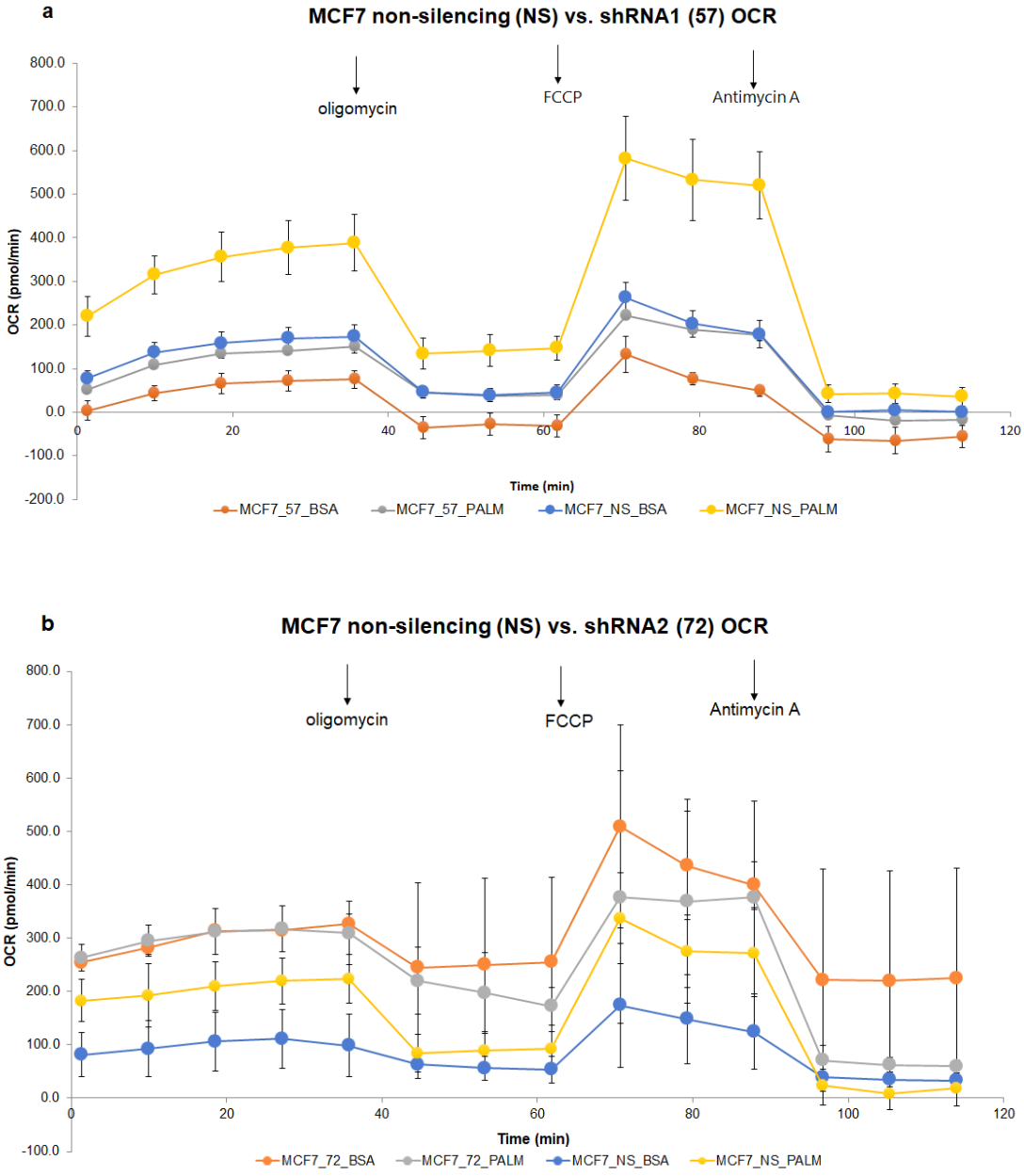

Figure 6.20: Real time oxygen consumption analysis in MCF7 cells after CPT1A knockdown. *CPT1A* expression was knocked down for one week, before seeding into XF24 well plates in substrate-limited media overnight. Error bars = standard deviation from 2 technical replicates from one experiment. Oxygen consumption analysis in (a) shRNA clone 1 and (b) shRNA clone 2. Arrows indicate when various mitochondrial inhibitors (oligomycin, FCCP and antimycin A) were introduced into the assay.

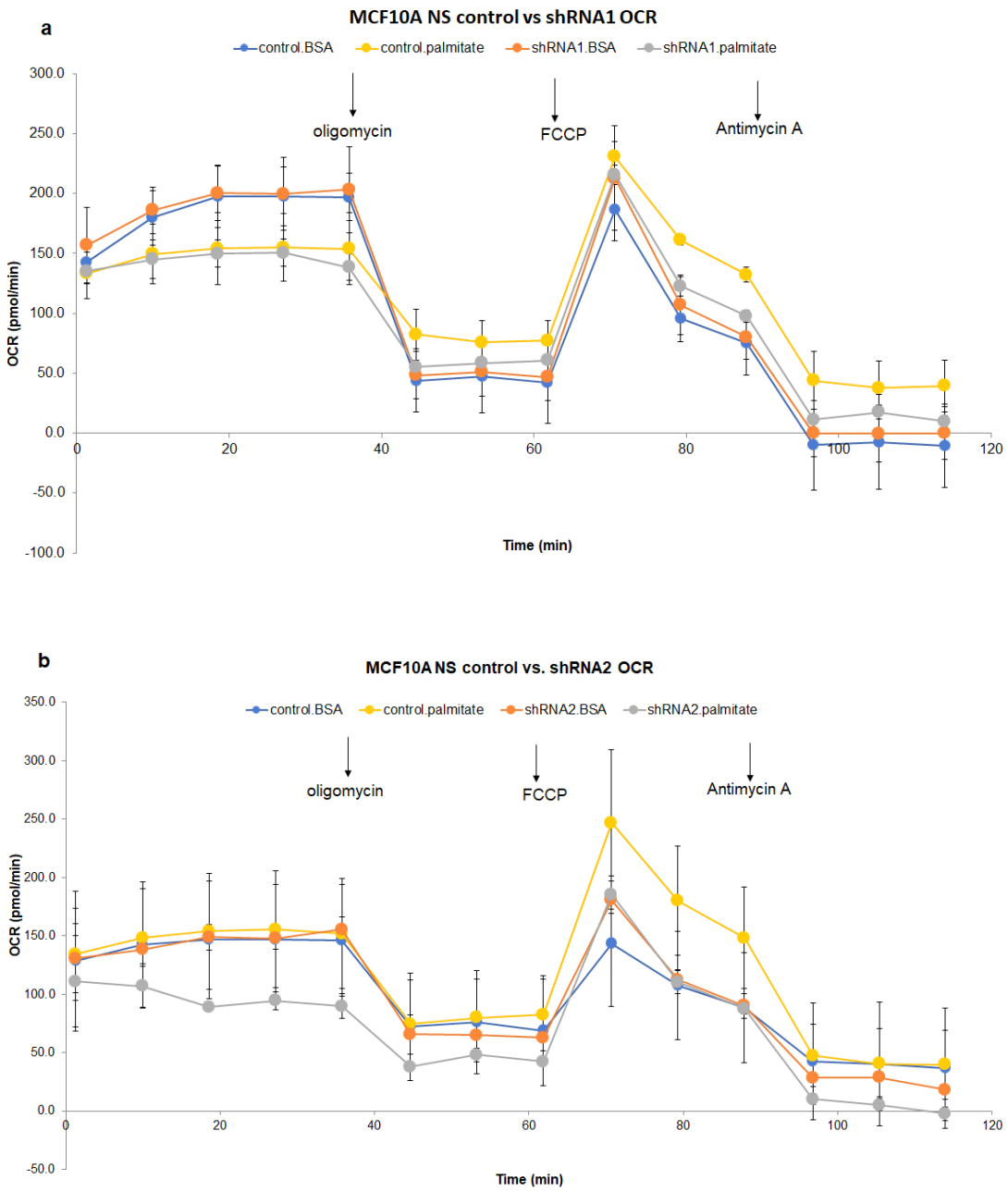

Figure 6.21: Real time oxygen consumption analysis in MCF10A cells after CPT1A knockdown. *CPT1A* expression was knocked down for one week, before seeding into XF24 well plates in substrate-limited media overnight. Error bars = standard deviation from 2 technical replicates from one experiment. Oxygen consumption analysis in (a) shRNA clone 1 and (b) shRNA clone 2. Arrows indicate when various mitochondrial inhibitors (oligomycin, FCCP and antimycin A) were introduced into the assay.

al., 2014). This is important as there are several ways mitochondrial respiration can be promoted, including glutamine oxidation, conversion of pyruvate to oxaloacetate by pyruvate carboxylase, and pyruvate and fatty acid oxidation. The standard Seahorse XF assay measures mitochondrial oxygen consumption from all sources mentioned. Therefore, it is possible that the contribution of each source may differ within and between cancer cell lines. Indeed, the oxidation rate of radiolabelled palmitate in MCF7 cells has been shown to be over 5 fold higher compared to MDA-MB231 cells (Balaban et al., 2017). Importantly, the protein expression of CPT1A is significantly higher in MCF7- compared to MDA-MB231 cells, which is consistent with the mRNA expression levels between these two cell lines (Figs 6.3, 6.2). In another study, CPT1A overexpression in interleukin-3 dependent cells resulted in approximately 9 fold increase in the oxidation of radiolabelled palmitate (Deberardinis, Lum, and Thompson, 2006). The implications of these findings are twofold: (i) FAO flux may vary between different cancer cell lines and (ii) CPT1A expression is associated with cellular FAO flux in these studies.

6.9.1 CPT1A modulation decreases growth and wound closure rates in MDA-MB231, but not MCF7 cells

Overexpression of CPT1A in MDA-MB231 cells was observed to decrease the proliferation rate by up to 30%, compared to Tet parental line. This suggests that in this genetic background, forced FAO can alter the growth kinetics of these cells. This finding is supported by that of DeBerardinis *et. al.*, who found that CPT1A overexpression in interleukin-3 dependent cells decreased the proliferation rate by approximately 33%, compared to empty vector control. MDA-MB231 has been shown to be highly glycolytic, and have low respiration capacity (Pelicano et al., 2014). Therefore, by upregulating FAO via CPT1A overexpression, it is likely that glycolytic rates would be reduced in this cell line. Given the central role of glycolysis for anabolic precursors and energetic needs for cellular growth, it could explain the cytostatic effect brought about by CPT1A

overexpression, compared to basal expression control.

However, the difference in proliferation observed was relatively modest. A possible explanation for this is that it may require more time for the metabolic rewiring to fully take effect. Oncogenic mutations can promote a glycolytic phenotype, and MDA-MB231 cells harbour mutations in *RAS* and *TP53*, both of which are key to activate glycolysis (Bryant et al., 2014; Ying et al., 2012; Berkers et al., 2013). Thus, competition between expression and activity of glycolytic enzymes driven by oncogenic mutations, and the transgenic expression of CPT1A and increased FAO flux could occur. Consequently, more time may be required before the molecular phenotype of CPT1A overexpression manifests.

Overexpression of CPT1A in MDA-MB231 was also observed to decrease the wound closure rate of by approximately 20%. However, validation of this finding using the transwell migration assay revealed no difference in migration between Tet and clone 3 overexpression lines. As such, it is possible that the differences observed in the scratch assay are due to differences in proliferation, rather than the direct effect of CPT1A overexpression on migration.

In MCF7 cells, no difference was observed in the proliferation rates of non-silencing control and *CPT1A* knockdown cells. The knockdown between the two shRNAs ranges between 40-60%, which indicates that substantial levels of CPT1A protein are still expressed in these cells. It is not clear what levels of CPT1A knockdown are required to effectively induce cells to switch to glycolysis. Furthermore, the MCF7 cells with shRNA knockdown may also increase pyruvate or glutamine oxidation to compensate for decreased acetyl-CoA to drive the citric acid cycle. It is also possible that assessing the effect of *CPT1A* knockdown in different cell lines could reveal stronger effects as other genetic changes in MCF7 cells could be masking the effect of decreased CPT1A

expression. This is supported by the findings of Chaneton *et. al.*, who reported decreased proliferation in HT29 and SW620, but not HCT116 colorectal cell lines when *PKM2* expression was knocked down (Chaneton et al., 2012). Taken together, more effective *CPT1A* knockdown in MCF7, or assaying other cell lines could reveal a potential effect of modulating *CPT1A* expression levels on cancer cell proliferation.

6.9.1.1 *Culture media constituents and concentrations are key in metabolism experiments*

The RPMI 1640 media used for experiments in this chapter has 11 mM of glucose, roughly twice the normoglycemic levels in human circulation. Therefore, it may be possible that repeating these experiments in 5.5 mM glucose may widen the difference in the basal and CPT1A overexpression isogenic MDA-MB231 cell line. Furthemore, many other nutrients, amino acids in particular, in standard commercial media are present in higher concentration than in human plasma or serum (Mayers and Vander Heiden, 2015). For instance, glutamine, an important anaplerotic substrate, is present at a concentration of 2 mM, approximately 2.5-5 fold higher compared to human circulation which ranges from 0.45 to 0.8 mM (Mayers and Vander Heiden, 2015). This is also true for several other amino acids, and is significant because amino acids has been shown to contribute to the majority of proliferating cell mass (Hosios et al., 2016). Serine and glycine, two other important amino acids for cancer cell proliferation, are present between 2-8 fold higher in RPMI media, compared to human plasma or serum. Hence, in using commercial media solutions, cells are cultured in pro-proliferative nutrient milieu which may confound the investigation of specific metabolic pathways.

In addition, while CPT1A expression can be manipulated, it is important that there is sufficient *substrate* available for the activity of this enzyme. The concentrations of fatty acids in fetal bovine serum that cells are routinely cultured in is unknown, although re-

cent analysis indicates a concentration of 260 μM (Mayers and Vander Heiden, 2015). Of note, this may be subject to variations between different commercial batches, although the same batch of serum was used for all experiments in this study. This potential lack of consistency in concentrations of the different lipid species in serum may result in lipotoxicity when experiments are supplemented with exogenous palmitic acid. Of note, in a small cohort of Canadian adults (n=826), analysis of serum lipids by gas chromatography determined the concentration of free fatty acids to be 474 $\pm$275 μM (Abdelmagid et al., 2015). This highlights potential interspecies differences in serum lipid profiles, which may affect interpretation of *in vitro* metabolism experiments.

6.9.2 CPT1A modulation does not affect anchorage-independent growth

The soft agar assay performed in this chapter on CPT1A overexpression or knockdown in MDA-MB231 or MCF7 cells, respectively, did not reveal any differences in the number of colonies, compared to controls. The lack of effect on three-dimensional growth is inconsistent with the observation that CPT1A overexpression resulted in decreased *monolayer* growth of MDA-MB231 cells. A straightforward explanation for this finding is that CPT1A overexpression may have different effects between monolayer, compared to anchorage-independent growth in MDA-MB231 cells. It is worth mentioning that the isogenic MDA-MB231 cell lines used in this experiments were observed to form small colonies, which could not be counted visually without the assistance of a microscope. This contrasts with several reports in the literature that reported this cell line to form sizeable colonies visible to the naked eye. One plausible explanation for this is that in generating these stable transgenic lines, the passages over time could have selected for cells that do not form colonies efficiently in soft agar. Furthermore, the soft agar assay may not be sensitive enough to detect small, but significant differences in colony size, and hence, modest decreases in CPT1A overexpressing MDA-MB231 cells may not be captured by the quantitation method utilised in this experiment. In MCF7 cells, knockdown of *CPT1A* did not result in significant difference in number of colonies, compared

to basal expression. Similar to the growth curve analysis, this could be explained by the possibility that the knockdown achieved in these clones were insufficient to trigger some form of metabolic or signalling pathway alterations that could affect colony formation.

The soft agar assay, which assesses how well single cells form colonies in response to an intervention, may reflect the efficiency of colony establishment after metastasis of tumour cells. While the FAO signature expression has been shown to be lower in primary and metastasis tumour tissues (Chapter 3, Figs 3.13d and 3.14d), how FAO functions during the *early* events of dissemination is not well understood. This question was attempted by Pascual *et.al.* who observed that overexpression of the lipid uptake receptor CD36 in patient-derived or established oral carcinoma cell lines with low metastatic propensity significantly promoted the ability of these cells to spread to the lymph nodes in mice (Pascual et al., 2017). The authors observed several genes involved in alpha and beta-oxidation to be upregulated in the CD36 overexpressing, compared to basal expression cells. Additionally, three enzymes involved in FAO - ACADM, ACADVL, HADHA - were upregulated based on flow cytometry analysis. Based on this, the authors concluded that CD36-mediated fatty acid uptake promotes FAO and facilitates oral squamous cell carcinoma metastasis.

However, there are several concerns that were apparent in the Pascual study. First, 4 of 9 genes (44%) that were observed to be involved in FAO also featured in another geneset involved in fatty acid synthesis. Two of these enzymes catalyse reversible reactions, and two were involved in steroid and lipid modification reactions. This highlights the importance of understanding the biology of curated genesets, and as such, the alpha/beta oxidation geneset should be interpreted cautiously. Secondly, the flow cytometry analysis of FAO enzymes did not quantify and provide a measure of certainty in the differences in expression between basal and CD36 overexpression. Interestingly, it is not clear why CPT1A expression or activity was not assessed in this study, even though the Taqman

qPCR probe sequence for this gene was listed in their supplementary material. Nevertheless, the authors provided compelling evidence in *in vitro* and *in vivo* systems of the role of CD36 *per se* in metastasis, although one should be wary of the conclusion that fatty acid uptake equates to oxidation to promote metastasis of cancer cells.

6.9.2.1 *Varied roles of metabolic pathways during anchorage-independent growth*

In light of the findings from the soft agar clonogenic assay in this chapter, it is worthwhile mentioning that metabolic pathways may serve different roles when cultured in adherent or non-adherent conditions. For instance, in H460 lung cancer cells, IDH1 and IDH2 have different functions when cultured as a monolayer or spheroids (Jiang, Deberardinis, and Boothman, 2015). Culture of cells under non-adherent conditions limits spheroid growth due to increased reactive oxygen production (ROS), which was mitigated by NAPDH generated from the oxidation of isocitrate by IDH2 in the mitochondria. The increased supply of citrate is provided by the reductive carboxylation of alpha-ketoglutarate by IDH1 in the cytosol. Importantly, knockout of IDH1/2 activity decreased spheroid size but had no effect on cells cultured as a monolayer. Based on this finding, one should be aware that modulating metabolic pathways, such as FAO, under non-adherent conditions may not necessarily reflect the findings observed from adherent setting.

6.9.3 Seahorse XF analysis of transgenic lines

Using the Seahorse XF extracellular flux technology, the FAO flux of cells in the transgenic cells was analysed. In all three cell lines with overexpression or knockdown of CPT1A, there was no apparent evidence of changes in oxygen consumption in response to exogenous palmitate. Notably, the OCR in response to different mitochondrial poi-

sons were in agreement with the expected output from a standard MitoStress assay. For instance, the ATP synthase inhibitor decreased oxygen consumption, while the mitochondrial uncoupler increased cellular oxygen consumption in all three cell lines assayed. Futhermore, MCF7 cells had higher basal OCR, compared to MDA-MB231 cells, which is consistent with the findings reported in the literature. Notwithstanding genetic differences between these two cell lines, differences in CPT1A *expression per se* reflects the approximately 5 fold difference in FAO flux between them. Why, then, was there negligible difference in OCR in the transgenic lines? This may be due to the cells being seeded overnight in media with higher concentration of glucose than recommended by the manufacturers, which was to avoid stressing cells. Furthermore, the recommended supplementation of glutamine may also allow another route of mitochondrial metabolism, which together with glucose, could meet the nutritional need of the cells, and hence, be less receptive of exogenous palmitic acid. Furthermore, some cell types may have endogenous lipid stores to utilise when under nutritional stress, and therefore, may not require exogenous palmitate.

Indeed, the manufacturer suggests that the constituents of the substrate-limited media and length of time cells are incubated in the substrate-limited media are potential variables amenable to optimisation for this assay. Of note, in the knockdown lines, strong RFP expression was observed in the presence of Dox during the pre-induction period prior to seeding into XF24 plates. Nonetheless, potential variations in knockdown between experiments cannot be eliminated, which may also contribute to the results observed from the Seahorse XF oxygen consumption analysis. On a more positive note, the increase in OCR in MCF7 non-silencing compared to *CPT1A* shRNA suggests that there is some evidence that knockdown of CPT1A does alter mitochondrial respiration in these cells.

Two potential experiments can be suggested from the preliminary Seahorse XF extracellular flux analysis. Firstly, it is imperative that the best knockdown of *CPT1A* is achieved to confidently observe the impact on FAO flux and oxygen consumption. An alternative option is to genetically knockdown *CPT1A* is through transient siRNA transfection which may achieve higher levels of knockdown before oxygen consumption analysis in response to exogenous palmitate is performed. Secondly, the Seahorse Mito Fuel Flex Test could be performed, which would allow the measurement of real time dependency of cells on three metabolic pathways: glycolysis, and glutamine- and fatty acid oxidation. This is more meaningful as it may identify adaptations in fluxes in response to modulating FAO in cell systems. For instance, by increasing FAO in MDA-MB231 (highly glycolytic), it may force the cells to respire and possibly rely less on glycolysis and glutamine oxidation. This information may complement findings from other experiments, such as differential expression of genes encoding enzymes from transcriptome analysis. Since this assay measures metabolic flux real time, it gives a good indicator of metabolic adaptation in response to genetic or pharmacologic manipulations, compared to end point assays (e.g., mRNA or protein expression, enzyme activity, metabolomics).

6.10 Summary, strengths and limitations

This chapter sought to experimentally characterise the association between FAO and cancer cell biology, in light of findings made in Chapter 3. Expression of *CPT1A* was higher in ER-positive, compared to ER-negative tumours and cell lines. Overexpression of CPT1A in MDA-MB231 was observed to significantly decrease proliferation and wound healing migration rates. In contrast, no significant differences were observed in proliferation rate of MCF7 cells with moderate CPT1A knockdown. Unexpectedly, modulation of CPT1A expression did not alter cellular oxygen consumption in response to exogenous palmitate in MDA-MB231, MCF7 and MCF10A cell lines.

The cell systems generated in this chapter was based on Dox induction, which allows controlled expression of transgenes. This helps to minimise potential artefacts that may arise from constitutive expression or knockdown of CPT1A. Importantly, the decrease in proliferation when CPT1A was inducibly overexpressed in MDA-MB231 was observed in two independent clones, which strengthens this finding. Of note, the MDA-MB231 cells have a mesenchymal morphology. It could be worthwhile studying the effects of CPT1A modulation on other ER-negative cell lines with epithelial morphology to verify whether the findings made in this chapter stand in other cell systems. Similarly, it is also possible that other ER-positive cell lines with a different genetic background, such as T47D, may be more amenable to genetic knockdown, and as such could facilitate studying the effects of altering FAO in this system.

This chapter also has a few limitations. The knockdown of CPT1A in MCF7 cells was not complete, which may explain some of the findings observed using this system. A potential experiment that may be performed in MCF7 cell line is highlighted in Chapter 8. The Seahorse XF technology may require further optimisation to establish conditions prior to formally measuring oxygen consumption in response to exogenous palmitate. This study was limited with regards to time, budget, and logistics to fully undertake this analysis to completion.

Chapter 7

Transcriptome analysis of breast cancer cell systems in response to CPT1A modulation

7.1 Background

In the previous chapter, the functional assays described revealed that increased *CPT1A* expression in MDA-MB231 cell line resulted in decreased proliferation and wound healing rates. As these assays analyse specific cellular characteristics, the information gleaned is rather limited. A more global approach to assess the molecular changes in response to *CPT1A* modulation may be more informative in understanding how alterations in FAO features in cancer cell biology.

Pharmacological activation of fatty acid oxidation in a lung cancer cell line has been shown to induce *transcriptional* changes, and activation of proteins involved in cell cycle arrest (Srivastava et al., 2014). However, the signalling pathways and cellular processes that are altered in response to FAO modulation to affect proliferation is poorly understood. To investigate this, RNA-sequencing analysis was performed to identify global

transcriptomic changes in MDA-MB231 and MCF7 cell systems in response to *CPT1A* modulation.

7.2 Results

This experiment compared the transcriptomes of:

(i) MDA-MB231 TetOn parental with and without Dox induction for 5 days (two biological duplicates per condition)
(ii) MDA-MB231 pTRE-CPT1A clones 3 and 17 with and without Dox induction for 5 days (two biological duplicates per condition)
(iii) MCF7 non-silencing, shRNA1 and shRNA2 clones induced with Dox for 5 days (two biological duplicates per condition)

Of note, qPCR was performed on samples to verify that knockdown and overexpression in the transgenic cell systems indeed occured prior to submitting for sequencing. RNA-Seq and alignment of raw reads was performed by New Zealand Genomics Limited, and a matrix of counts for each gene provided. Genes with zero counts across all samples were removed using the *RowSums*() function.

7.2.1 Differential expression analysis in MDA-MB231 cells with *CPT1A* overexpression

To identify genes that were differentially expressed between basal and *CPT1A* overexpression in the MDA-MB231 cell line, the 'limma' package and its associated functions were applied to the expression matrix (Ritchie et al., 2015; Phipson et al., 2016; Liu et al., 2015). After fitting a linear model using the *lmfit*() function, the *eBayes*() function was applied to determine the log odds of differential expression for each particular gene.

Multiple hypothesis testing was adjusted for by the false discovery rate method, and genes with an adjusted p-value threshold of 0.2 were considered significantly differentially expressed. This relatively liberal threshold was defined *a priori*, based on the possibility that this RNA-Seq analysis may be under-powered to detect small, biologically meaningful fold changes. This threshold does increase the possibility of false-positives in this analysis; and genes identified to be significantly, differentially expressed would require validation by alternative methods (e.g., qPCR).

Tables 7.1 and 7.2 provide a summary of the differentially expressed genes from the *toptable*() function from the limma package. As expected, *CPT1A* expression was significantly increased in pTRE-CPT1A overexpressing clones 3 and 17, but not in the TetOn parental line. However, only one gene in clone 3 (*RP11-563J2.2*) was differentially expressed with an adjusted p-value of 0.01. This gene encodes a long noncoding RNA, and very little is reported about this gene apart from the study by Drummond *et. al.*, who found the expression of this gene to be downregulated in three- compared to two-dimensional cultures of Caco-2 cells infected with coxsackie virus (Drummond, Nickerson, and Coyne, 2016).

Three other genes - *LAD1*, *C22orf15* and *LPAR4* - had an adjusted p-value of < 0.2 in pTRE-CPT1A clone 3. The gene *LAD1* (log2 fold change 1.11; adjusted p=0.205) encodes an anchoring filament as a component of the basement membrane (Groger et al., 2012). This gene was reported to be downregulated during EMT, and low expression was correlated with low rates of pathological complete response from a cohort of breast cancer patients (Hess et al., 2006). Furthemore, promoter methylation was associated with poorer outcome in ccRCC (Vlodrop et al., 2017). The *LPAR4* gene (log2 fold change -0.99; adjusted p=0.205) encodes a lysophospatidic acid receptor, and its role in cancer is not well characterised, apart from a mutation reported in a cohort of Chinese patients with papillary thyroid carcinoma (Pan et al., 2016). However, none of these

Table 7.1: Top 20 genes differentially expressed in CPT1A overexpression clone 3. The ID column represents the gene symbol, logFC indicates the log2 fold change between pTRE-CPT1A clone 3 +Dox and -Dox clone, the AveExpr column corresponds to the average log2 expression of genes, the t column represents the moderated t-statistic, the P.Value column denotes nominal, unadjusted *p*-value, the adj.P.Val indicates the FDR-adjusted *p*-value, and B is the Bayes factor, which indicates the log-odds that the gene is differentially expressed. Table is sorted according to adjusted p value.

ID	logFC	AveExpr	t	P.Value	adj.P.Val	B
CPT1A	3.562	5.864	34.879	2.05E-10	4.09E-06	2.214
RP11-563J2.2	-1.535	-2.502	-11.936	1.43E-06	0.014	1.356
C22orf15	-0.761	-2.782	-8.026	3.15E-05	0.203	0.483
LAD1	1.112	-2.622	7.763	4.05E-05	0.203	0.391
LPAR4	-0.998	-2.362	-7.522	5.13E-05	0.205	0.301
TFF1	1.548	-2.581	6.790	0.0001	0.312	-0.008
SPON2	1.037	0.960	6.787	0.0001	0.312	-0.009
RP11-440G9.1	-0.889	-2.725	-6.164	0.0002	0.533	-0.321
SOWAHB	-1.147	-2.035	-6.077	0.0002	0.533	-0.368
ZMYND10	1.110	-1.795	5.846	0.0003	0.575	-0.500
AP4B1-AS1	0.738	-2.754	5.668	0.0004	0.575	-0.607
CCER2	-0.889	-2.529	-5.381	0.0006	0.575	-0.790
MIR10A	-0.586	-2.811	-5.326	0.0006	0.575	-0.826
LOC101928870	-0.586	-2.744	-5.326	0.0006	0.575	-0.826
RP11-486A14.2	-1.045	-2.301	-5.041	0.0009	0.575	-1.024
ZSWIM8-AS1	-1.031	-0.541	-4.967	0.0009	0.575	-1.077
LOC100132815	-0.646	2.375	-4.960	0.0009	0.575	-1.082
C4orf47	-1.030	-2.292	-4.899	0.0010	0.575	-1.127
GBGT1	1.373	-0.398	4.863	0.0011	0.575	-1.154
RERGL	0.575	-2.813	4.857	0.0011	0.575	-1.159

were observed to be significant in pTRE-CPT1A clone 17, and hence may possibly be unique to pTRE-CPT1A clone 3, and are potentially false-positives.

Table 7.2: Top 20 genes differentially expressed in CPT1A overexpression clone 17. The ID column represents the gene symbol, logFC indicates the log2 fold change between pTRE-CPT1A clone 17 +Dox and -Dox clone, the AveExpr column corresponds to the average log2 expression of genes, the t column represents the moderated t-statistic, the P.Value column denotes nominal, unadjusted *p*-value, the adj.P.Val indicates the FDR-adjusted *p*-value, and B is the Bayes factor, which indicates the log-odds that the gene is differentially expressed. Table is sorted according to adjusted p value.

ID	logFC	AveExpr	t	P.Value	adj.P.Val	B
CPT1A	3.728	5.864	36.497	1.40E-10	2.80E-06	0.678
DUOXA1	-0.718	-2.720	-7.827	3.81E-05	0.234	-0.517
RP11-178C3.2	0.691	-2.724	7.457	5.48E-05	0.234	-0.615
ANGPT2	1.228	-1.936	7.338	6.17E-05	0.234	-0.648
RP11-392P7.6	1.440	-1.566	7.274	6.58E-05	0.234	-0.667
LOC101928117	-0.901	-0.804	-7.210	7.02E-05	0.234	-0.685
RP5-1057J7.6	1.526	-0.731	7.002	8.70E-05	0.249	-0.749
RP11-60I3.5	1.247	-2.537	6.630	0.0001	0.323	-0.872
ZNF599	1.077	-0.747	5.706	0.0004	0.784	-1.239
SLC27A5	0.813	-1.422	5.428	0.0005	0.784	-1.370
CCDC78	0.983	-0.874	5.312	0.0006	0.784	-1.428
FBXO16	-1.245	-0.471	-5.301	0.0006	0.784	-1.434
LOC101928126	0.813	-2.615	5.293	0.0006	0.784	-1.437
LOC101927374	-0.938	-1.639	-5.100	0.0008	0.784	-1.538
NAPB	0.887	2.752	4.976	0.0009	0.784	-1.606
LOC102724642	0.998	0.191	4.964	0.0009	0.784	-1.613
LINC01011	0.989	-0.205	4.925	0.0010	0.784	-1.635
CD81-AS1	-1.250	-2.239	-4.855	0.0011	0.784	-1.675
ZNF793	-0.809	-1.200	-4.850	0.0011	0.784	-1.677
RPP21	-0.809	-1.993	-4.823	0.0011	0.784	-1.694

7.2.1.1 *Gene set enrichment analysis*

To identify the pathways and processes significantly differentially expressed in response to *CPT1A* overexpression, gene set enrichment analysis was performed using the Enrichr online software. Up- and downregulated genes were analysed individually, sorted ascendingly according to their adjusted *p*-value (i.e., most to least significant) and the pre-ranked gene list was provided for enrichment analysis. Four different databases - KEGG, Reactome, WikiPathways, and Panther - were utilised to identify pathways that

were enriched in this analysis.

Genes that were upregulated in clone 3 in response to CPT1A overexpression compared to basal expression showed enrichment of genesets involved in mitochondrial metabolism (Fig 7.1a,c; yellow arrows). Downregulated genes in this clone showed enrichment of cell cycle-related genesets in all four databases (Fig 7.1e-h). However, while the nominal p-values of these genesets were significant, none of these enrichments were statistically significant after adjustment. All statistical values for enrichment analysis in this chapter are provided in Supp Tables B.3 to B.58.

Figure 7.1: Genesets enriched in pTRE-CPT1A clone 3 overexpressing *CPT1A*, relative to basal expression. (**a,b,c,d**) Genesets that were *upregulated* from (a) KEGG, (b) Reactome, (c) WikiPathways and (d) Panther databases from the Enrichr analysis. (**e,f,g,h**) Genesets that were *downregulated* from (e) KEGG, (f) Reactome, (g) WikiPathways and (h) Panther databases. The length and brightness of the bars are positively correlated with how statistically significant the enrichments were. In panels (b) and (c), yellow arrows indicate the upregulated genesets involved in citric acid cycle, and the navy blue arrows in panels (e-h) indicate the genesets involved in cell cycle that were downregulated in response to CPT1A overexpression. Pink and red/brown coloured bars indicate genesets with nominal p-value of < 0.05. Length and brightness of coloured bars are correlated with lower p-values. Genesets represented with grey bars are not statistically significant.

Genes that were downregulated in clone 17 with CPT1A overexpression compared to basal expression showed a significant, concordant enrichment for processes involved in mRNA processing (Fig 7.2e,f,g; yellow arrows). Genes upregulated in clone 17 with CPT1A overexpression showed enrichment in genesets associated with proliferation (Fig 7.2b-d, yellow arrows). This is in contrast with the findings observed in clone 3, where proliferation genesets were enriched in genes downregulated in response CPT1A overexpression.

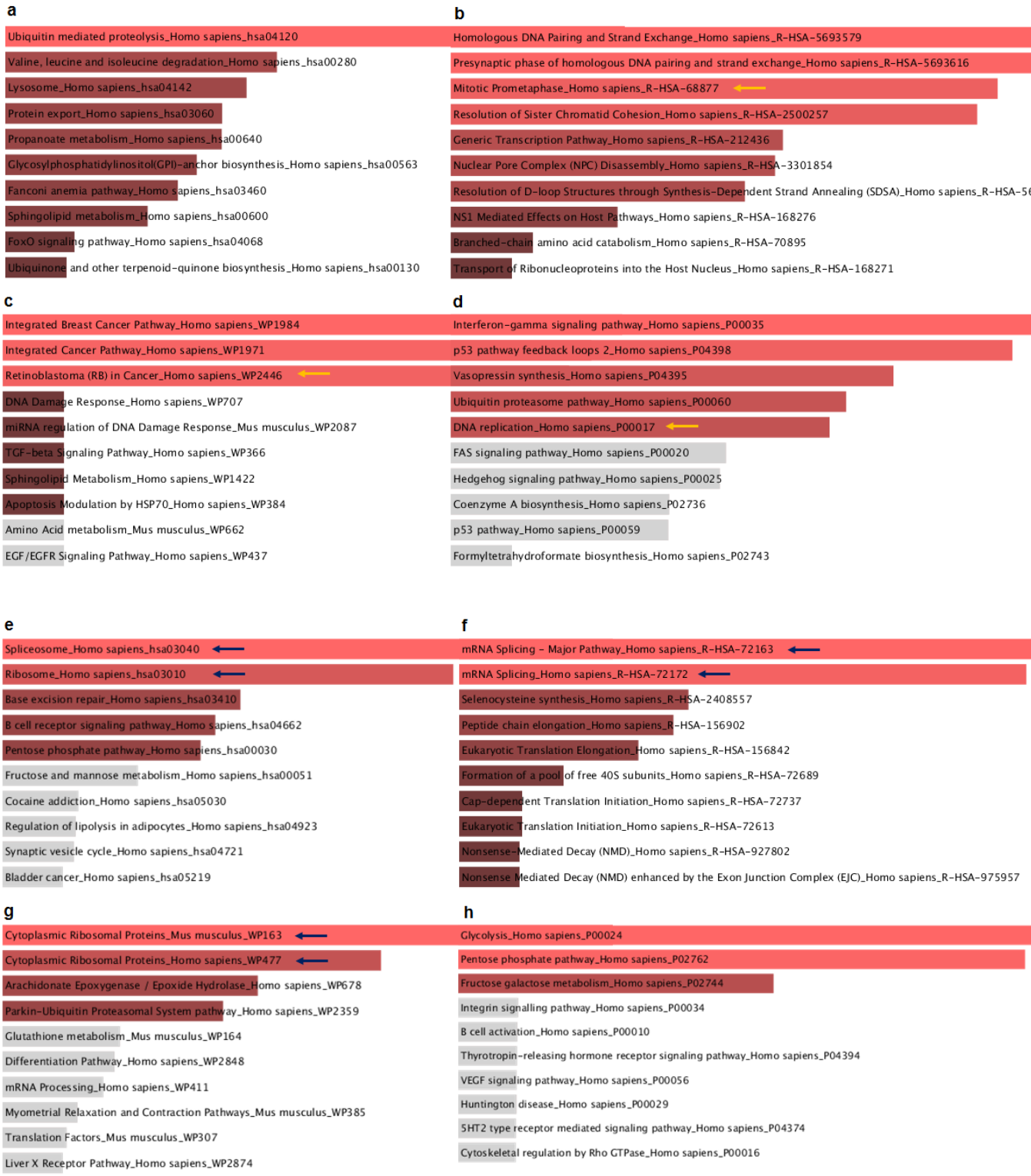

Figure 7.2: Genesets enriched in pTRE-CPT1A clone 17 overexpressing *CPT1A*, relative to basal expression. (**a,b,c,d**) Genesets that were *upregulated* from (a) KEGG, (b) Reactome, (c) WikiPathways and (d) Panther databases from the Enrichr analysis. (**e,f,g,h**) Genesets that were *downregulated* from (e) KEGG, (f) Reactome, (g) WikiPathways and (h) Panther databases. Yellow arrows in panels (b-d) indicate the upregulated genesets involved in cell cycle, and the navy blue arrows in panels (e-g) indicate downregulated genesets involved in ribosomal processes in response to CPT1A overexpression. Pink and red/brown coloured bars indicate genesets with nominal p-value of < 0.05. Length and brightness of coloured bars are correlated with lower p-values. Genesets represented with grey bars are not statistically significant.

Next, to explore whether combining the clones together to perform differential analysis may improve the power to detect significant pathway enrichment, the analysis was repeated with the four combined pTRE-CPT1A -Dox and +Dox replicates. Genes that were upregulated when *CPT1A* was overexpressed did not show consistent pathway enrichment across all four databases (Fig 7.3a-d).

Genes downregulated in response to *CPT1A* overexpression, however, were enriched for ribosomal and RNA processing associated processes (Fig 7.3e-h, yellow arrows). Of note, the enrichment of these genesets were also observed in genes that were downregulated in response to Dox treatment in the TetOn parental line (Supp Fig A.11, yellow arrows).

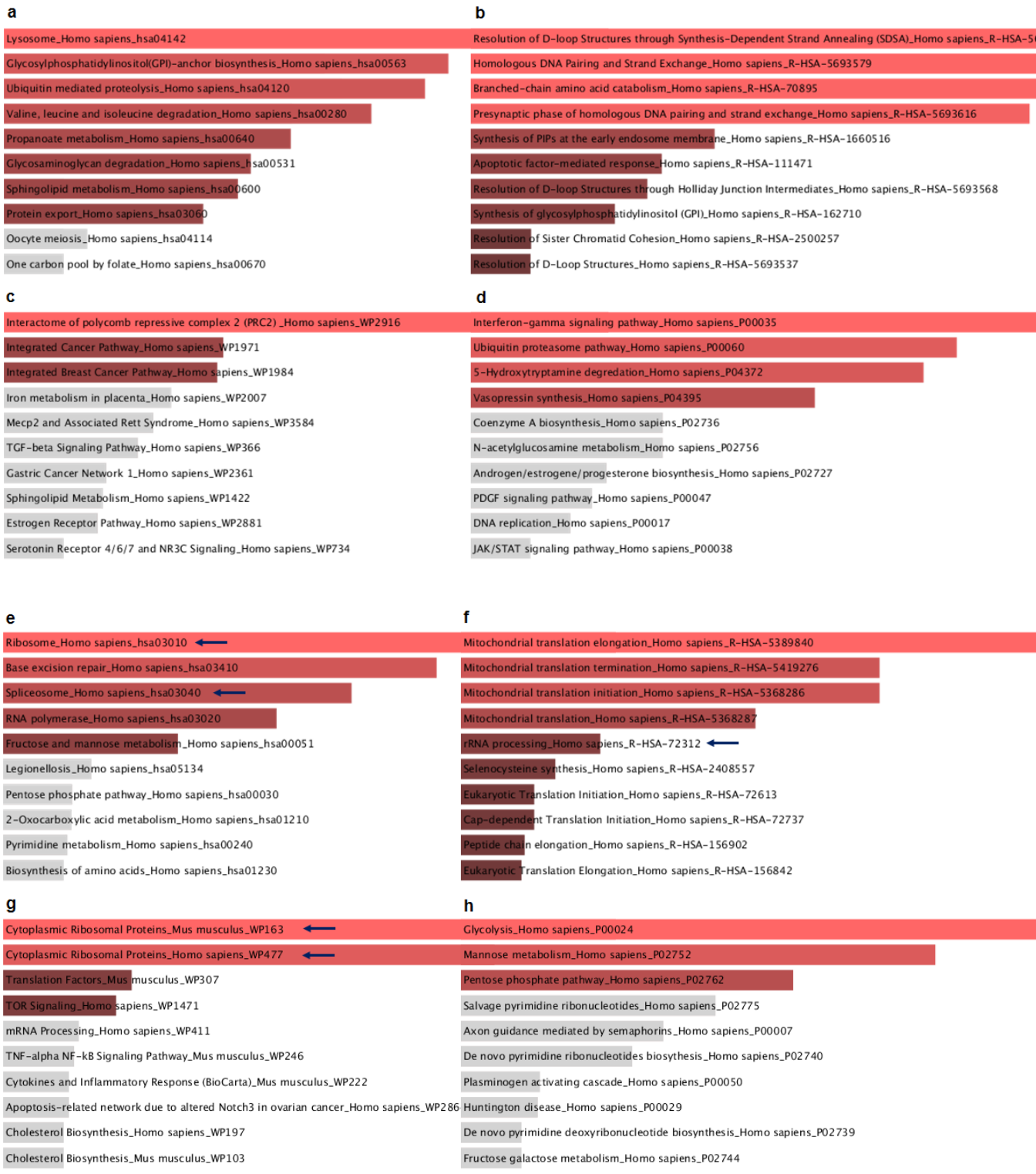

Figure 7.3: Genesets enriched in pTRE-CPT1A clones 3 and 17 overexpressing *CPT1A*, relative to basal expression. (**a,b,c,d**) Genesets that were *upregulated* from (a) KEGG, (b) Reactome, (c) WikiPathways and (d) Panther databases from the Enrichr analysis. (**e,f,g,h**) Genesets that were *downregulated* from (e) KEGG, (f) Reactome, (g) WikiPathways and (h) Panther databases. Navy blue arrows in panels (e-g) indicate the genesets involved in ribosomal processes that were downregulated in pTRE-CPT1A clones treated with Dox. Pink and red/brown coloured bars indicate genesets with nominal p-value of < 0.05. Length and brightness of coloured bars are correlated with lower p-values. Genesets represented with grey bars are not statistically significant.

Table 7.3: Top 20 genes differentially expressed in shRNA clone 1.The ID column represents the gene symbol, logFC indicates the log2 fold change between shRNA clone 1 and non-silencing clone, the AveExpr column corresponds to the average log2 expression of genes, the t column represents the moderated t-statistic, the P.Value column denotes nominal, unadjusted p-value, the adj.P.Val indicates the FDR-adjusted p-value, and B is the Bayes factor, which indicates the log-odds that the gene is differentially expressed. Table is sorted according to adjusted p value. *CPT1A* log2 fold change = -1.03, adjusted p= 0.2.

ID	logFC	AveExpr	t	P.Value	adj.P.Val	B
TRPM2	-6.805	1.871	-18.366	1.14E-06	0.004	5.184
KCND1	-6.531	1.467	-11.878	1.62E-05	0.021	3.487
PKIA	-5.347	-0.207	-17.697	1.44E-06	0.004	5.063
TRPM2-AS	-4.277	-0.357	-21.009	5.01E-07	0.003	5.583
CACNA2D1	-3.803	3.295	-6.586	0.000501	0.085	0.487
MSH5-SAPCD1	-3.798	0.125	-5.561	0.001256	0.113	-0.421
PCDH10	-3.786	1.796	-19.594	7.69E-07	0.004	5.384
ARMCX1	-3.651	-1.643	-18.963	9.41E-07	0.004	5.285
ASCL1	-3.571	-0.884	-5.582	0.001231	0.113	-0.400
MAGEA4	-3.476	-0.082	-5.621	0.001186	0.111	-0.363
LEF1	-3.463	0.148	-6.333	0.000622	0.090	0.276
ELOVL2	-3.453	3.470	-8.936	8.77E-05	0.046	2.102
PCDH19	-3.299	2.310	-11.571	1.90E-05	0.022	3.367
C1orf168	-3.291	0.363	-6.244	0.000672	0.092	0.200
PGR	-3.268	4.482	-8.105	0.000155	0.053	1.594
SLC4A10	-3.196	0.840	-6.415	0.000579	0.087	0.345
SGCG	-3.135	0.207	-10.602	3.20E-05	0.026	2.954
SCNN1G	-3.076	1.058	-4.882	0.002475	0.144	-1.105
VWDE	-2.967	0.468	-6.435	0.000569	0.086	0.362
PKDCC	-2.952	-0.376	-11.716	1.76E-05	0.021	3.424

7.2.2 Differential expression analysis in MCF7 cells with *CPT1A* knockdown

To identify genes that were differentially expressed between basal and *CPT1A* knockdown in MCF7 cells, the differential analysis pipeline described earlier was applied to the MCF7 *CPT1A* knockdown versus non-silencing expression data.

Tables 7.3 and 7.4 summarises the output from the *toptable*() function from the limma package. Of note, *CPT1A* expression was downregulated by 50% in shRNA1 (adjusted $p = 0.19$) and 67% in shRNA2 (adjusted $p = 0.17$), compared to non-silencing control.

Table 7.4: Top 20 genes differentially expressed in shRNA clone 2. The ID column represents the gene symbol, logFC indicates the log2 fold change between shRNA clone 2 and non-silencing clone, the AveExpr column corresponds to the average log2 expression of genes, the t column represents the moderated t-statistic, the P.Value column denotes nominal, unadjusted p-value, the adj.P.Val indicates the FDR-adjusted p-value, and B is the Bayes factor, which indicates the log-odds that the gene is differentially expressed. Table is sorted according to adjusted p value. *CPT1A* log2 fold change = -1.43, adjusted p= 0.17.

ID	**logFC**	**AveExpr**	**t**	**P.Value**	**adj.P.Val**	**B**
ATP6V1G3	6.112	-0.823	28.359	7.84E-08	0.002	5.388
NCMAP	3.913	-0.400	19.283	8.49E-07	0.005	4.679
ARMCX1	-3.651	-1.643	-18.963	9.41E-07	0.005	4.639
PKIA	-5.651	-0.207	-18.702	1.02E-06	0.005	4.605
PCDHGB5	3.044	0.220	12.388	1.26E-05	0.046	3.320
UNC13D	-2.704	3.160	-12.153	1.41E-05	0.046	3.247
CALB2	-2.310	-0.715	-11.614	1.86E-05	0.052	3.071
PCDH10	-2.089	1.796	-10.810	2.85E-05	0.068	2.780
KCND1	-5.790	1.467	-10.531	3.33E-05	0.068	2.670
CABYR	-2.600	-0.624	-10.458	3.47E-05	0.068	2.640
ST3GAL5	2.076	2.261	10.220	3.98E-05	0.071	2.542
RORC	2.133	3.383	9.488	6.18E-05	0.082	2.215
SP100	-2.426	-0.844	-9.372	6.64E-05	0.082	2.160
MAST4	-1.978	1.853	-9.365	6.67E-05	0.082	2.156
LINC00458	2.998	-1.861	9.207	7.37E-05	0.082	2.079
SH3BGRL	-2.301	1.279	-9.133	7.73E-05	0.082	2.042
KCNJ8	-2.145	0.298	-8.943	8.74E-05	0.082	1.945
NBPF13P	-1.843	-0.821	-8.874	9.14E-05	0.082	1.910
BRINP2	2.282	-0.740	8.849	9.29E-05	0.082	1.897
FAXDC2	1.652	-1.603	8.834	9.38E-05	0.082	1.889

Since there were more genes that were significantly differentially expressed between the CPT1A knockdown in MCF7- compared to overexpression in MDA-MB231 cells, gene ontology analysis was performed to identify cellular processes that may be enriched in MCF7 cells in response to CPT1A knockdown. In shRNA1 clone, there were 541 genes that were differentially expressed below the adjusted p-value threshold of 0.2. These genes were sorted into up- and downregulated, and gene ontology analysis using the GATHER online software was conducted to investigate for enriched biological processes (Chang and Nevins, 2006). Genes that were upregulated were enriched for functions associated with metabolism, antigen presentation and processing, and cell-to-cell communication (Fig 7.4a). Downregulated genes were enriched for processes involved in developmental processes, including neurogenesis, organ development, cell adhesion and morphogenesis (Fig 7.4b).

In shRNA2 clone, there were 197 genes that were differentially expressed below the adjusted p-value threshold of 0.2. Gene ontology analysis of the upregulated genes found enrichment for processes involved in vitamin, ganglioside and sphingolipid metabolism (Fig 7.5a). Genes that were downregulated were enriched for localisation, ion transport, frizzled-2 signalling and hepatocyte growth factor biosynthesis (Fig 7.5b).

7.2.2.1 *Gene set enrichment analysis*

To determine pathways that are differentially expressed between *CPT1A* basal and knockdown MCF7 cells, a pre-ranked gene set enrichment analysis was performed as previously.

Genes that were downregulated in shRNA1 and shRNA2 clones with CPT1A knockdown compared to non-silencing control showed an enrichment for ribosomal and RNA processing genesets (Fig 7.6e-h, yellow arrows). Genes that were upregulated in shRNA1

a

Gene Ontology	# Genes	p Value	Bayes Factor
1. GO:0008152 [3]: metabolism	56 [show]	0.0003	4
2. GO:0044237 [4]: cellular metabolism	53 [show]	0.0008	4
3. GO:0019883 [6]: antigen presentation, endogenous antigen	3 [show]	0.001	3
4. GO:0019885 [6]: antigen processing, endogenous antigen vi...	3 [show]	0.001	3
5. GO:0044238 [4]: primary metabolism	53 [show]	0.006	2
6. GO:0007267 [4]: cell-cell signaling	14 [show]	0.008	2
7. GO:0019932 [6]: second-messenger-mediated signaling	7 [show]	0.01	1
8. GO:0007154 [3]: cell communication	52 [show]	0.01	1

b

Gene Ontology	# Genes	p Value	Bayes Factor
1. GO:0007399 [5]: neurogenesis	19 [show]	< 0.0001	10
2. GO:0016339 [6]: calcium-dependent cell-cell adhesion	5 [show]	< 0.0001	9
3. GO:0009887 [4]: organogenesis	28 [show]	< 0.0001	8
4. GO:0048513 [3]: organ development	28 [show]	< 0.0001	8
5. GO:0009653 [3]: morphogenesis	32 [show]	< 0.0001	8
6. GO:0007155 [4]: cell adhesion	21 [show]	< 0.0001	8
7. GO:0007416 [6]: synaptogenesis	5 [show]	< 0.0001	7
8. GO:0050808 [5]: synapse organization and biogenesis	5 [show]	< 0.0001	7

Figure 7.4: Processes enriched in MCF7 shRNA1 clone compared to non-silencing basal expression. Processes that were (a) upregulated and (b) downregulated in response to *CPT1A* knockdown in shRNA1 clone relative to non-silencing control.

a

Gene Ontology	# Genes	*p* Value	Bayes Factor
1. GO:0015993 [6]: molecular hydrogen transport	1 [show]	0.006	2
2. GO:0019852 [7]: L-ascorbic acid metabolism	1 [show]	0.006	2
3. GO:0001574 [10]: ganglioside biosynthesis	1 [show]	0.006	2
4. GO:0006767 [6]: water-soluble vitamin metabolism	2 [show]	0.01	1
5. GO:0001573 [9]: ganglioside metabolism	1 [show]	0.01	1
6. GO:0007612 [4]: learning	1 [show]	0.01	1
7. GO:0006665 [7]: sphingolipid metabolism	2 [show]	0.02	1
8. GO:0006766 [5]: vitamin metabolism	2 [show]	0.02	1

b

Gene Ontology	# Genes	*p* Value	Bayes Factor
1. GO:0051179 [3]: localization	19 [show]	0.001	3
2. GO:0006810 [4]: transport	18 [show]	0.003	3
3. GO:0051234 [4]: establishment of localization	18 [show]	0.003	3
4. GO:0006811 [5]: ion transport	9 [show]	0.007	2
5. GO:0007223 [7]: frizzled-2 signaling pathway	2 [show]	0.007	2
6. GO:0015698 [7]: inorganic anion transport	4 [show]	0.008	2
7. GO:0048175 [7]: hepatocyte growth factor biosynthesis	1 [show]	0.01	1
8. GO:0048176 [8]: regulation of hepatocyte growth factor bi...	1 [show]	0.01	1

Figure 7.5: Processes enriched in MCF7 shRNA2 clone compared to non-silencing basal expression. Processes that were (a) upregulated and (b) downregulated in response to *CPT1A* knockdown in shRNA2 clone relative to non-silencing control.

clone were over-represented for signalling pathways, including EGF signalling (Fig 7.6b-d, yellow arrows). Partly consistent with shRNA1 clone, genes upregulated in shRNA2 in response to CPT1A knockdown were also enriched for EGF signalling pathway. However, for this clone, the enrichment was only seen in the Panther database (Fig 7.7d, yellow arrow).

Figure 7.6: Genesets enriched in MCF7 shRNA1 *CPT1A* knockdown, relative to basal non-silencing cells. (**a,b,c,d**) Genesets that were *upregulated* from (a) KEGG, (b) Reactome, (c) WikiPathways and (d) Panther databases from the Enrichr analysis. (**e,f,g,h**) Genesets that were *downregulated* from (e) KEGG, (f) Reactome, (g) WikiPathways and (h) Panther databases. Yellow arrow in panels (b-d) indicate the genesets associated with signalling pathways that were upregulated, while the navy blue arrows in panels (e-g) indicate ribosomal-associated processes that were downregulated in shRNA clone 1, relative to non-silencing control. Pink and red/brown coloured bars indicate genesets with nominal p-value of < 0.05. Length and brightness of coloured bars are correlated with lower p-values. Genesets represented with grey bars are not statistically significant.

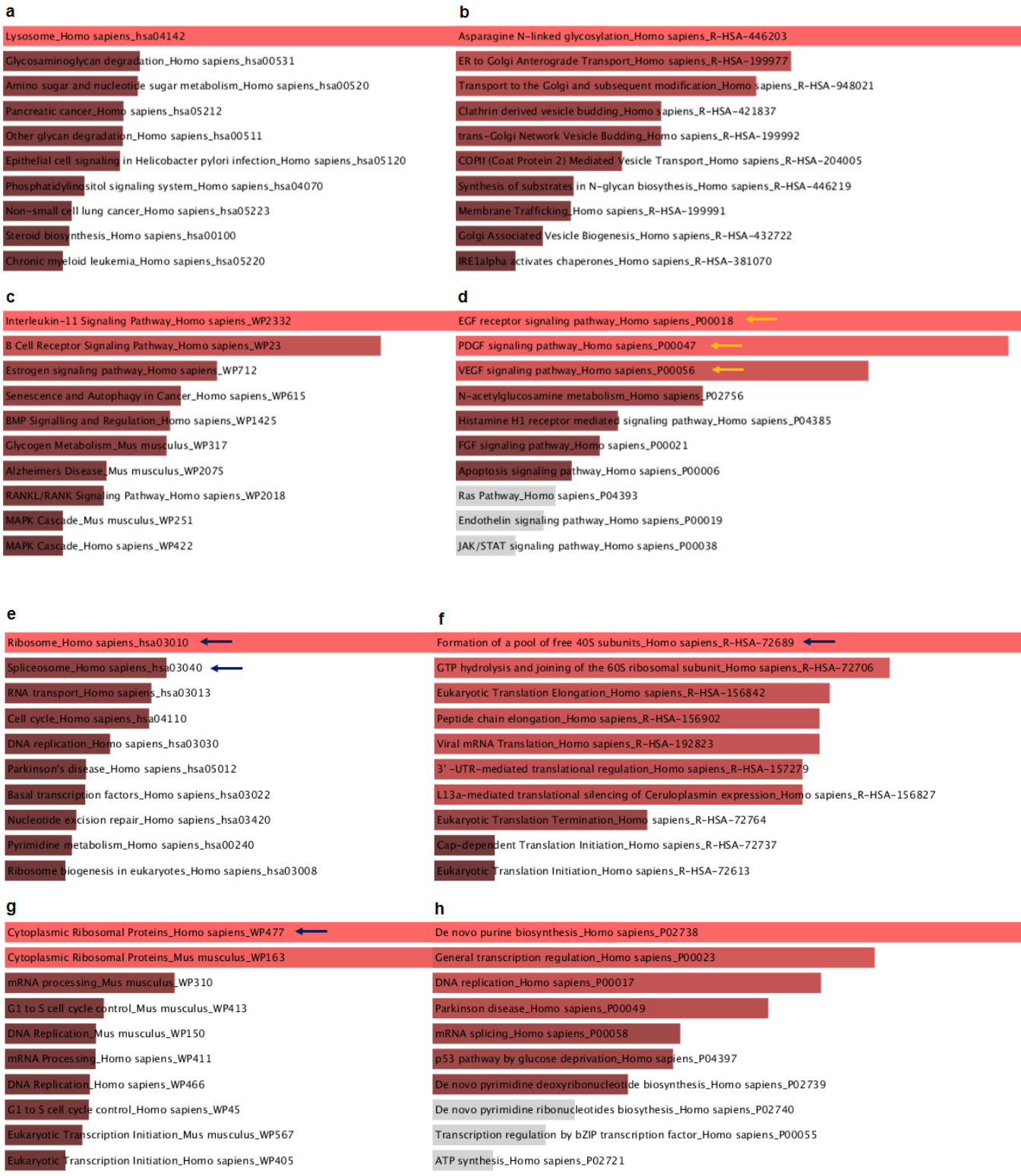

Figure 7.7: Genesets enriched in MCF7 shRNA2 *CPT1A* knockdown, relative to basal non-silencing cells. (**a,b,c,d**) Genesets that were *upregulated* from (a) KEGG, (b) Reactome, (c) WikiPathways and (d) Panther databases from the Enrichr analysis. (**e,f,g,h**) Genesets that were *downregulated* from (e) KEGG, (f) Reactome, (g) WikiPathways and (h) Panther databases. Yellow arrows in panel (d) indicate the genesets involved signalling pathways that were upregulated, while navy blue arrows in panels (e-g) indicate the ribosomal processes that were downregulated in shRNA clone 2, relative to non-silencing control. Pink and red/brown coloured bars indicate genesets with nominal p-value of < 0.05. Length and brightness of coloured bars are correlated with lower p-values. Genesets represented with grey bars are not statistically significant.

Next, the two knockdown clones were combined to explore for genesets enriched with larger sample size. Genes that were upregulated in this analysis were enriched for signalling associated genesets, in agreement with the individual differential analysis (Fig 7.8a-d, yellow arrows). Consistent with the findings from analysis of individual shRNA clones, ribosomal and RNA processing genesets were enriched in genes downregulated in response to CPT1A knockdown (Fig 7.8e-h, yellow arrows).

Figure 7.8: Genesets enriched in MCF7 shRNA1 and shRNA2 combined *CPT1A* knockdown, relative to basal non-silencing cells. (**a,b,c,d**) Genesets that were *upregulated*from (a) KEGG, (b) Reactome, (c) WikiPathways and (d) Panther databases from the Enrichr analysis. (**e,f,g,h**) Genesets that were *downregulated* from (e) KEGG, (f) Reactome, (g) WikiPathways and (h) Panther databases. Genesets that were *downregulated* from (e) KEGG, (f) Reactome, (g) WikiPathways and (h) Panther databases. Yellow arrows in panels (b-d) indicate the signalling pathways that were upregulated, while the navy blue arrows in panels (e-h) indicate the ribosomal associated processes that were downregulated when both shRNA clones were combined, compared to non-silencing control. Pink and red/brown coloured bars indicate genesets with nominal p-value of < 0.05. Length and brightness of coloured bars are correlated with lower p-values. Genesets represented with grey bars are not statistically significant.

7.2.3 Targeted pathway analysis

Chapters 4 and 5 in this thesis demonstrated a correlation between EMT, Wnt and MAPK pathways and the FAO signature expression. To explore whether alterations in *CPT1A* expression in MDA-MB231 and MCF7 cell lines affect these pathways, a targeted pathway analysis between the FAO and gene signatures corresponding to each of the pathways were conducted.

7.2.3.1 *Wnt, MAPK and EMT signature expression in MDA-MB231 transgenic systems*

7.2.3.1.1 ***Wnt signature expression*** The Wnt signature showed a trend of increased expression in the TetOn parental cells treated with Dox, albeit not statistically significant (Fig 7.9a). However, no clear trend could be deduced when CPT1A was overexpressed in pTRE-CPT1A clones 3 and 17. Furthermore, combination of both overexpression clones together did not reveal a significant difference in the Wnt signature expression between pTRE-CPT1A clones with and without Dox treatment (t-test p=0.79).

7.2.3.1.2 ***MAPK signature expression*** The MAPK signature showed a trend of increased expression in TetOn and pTRE-CPT1A clone 3, but not pTRE-CPT1A clone 17 cells in response to Dox, although none of these were statistically significant (Fig 7.9b). Combination of both overexpression clones together did not reveal a significant difference in the MAPK signature expression between pTRE-CPT1A clones with and without Dox treatment (t-test p=0.68).

7.2.3.1.3 ***EMT signature expression*** As with the earlier two signatures, the TetOn parental cells were observed to have a non-significant trend of increased expression of the EMT signature in response to Dox treatment (Fig 7.9c). However, the EMT signature was not significantly differentially expressed in either pTRE-CPT1A overexpression clone. The EMT signature was also not significantly differentially expressed abetween pTRE-CPT1A clones with and without Dox treatment when the two overexpression clones were combined (t-test p=0.91).

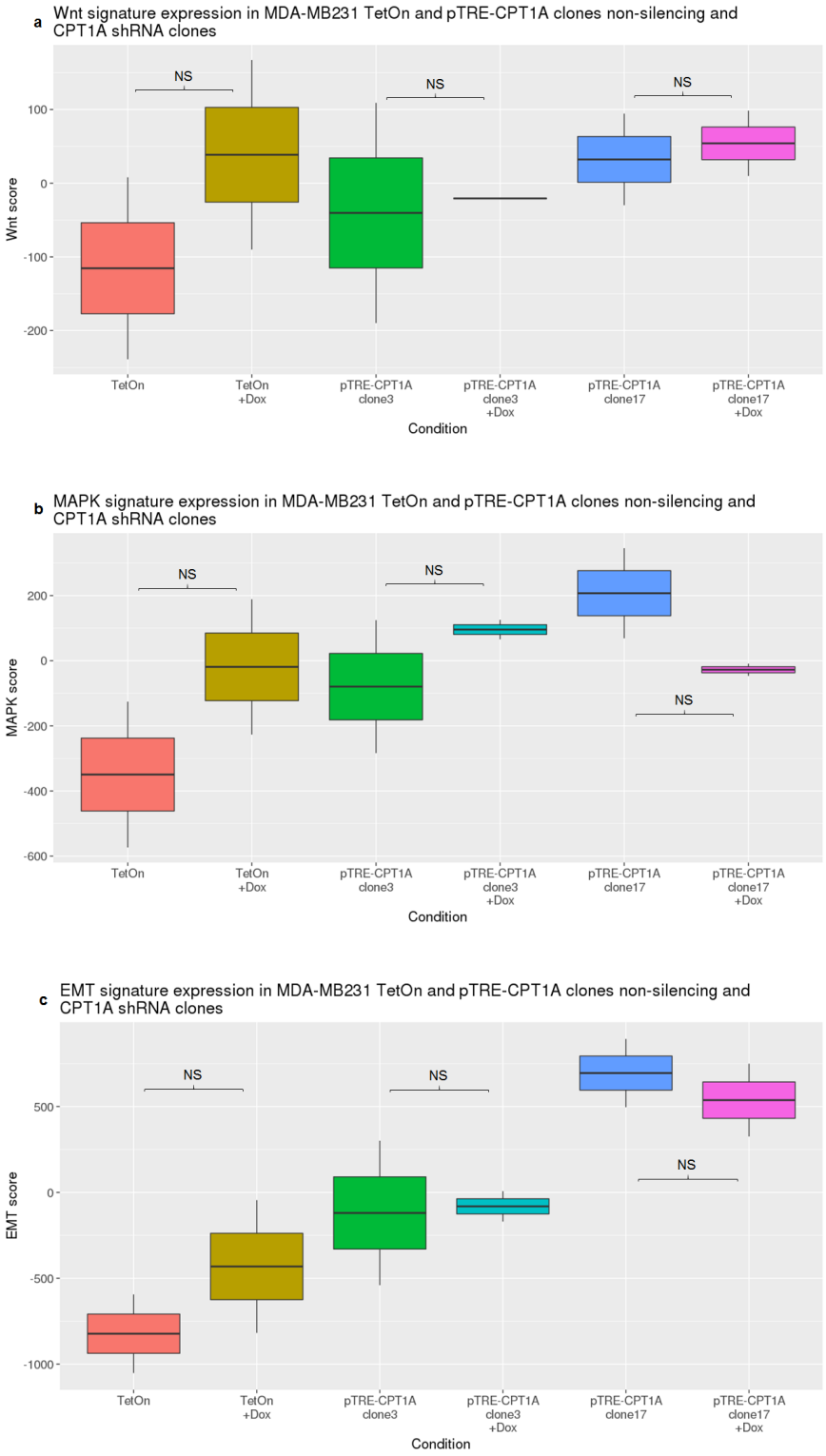

Figure 7.9: Wnt, MAPK and EMT signature expression analysis in MDA-MB231 TetOn and pTRE-CPT1A clones. (a) Wnt, (b) MAPK, and (c) EMT signature expression in TetOn and pTRE-CPT1A in the presence or absence of Dox.

7.2.3.2 *Wnt, MAPK and EMT signature expression in MCF7 transgenic systems*

7.2.3.2.1 ***Wnt signature expression*** In both shRNA knockdown clones, the Wnt signature expression was higher than the non-silencing control, but these differences were not significant.(Fig 7.10a). When the two different shRNA knockdown clones were combined (n=4 total) and expression of the Wnt signature was compared to the non-silencing control, the difference was not significant (t-test $p = 0.18$). However, when one outlier value from shRNA1 clone was removed, the Wnt signature showed a trend of increased expression in the *CPT1A* knockdown combined clones ($p = 0.063$) (Fig 7.10d).

7.2.3.2.2 ***MAPK signature expression*** The MAPK signature expression was higher in both shRNA knockdown clones compared to the non-silencing control, but these differences were not significant.(Fig 7.10b). Furthermore, the MAPK signature expression also showed no evidence of being significantly differentially expressed when the two knockdown clones were combined, compared to the non-silencing control (t-test $p = 0.23$). However, when the same outlier value from the Wnt signature expression analysis was removed, the MAPK signature was expressed higher in the *CPT1A* knockdown line, with a favourable statistical trend ($p = 0.09$) (Fig 7.10e).

7.2.3.2.3 ***EMT signature expression*** The EMT signature expression was higher than the non-silencing control, but these differences were not significant (Fig 7.10c). Additionally, when the two knockdown clones were combined and EMT signature expression compared to the non-silencing control, the differences were not significant (t-test $p = 0.16$). Removal of the outlier value from the combined clones as above resulted in increased EMT signature expression when *CPT1A* was knocked down, which was

marginally close to statistical significance (p value of 0.073) (Fig 7.10f).

7.2.4 Analysis of publicly available datasets that modulate FAO in different cell systems

To explore molecular changes that occur in response to alterations in FAO in other cell systems by different means investigated in this thesis, two publicly available datasets were analysed. The first dataset was generated by Torrano *et. al.*, who reported that increased expression of PGC1A - a key co-regulator of fatty acid oxidation - increased FAO flux and mitochondrial respiration, which resulted in decreased proliferation rates of prostate cancer cell lines *in vitro*, and decreased metastasis in xenograft mice studies (Torrano et al., 2016). The authors performed microarray analysis to compare the transcriptome of PC3 prostate cancer cells with basal and PGC1A overexpression. The second dataset analysed was generated by Srivastava *et. al.*, who reported that treatment of NCI-H2347 lung cancer cell line with pioglitazone - a PPARG agonist - resulted in increased FAO and cell cycle arrest, both in *in vitro* and *in vivo* settings (Srivastava et al., 2014). The authors performed transcriptome analysis of NCI-H2347 cells treated with pioglitazone for 12-, 24- and 48 hours.

7.2.4.1 *Wnt, MAPK and EMT signature expression in PC3 cells with PGC1A overexpression and NCI-H2347 cells treated with pioglitazone*

PGC1A overexpression in PC3 cells resulted in decreased expression of the Wnt signature, and showed a trend towards decreased expression of the MAPK signature (Fig 7.11a,b). Notably, the EMT signature was significantly downregulated in response to PGC1A overexpression (Fig 7.11c).

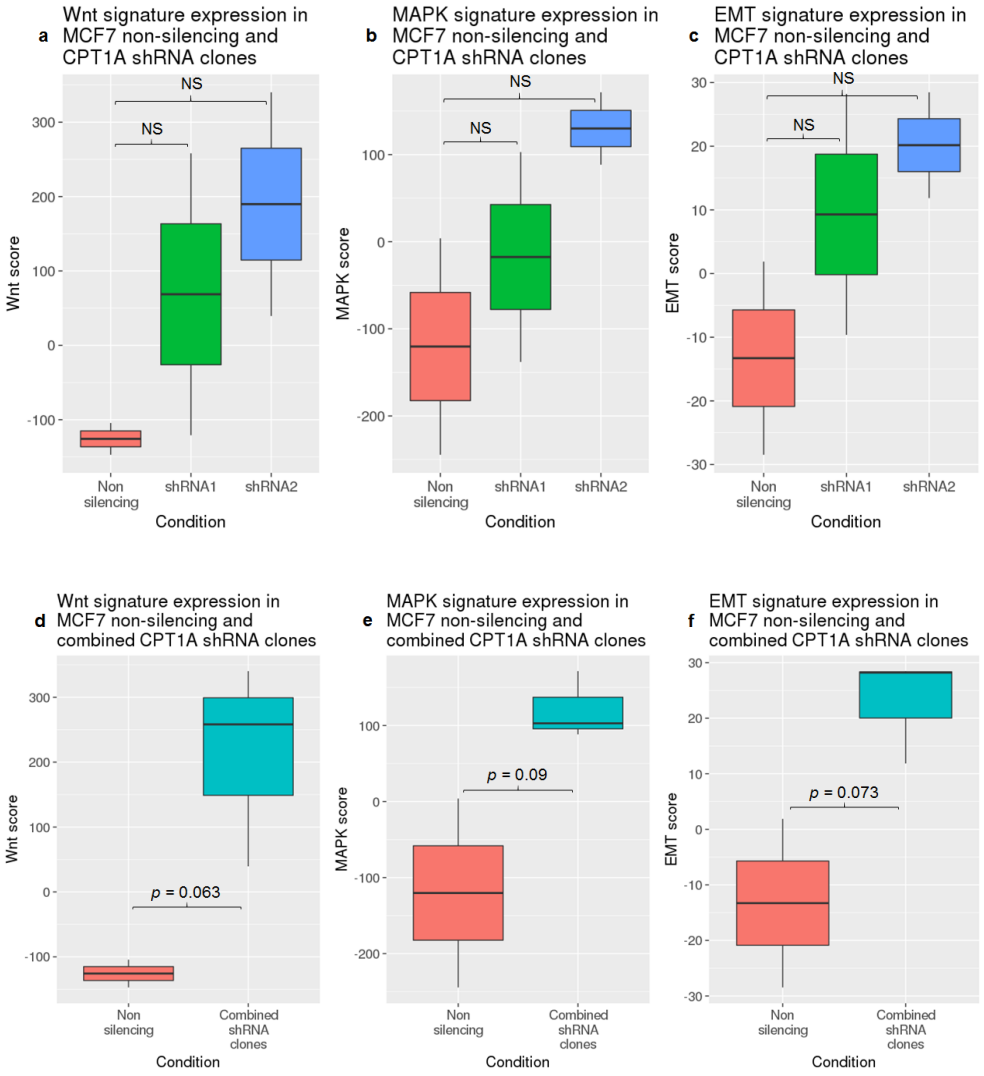

Figure 7.10: Wnt, MAPK and EMT signature expression analysis in MCF7 non-silencing and *CPT1A* shRNA1 and shRNA2 clones. (a) Wnt, (b) MAPK, and (c) EMT signature expression in non-silencing and shRNA clones. (d) Wnt, (e) MAPK, and (f) EMT signature expression in non-silencing and combined shRNA clones after removal of one outlier value.

Treatment of NCI-H2347 cells with pioglitazone over a time course led to significant decreases in the Wnt signature expression across all time points. However, no significant differences in MAPK signature expression were observed (Fig 7.11d,e). The EMT signature showed no evidence of being differentially expressed at the earlier time points, but pioglitazone treatment at 48 hrs increased the expression of this signature, albeit with a fairly large variation, compared to vehicle treatment (Fig 7.11f).

7.2.4.2 *Differential expression analysis of transcriptome data from PC3 cells with PCG1A overexpression*

Differential and enrichment analysis between basal and PGC1A overexpressing PC3 cells was performed as for MDA-MB231 and MCF7 RNA-seq analysis. Genesets that are upregulated were concordant with those reported by the authors and presented in the supplementary for brevity (Supp Fig A.14. Briefly, as expected, genesets that were involved in oxidative metabolism were significantly enriched in genes that were upregulated by PGC1A overexpression in PC3 cells. All of the curated databases consistently identified enrichment of genesets involved in oxidative phosphorylation and electron transport chain, while only the WikiPathways database was observed to have a geneset involved in FAO enriched (Supp Fig A.14c).

In agreement with the findings of the authors that generated this dataset, genesets that were significantly downregulated in PC3 cells with PGC1A overexpression were primarily involved in cell proliferation. However, this analysis also identified several immune- or inflammation-related genesets that were *downregulated* when PGC1A was overexpressed in PC3 cells (Supp Fig A.13, blue arrows).

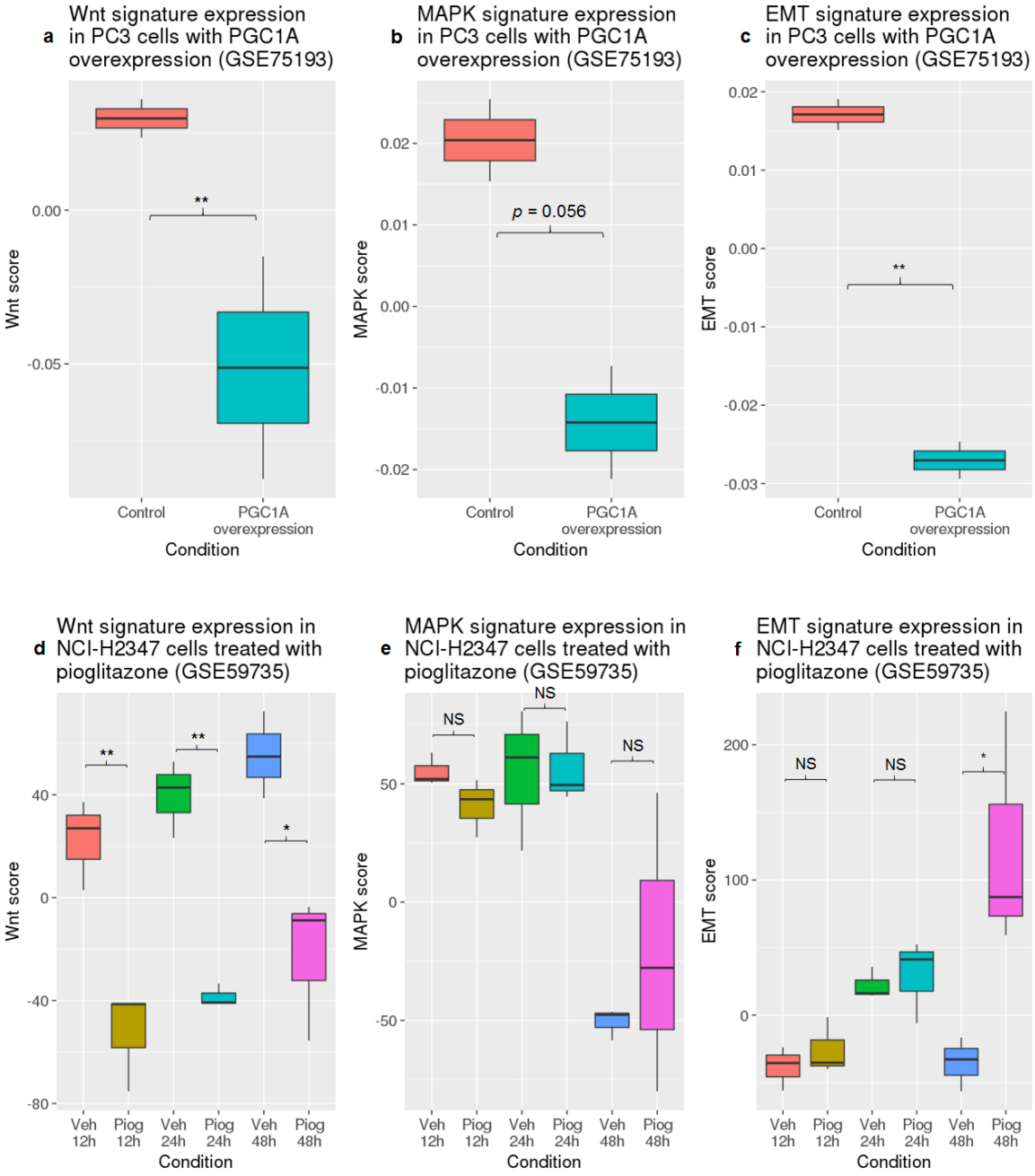

Figure 7.11: Wnt, MAPK and EMT signature expression analysis in PC3 cells with PGC1A overexpression or NCI-H2347 cells treated with pioglitazone. (**a-c**) (a) Wnt, (b) MAPK, and (c) EMT signature expression in PC3 cells with PGC1A overexpression. (**d-f**) (d) Wnt, (e) MAPK, and (f) EMT signature expression in NCI-H2347 cells treated with pioglitazone. Veh = vehicle, Piog = pioglitazone.

7.2.4.3 *Differential expression analysis of transcriptome data from NCI-H2347 cells treated with pioglitazone*

To identify genes involved in signalling pathways that were enriched in NCI-H2347 cells in response to pioglitazone, differential and enrichment analysis was performed on the Srivastava *et. al.* dataset. At 12 hours post-treatment, genesets involved in fatty acid metabolism were upregulated (Supp Fig A.18, yellow arrows). This was also true at 24 hours post-treatment (Supp Fig A.19, yellow arrows); while at 48 hours, genesets involved in glycolysis were enriched in genes upregulated in response to PGC1A expression, presumably to generate NADPH via the pentose phosphate pathway to neutralise increased free radical species from enhanced mitochondrial respiration (Supp Fig A.20, cyan arrows).

As shown by the authors, genesets involved in proliferation were also significantly downregulated by 12 hours (Supp Fig A.15, cyan arrows). Similar to the observations made in analysis of Torrano *et. al.* dataset, genesets associated with immune function were downregulated in response to pioglitazone treatment (blue arrows). However, at 24- and 48 hours post-treatment, the immune-related genesets were no longer enriched, and overrepresentation of other signalling pathways was not observed (Supp Figs A.16, A.17). Notably, proliferation genesets continued to be downregulated in treated cells over these time points.

7.3 Discussion

This chapter sought to characterise the transcriptomic features that were differentially regulated in response to *CPT1A* modulation in MDA-MB231 and MCF7 cells. In particular, this hypothesis-generating exercise was focused on identifying the *signalling*

pathways that may be altered between the conditions.

7.3.1 Differential and gene set enrichment analysis

7.3.1.1 MDA-MB231 *CPT1A* overexpression

In MDA-MB231 pTRE-CPT1A clones, apart from *CPT1A*, no other genes were significantly differentially expressed. Gene set enrichment analysis suggests that genes downregulated in pTRE-CPT1A clone 3 were enriched for cell cycle processes, which is consistent with the results from the growth curve analysis performed in Chapter 6. In contrast, cell cycle genesets were enriched in genes that were upregulated in clone 17. Given that the growth curve analysis of this clone also showed slower growth when CPT1A was overexpressed, it is not entirely clear why genes involved in proliferation were higher in basal compared to CPT1A overexpression in clone 17. Additionally, there were no other genesets that were commonly enriched between these two clones. Differential analysis by combining the two overexpression clones together did not show consistent enrichment for genes that were upregulated. In contrast, genesets that were commonly identified to be downregulated were involved in ribosomal processes. Two studies have documented that doxycycline can affect mitochondrial ribosomal processes, which may account for the enrichment of these processes in the pTRE-CPT1A and TetOn parental cell lines (Ahler et al., 2013; Moullan et al., 2015). Another possible reason why genes involved in signalling pathways are not enriched in this analysis could be that *CPT1A* may indirectly induce an increased activity of one or a few key tumour suppressor *proteins*, such as pRb, and destabilisation of cell cycle-related proteins, thereby leading to decreased proliferation rates observed in the growth curves of these clones.

7.3.1.2 MCF7 *CPT1A* knockdown

In MCF7 cells with CPT1A knockdown relative to basal non-silencing expression, cell signalling genesets were enriched in the knockdown clones. In particular, an EGF signalling geneset was a common geneset enriched in both knockdown clones. Notably, this enrichment was also observed when both knockdown clones were combined for differential analysis. This supports the trend observed from the targeted analysis, where the MAPK signature was trending towards increased expression upon *CPT1A* knockdown. However, the growth curve analysis performed on this cell system did not suggest differences in proliferation rates between *CPT1A* knockdown and basal expression. This raises the possibility that there may be other signalling pathways that drive MCF7 cell proliferation that are not affected by *CPT1A* knockdown. Another plausible explanation is that under the experimental conditions for this analysis, the magnitude of EGF signalling downregulation may not be sufficient to alter the cell division rates in MCF7 cells. Perhaps stronger or longer knockdown of *CPT1A* in MCF7 cells may amplify its effect on EGF signalling. As for genes that were downregulated by *CPT1A* knockdown, genesets involved in ribosomal processes were enriched for, in line with the observation in MDA-MB231 cells. Hence, this could be attributed to the effect of Dox on mitochondrial RNA metabolism.

7.3.1.3 Public datasets

The geneset enrichment analysis was also performed on two publicly available datasets that modulated FAO in different cell systems. Between both datasets, enriched genesets that were commonly downregulated were associated with immune function. Of note, in NCI-H2347 cells treated with pioglitazone, this enrichment was only observed at the 12h, but not later time points. Validation of these genesets on other datasets which may be available in future should be a priority, before investing experimental resources

to pursue this finding.

7.3.2 Targeted analysis

7.3.2.1 MDA-MB231 *CPT1A* overexpression

The expression of specific pathways were also analysed in the MDA-MB231 and MCF7 transgenic systems. In pTRE-CPT1A MDA-MB231 cells, no significant differences were found in the expression of gene signatures that represent the EMT, Wnt and MAPK signalling pathways, compared to TetOn parental line. The most obvious explanation for this observation is that these genesets are not altered by potential metabolic rewiring brought about by *CPT1A* overexpression.

While the targeted analysis conducted was exploratory, it is possible that the cell lines used in this study may not be entirely suitable to observe changes in the three targeted pathways in response to *CPT1A* modulation. Due to the crosstalk between pathways, cancer cells may also activate several signalling cascades that may feed into the MAPK pathway en route to the nucleus to activate transcriptional programs for proliferation (Mendoza, Er, and Blenis, 2011). Hence, the *linear* enrichment of genes, from say, the MAPK pathway (i.e, RAS - RAF - MEK - ERK) may not be strongly enriched in certain cell types. Alternatively, certain cell lines may prefer to activate other signalling pathways independently of the MAPK cascade to proliferate. These two points taken together may explain the lack of association between *CPT1A* overexpression and expression of the Wnt and MAPK gene signatures in the MDA-MB231 cell system. One suggestion could be to modulate FAO in cell systems with activation in these pathways - such as BRAF V600E mutant melanoma cell lines, or colorectal cancer cell lines with mutation in *APC* or some other Wnt signalling components. As for the EMT gene signature, it is possible that *CPT1A* overexpression alone is sufficient to reverse the

mesenchymal features of MDA-MB231 cells.

7.3.2.2 MCF7 *CPT1A* knockdown

In MCF7 cells with *CPT1A* knockdown, analysis of individual clones compared to non-silencing control suggests a trend of increased expression of the EMT, Wnt, and MAPK signatures, particularly in shRNA2 clone, which had stronger *CPT1A* knockdown (67% knockdown in shRNA2 clone vs 50% in shRNA1 clone). However, these differeces were not statistically significant. After combining the knockdown clones and removing one outlier value, the p-values obtained were trending towards significance for all three signatures analysed. Hence, it is possible that stronger *CPT1A* inhibition may further enhance the increased expression of these signatures in this cell line. These increased proliferation and migration associated signatures in response to *CPT1A* knockdown may be accounted for by increased glycolytic flux, which on top of ATP, is key to generate metabolites for proliferation (Lunt and Vander Heiden, 2011; Hay, 2016).

Notably, while the MAPK and Wnt signatures were upregulated, no difference in growth rates between basal and *CPT1A* knockdown in MCF7 were observed as described in Chapter 6. A potential explanation for this is that while these pathways were activated at the *transcript* level under the experimental conditions conducted for this RNA-Seq analysis, it may take longer for the complete metabolic and molecular reprogramming to manifest and impact cell division rates.

The level of *CPT1A* knockdown observed in this RNA-Seq analysis is consistent with multiple, previous experiments. Therefore, this warrants verification of the findings from the targeted analysis by alternative methods such as using small interfering RNA knockdown, or CPT1A inhibition with etomoxir. Key genes from each of the three signatures analysed can then be measured by qPCR. Taken together, this analysis, while prelimi-

nary, suggests that altering *CPT1A* expression in MCF7 cells can affect key oncogenic pathways. It may also be worthwhile to advance these findings using cancer cell lines with pathway activation of the signatures analysed, such as selected melanoma and lung (MAPK), and colorectal (Wnt) cancer cell lines.

7.3.2.3 Public datasets

The analysis of published gene expression data from PC3 cells with PGC1A overexpression revealed a significant difference in the expression of the EMT geneset. This supports the decreased lung and bone metastasis *in vivo* of PGC1A overexpressing PC3 cells, compared to basal expression, reported by the authors. However, even though the authors of this dataset demonstrated significant decrease in proliferation when PGC1A was overexpressed, the MAPK and Wnt signalling signatures showed no evidence of significant differential expression between the two conditions. This suggests that the PC3 cells utilised in this study may not be reliant on Wnt or MAPK signalling for proliferation.

In the second dataset analysed, NCI-H2347 cells treated with pioglitazone over a time course were observed to downregulate Wnt signalling signature expression. The MAPK signature expression, however, showed no evidence of differential expression over the time point. Interestingly, the EMT signature was observed to be significantly *upregulated* in pioglitazone treated cells at 48 hours post-treatment, compared to earlier time points, which suggests that pioglitazone can induce EMT in this cell system. However, the variation observed in the vehicle-treated cells between time points suggest that one should be cautious to interpret this finding and more in-depth analysis is required to verify this observation. In summary, analysis of the two publicly available datasets did not reveal any outstanding signalling pathway members that were altered at the transcript level.

7.3.3 Conclusions and limitations

This chapter sought to identify enriched processes at the transcriptome level in MDA-MB231 cells with *CPT1A* overexpression and MCF7 cells with *CPT1A* knockdown. No genesets were reproducibly up- or downregulated in the MDA-MB231 pTRE-CPT1A clones 3 and 17. Consistent enrichment in ribosomal and RNA processing genesets were found between pTRE-CPT1A and TetOn cell lines, as well as between non-silencing and *CPT1A* shRNA MCF7 cell lines. Some enrichment in EGF signalling was observed in genes upregulated by *CPT1A* knockdown, which may be worth further investigation.

The ability to detect small differences in gene expression in this study may have been limited by the number of replicates assayed. From the growth curve analysis described in Chapter 6, the modest decrease in proliferation (33%) in pTRE-CPT1A cells after one week suggests a fairly small effect size. The budget of this project allowed the sequencing of biological duplicates for each condition. Sequencing 2-3 more biological replicates may possibly identify smaller, but biologically meaningful, fold changes, while meeting the predefined statistical threshold. Hence, one cannot discount the possibility that transcriptional changes may be occurring in these systems in response to *CPT1A* modulation. Alternatively, this work could be followed up with panel-based gene expression analysis of selected pathways by either qPCR or the NanoString nCounter platform.

The analysis performed on the public datasets are also subject to some caveats. While PGC1A is a key transcriptional co-regulator of genes involved in FAO, one cannot discount other processes directly or indirectly activated or inhibited by this protein. Hence, it is possible that the downregulation of the EMT geneset by PGC1A overexpression is not due to activation of FAO and overall mitochondrial respiration, but also other cues modulated by PGC1A. Similarly, given that the pioglitazone concentration used to treat NCI-H2347 cells was in the micromolar range, the effect of this drug may not be specifically attributable to the activation of its cognate target *per se*, but may be due

to off-target effects.

Chapter 8

Conclusions and future directions

8.1 General discussion

This thesis sought to identify and investigate the metabolic correlates of prognosis in ER-positive breast cancer patients. Analysis of a large training dataset from a cohort of primary breast tumours identified high expression of a 19-gene signature involved in FAO that is significantly associated with better disease-specific survival. This finding was validated in multiple, independent datasets from breast, and other cancer types. Additionally, analysis of the FAO signature expression in tumour-normal tissues from different tissues revealed downregulation of the signature in tumour, relative to normal tissues. This finding suggests that expression of genes involved in FAO is downregulated during tumourigenesis, and may be part of a larger metabolic rewiring that occurs in a cancer cell.

Since low expression of the FAO signature is associated with disease recurrence, a relationship between the FAO signature expression and EMT - a process implicated in metastasis - was explored. Different modalities of EMT induction - a process understood to be important for metastasis - resulted in the decreased expression of the FAO signature in different cell and organoid systems. This may potentially explain why

patients with low FAO signature expression have a poorer outcome. Importantly, as demonstrated by Kang *et. al.*, expression of EMT markers in kidney fibrosis model was reduced in response to activation of FAO by treatment with fenofibrate (Kang et al., 2015). These findings warrant further investigation into how activation of FAO may alter EMT-induced migration and/or invasion in cancer cell systems.

Understanding how oncogenic signalling affects cancer cell metabolism is an ongoing effort in the field of tumour metabolism (Nagarajan, Malvi, and Wajapeyee, 2016). In Chapter 5, the association between the FAO signature expression and two key signalling pathways frequently altered in cancer - MAPK and Wnt - was explored. Activation of both signalling pathways in cell and organoid systems resulted in the significant down-regulation of the FAO signature expression. Since both pathways induce cancer cell proliferation, and Chapter 3 has shown a negative correlation between a proliferation gene signature and the FAO signature expression, it is possible that the finding above may be an indirect consequence of activating the MAPK and Wnt pathways. Interestingly, the two oncogenic signalling pathways - MAPK and Wnt - explored in Chapter 5 have also been shown to be involved in EMT induction (Lamouille, Xu, and Derynck, 2014). However, the studies that generated the gene expression datasets analysed in Chapter 5 did not focus on analysing EMT in response to modulation of the two oncogenic signalling pathways in different systems. Furthermore, as suggested by the findings of Mitra *et. al.* (Mitra and Roy, 2017), the simultaneous activation of TGFβ and Wnt signalling pathways can negate EMT induction in ovarian cancer cells. Hence, this suggests that the relationship between EMT and oncogenic signalling is complex, and while this thesis has shown that activation of the Wnt, MAPK and EMT signalling converge on decreased FAO signature expression, a mechanistic relationship between these three processes require experimental investigation.

Based on the computational findings, the effect of experimentally modulating FAO was investigated in two breast cancer cell systems. Due to the impracticalities of modulating all the 19 genes in the FAO signature, this thesis generated cell systems that modulate CPT1A - the rate-limiting enzyme in FAO. Overexpression of *CPT1A* in MDA-MB231 breast cancer cells decreased the proliferation and wound healing rates. In contrast, CPT1A knockdown in MCF7 cells did not alter proliferation rates, compared to basal expression control. A single attempt at measuring oxygen consumption rates in response to *CPT1A* expression did not reveal significant differences in oxygen consumption in response to exogenous palmitate. Global transcriptome analyses did not reveal pathways that were significantly altered in response to modulation of *CPT1A* expression in either cell systems. However, targeted analysis of EMT, MAPK and Wnt pathways in MCF7 cells with *CPT1A* knockdown suggests a trend towards increased transcriptional activity of these pathways in this cell system. Taken together, while this thesis has provided novel evidence on how modulating FAO in cell systems can alter cancer cell proliferation, future efforts should focus on analysing other cell lines using different means of modulating FAO.

8.1.1 Conclusion

In conclusion, this thesis has highlighted the novel association between expression of a gene signature involved in FAO and prognosis in some cancers. What are potential clinical implications of these findings? Firstly, this study suggests that having an estimate of how FAO status in a primary tumour may provide useful prognostic information. One possible avenue of achieving this in presented in the future directions section below (Section 8.3.1). Tumours identified with low FAO could be treated with agents that can upregulate FAO, which may improve survival for some cancers.

8.1.2 Overall strengths and limitations

The basis of this thesis is based on compelling, robust data from computational analyses of publicly available gene expression datasets. These data sets the scene for future experimental work to dissect the molecular underpinnings described in Chapters 3 to 5. Some of these findings are in agreement of recent literature, which lends support to pursue them further experimentally. While this thesis has contributed significant findings as to the relationship between the FAO signature expression and EMT and activation of oncogenic signalling, due to time constraints, it was limited by the lack of experimental analysis to further characterise these findings in cell systems. Nevertheless, this thesis has presented a novel perspective into the role of FAO in cancer biology and prognosis. Further work, some of which is proposed below, is required to better appreciate the significance of this metabolic pathway.

8.2 Future directions

This chapter proposes several conceptual applications of how the FAO pathway can be studied in various different contexts, which could enhance our understanding of tumour metabolism. This will be followed by suggestions on how the FAO pathway can be studied at a different scale by harnessing technologies to image and actively monitor this metabolic pathway in the management of cancer patients.

8.2.1 *siRNA knockdown of CPT1A in ER-positive breast cancer cell lines*

This thesis investigated the effects of knocking down CPT1A expression in MCF7 cells using the shRNA system. However, after one week of knockdown, substantial CPT1A expression could still be detected by immunoblot analysis. Hence, it is possible that

there was not sufficient knockdown of CPT1A to alter cellular characteristics such as proliferation. Hence, future work could explore an alternative method of CPT1A knockdown such as siRNA. It is worthwhile noting that this method, unlike the stable shRNA expression performed in this thesis, would be more suitable to study the short term effects of knocking down the expression of a gene. If the cellular effects of knocking down CPT1A requires time to manifest, siRNA may not be capture them.

8.2.2 *Pharmacologic activation or inhibition of FAO in cancer cell lines*

For experiments that involved looking at the effects of CPT1A knockdown in MCF10A and MCF7 cells, there was substantial protein expression even after 5-7 days of shRNA expression, which suggests that the protein has a long half-life. Future work could use small interfering RNAs against *CPT1A* or the small molecule etomoxir to inhibit CPT1A enzyme, and observe whether this intervention affects proliferation, migration and anchorage-independent growth in breast cancer cell lines. Additionally, the decreased proliferation observed when *CPT1A* was overexpressed in MDA-MB231 cells could be followed up with pharmacologic activation of FAO in other ER-negative cell lines.

The drugging exercise can also be extended to other cancer types, which may inform whether findings from this experiment can be applied to different cancers. Furthermore, because the genomic profile of most these cell lines have been characterised, observations from the drugging experiments can be associated with particular genetic profiles, which may identify genomic correlates of FAO.

Moving away from breast cancer, this thesis found that the FAO signature expression was expressed lower in several cancers compared to normal tissues. This suggests that

there may be common feature/s associated with FAO regulation across different cancers. ccRCC is particularly intriguing, as the inactivation of *VHL* which occurs in approximately 90% of cases, results in the stabilisation of HIF1A, which drives a glycolytic phenotype. The use of dichloroacetate (DCA) reversed the Warburg effect and increased oxidative metabolism, resulting in increased p53 activation and apoptosis, and decreased proliferation in 786-O ccRCC cell line (Kinnaird et al., 2016). Additionally, DCA inhibited angiogenesis and tumour growth *in vivo*. Using ccRCC cell lines with *VHL* inactivation, one can ask: what is the effect of enforcing FAO in these cell lines? Findings from this experiment may provide an understanding of how altered FAO features in HIF1A metabolic rewiring in *VHL*-mutant ccRCCs.

8.2.3 *Analysis of other platforms to identify novel regulators and correlates of FAO*

This thesis primarily focused on the computational analysis of *mRNA* expression data. Pathways can also be regulated by other means, such as at the post-transcriptional and epigenetic levels. The TCGA database has microRNA and DNA methylation data available for most cancer types. By first separating patients into low and high FAO gene signature expression groups using RNAseq data, differential analysis of miRNA and DNA methylation can be conducted to identify novel regulators of FAO, as well as other pathways whose activity are correlated with FAO. As with the drugging experiment, this analysis ought to be performed in several cancers to identify the common molecular denominators, and unique findings can be further pursued separately, taking into account the genetics of each cancer.

Assuming a particular miRNA is enriched in the high FAO group, the expression of this miRNA could be analysed by qPCR in several cancer cell lines. This miRNA could then be overexpressed in cell lines with low expression, and transcriptome analysis performed

to identify genes and pathways regulated by the transgenic expression of this miRNA. Conversely, enriched miRNAs in the low FAO group could be overexpressed in cell lines with low expression of this miRNA (which presumably, has high FAO). The FAO flux in response to transgenic expression of this miRNA can be measured using the Seahorse XF system. Transcriptome analysis after overexpression of this miRNA may identify genes and pathways that are correlated with, or possibly drive, the decrease in FAO in cancer cells.

8.2.4 *How does hypoxia affect FAO flux?*

The diffusion limit for oxygen ranges between 100-200 microns, and cells must be within this radius for adequate oxygenation (Eales, Hollinshead, and Tennant, 2016). As cancer cells proliferate, regions of the tumour will be spatially withdrawn from the vasculature, hence, affecting the supply of oxygen and nutrients. This triggers activation of HIF1A, which drives a slew of molecular changes, including upregulation of genes that facilitate glycolysis. Of note, the electron transport chain (ETC) has been shown to still be functional at 0.5% oxygen levels, and hypoxic ($< 2\%$ oxygen) tumour cells can oxidise glutamine to generate ATP through the ETC (Chandel et al., 1997; Fan et al., 2013; Le et al., 2012; Le et al., 2014). Therefore, low oxygen tension does not necessarily imply the complete ablation of mitochondrial metabolism. However, how FAO is affected during hypoxia is poorly understood.

In hepatocellular carcinoma, HIF2A repressed the mRNA expression of two key FAO genes: *ACADM* and *ACADL*, resulting in decreased palmitate and oleate oxidation (Huang et al., 2014). Whether this finding can be extended to other cancer types remains unclear. Short of culturing cells under hypoxic conditions, treatment with cobalt chloride or desferrioxamine has been used to mimic hypoxia, which functions by either displacing or chelating iron atoms that are required for prolyl hydroxylase activity (Xia

et al., 2009). This enzyme serves to initiate the proteosomal degradation of HIF1A under normoxic condition. Therefore, these agents may be a good starting point to study the effect of hypoxia on FAO. Selected cancer cell lines can be treated with cobalt chloride, and gene expression of key FAO genes such as *CPT1A*, and the *ACAD* gene family measured by qPCR. This information is important because much emphasis has been placed on the role glycolysis and glutamine oxidation in hypoxic adaptation, but less is known about FAO. Findings from this experiment may add another piece to the puzzle as to the overall metabolic adaptations during decreased oxygen tension in cancer cells.

Recently, the efficacy of a small molecule inhibitor against HIF2A - PT2399 in ccRCC was reported by two independent groups (Cho et al., 2016; Chen et al., 2016). These initial studies focused on the pharmacokinetics and dynamics of the molecule, and identifying biomarkers of response. This presents an opportunity to compare the global metabolic adaptations and flux of pseudohypoxic ccRCC cell lines treated with PT2399 and vehicle control.

8.2.5 *Targeting co-dependencies in tumours with low FAO*

Altered cellular metabolism is now considered a hallmark of cancer (Ward and Thompson, 2012). In his commentary in Lancet, Professor Douglas Hanahan proposes that one solution to overcome the disheartening, inevitable resistance acquired to monotherapy against one hallmark is to target other hallmarks where possible:

"If one accepts the premise that most cancers acquire a similar armamentarium of capabilities, then a logical strategy is to remove as many of these capabilities as possible, rather than merely to target a single mechanism. Such a strategic shift can be thought of as a plan, of co-targeting of multiple capabilities, especially co-targeting of hallmarks

that can provide cross-support, whereby the power of one hallmark capability can help compensate for the therapeutic impairment of another." (Hanahan, 2014)

Since deregulated cellular metabolism is a hallmark of cancer, targeting metabolic vulnerabilities, in tandem with other hallmarks may provide more efficacious for the treatment of certain cancers. The FAO signature expression has been shown to be *lower* in several cancers, compared to normal tissues. The first, obvious strategy is to treat cancers with agents that upregulate FAO. This can be achieved using a PPAR alpha agonist such as fenofibrate, which has been shown to activate FAO in kidney epithelial cells (Kang et al., 2015). Additionally, Zeng *et.al.* described a molecule (Yhhu981) synthesised in-house that increased FAO in the C2C12 skeletal muscle cell line and ob/ob mice, an *in vivo* model of obesity (Zeng et al., 2015). Hence, these two molecules provide a starting point to study the effects of pharmacologically upregulating FAO in cancer cell lines.

Another option would be to identify other metabolic or signalling pathways correlated with low FAO. The conceptual framework has also been applied, at least in the preclinical setting, to other aspects of cancer metabolism. Some examples include co-administration of 2-deoxyglucose and metformin in mouse xenograft models; whereby inhibiting glycolysis induces cells to adopt oxidative metabolism, and this dependency can be targeted with metformin (Cheong et al., 2011). In lymphoma, therapy-induced senescence resulted in increased glycolysis and ATP production, and inhibition of glycolysis or autophagy further improved treatment outcome *in vivo* (Dorr et al., 2013).

Based on these findings, it is possible that other dependencies will emerge in response to different tumour FAO flux. For example, when FAO is high, cancer cells may be less dependent on glycolysis. Consequently, flux through the pentose phosphate pathway would be lower, which results in lesser reducing equivalents available to buffer against

acute oxidative stress. A small molecule screen performed on normal and cancer lines by Raj *et. al.* identified piperlongumine to be selectively cytotoxic to cancer cells via generation of reactive oxygen species (Raj et al., 2011). Based on this, one may postulate that the combination of agents that increase FAO (e.g., fenofibrate, Yhhu981) *and* induces oxidative stress (e.g., piperlongumine) may be cytotoxic to high glycolysis/low FAO tumours.

8.2.6 *Elucidating the interaction between tumour metabolism and microenvironment*

This thesis has considered the FAO signature expression in tumours as a cell autonomous process. Indeed, laser capture microdissected colorectal tumour tissue was found to have lower FAO signature expression, compared to bulk tumour tissues (Supp Fig A.2). Nevertheless, there are several studies that suggest the tumour microenvironment can influence the metabolism of tumour cells (Anastasiou, 2017).

Altering metabolic flux through pharmacologic interventions in the tumour may make substrates available for the stromal components such as infiltrating immune cells. For instance, decreasing glycolytic flux in cancer cells may make more glucose available for T lymphocyte cell function (Chang et al., 2013; Ho et al., 2015). Arginine promotes T lymphocyte cell anti-tumour activity, and consequently, arginine deprivation may bring about an immune-suppressive effect (Fletcher et al., 2015). Excess lactate secreted from tumour cells can blunt natural killer cell and T lymphocyte cell function (Brand et al., 2016).

Taken together, targeting the metabolic pathways in tumours may have a positive or negative collateral effect on its immediate environment. This presents an opportunity to develop metabolic therapies that have a negative impact on the tumour, but also pro-

mote anti-tumour stromal activity that may further potentiate its treatment efficacy.

8.2.7 *Xenopus laevis appendage regeneration as a model system to understand metabolic correlates of cancer initiation and progression*

The use of model organisms has led to the characterisation of several processes that are key in tumourigenesis. The nematode *Caenorhabditis elegans* was key in understanding apoptosis and hypoxia, and the fruitfly *Drosophila melanogaster* was integral in elucidating the Notch and Hippo pathways - all highly relevant pathways and processes in several human cancers (Potts and Cameron, 2011; Epstein et al., 2001; Gonzalez, 2013).

The tadpole *Xenopus laevis* has a remarkable ability to regenerate its appendages (fins, tails and limbs), and is a model organism to study regeneration (Beck, Izpisua Belmonte, and Christen, 2009; Beck, Christen, and Slack, 2003). Love *et. al.* investigated the molecular alterations in response to regeneration of *Xenopus* tail appendage, and observed genes such as *leptin*, *proinsulin*, *hif1a* - all of which regulate the activity of glucose transporters and glycolysis - to be up regulated upon tail amputation. Furthermore, tail regeneration also activates pathways often implicated in cancer such as Wnt, FGF and leptin-mediated PI3K/Akt signalling (Lin and Slack, 2008; Donato, Frazao, and Elias, 2010).

The regeneration of *Xenopus* can be divided into three phases: early, intermediate, and late. This regenerative process involves proliferation, migration and differentiation - processes involved in cancer initiation and progression. While Love *et. al.* has reported the importance of the Warburg effect in *Xenopus* tail regeneration, the *global* metabolic correlates associated with each regenerative phase remains to be defined. Since the *Xenopus*

model is amenable to genetic modification procedures such as genetic editing and development of transgenic lines, expression of key, rate-limiting enzymes can be modulated and their effect on the different phases of regeneration monitored (Ishibashi, Cliffe, and Amaya, 2012; Love et al., 2011). The power of this system lies in the linear, continuum regenerative process, which allows identification of the metabolic shifts between the proliferation and migration- (pro-tumourigenic), and differentiation (tumour-suppressive) phases. Since *Xenopus* are unlikely to be mired by various genomic aberrations observed in cancers, the metabolic correlates of regeneration can be attributed to these processes *per se*. The findings from this analysis can then be further explored in cancer cell systems with progressive malignant features, such as the commercially available RWPE1 prostate cell line series.

8.3 Potential translational relevance of FAO in oncology

8.3.1 *Radiolabelled fatty acid to image tumours*

In oncology, fluoro-deoxyglucose positron emission tomography (FDG-PET) has been utilised for over 35 years to diagnose and stage tumours (Kelloff et al., 2005). FDG-PET takes advantage of the avidity for glucose displayed in many tumour types. Upon uptake via glucose transporters, FDG is phosphorylated to form 2-FDG-phosphate by hexokinase. The subsequent isomerisation to fructose-6-phosphate is inhibited due to the absence of an oxygen atom at the C2 position. Hence, it is trapped in the cell and its accumulation is correlated with the cellular glycolytic rate. The decay of 18-fluorine in FDG can then be detected by a PET scanner. Apart from diagnosing and staging tumours, FDG-PET has also been used to monitor therapy response in advanced and metastatic breast cancers (Lewis, Soloviev, and Brindle, 2015; Brindle, 2008). Another highly consumed nutrient in cancer is glutamine, and imaging of labelled glutamine has been reported to be superior compared to FDG to delineate tumour and normal brain

tissue in glioma patients (Venneti et al., 2015).

8.3.1.1 *PET imaging of FAO in cancer*

This thesis has shown that genes involved in FAO are downregulated in many cancers, and is supported by several other studies examining the protein levels and FAO flux of cancer cells. However, currently, no assays are utilised as part of standard clinical practise to estimate the FAO status in primary tumours. Several radiolabelled FAO probes such as fluoro-thia-palmitate (FTP) and fluoro-thio-oleate (FTO) have been developed and studied in a mouse model (DeGrado et al., 2010). This provides an opportunity to glean the FAO status of tumours *in vivo*. By imaging FDG, glutamine and thio-palmitate/oleate uptake, one may non-invasively infer the metabolic 'score' based on the ratios of the uptake values for a particular tumour. With follow up data, one could correlate the metabolic score with outcome, and potentially establish a novel prognostic or predictive variable of clinical significance.

8.3.2 *Using genomic correlates of tumour metabolism to actively target metabolic dependencies*

The relationship between key oncogenes and tumour metabolism is well documented. Furthermore, apart from synthetic lethal approaches, there are little therapeutic options available to treat tumours with tumour suppressor (e.g., *CDH1*, *TP53*) inactivation. Hence, targeting specific metabolic dependencies in this instance would provide another therapeutic avenue for cancer treatment. For example, metformin was shown to selectively suppress the growth of p53-null, compared to wildtype expression HCT116 isogenic colon cancer cell lines (Buzzai et al., 2005). Mutations in the tumour suppressor *LKB1*, which activates AMPK, have been shown to be susceptible to phenformin treatment in non-small cell lung cancer cell lines (Shackelford et al., 2013). Interestingly, in

mice, mutations in *Lkb1* and *Kras*, but not *Kras* and *p53*, were susceptible to phenformin treatment, resulting in increased survival. Taken together, these data suggests clinically actionable metabolic dependencies associated with particular mutations.

Based on this, patients can be administered inhibitors or activators of specific metabolic pathways, according to the mutational profile of their tumour. Using liquid biopsies, the efficacy of the treatment can be monitored based on quantity of these mutations in the circulation (Wan et al., 2017). During the course of treatment, emergence of other mutations that drive resistance or disease progression may correlate with some other metabolic dependencies, which could then be targeted. Experimental analyses described in Chapter 6 suggest that CPT1A modulation in MDA-MB231 and MCF7 cell lines, subject to the discussed limitations, does not consistently converge on influencing the cell cycle. In other words, the cell systems studied in this thesis suggest that overexpression or knockdown on CPT1A expression does not affect proliferation in an opposing manner. Furthermore, *in silico* analysis of *CPT1A* mRNA expression in a panel of breast cancer cell lines suggest that while ER-positive cell lines have higher *CPT1A* expression compared to ER-negative cell lines, there were substantial differences in *CPT1A* expression *within* these two groups. Hence, it is possible that other genomic aberrations, in addition to ER status, may be associated with *CPT1A* expression in these cell lines. This highlights the need to characterise the genomic correlates associated with *CPT1A* expression, which may assist identifying mutations that best explain the variation observed within the two ER subgroups. To summarise, future efforts could focus on refining our knowledge regarding mutations and their metabolic correlates, which may be translated in the clinic with potential therapies and active, non-invasive methods to monitor response.

Appendix A

Supplementary Figures

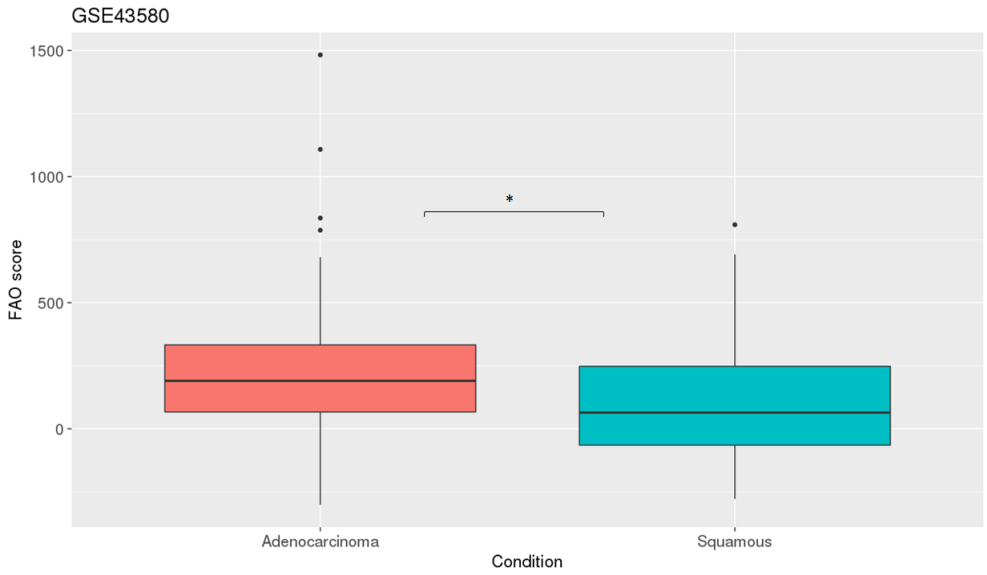

Figure A.1: FAO signature is expressed higher in lung adenocarcinoma compared to squamous cell carcinoma. t-test p * ≤ 0.05.

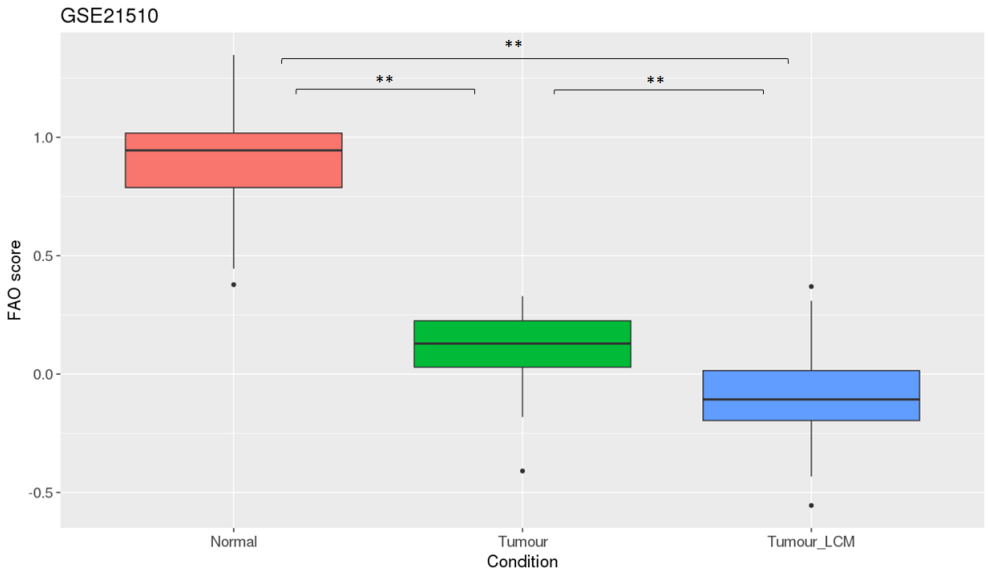

Figure A.2: FAO signature is expressed lower in laser capture microdissected (LCM) compared to bulk biopsy colon tumours and normal colon tissue. t-test p ** ≤ 0.01.

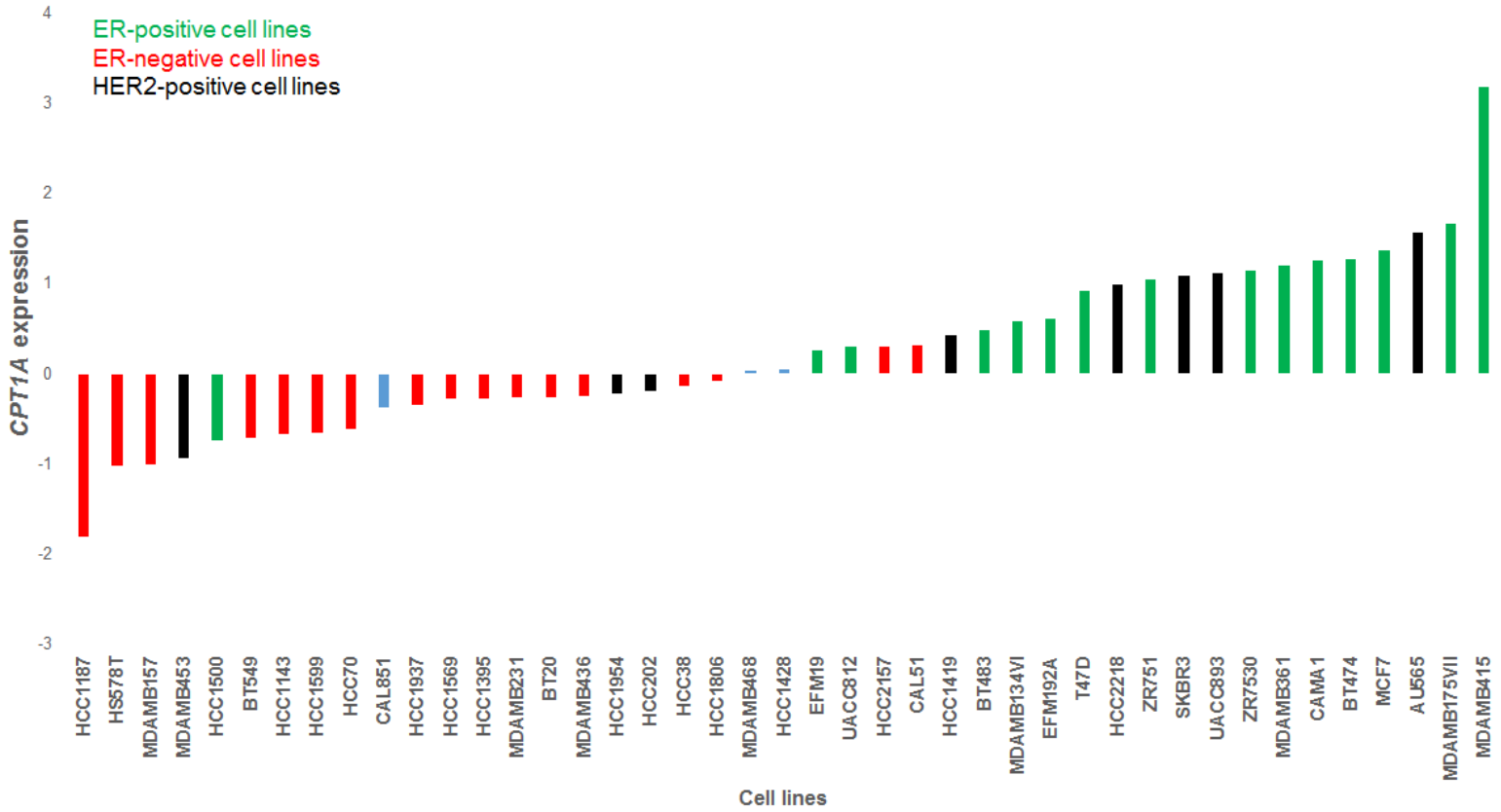

Figure A.3: ER-positive cell lines have higher *CPT1A* mRNA expression compared to ER-negative cell lines (GSE41313 dataset).

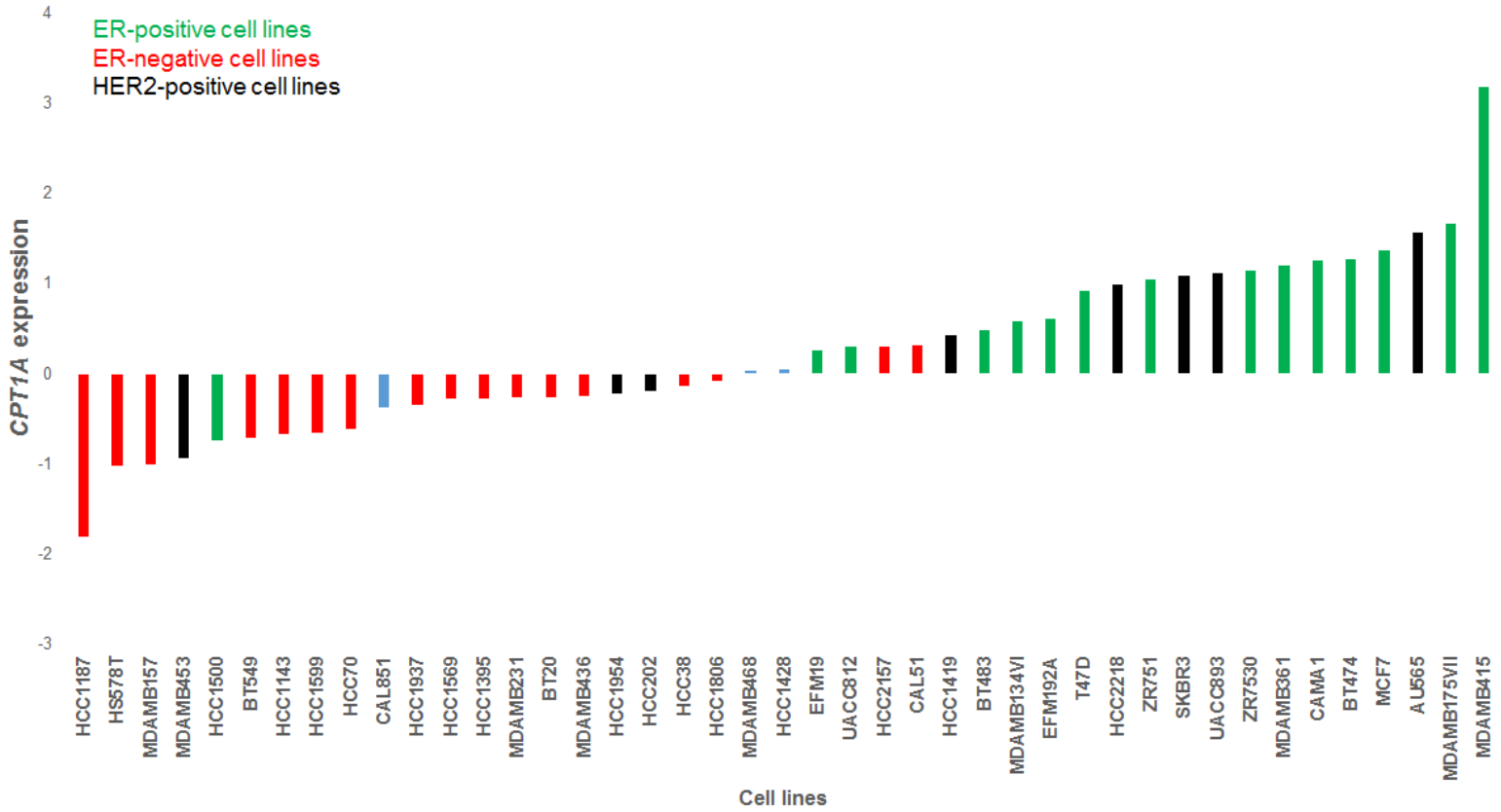

Figure A.4: ER-positive cell lines have higher *CPT1A* mRNA expression compared to ER-negative cell lines (Cancer Cell Line Encyclopedia dataset).

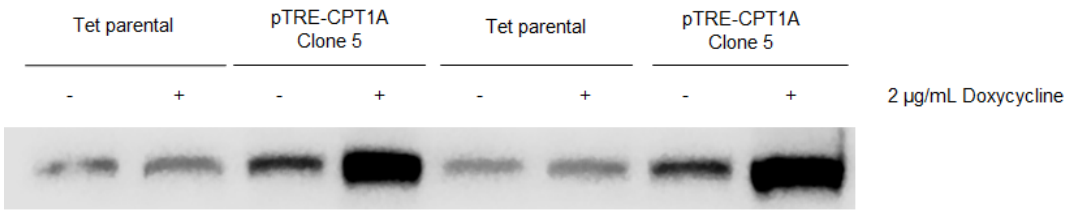

Figure A.5: Leaky CPT1A expression in pTRE-CPT1A clone 5 in the absence of Dox induction.

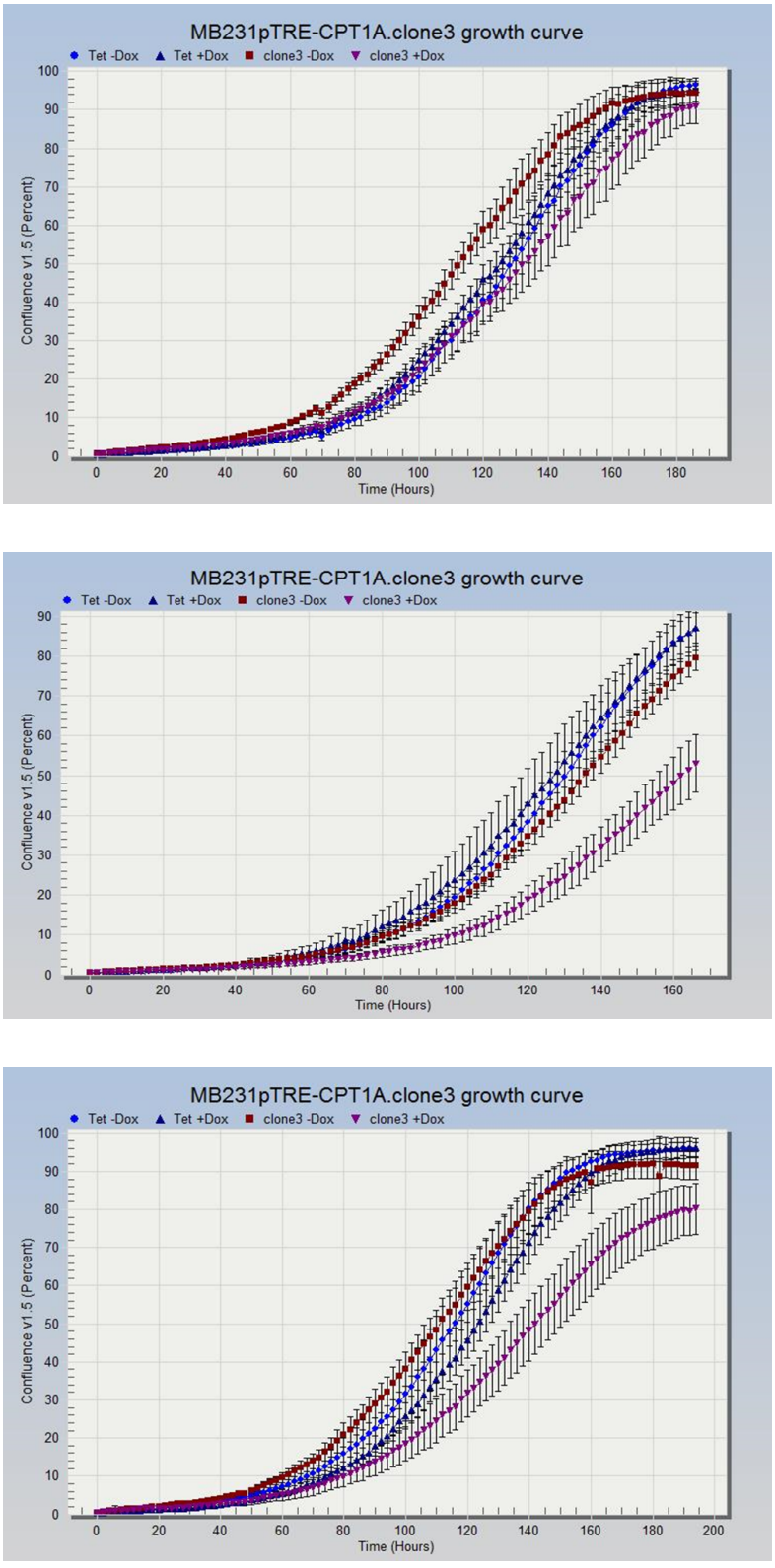

Figure A.6: Growth curves of pTRE-CPT1A clone 3 with basal and CPT1A overexpression. Error bars = standard deviation. Blue cirles: Tet -Dox; Navy squares: Tet +Dox; Red squares: pTRE-CPT1A clone 3 -Dox; Pink triangles: pTRE-CPT1A clone 3 +Dox.

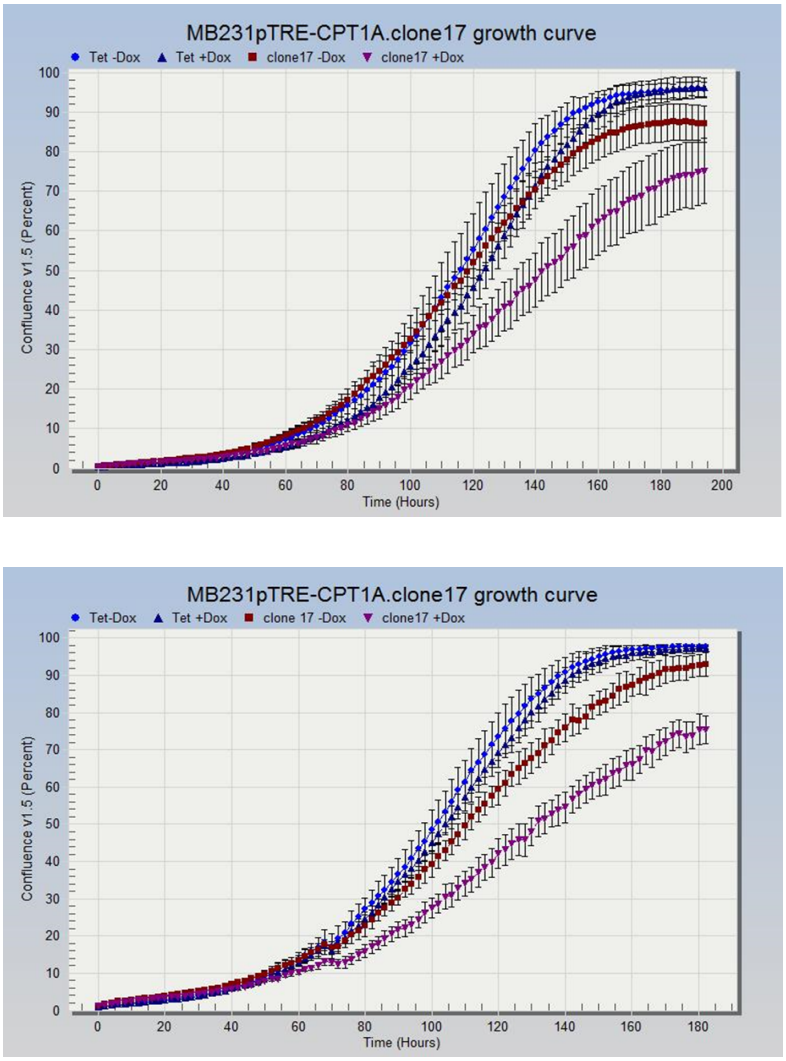

Figure A.7: Growth curves of pTRE-CPT1A clone 17 with basal and CPT1A overexpression. Error bars = standard deviation. Blue cirles: Tet -Dox; Navy squares: Tet +Dox; Red squares: pTRE-CPT1A clone 17 -Dox; Pink triangles: pTRE-CPT1A clone 17 +Dox.

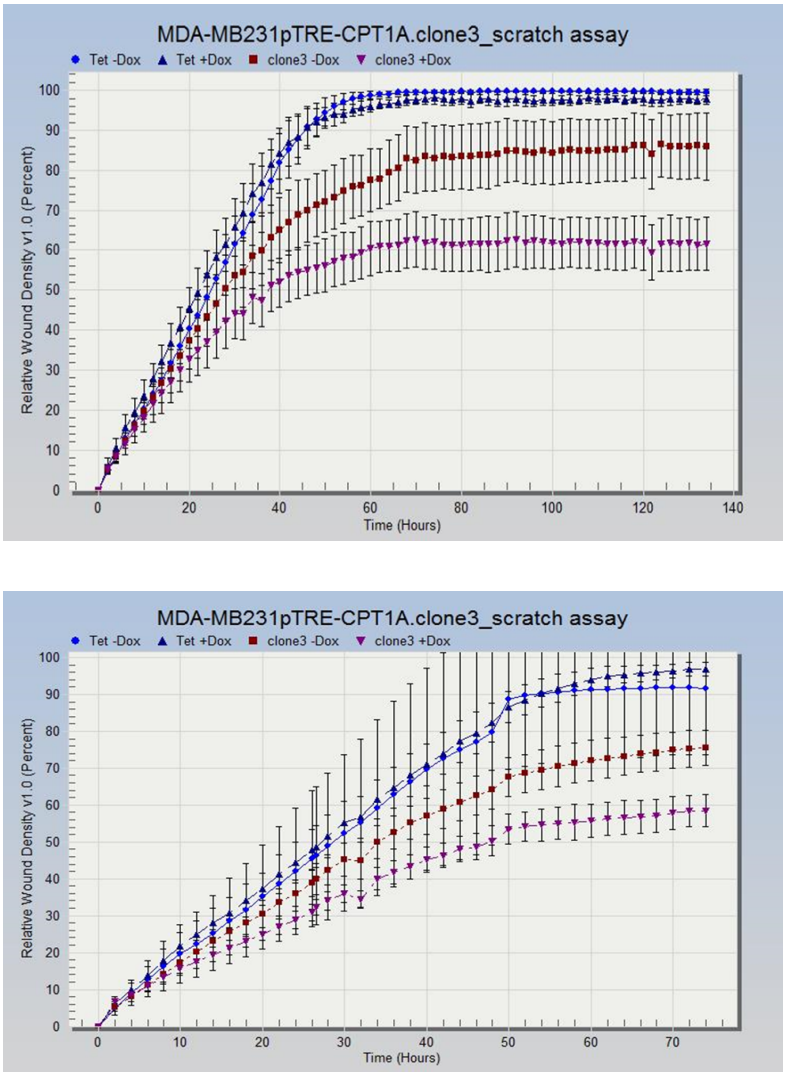

Figure A.8: Would healing rate of pTRE-CPT1A clone 3 with basal and CPT1A overexpression. Error bars = standard deviation. Blue cirles: Tet -Dox; Navy squares: Tet +Dox; Red squares: pTRE-CPT1A clone 3 -Dox; Pink triangles: pTRE-CPT1A clone 3 +Dox.

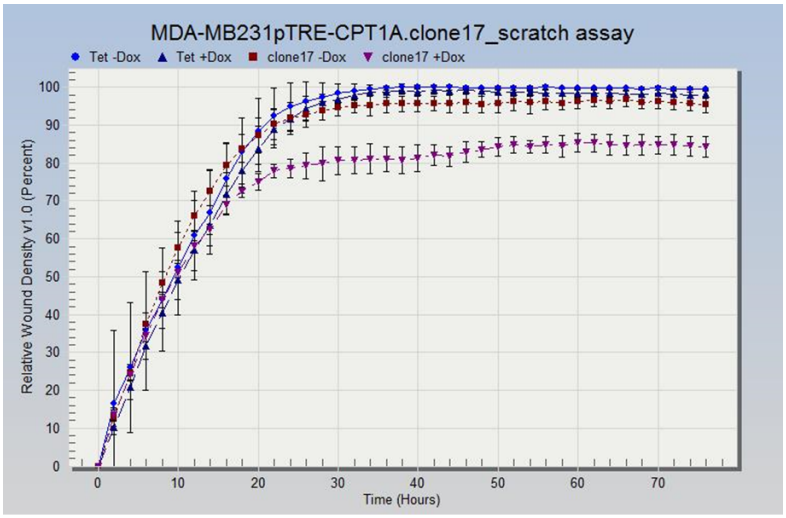

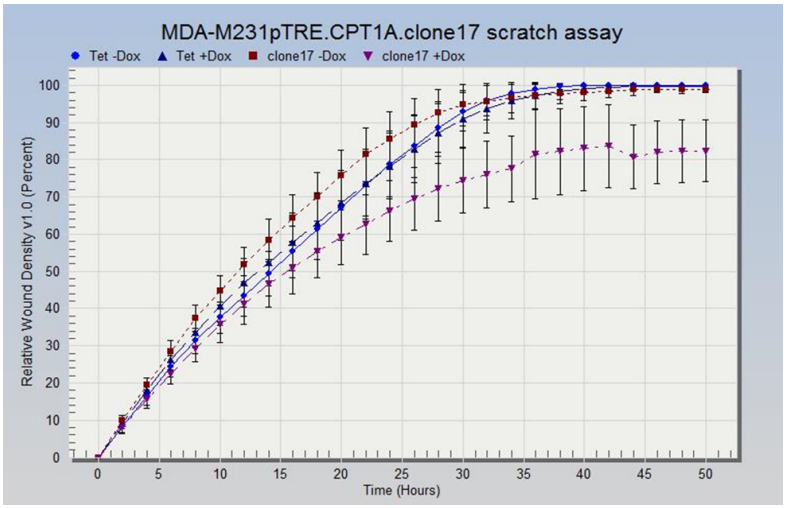

Figure A.9: Would healing rate of pTRE-CPT1A clone 17 with basal and CPT1A overexpression. Erro bars = standard deviation. Blue cirles: Tet -Dox; Navy squares: Tet +Dox; Red squares: pTRE-CPT1A clone 17 -Dox; Pink triangles: pTRE-CPT1A clone 17 +Dox.

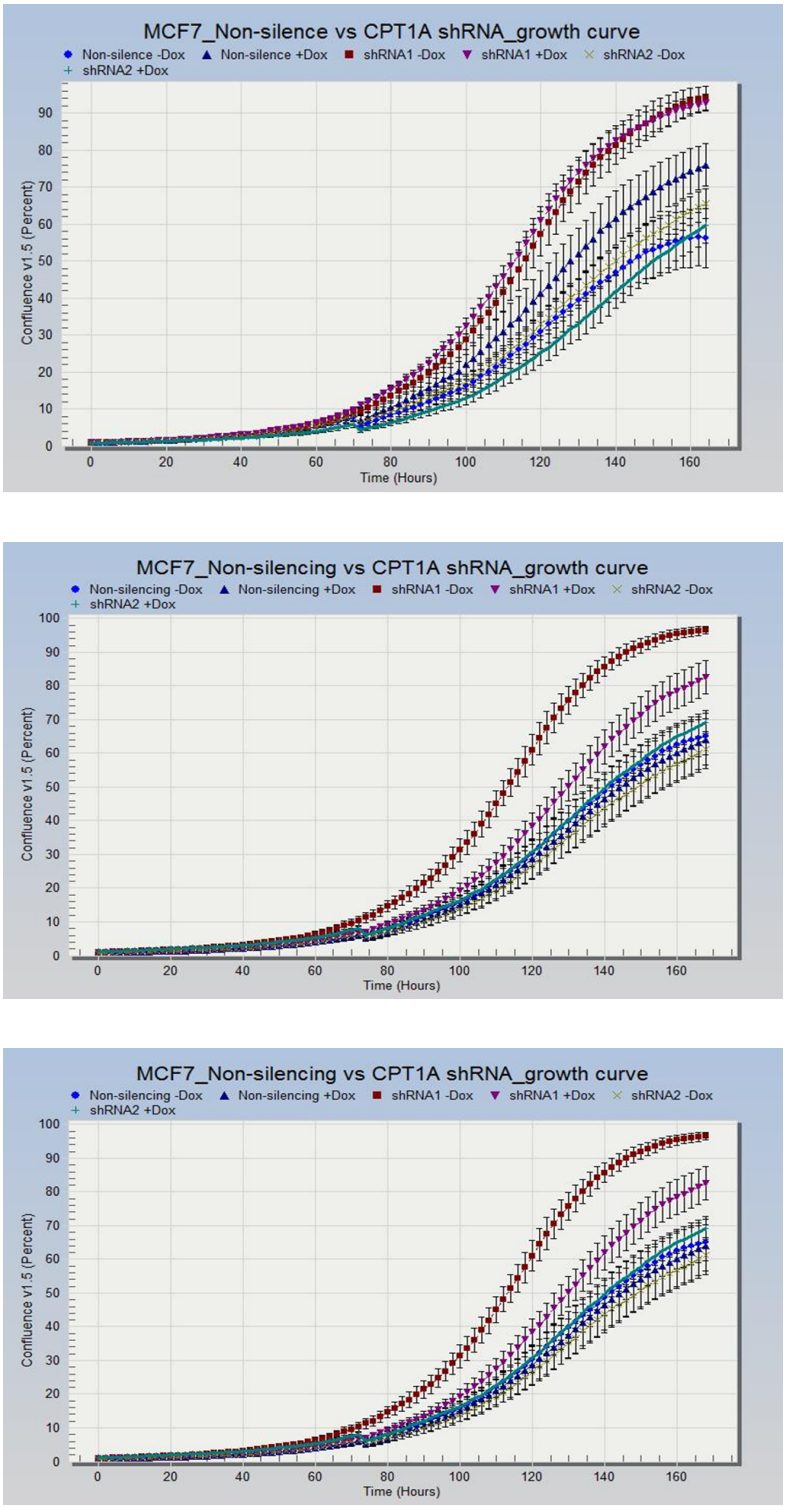

Figure A.10: Growth curves of MCF7 non-silencing, shRNA clones 1 and 2. Error bars = standard deviation. Blue cirles: Non-silencing -Dox; Navy squares: Non-silencing +Dox; Red squares: shRNA1 -Dox; Pink triangles: shRNA1 +Dox; golden crosses: shRNA2 -Dox,; green line: shRNA2 +Dox.

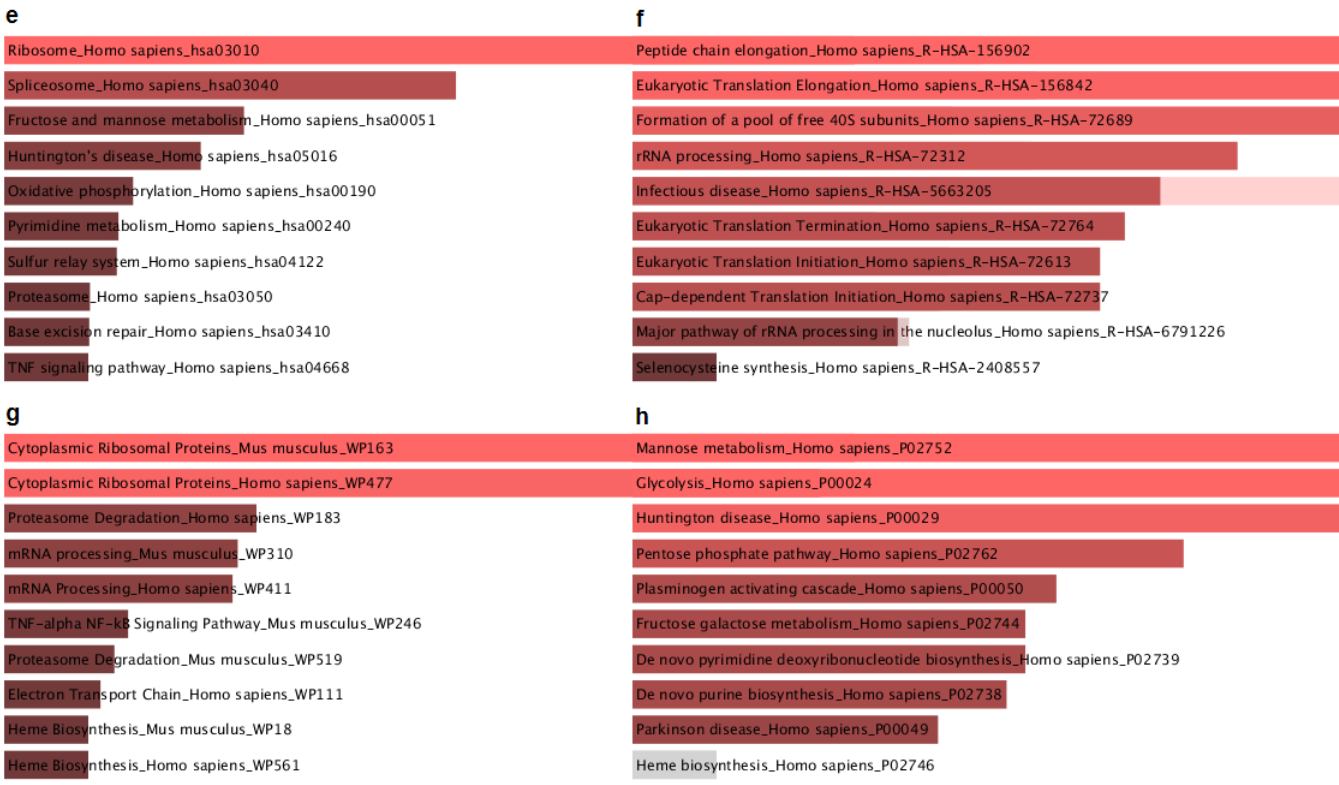

Figure A.11: Geneset enrichment analysis of TetOn cells with Dox treatment. (**a,b,c,d**) Genesets that were *downregulated* in Dox-treated TetOn cells from (a) KEGG, (b) Reactome, (c) WikiPathways and (d) Panther databases from the Enrichr analysis.

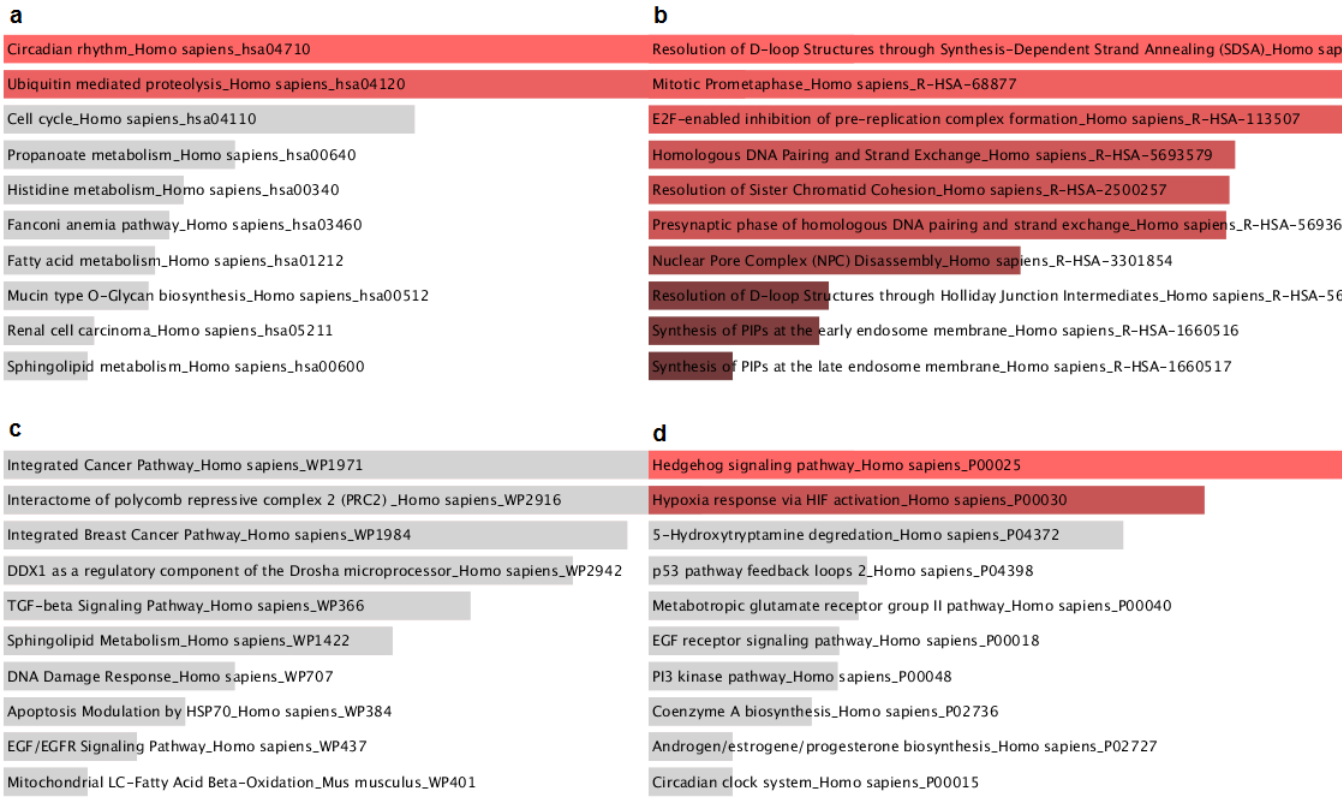

Figure A.12: Geneset enrichment analysis of TetOn cells with Dox treatment. (**a,b,c,d**) Genesets that were *upregulated* in Dox-treated TetOn cells from (a) KEGG, (b) Reactome, (c) WikiPathways and (d) Panther databases from the Enrichr analysis.

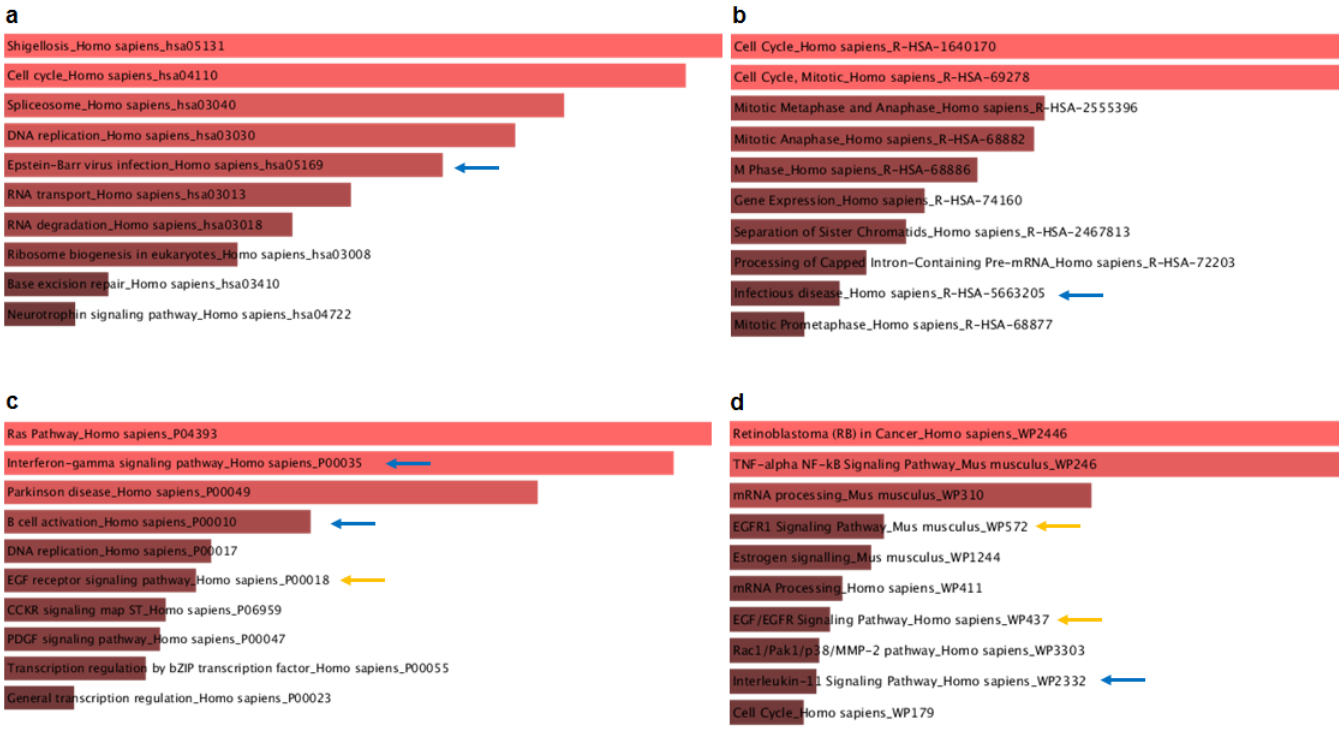

Figure A.13: Geneset enrichment analysis of PC3 cells with basal or PGC1A overexpression. (**a,b,c,d**) Genesets that were *downregulated* in PGC1A overexpressing cells from (a) KEGG, (b) Reactome, (c) WikiPathways and (d) Panther databases from the Enrichr analysis.

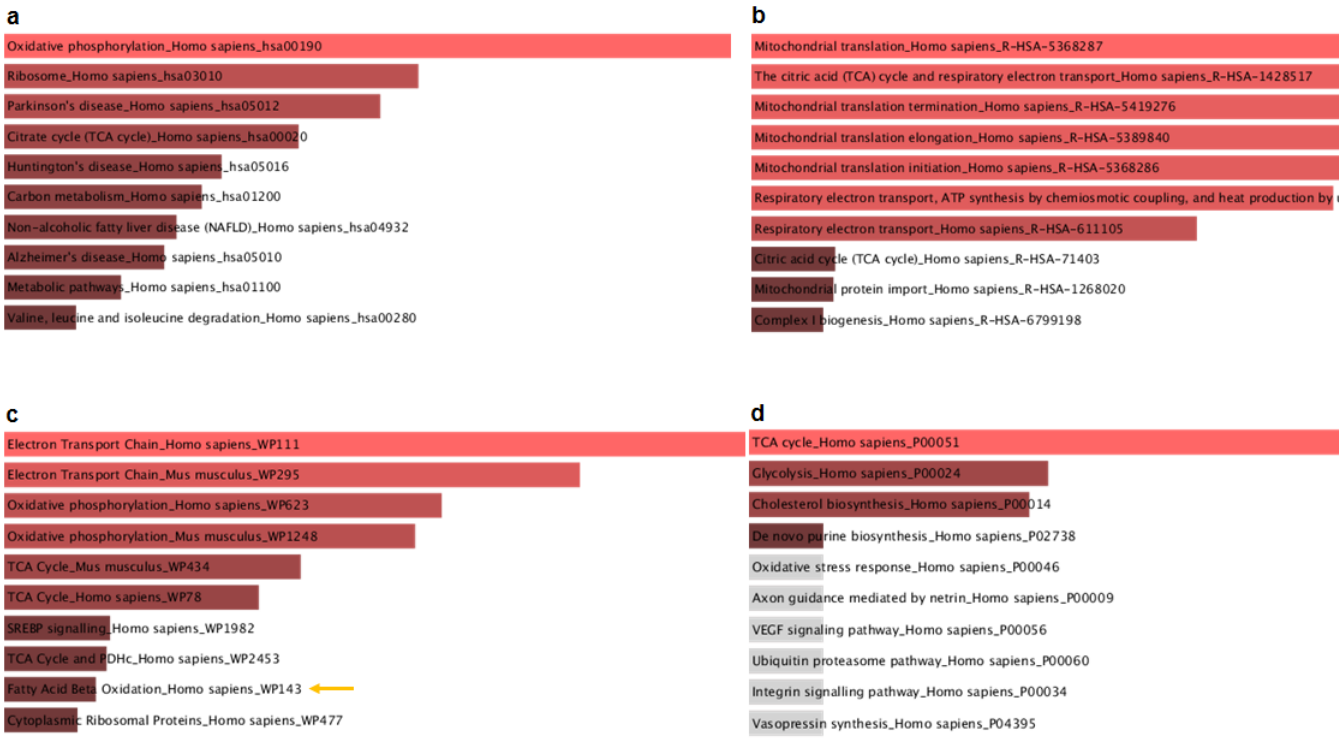

Figure A.14: Geneset enrichment analysis of PC3 cells with basal or PGC1A overexpression. (**a,b,c,d**) Genesets that were *upregulated* in PGC1A overexpressing cells from (a) KEGG, (b) Reactome, (c) WikiPathways and (d) Panther databases from the Enrichr analysis.

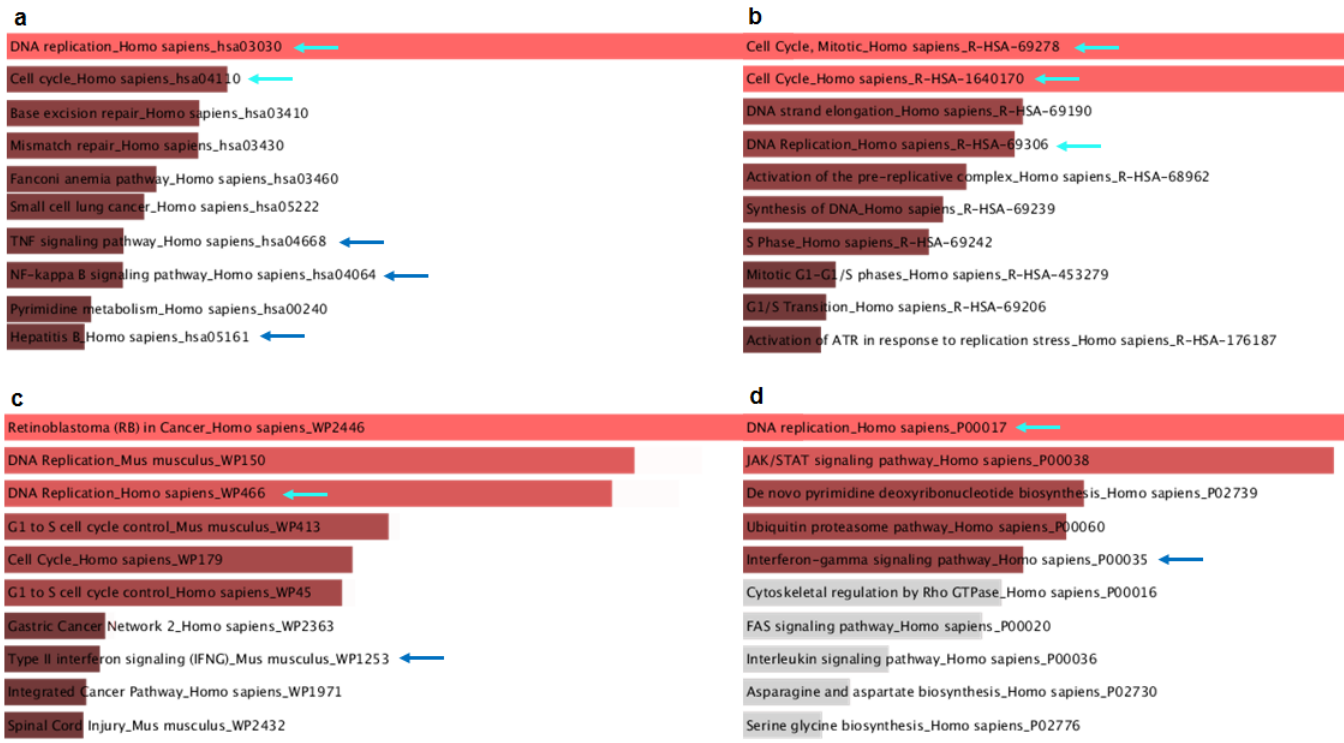

Figure A.15: Genesets enriched in NCI-H2347 cells 12 hrs after pioglitazone treatment. (**a,b,c,d**) Genesets that were *downregulated* in pioglitazone-treated cells from (a) KEGG, (b) Reactome, (c) WikiPathways and (d) Panther databases from the Enrichr analysis.

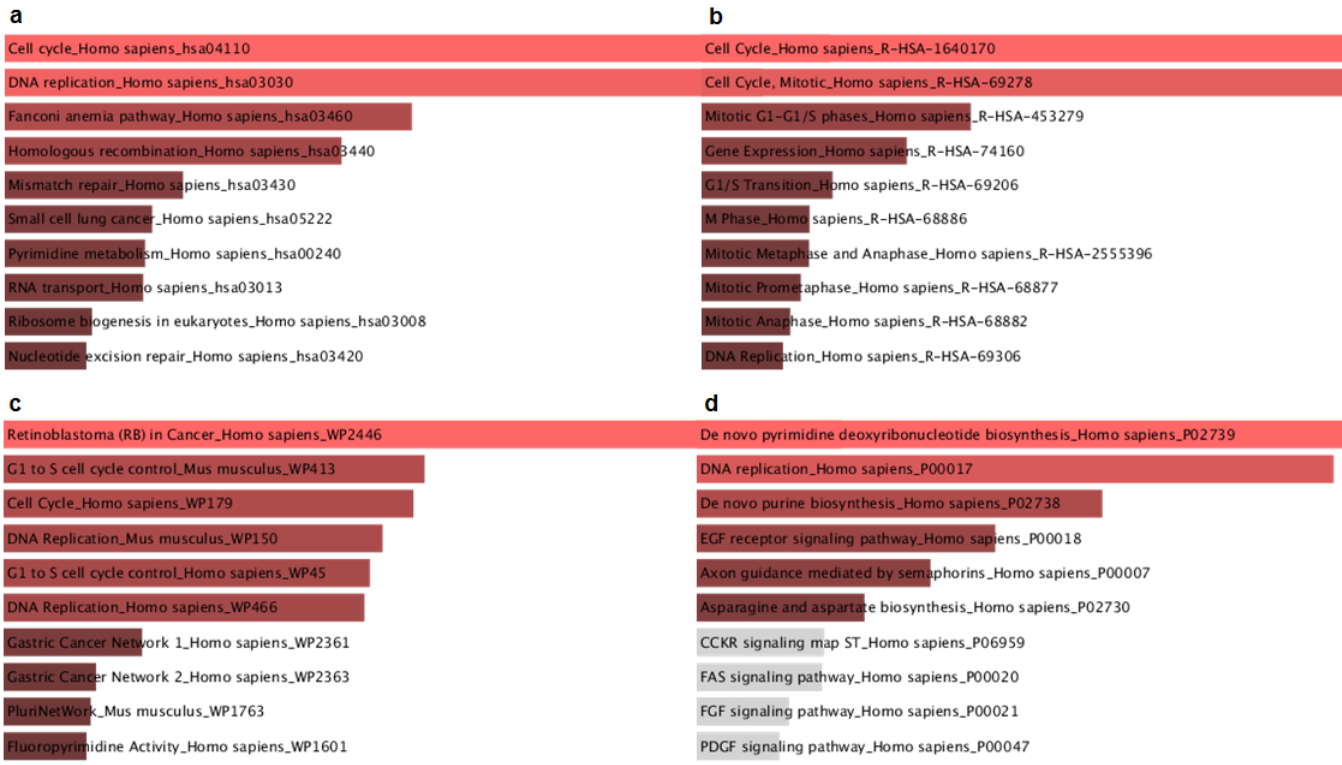

Figure A.16: Genesets enriched in NCI-H2347 cells 24 hrs after pioglitazone treatment. (**a,b,c,d**) Genesets that were *downregulated* in pioglitazone-treated cells from (a) KEGG, (b) Reactome, (c) WikiPathways and (d) Panther databases from the Enrichr analysis.

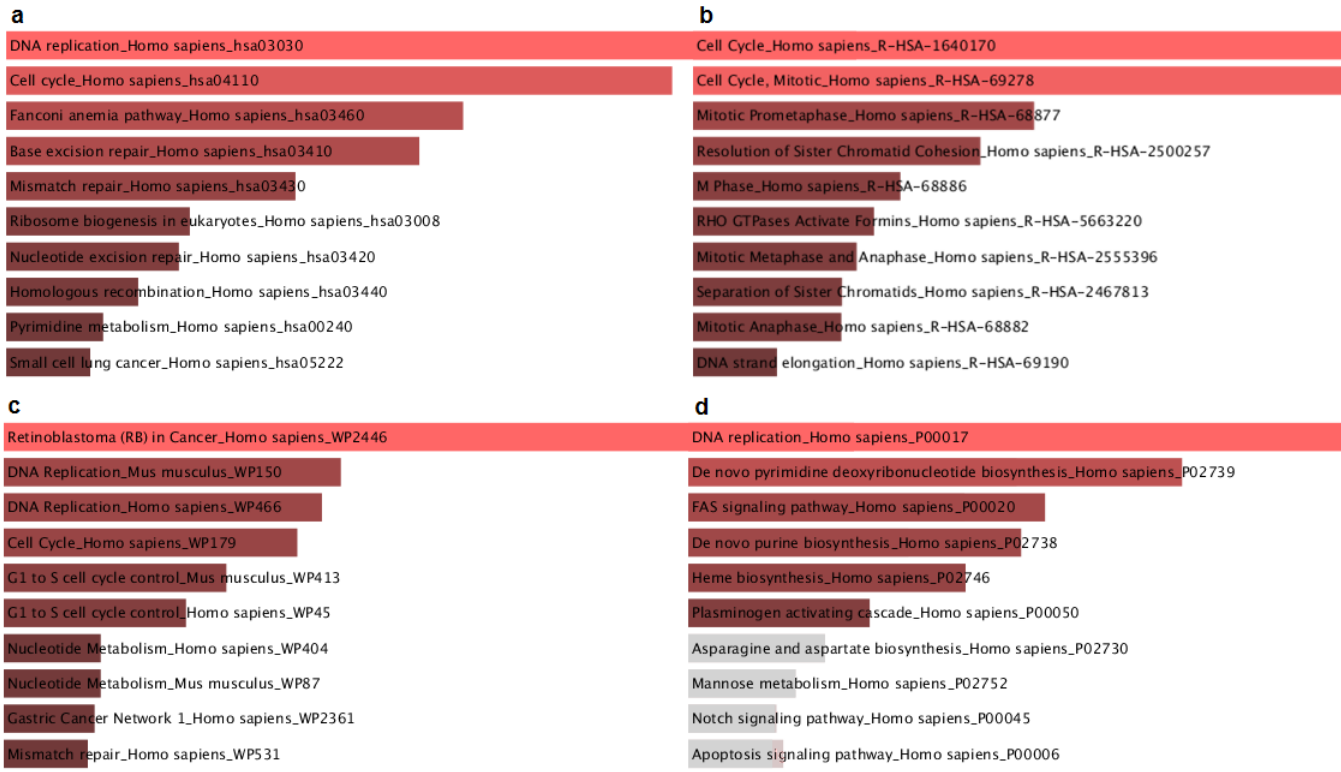

Figure A.17: Genesets enriched in NCI-H2347 cells 48 hrs after pioglitazone treatment. (**a,b,c,d**) Genesets that were *downregulated* in pioglitazone-treated cells from (a) KEGG, (b) Reactome, (c) WikiPathways and (d) Panther databases from the Enrichr analysis.

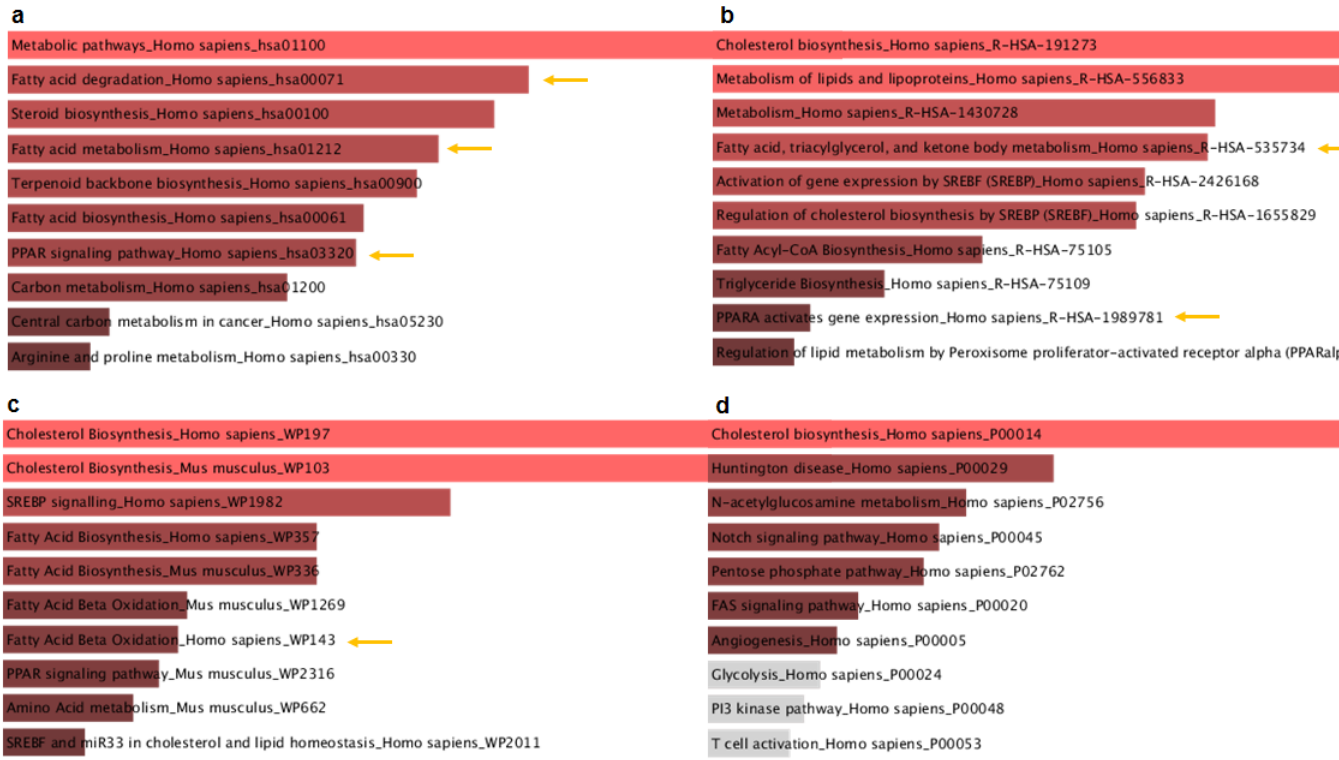

Figure A.18: Genesets enriched in NCI-H2347 cells 12 hrs after pioglitazone treatment. (**a,b,c,d**) Genesets that were *upregulated* in pioglitazone-treated cells from (a) KEGG, (b) Reactome, (c) WikiPathways and (d) Panther databases from the Enrichr analysis.

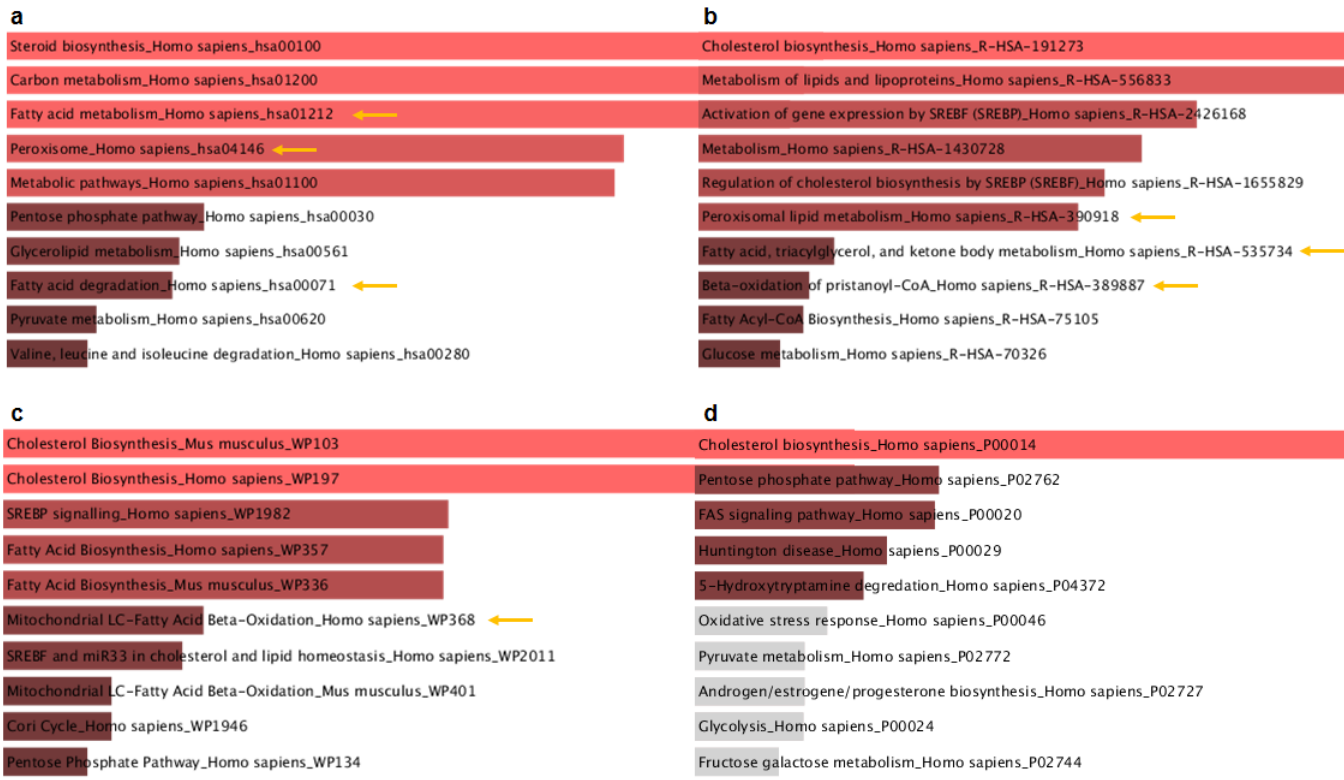

Figure A.19: Genesets enriched in NCI-H2347 cells 24 hrs after pioglitazone treatment. (**a,b,c,d**) Genesets that were *upregulated* in pioglitazone-treated cells from (a) KEGG, (b) Reactome, (c) WikiPathways and (d) Panther databases from the Enrichr analysis.

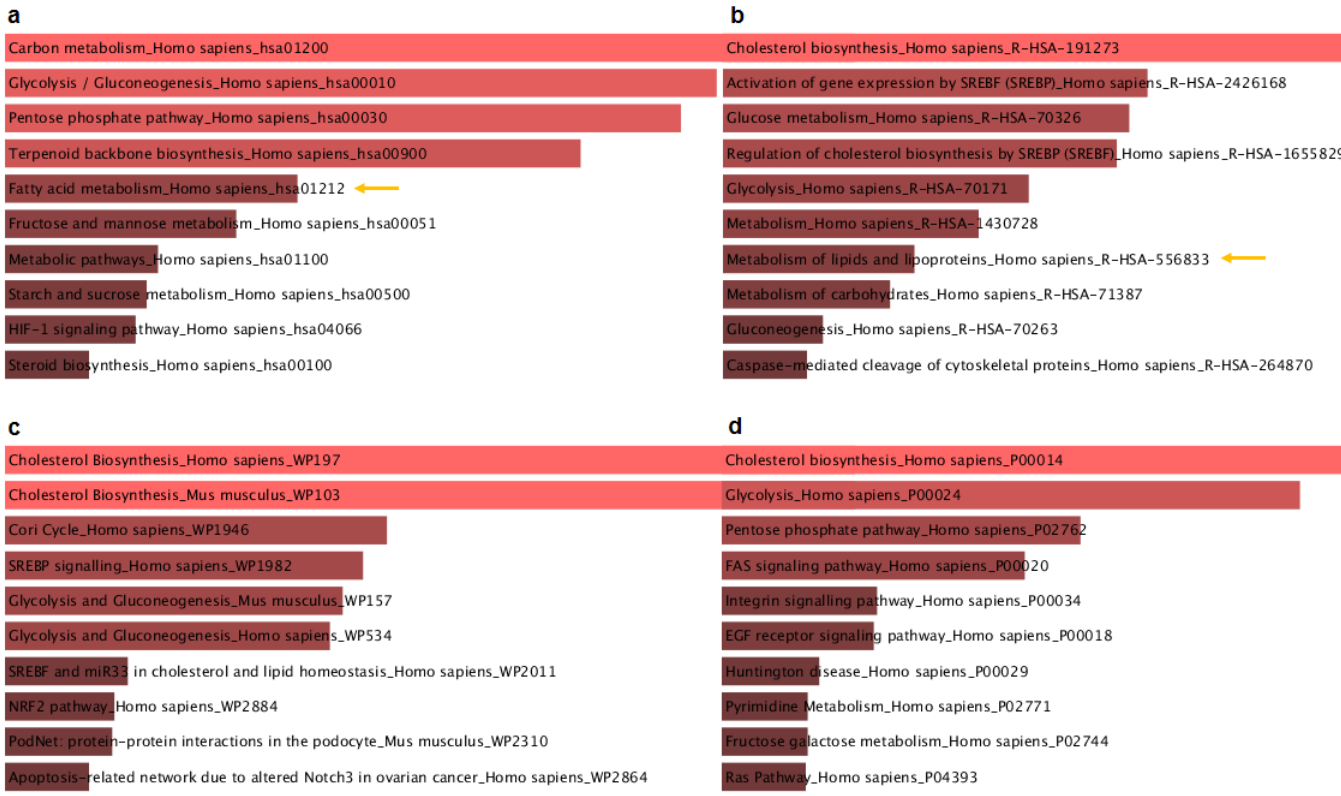

Figure A.20: Genesets enriched in NCI-H2347 cells 48 hrs after pioglitazone treatment. (**a,b,c,d**) Genesets that were *upregulated* in pioglitazone-treated cells from (a) KEGG, (b) Reactome, (c) WikiPathways and (d) Panther databases from the Enrichr analysis.

Appendix B

Supplementary Tables

Table B.1: Clinical information of METABRIC training data.

Median age at diagnosis (years)	61.84 (51.45-70.64)
Median tumour size (mm)	23 (17-30)
Lymph nodes involved	-
1-3	806
4-9	132
>9	36
NA	2
Tumour grade	-
I	99
II	439
III	397
NA	38
ER status	-
Positive	973
Treatment	-
Hormone therapy only	388
Hormone plus radiation therapy	585
PAM50 subtype	-
Luminal A	431
Luminal B	346
HER2-enriched	69
Basal-like	32
Normal	91
Not classified	4
Median Nottingham Prognostic Index	4.04 (1.02-6.03)

Table B.2: Cell lines with *CCND1* and *CPT1A* co-amplification.

Cell lines	**Tissue**
143B, G292CLONEA141B1, HOS, RDES, SJSA1	Bone
BT474, CAMA1, HCC1395, HDQP1, MDA-MB134VI, MDA-MB175VII, MDA-MB415, MDA-MB453, ZR751, EVSAT	Breast
ME1, OCIM1, REC1	Haematopoetic
HUH7, JHH5, JHH7, SNU387, SNU475, SNU878, SNU886	Liver
DMS114, EPLC272H, NCI1395, NCIH1437, NCIH1573, NCIH1975, NCIH211, NCIH23, NCIH441, HCIH838	Lung
COLO680N, KYSE140, KYSE180, KYSE510, OE19, TE11, TE15, TE8, TE9, TT	Oesphagus
COV362, JHM1, OVKATE	Ovary
YAPC	Pancreas
HS852T, MELHO, MEWO, SKMEL30, SKMEL5	Skin
HS746T, KE39, SNU668,	Stomach
CGTHW1	Thyroid

Table B.3: Upregulated KEGG genesets in pTRE-CPT1A clone 3 in response to *CPT1A* overexpression

Term	P-value	Adjusted P-value	Old P-value	Old Adjusted P-value	Z-score	Combined Score
Cell cycle_Homo sapiens_hsa04110	0.044028997	1	0.003235071	0.927158974	-1.733198335	5.412616937
DNA replication_Homo sapiens_ hsa03030	0.073517601	1	0.042440959	0.927158974	-1.935236309	5.051412699
RNA polymerase_Homo sapiens_ hsa03020	0.11023229	1	0.060979109	0.927158974	-1.746633355	3.851615457
Biosynthesis of unsaturated fatty acids_ Homo sapiens_hsa01040	0.086307178	1	0.070731211	0.927158974	-1.507461721	3.693043803
p53 signaling pathway_Homo sapiens_ hsa04115	0.126380809	1	0.025963106	0.927158974	-1.633457981	3.378735368
Nucleotide excision repair_Homo sapiens_ hsa03420	0.156176381	1	0.051438651	0.927158974	-1.662043401	3.086031098
Proteasome_Homo sapiens_ hsa03050	0.178298172	1	0.061072645	0.927158974	-1.428779059	2.463640885
Ribosome biogenesis in eukaryotes_ Homo sapiens_hsa03008	0.330687642	1	0.041842766	0.927158974	-1.614194189	1.786236664
Base excision repair_Homo sapiens_ hsa03410	0.253114053	1	0.104298692	0.927158974	-1.178095782	1.618603571
Circadian rhythm_Homo sapiens_ hsa04710	0.291313663	1	0.125216534	0.927158974	-1.185944072	1.462689708

Table B.4: Upregulated Reactome genesets in pTRE-CPT1A clone 3 in response to *CPT1A* overexpression

Term	P-value	Adjusted P-value	Old P-value	Old Adjusted P-value	Z-score	Combined Score
HIV Infection_Homo sapiens_ R-HSA-162906	0.000486535	0.369036917	4.42602E-05	0.022380906	-2.376987336	2.369520256
Host Interactions of HIV factors_ Homo sapiens_R-HSA-162909	0.000387008	0.369036917	0.00033183	0.083897787	-2.275378521	2.268230636
Cell Cycle, Mitotic_Homo sapiens_ R-HSA-69278	0.006449666	0.404969749	3.50651E-06	0.002659689	-2.323067069	2.099920003
APC/C:Cdh1 mediated degradation of Cdc20 and other APC/C:Cdh1 targeted proteins in late mitosis/early G1_Homo sapiens_R-HSA-174178	0.002399061	0.404969749	0.003776443	0.229154539	-2.248536738	2.032548838
SUMOylation of DNA replication proteins_Homo sapiens_R-HSA-4615885	0.00257268	0.404969749	0.008923074	0.317916072	-2.248491597	2.032508034
Regulation of mitotic cell cycle_ Homo sapiens_R-HSA-453276	0.003580122	0.404969749	0.003164282	0.229154539	-2.237066269	2.02218019
DNA Replication_Homo sapiens_ R-HSA-69306	0.003658523	0.404969749	0.001958131	0.198032266	-2.234778521	2.020112196
APC/C-mediated degradation of cell cycle proteins_Homo sapiens_ R-HSA-174143	0.003580122	0.404969749	0.003164282	0.229154539	-2.228739112	2.014652915
M/G1 Transition_Homo sapiens_ R-HSA-68874	0.004051093	0.404969749	0.003639741	0.229154539	-2.205359518	1.993519097
DNA Replication Pre-Initiation_ Homo sapiens_R-HSA-69002	0.004051093	0.404969749	0.003639741	0.229154539	-2.194796457	1.983970693

Table B.5: Upregulated WikiPathways genesets in pTRE-CPT1A clone 3 in response to *CPT1A* overexpression

Term	P-value	Adjusted P-value	Old P-value	Old Adjusted P-value	Z-score	Combined Score
DNA Replication_Homo sapiens_WP466	0.005222081	1	0.014265782	0.913978164	-2.185699155	3.17111E-10
DNA Replication_Mus musculus_WP150	0.010302767	1	0.020320329	0.913978164	-2.020056622	2.93078E-10
TNF-alpha NF-kB Signaling Pathway_ Mus musculus_WP246	0.221551491	1	0.012917743	0.913978164	-1.793442026	2.602E-10
Parkin-Ubiquitin Proteasomal System pathway_Homo sapiens_WP2359	0.023797604	1	0.014422241	0.913978164	-1.792263771	2.60029E-10
Cell Cycle_Homo sapiens_WP179	0.017278528	1	0.005962476	0.913978164	-1.79008958	2.59714E-10
Cholesterol Biosynthesis_ Homo sapiens_WP197	0.007516368	1	0.046654349	0.913978164	-1.762215697	2.5567E-10
Eukaryotic Transcription Initiation_ Homo sapiens_WP405	0.062249762	1	0.044378143	0.913978164	-1.74801357	2.53609E-10
G1 to S cell cycle control_ Mus musculus_WP413	0.075442072	1	0.035207801	0.913978164	-1.707844746	2.47781E-10
Proteasome Degradation_ Mus musculus_WP519	0.036126732	1	0.024911558	0.913978164	-1.703574558	2.47162E-10
Eukaryotic Transcription Initiation_ Mus musculus_WP567	0.037075337	1	0.036207816	0.913978164	-1.702185739	2.4696E-10

Table B.6: Upregulated Panther genesets in pTRE-CPT1A clone 3 in response to *CPT1A* overexpression.

Term	P-value	Adjusted P-value	Old P-value	Old Adjusted P-value	Z-score	Combined Score
Cell cycle_Homo sapiens_P00013	0.020467664	0.999895948	0.076948172	0.882298466	-1.281527657	0.000133353
Oxytocin receptor mediated signaling pathway_Homo sapiens_P04391	0.11583907	0.999895948	0.095635256	0.882298466	-1.222159907	0.000127175
5HT2 type receptor mediated signaling pathway_Homo sapiens_P04374	0.118821009	0.999895948	0.086369505	0.882298466	-1.209273718	0.000125834
Ubiquitin proteasome pathway_ Homo sapiens_P00060	0.042571799	0.999895948	0.052698239	0.882298466	-1.19612574	0.000124466
Mannose metabolism_Homo sapiens_ P02752	0.022899884	0.999895948	0.129913711	0.882298466	-0.479838756	4.9931E-05
Plasminogen activating cascade_ Homo sapiens_P00050	0.095785002	0.999895948	0.143365747	0.882298466	-0.295053675	3.07027E-05
Thyrotropin-releasing hormone receptor signaling pathway_Homo sapiens_P04394	0.303846683	0.999895948	0.170179799	0.882298466	-0.005802686	6.03815E-07
Histamine H1 receptor mediated signaling pathway_Homo sapiens_P04385	0.260284061	0.999895948	0.19124416	0.882298466	0.275258882	-2.86429E-05
p53 pathway feedback loops 2_ Homo sapiens_P04398	0.326165482	0.999895948	0.170219374	0.882298466	0.286631442	-2.98263E-05
Cortocotropin releasing factor receptor signaling pathway_Homo sapiens_P04380	0.291313663	0.999895948	0.193108418	0.882298466	0.299677459	-3.11838E-05

Table B.7: Downregulated KEGG genesets in pTRE-CPT1A clone 3 in response to *CPT1A* overexpression.

Term	P-value	Adjusted P-value	Old P-value	Old Adjusted P-value	Z-score	Combined Score
Cell cycle_Homo sapiens_ hsa04110	0.044028997	1	0.003235071	0.927158974	-1.733198335	5.412616937
DNA replication_Homo sapiens_ hsa03030	0.073517601	1	0.042440959	0.927158974	-1.935236309	5.051412699
RNA polymerase_Homo sapiens_ hsa03020	0.11023229	1	0.060979109	0.927158974	-1.746633355	3.851615457
Biosynthesis of unsaturated fatty acids_ Homo sapiens_hsa01040	0.086307178	1	0.070731211	0.927158974	-1.507461721	3.693043803
p53 signaling pathway_Homo sapiens_ hsa04115	0.126380809	1	0.025963106	0.927158974	-1.633457981	3.378735368
Nucleotide excision repair_Homo sapiens_ hsa03420	0.156176381	1	0.051438651	0.927158974	-1.662043401	3.086031098
Proteasome_Homo sapiens_hsa03050	0.178298172	1	0.061072645	0.927158974	-1.428779059	2.463640885
Ribosome biogenesis in eukaryotes_ Homo sapiens_hsa03008	0.330687642	1	0.041842766	0.927158974	-1.614194189	1.786236664
Base excision repair_Homo sapiens_ hsa03410	0.253114053	1	0.104298692	0.927158974	-1.178095782	1.618603571
Circadian rhythm_Homo sapiens_ hsa04710	0.291313663	1	0.125216534	0.927158974	-1.185944072	1.462689708

Table B.8: Downregulated Reactome genesets in pTRE-CPT1A clone 3 in response to *CPT1A* overexpression.

Term	P-value	Adjusted P-value	Old P-value	Old Adjusted P-value	Z-score	Combined Score
HIV Infection_Homo sapiens_R-HSA-162906	0.000486535	0.369036917	4.42602E-05	0.022380906	-2.376987336	2.369520256
Host Interactions of HIV factors_Homo sapiens_ R-HSA-162909	0.000387008	0.369036917	0.00033183	0.083897787	-2.275378521	2.268230636
Cell Cycle, Mitotic_Homo sapiens_R-HSA-69278	0.006449666	0.404969749	3.50651E-06	0.002659689	-2.323067069	2.099920003
APC/C:Cdh1 mediated degradation of Cdc20 and other APC/C:Cdh1 targeted proteins in late mitosis/early G1_ Homo sapiens_R-HSA-174178	0.002399061	0.404969749	0.003776443	0.229154539	-2.248536738	2.032548838
SUMOylation of DNA replication proteins_ Homo sapiens_R-HSA-4615885	0.00257268	0.404969749	0.008923074	0.317916072	-2.248491597	2.032508034
APC/C-mediated degradation of cell cycle proteins_ Homo sapiens_R-HSA-174143	0.003580122	0.404969749	0.003164282	0.229154539	-2.238062993	2.023081171
DNA Replication_Homo sapiens_R-HSA-69306	0.003658523	0.404969749	0.001958131	0.198032266	-2.234778521	2.020112196
Regulation of mitotic cell cycle_Homo sapiens_ R-HSA-453276	0.003580122	0.404969749	0.003164282	0.229154539	-2.227747576	2.013756623
DNA Replication Pre-Initiation_Homo sapiens_ R-HSA-69002	0.004051093	0.404969749	0.003639741	0.229154539	-2.204440342	1.992688214
M/G1 Transition_Homo sapiens_R-HSA-68874	0.004051093	0.404969749	0.003639741	0.229154539	-2.195702879	1.984790046

Table B.9: Downregulated WikiPathways genesets in pTRE-CPT1A clone 3 in response to *CPT1A* overexpression.

Term	P-value	Adjusted P-value	Old P-value	Old Adjusted P-value	Z-score	Combined Score
DNA Replication_Homo sapiens_WP466	0.005222081	1	0.014265782	0.913978164	-2.185699155	3.17111E-10
DNA Replication_Mus musculus_WP150	0.010302767	1	0.020320329	0.913978164	-2.020056622	2.93078E-10
TNF-alpha NF-kB Signaling Pathway_ Mus musculus_WP246	0.221551491	1	0.012917743	0.913978164	-1.793442026	2.602E-10
Parkin-Ubiquitin Proteasomal System pathway_ Homo sapiens_WP2359	0.023797604	1	0.014422241	0.913978164	-1.792263771	2.60029E-10
Cell Cycle_Homo sapiens_WP179	0.017278528	1	0.005962476	0.913978164	-1.79008958	2.59714E-10
Cholesterol Biosynthesis_Mus musculus_WP103	0.007516368	1	0.046654349	0.913978164	-1.752329034	2.54235E-10
Eukaryotic Transcription Initiation_ Homo sapiens_WP405	0.062249762	1	0.044378143	0.913978164	-1.74801357	2.53609E-10
G1 to S cell cycle control_Mus musculus_WP413	0.075442072	1	0.035207801	0.913978164	-1.707844746	2.47781E-10
Proteasome Degradation_Mus musculus_WP519	0.036126732	1	0.024911558	0.913978164	-1.703574558	2.47162E-10
Eukaryotic Transcription Initiation_ Mus musculus_WP567	0.037075337	1	0.036207816	0.913978164	-1.702185739	2.4696E-10

Table B.10: Downregulated Panther genesets in pTRE-CPT1A clone 3 in response to *CPT1A* overexpression.

Term	P-value	Adjusted P-value	Old P-value	Old Adjusted P-value	Z-score	Combined Score
Cell cycle_Homo sapiens_P00013	0.020467664	0.999895948	0.076948172	0.882298466	-1.281527657	0.000133353
Oxytocin receptor mediated signaling pathway_ Homo sapiens_P04391	0.11583907	0.999895948	0.095635256	0.882298466	-1.222159907	0.000127175
5HT2 type receptor mediated signaling pathway_ Homo sapiens_P04374	0.118821009	0.999895948	0.086369505	0.882298466	-1.209273718	0.000125834
Ubiquitin proteasome pathway_Homo sapiens_ P00060	0.042571799	0.999895948	0.052698239	0.882298466	-1.19612574	0.000124466
Mannose metabolism_Homo sapiens_P02752	0.022899884	0.999895948	0.129913711	0.882298466	-0.479838756	4.9931E-05
Plasminogen activating cascade_Homo sapiens_P00050	0.095785002	0.999895948	0.143365747	0.882298466	-0.295053675	3.07027E-05
Thyrotropin-releasing hormone receptor signaling pathway_Homo sapiens_P04394	0.303846683	0.999895948	0.170179799	0.882298466	-0.005802686	6.03815E-07
Histamine H1 receptor mediated signaling pathway_ Homo sapiens_P04385	0.260284061	0.999895948	0.19124416	0.882298466	0.275258882	-2.86429E-05
p53 pathway feedback loops 2_Homo sapiens_P04398	0.326165482	0.999895948	0.170219374	0.882298466	0.286631442	-2.98263E-05
Cortocotropin releasing factor receptor signaling pathway_Homo sapiens_P04380	0.291313663	0.999895948	0.193108418	0.882298466	0.299677459	-3.11838E-05

Table B.11: Upregulated KEGG genesets in combined pTRE-CPT1A clones 3 and 17 in response to *CPT1A* overexpression.

Term	Overlap	P-value	Adjusted P-value	Old P-value	Old Adjusted P-value	Z-score	Combined Score
Ribosome_Homo sapiens_hsa03010	89/137	0.000649568	0.190323372	0.000514486	0.15074431	-1.746138049	2.89689662
Base excision repair_Homo sapiens_hsa03410	25/33	0.003215776	0.471111128	0.015799542	0.679562894	-1.626543214	1.224236085
Spliceosome_Homo sapiens_hsa03040	83/134	0.006878816	0.671831062	0.002124723	0.311271983	-1.747319798	0.694993593
RNA polymerase_Homo sapiens_hsa03020	23/32	0.01343285	0.983956234	0.029471814	0.679562894	-1.746633355	0.028249804
Legionellosis_Homo sapiens_hsa05134	34/55	0.07020851	1	0.039922133	0.679562894	-1.709516338	4.93928E-10
Epstein-Barr virus infection_ Homo sapiens_hsa05169	112/202	0.115620096	1	0.006221447	0.541036272	-1.701033337	4.91477E-10
Huntington's disease_ Homo sapiens_ hsa05016	107/193	0.121965076	1	0.007386161	0.541036272	-1.628205797	4.70435E-10
Pyrimidine metabolism_Homo sapiens_ hsa00240	61/105	0.086954367	1	0.019431436	0.679562894	-1.571024109	4.53914E-10
Neurotrophin signaling pathway_ Homo sapiens_hsa04722	66/120	0.216241679	1	0.03374291	0.679562894	-1.539869748	4.44913E-10
Non-small cell lung cancer_ Homo sapiens_hsa05223	32/56	0.216318549	1	0.084558063	0.72160196	-1.513766213	4.3737E-10

Table B.12: Upregulated Reactome genesets in combined pTRE-CPT1A clones 3 and 17 in response to *CPT1A* overexpression.

Term	Overlap	P-value	Adjusted P-value	Old P-value	Old Adjusted P-value	Z-score
Mitochondrial translation elongation_ Homo sapiens_R-HSA-5389840	62/84	1.58985E-05	0.02149842	0.000540715	0.11093287	-2.079555632
Mitochondrial translation termination_ Homo sapiens_R-HSA-5419276	61/84	4.27121E-05	0.02149842	0.000796536	0.11093287	-2.073160826
Mitochondrial translation initiation_ Homo sapiens_R-HSA-5368286	61/84	4.27121E-05	0.02149842	0.000796536	0.11093287	-2.045413922
Mitochondrial translation_ Homo sapiens_R-HSA-5368287	64/90	8.03486E-05	0.030331602	0.000881586	0.11093287	-2.083609973
rRNA processing_Homo sapiens_ R-HSA-72312	116/180	0.000177018	0.039929015	0.000190545	0.095907895	-1.996434028
Eukaryotic Translation Initiation_ Homo sapiens_R-HSA-72613	77/114	0.00024792	0.039929015	0.000832051	0.11093287	-1.93903209
Eukaryotic Translation Elongation_ Homo sapiens_R-HSA-156842	62/89	0.000264431	0.039929015	0.001503239	0.118327548	-1.937632272
Major pathway of rRNA processing in the nucleolus_Homo sapiens_R-HSA-6791226	107/166	0.000305804	0.041978491	0.000329529	0.11093287	-1.966950476
Cap-dependent Translation Initiation_ Homo sapiens_R-HSA-72737	77/114	0.00024792	0.039929015	0.000832051	0.11093287	-1.931661151
Selenocysteine synthesis_Homo sapiens_ R-HSA-2408557	61/87	0.000222583	0.039929015	0.001463194	0.118327548	-1.896405961

Table B.13: Upregulated WikiPathways genesets in combined pTRE-CPT1A clones 3 and 17 in response to *CPT1A* overexpression.

Term	Overlap	P-value	Adjusted P-value	Old P-value	Old Adjusted P-value	Z-score
Mitochondrial translation elongation_ Homo sapiens_R-HSA-5389840	62/84	1.58985E-05	0.02149842	0.000540715	0.11093287	-2.079555632
Mitochondrial translation termination_ Homo sapiens_R-HSA-5419276	61/84	4.27121E-05	0.02149842	0.000796536	0.11093287	-2.073160826
Mitochondrial translation initiation_ Homo sapiens_R-HSA-5368286	61/84	4.27121E-05	0.02149842	0.000796536	0.11093287	-2.045413922
Mitochondrial translation_ Homo sapiens_R-HSA-5368287	64/90	8.03486E-05	0.030331602	0.000881586	0.11093287	-2.083609973
rRNA processing_Homo sapiens_ R-HSA-72312	116/180	0.000177018	0.039929015	0.000190545	0.095907895	-1.996434028
Eukaryotic Translation Initiation_ Homo sapiens_R-HSA-72613	77/114	0.00024792	0.039929015	0.000832051	0.11093287	-1.93903209
Eukaryotic Translation Elongation_ Homo sapiens_R-HSA-156842	62/89	0.000264431	0.039929015	0.001503239	0.118327548	-1.937632272
Major pathway of rRNA processing in the nucleolus_Homo sapiens_R-HSA-6791226	107/166	0.000305804	0.041978491	0.000329529	0.11093287	-1.966950476
Cap-dependent Translation Initiation_ Homo sapiens_R-HSA-72737	77/114	0.00024792	0.039929015	0.000832051	0.11093287	-1.931661151
Selenocysteine synthesis_Homo sapiens_ R-HSA-2408557	61/87	0.000222583	0.039929015	0.001463194	0.118327548	-1.896405961

Table B.14: Upregulated Panther genesets in combined pTRE-CPT1A clones 3 and 17 in response to *CPT1A* overexpression.

Term	Overlap	P-value	Adjusted P-value	Old P-value	Old Adjusted P-value	Z-score	Combined Score
Glycolysis_Homo sapiens_P00024	14/17	0.007965496	0.876204516	0.065198289	0.901647286	-1.291884483	0.170729962
Mannose metabolism_Homo sapiens_P02752	6/6	0.017604311	0.968237109	0.131498607	0.901647286	-0.479838756	0.015488367
Huntington disease_Homo sapiens_P00029	69/124	0.172205038	0.998686368	0.076022202	0.901647286	-0.977492555	0.00128491
Axon guidance mediated by semaphorins_ Homo sapiens_P00007	12/17	0.083793761	0.998686368	0.151495636	0.901647286	-0.411028002	0.000540295
Salvage pyrimidine ribonucleotides_ Homo sapiens_P02775	8/10	0.062108649	0.998686368	0.15931664	0.901647286	-0.385744902	0.00050706
Ras Pathway_Homo sapiens_P04393	38/69	0.289599375	0.998686368	0.169485459	0.901647286	-0.328050215	0.000431221
Pentose phosphate pathway_ Homo sapiens_P02762	7/8	0.039774248	0.998686368	0.147449453	0.901647286	-0.009071811	1.19249E-05
Integrin signalling pathway_ Homo sapiens_P00034	82/156	0.378740481	0.998686368	0.119852308	0.901647286	0.129320763	-0.000169992
Nicotine pharmacodynamics pathway_ Homo sapiens_P06587	17/28	0.201149592	0.998686368	0.196202219	0.901647286	0.16834715	-0.000221292
p38 MAPK pathway_ Homo sapiens_P05918	19/32	0.220950709	0.998686368	0.197741402	0.901647286	0.173593209	-0.000228188

Table B.15: Downregulated KEGG genesets in combined pTRE-CPT1A clones 3 and 17 in response to *CPT1A* overexpression.

Term	Overlap	P-value	Adjusted P-value	Old P-value	Old Adjusted P-value	Z-score	Combined Score
Ribosome_Homo sapiens_ hsa03010	89/137	0.000649568	0.190323372	0.000514486	0.15074431	-1.746138049	2.89689662
Base excision repair_Homo sapiens_ hsa03410	25/33	0.003215776	0.471111128	0.015799542	0.679562894	-1.626543214	1.224236085
Spliceosome_Homo sapiens_ hsa03040	83/134	0.006878816	0.671831062	0.002124723	0.311271983	-1.747319798	0.694993593
RNA polymerase_Homo sapiens_ hsa03020	23/32	0.01343285	0.983956234	0.029471814	0.679562894	-1.746633355	0.028249804
Legionellosis_Homo sapiens_ hsa05134	34/55	0.07020851	1	0.039922133	0.679562894	-1.709516338	4.93928E-10
Epstein-Barr virus infection_ Homo sapiens_hsa05169	112/202	0.115620096	1	0.006221447	0.541036272	-1.701033337	4.91477E-10
Huntington's disease_Homo sapiens_ hsa05016	107/193	0.121965076	1	0.007386161	0.541036272	-1.628205797	4.70435E-10
Pyrimidine metabolism_Homo sapiens_ hsa00240	61/105	0.086954367	1	0.019431436	0.679562894	-1.571024109	4.53914E-10
Neurotrophin signaling pathway_ Homo sapiens_hsa04722	66/120	0.216241679	1	0.03374291	0.679562894	-1.539869748	4.44913E-10
Non-small cell lung cancer_ Homo sapiens_hsa05223	32/56	0.216318549	1	0.084558063	0.72160196	-1.513766213	4.3737E-10

Table B.16: Downregulated Reactome genesets in combined pTRE-CPT1A clones 3 and 17 in response to *CPT1A* overexpression.

Term	Overlap	P-value	Adjusted P-value	Old P-value	Old Adjusted P-value	Z-score	Combined Score
Mitochondrial translation termination_ Homo sapiens_R-HSA-5419276	61/84	4.27121E-05	0.02149842	0.000796536	0.11093287	-2.082500048	7.996333396
Mitochondrial translation elongation_ Homo sapiens_R-HSA-5389840	62/84	1.58985E-05	0.02149842	0.000540715	0.11093287	-2.079555632	7.985027497
Mitochondrial translation initiation_ Homo sapiens_R-HSA-5368286	61/84	4.27121E-05	0.02149842	0.000796536	0.11093287	-2.036255914	7.818766286
Mitochondrial translation_Homo sapiens_ R-HSA-5368287	64/90	8.03486E-05	0.030331602	0.000881586	0.11093287	-2.083609973	7.28339438
rRNA processing_Homo sapiens_R-HSA-72312	116/180	0.000177018	0.039929015	0.000190545	0.095907895	-1.996434028	6.429819304
Eukaryotic Translation Initiation_ Homo sapiens_R-HSA-72613	77/114	0.00024792	0.039929015	0.000832051	0.11093287	-1.93903209	6.244947635
Eukaryotic Translation Elongation_ Homo sapiens_R-HSA-156842	62/89	0.000264431	0.039929015	0.001503239	0.118327548	-1.937632272	6.240439307
Major pathway of rRNA processing in the nucleolus_ Homo sapiens_R-HSA-6791226	107/166	0.000305804	0.041978491	0.000329529	0.11093287	-1.966950476	6.236409091
Cap-dependent Translation Initiation_Homo sapiens_ R-HSA-72737	77/114	0.00024792	0.039929015	0.000832051	0.11093287	-1.931661151	6.221208406
Selenocysteine synthesis_Homo sapiens_ R-HSA-2408557	61/87	0.000222583	0.039929015	0.001463194	0.118327548	-1.896405961	6.107663706

Table B.17: Downregulated WikiPathways genesets in combined pTRE-CPT1A clones 3 and 17 in response to *CPT1A* overexpression.

Term	Overlap	P-value	Adjusted P-value	Old P-value	Old Adjusted P-value	Z-score	Combined Score
Cytoplasmic Ribosomal Proteins_ Mus musculus_WP163	50/70	0.000399101	0.173608941	0.004502397	0.821667801	-2.034709977	3.562675385
Cytoplasmic Ribosomal Proteins_ Homo sapiens_WP477	60/89	0.001240039	0.269708474	0.0049864	0.821667801	-1.982224342	2.597533795
TNF-alpha NF-kB Signaling Pathway_ Mus musculus_WP246	102/179	0.062714727	1	0.013923321	0.881128797	-2.147111963	6.6542E-10
Translation Factors_Mus musculus _WP307	30/46	0.03660629	1	0.050987836	0.881128797	-1.918584981	5.94597E-10
TOR Signaling_Homo sapiens _WP1471	24/36	0.04234669	1	0.065278922	0.881128797	-1.917167782	5.94157E-10
mRNA Processing_Homo sapiens _WP411	74/127	0.060022229	1	0.023370443	0.881128797	-1.861148938	5.76796E-10
Apoptosis-related network due to altered Notch3 in ovarian cancer_ Homo sapiens_WP2864	33/53	0.065812912	1	0.061880935	0.881128797	-1.793382185	5.55794E-10
MicroRNAs in Cardiomyocyte Hypertrophy_Mus musculus_WP1560	47/79	0.080643871	1	0.04927221	0.881128797	-1.713925724	5.3117E-10
Differentiation Pathway_Homo sapiens_WP2848	30/48	0.073023164	1	0.070507674	0.881128797	-1.650855231	5.11623E-10
Cytokines and Inflammatory Response (BioCarta)_Mus musculus_WP222	17/25	0.065748844	1	0.099304487	0.881128797	-1.643670211	5.09397E-10

Table B.18: Downregulated Panther genesets in combined pTRE-CPT1A clones 3 and 17 in response to *CPT1A* overexpression.

Term	Overlap	P-value	Adjusted P-value	Old P-value	Old Adjusted P-value	Z-score	Combined Score
Glycolysis_Homo sapiens_P00024	14/17	0.007965496	0.876204516	0.065198289	0.901647286	-1.291884483	0.170729962
Mannose metabolism_Homo sapiens_P02752	6/6	0.017604311	0.968237109	0.131498607	0.901647286	-0.479838756	0.015488367
Huntington disease_Homo sapiens_P00029	6/6	0.172205038	0.998686368	0.076022202	0.901647286	-0.977492555	0.00128491
Axon guidance mediated by semaphorins_ Homo sapiens_P00007	12/17	0.083793761	0.998686368	0.151495636	0.901647286	-0.411028002	0.000540295
Salvage pyrimidine ribonucleotides_ Homo sapiens_P02775	8/10	0.062108649	0.998686368	0.15931664	0.901647286	-0.385744902	0.00050706
Ras Pathway_Homo sapiens_P04393	38/69	0.289599375	0.998686368	0.169485459	0.901647286	-0.328050215	0.000431221
Pentose phosphate pathway_ Homo sapiens_P02762	7/8	0.039774248	0.998686368	0.147449453	0.901647286	-0.009071811	1.19249E-05
Integrin signalling pathway_ Homo sapiens_P00034	82/156	0.378740481	0.998686368	0.119852308	0.901647286	0.129320763	-0.000169992
Nicotine pharmacodynamics pathway_ Homo sapiens_P06587	17/28	0.201149592	0.998686368	0.196202219	0.901647286	0.16834715	-0.000221292
p38 MAPK pathway_ Homo sapiens_P05918	19/32	0.220950709	0.998686368	0.197741402	0.901647286	0.173593209	-0.000228188

Table B.19: Upregulated KEGG genesets in TetOn parental cells in response to Dox treatment.

Term	Overlap	P-value	Adjusted P-value	Old P-value	Old Adjusted P-value	Z-score	Combined Score
Circadian rhythm_Homo sapiens_ hsa04710	22/30	0.032270794	1	0.02778209	0.738789204	-1.972723766	6.82952E-11
Cell cycle_Homo sapiens_hsa04110	76/124	0.098320076	1	0.003619894	0.530314447	-1.682638698	5.82525E-11
Propanoate metabolism_Homo sapiens_ hsa00640	21/32	0.155124276	1	0.06332509	0.738789204	-1.637436576	5.66876E-11
Renal cell carcinoma_Homo sapiens_ hsa05211	40/66	0.22166039	1	0.032469873	0.738789204	-1.632964146	5.65328E-11
Ubiquitin mediated proteolysis_ Homo sapiens_hsa04120	86/137	0.042532691	1	0.001239755	0.363248099	-1.62124378	5.61271E-11
Fatty acid metabolism_Homo sapiens_ hsa01212	30/48	0.18988777	1	0.045639782	0.738789204	-1.596357117	5.52655E-11
Histidine metabolism_Homo sapiens_ hsa00340	16/24	0.1766657	1	0.090017508	0.738789204	-1.584602029	5.48585E-11
Fanconi anemia pathway_Homo sapiens_ hsa03460	33/53	0.183179506	1	0.038648303	0.738789204	-1.575371809	5.4539E-11
Sphingolipid metabolism_Homo sapiens_ hsa00600	29/47	0.225232391	1	0.053897066	0.738789204	-1.524343129	5.27724E-11
Valine, leucine and isoleucine egradation_Homo sapiens_hsa00280	29/48	0.279179444	1	0.063216129	0.738789204	-1.425205952	4.93403E-11

Table B.20: Upregulated Reactome genesets in TetOn parental cells in response to Dox treatment.

Term	Overlap	P-value	Adjusted P-value	Old P-value	Old Adjusted P-value	Z-score	Combined Score
Resolution of D-loop Structures through Synthesis-Dependent Strand Annealing (SDSA)_Homo sapiens_R-HSA-5693554	22/26	0.001549312	1	0.016869381	1	-2.121040787	13.72301632
E2F-enabled inhibition of pre-replication complex formation_Homo sapiens_R-HSA-113507	10-Oct	0.002598126	1	0.051521677	1	-2.15552297	12.8317528
Mitotic Prometaphase_Homo sapiens_R-HSA-68877	74/107	0.002089202	1	0.001567034	0.512216497	-2.040727035	12.59327132
Homologous DNA Pairing and Strand Exchange_Homo sapiens_R-HSA-5693579	32/42	0.003966061	1	0.012606959	1	-2.110628714	11.67173851
Presynaptic phase of homologous DNA pairing and strand exchange_Homo sapiens_R-HSA-5693616	30/39	0.004093873	1	0.014132866	1	-2.061851432	11.33660329
Resolution of Sister Chromatid Cohesion_Homo sapiens_R-HSA-2500257	68/99	0.004047488	1	0.00266868	0.673397014	-2.055766103	11.32657006
Nuclear Pore Complex (NPC) Disassembly_Homo sapiens_R-HSA-3301854	26/34	0.008520672	1	0.022415359	1	-2.131943316	10.15926432
Resolution of D-loop Structures through Holliday Junction Intermediates_Homo sapiens_R-HSA-5693568	24/32	0.016861236	1	0.031711902	1	-2.007564692	8.196360665
Synthesis of PIPs at the early endosome membrane_Homo sapiens_R-HSA-1660516	Dec-14	0.017443534	1	0.065134982	1	-1.794672654	7.266245924
Sphingolipid de novo biosynthesis_Homo sapiens_R-HSA-1660661	24/33	0.029735483	1	0.039411741	1	-2.011389469	7.070867154

Table B.21: Upregulated WikiPathways genesets in TetOn parental cells in response to Dox treatment.

Term	Overlap	P-value	Adjusted P-value	Old P-value	Old Adjusted P-value	Z-score	Combined Score
Integrated Breast Cancer Pathway_ Homo sapiens_WP1984	94/155	0.096407157	1	0.003626549	0.953513783	-2.127329909	4.15732E-10
Integrated Cancer Pathway_ Homo sapiens_WP1971	32/48	0.070814326	1	0.031532034	0.953513783	-2.009492422	3.92704E-10
Interactome of polycomb repressive complex 2 (PRC2) _Homo sapiens_WP2916	Dec-16	0.087109788	1	0.097098961	0.953513783	-1.952583354	3.81582E-10
TGF-beta Signaling Pathway_ Homo sapiens_WP366	80/132	0.11934912	1	0.006995534	0.953513783	-1.906446959	3.72566E-10
EGF/EGFR Signaling Pathway_ Homo sapiens_WP437	96/163	0.187874277	1	0.006093841	0.953513783	-1.87418167	3.66261E-10
DNA Damage Response_Homo sapiens_WP707	42/68	0.16447303	1	0.034736318	0.953513783	-1.870598454	3.6556E-10
Retinoblastoma (RB) in Cancer_ Homo sapiens_WP2446	54/90	0.20622926	1	0.026683119	0.953513783	-1.646304923	3.21728E-10
miRNA regulation of DNA Damage Response_Mus musculus _WP2087	39/64	0.210506177	1	0.046288023	0.953513783	-1.611742187	3.14974E-10
Signaling Pathways in Glioblastoma_ Homo sapiens_WP2261	48/83	0.352700157	1	0.052068364	0.953513783	-1.51338035	2.95751E-10
EGFR1 Signaling Pathway_ Mus musculus_WP572	97/171	0.368334943	1	0.01231713	0.953513783	-1.447872511	2.83E-10

Table B.22: Upregulated Panther genesets in TetOn parental cells in response to Dox treatment.

Term	Overlap	P-value	Adjusted P-value	Old P-value	Old Adjusted P-value	Z-score	Combined Score
Hypoxia response via HIF activation_ Homo sapiens_P00030	18/24	0.03751418	0.999921119	0.07386194	0.825188466	-1.475088254	0.000116361
p53 pathway feedback loops 2_ Homo sapiens_P04398	29/45	0.134231595	0.999921119	0.08801102	0.825188466	-1.292571313	0.000101964
EGF receptor signaling pathway_ Homo sapiens_P00018	66/109	0.149039656	0.999921119	0.036149254	0.825188466	-1.27730461	0.000100759
Hedgehog signaling pathway_Homo sapiens_P00025	15/18	0.012347547	0.999921119	0.06001324	0.825188466	-1.273353241	0.000100448
Metabotropic glutamate receptor group II pathway_Homo sapiens_P00040	20/30	0.138475226	0.999921119	0.11795991	0.825188466	-1.179608412	9.30527E-05
PI3 kinase pathway_Homo sapiens_P00048	27/42	0.149885392	0.999921119	0.098950557	0.825188466	-0.815089955	6.42979E-05
Axon guidance mediated by netrin_ Homo sapiens_P00009	19/30	0.237606658	0.999921119	0.160970229	0.825188466	0.021768899	-1.71723E-06
Ubiquitin proteasome pathway_ Homo sapiens_P00060	26/43	0.293371619	0.999921119	0.150802686	0.825188466	0.263729867	-2.08042E-05
Adrenaline and noradrenaline biosynthesis_ Homo sapiens_P00001	16/25	0.246985848	0.999921119	0.180200431	0.825188466	0.268674917	-2.11943E-05
5-Hydroxytryptamine degredation_ Homo sapiens_P04372	5/5	0.050997743	0.999921119	0.172276188	0.825188466	0.446757952	-3.52422E-05

Table B.23: Downregulated KEGG genesets in TetOn parental cells in response to Dox treatment.

Term	Overlap	P-value	Adjusted P-value	Old P-value	Old Adjusted P-value	Z-score	Combined Score
Ribosome_Homo sapiens_hsa03010	101/137	5.23703E-12	1.52921E-09	1.08251E-06	0.000316093	-1.746138049	35.44400421
Spliceosome_Homo sapiens_hsa03040	89/134	3.44946E-07	5.03621E-05	7.77281E-05	0.011348299	-1.77196951	17.53589228
Fructose and mannose metabolism_ Homo sapiens_hsa00051	25/32	0.000125783	0.012242902	0.00762193	0.370933912	-1.55094245	6.828503249
Huntington's disease_ Homo sapiens_hsa05016	110/193	0.000419006	0.030587457	0.000959826	0.093423109	-1.826574114	6.369565818
Oxidative phosphorylation_ Homo sapiens_hsa00190	76/133	0.002751738	0.160701494	0.005204621	0.366420156	-1.724055636	3.151930079
Pyrimidine metabolism_ Homo sapiens_hsa00240	61/105	0.004137115	0.180640379	0.008923645	0.372243492	-1.652908426	2.828534718
TNF signaling pathway_ Homo sapiens_hsa04668	62/110	0.009576391	0.279630609	0.013287333	0.484987638	-1.672329193	2.131025345
Epstein-Barr virus infection_ Homo sapiens_hsa05169	107/202	0.011613617	0.308288747	0.006274318	0.366420156	-1.701033337	2.001637304
Proteasome_Homo sapiens_hsa03050	28/44	0.009137396	0.279630609	0.030335664	0.555387316	-1.37701027	1.754704634
Base excision repair_ Homo sapiens_hsa03410	22/33	0.009327733	0.279630609	0.037348407	0.555387316	-1.178095782	1.501230727

Table B.24: Downregulated Reactome genesets in TetOn parental cells in response to Dox treatment.

Term	Overlap	P-value	Adjusted P-value	Old P-value	Old Adjusted P-value	Z-score	Combined Score
Infectious disease_Homo sapiens_ R-HSA-5663205	210/348	3.06872E-09	7.03286E-07	2.62789E-07	0.00039576	-2.368730796	33.55899794
Eukaryotic Translation Elongation_ Homo sapiens_R-HSA-156842	68/89	1.17069E-09	7.03286E-07	2.4763E-05	0.003818097	-2.008387964	28.45384019
rRNA processing_Homo sapiens_ R-HSA-72312	120/180	2.38445E-09	7.03286E-07	3.6581E-06	0.002754552	-2.004201911	28.39453428
Peptide chain elongation_Homo sapiens_ R-HSA-156902	65/84	1.06954E-09	7.03286E-07	2.82233E-05	0.003818097	-1.965461354	27.84567736
Formation of a pool of free 40S subunits_ Homo sapiens_R-HSA-72689	72/96	1.62274E-09	7.03286E-07	2.23632E-05	0.003818097	-1.941052342	27.49986265
Cap-dependent Translation Initiation_ Homo sapiens_R-HSA-72737	82/114	3.73592E-09	7.03286E-07	1.84552E-05	0.003818097	-1.939670905	27.48029114
Eukaryotic Translation Initiation_ Homo sapiens_R-HSA-72613	82/114	3.73592E-09	7.03286E-07	1.84552E-05	0.003818097	-1.931022481	27.35776457
Major pathway of rRNA processing in the nucleolus_Homo sapiens_R-HSA-6791226	111/166	7.23614E-09	1.21085E-06	7.59972E-06	0.00381506	-1.982525455	27.0103036
Eukaryotic Translation Termination_ Homo sapiens_R-HSA-72764	66/87	3.44592E-09	7.03286E-07	3.77586E-05	0.003818097	-1.879954752	26.63426243
Nonsense Mediated Decay (NMD) independent of the Exon Junction Complex (EJC)_Homo sapiens_ R-HSA-975956	66/89	1.68554E-08	1.63909E-06	6.13216E-05	0.00486054	-1.862683657	24.81350144

Table B.25: Downregulated WikiPathways genesets in TetOn parental cells in response to Dox treatment.

Term	Overlap	P-value	Adjusted P-value	Old P-value	Old Adjusted P-value	Z-score	Combined Score
Ribosome_Homo sapiens_hsa03010	101/137	5.23703E-12	1.52921E-09	1.08251E-06	0.000316093	-1.746138049	35.44400421
Spliceosome_Homo sapiens_hsa03040	89/134	3.44946E-07	5.03621E-05	7.77281E-05	0.011348299	-1.77196951	17.53589228
Fructose and mannose metabolism_ Homo sapiens_hsa00051	25/32	0.000125783	0.012242902	0.00762193	0.370933912	-1.55094245	6.828503249
Huntington's disease_ Homo sapiens_hsa05016	110/193	0.000419006	0.030587457	0.000959826	0.093423109	-1.826574114	6.369565818
Oxidative phosphorylation_ Homo sapiens_hsa00190	76/133	0.002751738	0.160701494	0.005204621	0.366420156	-1.724055636	3.151930079
Pyrimidine metabolism_ Homo sapiens_hsa00240	61/105	0.004137115	0.180640379	0.008923645	0.372243492	-1.652908426	2.828534718
TNF signaling pathway_ Homo sapiens_hsa04668	62/110	0.009576391	0.279630609	0.013287333	0.484987638	-1.672329193	2.131025345
Epstein-Barr virus infection_ Homo sapiens_hsa05169	107/202	0.011613617	0.308288747	0.006274318	0.366420156	-1.701033337	2.001637304
Proteasome_ Homo sapiens_hsa03050	28/44	0.009137396	0.279630609	0.030335664	0.555387316	-1.37701027	1.754704634
Base excision repair_ Homo sapiens_hsa03410	22/33	0.009327733	0.279630609	0.037348407	0.555387316	-1.178095782	1.501230727

Table B.26: Downregulated Panther genesets in TetOn parental cells in response to Dox treatment.

Term	Overlap	P-value	Adjusted P-value	Old P-value	Old Adjusted P-value	Z-score	Combined Score
Huntington disease_Homo sapiens_ P00029	69/124	0.009678337	0.358098456	0.032565816	0.99580555	-1.459003251	1.498319468
Glycolysis_ Homo sapiens_P00024	13/17	0.00821785	0.358098456	0.075444228	0.99580555	-1.056996395	1.085479608
Mannose metabolism_ Homo sapiens_P02752	06-Jun	0.008077308	0.358098456	0.110722342	0.99580555	-1.008891743	1.036078665
Parkinson disease_ Homo sapiens_P00049	45/81	0.033334402	0.41112429	0.075903745	0.99580555	-0.714215843	0.634837682
De novo purine biosynthesis_ Homo sapiens_P02738	17/26	0.02789128	0.386991515	0.103273668	0.99580555	-0.09669066	0.091793521
Apoptosis signaling pathway_ Homo sapiens_P00006	53/102	0.087507397	0.883029192	0.114861677	0.99580555	-0.676005058	0.084093014
Cytoskeletal regulation by Rho GTPase_Homo sapiens_P00016	37/70	0.108200266	0.92386381	0.147399165	0.99580555	-0.190407529	0.015078488
Integrin signalling pathway_ Homo sapiens_P00034	74/156	0.279126566	0.99992324	0.203683171	0.99580555	0.606925854	-4.65894E-05
Blood coagulation_ Homo sapiens_P00011	20/38	0.209021966	0.99992324	0.244374558	0.99580555	0.89060768	-6.83657E-05
Toll receptor signaling pathway_ Homo sapiens_P00054	25/49	0.231290334	0.99992324	0.246989832	0.99580555	0.97075554	-7.45181E-05

Table B.27: Upregulated KEGG genesets in pTRE-CPT1A clone 17 in response to *CPT1A* overexpression.

Term	Overlap	P-value	Adjusted P-value	Old P-value	Old Adjusted P-value	Z-score	Combined Score
Huntington disease_Homo sapiens_ P00029	69/124	0.009678337	0.358098456	0.032565816	0.99580555	-1.459003251	1.498319468
Glycolysis_ Homo sapiens_P00024	13/17	0.00821785	0.358098456	0.075444228	0.99580555	-1.056996395	1.085479608
Mannose metabolism_ Homo sapiens_P02752	06-Jun	0.008077308	0.358098456	0.110722342	0.99580555	-1.008891743	1.036078665
Parkinson disease_ Homo sapiens_P00049	45/81	0.033334402	0.41112429	0.075903745	0.99580555	-0.714215843	0.634837682
De novo purine biosynthesis_ Homo sapiens_P02738	17/26	0.02789128	0.386991515	0.103273668	0.99580555	-0.09669066	0.091793521
Apoptosis signaling pathway_ Homo sapiens_P00006	53/102	0.087507397	0.883029192	0.114861677	0.99580555	-0.676005058	0.084093014
Cytoskeletal regulation by Rho GTPase_Homo sapiens_P00016	37/70	0.108200266	0.92386381	0.147399165	0.99580555	-0.190407529	0.015078488
Integrin signalling pathway_ Homo sapiens_P00034	74/156	0.279126566	0.99992324	0.203683171	0.99580555	0.606925854	-4.65894E-05
Blood coagulation_ Homo sapiens_P00011	20/38	0.209021966	0.99992324	0.244374558	0.99580555	0.89060768	-6.83657E-05
Toll receptor signaling pathway_ Homo sapiens_P00054	25/49	0.231290334	0.99992324	0.246989832	0.99580555	0.97075554	-7.45181E-05

Table B.28: Upregulated Reactome genesets in pTRE-CPT1A clone 17 in response to *CPT1A* overexpression.

Term	Overlap	P-value	Adjusted P-value	Old P-value	Old Adjusted P-value	Z-score	Combined Score
Homologous DNA Pairing and Strand Exchange_Homo sapiens_ R-HSA-5693579	33/42	1.35786E-05	0.012268241	0.002214407	0.256360162	-2.150062576	9.461869426
Presynaptic phase of homologous DNA pairing and strand exchange_ Homo sapiens_R-HSA-5693616	31/39	1.63033E-05	0.012268241	0.002626843	0.28238563	-2.116898092	9.315921104
Mitotic Prometaphase_ Homo sapiens_R-HSA-68877	70/107	2.94451E-05	0.014771646	0.000589317	0.159346453	-2.032383599	8.566589857
Resolution of Sister Chromatid Cohesion_ Homo sapiens_R-HSA-2500257	65/99	4.73832E-05	0.017827915	0.000848069	0.159346453	-2.064423139	8.313410887
Nuclear Pore Complex (NPC) Disassembly_ Homo sapiens_R-HSA-3301854	26/34	0.00025457	0.067761606	0.007901028	0.503811279	-2.161900365	5.819315901
Resolution of D-loop Structures through Synthesis-Dependent Strand Annealing (SDSA)_Homo sapiens_R-HSA-5693554	21/26	0.000270146	0.067761606	0.010797081	0.541653561	-2.023745338	5.447435791
Generic Transcription Pathway_Homo sapiens_ R-HSA-212436	419/812	0.000321913	0.069211402	7.80122E-07	0.001174084	-2.21539766	5.916418073
NS1 Mediated Effects on Host Pathways_ Homo sapiens_R-HSA-168276	28/39	0.000860423	0.161866993	0.010681099	0.541653561	-2.128454739	3.875874173
Branched-chain amino acid catabolism_ Homo sapiens_R-HSA-70895	18/23	0.001502051	0.251176373	0.021472843	0.719285486	-2.049153276	2.831109969
Transport of Ribonucleoproteins into the Host Nucleus_Homo sapiens_R-HSA-168271	22/30	0.001991403	0.272390972	0.018959846	0.711796498	-1.961893148	2.551475094

Table B.29: Upregulated WikiPathways genesets in pTRE-CPT1A clone 17 in response to *CPT1A* overexpression.

Term	Overlap	P-value	Adjusted P-value	Old P-value	Old Adjusted P-value	Z-score	Combined Score
Integrated Cancer Pathway_ Homo sapiens_WP1971	32/48	0.002707704	0.809187378	0.006865658	0.739774697	-2.009492422	0.425459324
Retinoblastoma (RB) in Cancer_ Homo sapiens_WP2446	54/90	0.00436095	0.809187378	0.003050389	0.657358867	-1.925101836	0.407591746
Integrated Breast Cancer Pathway_ Homo sapiens_WP1984	87/155	0.005632395	0.809187378	0.000975001	0.420225539	-2.127329909	0.450408439
Sphingolipid Metabolism_ Homo sapiens_WP1422	14/20	0.02475276	1	0.048798684	0.86872574	-1.583707823	3.13571E-10
miRNA regulation of DNA Damage Response_Mus musculus_WP2087	37/64	0.034208996	1	0.01891683	0.86872574	-1.861744519	3.68622E-10
DNA Damage Response_ Homo sapiens_WP707	39/68	0.035150165	1	0.017754816	0.86872574	-1.900460742	3.76288E-10
TGF-beta Signaling Pathway_ Homo sapiens_WP366	71/132	0.037178195	1	0.005902796	0.739774697	-1.852717473	3.66835E-10
Apoptosis Modulation by HSP70_ Homo sapiens_WP384	13/19	0.03902709	1	0.062750749	0.86872574	-1.414082763	2.79986E-10
Amino Acid metabolism_ Mus musculus_WP662	48/92	0.125725356	1	0.029986198	0.86872574	-1.386201539	2.74466E-10
EGF/EGFR Signaling Pathway_ Homo sapiens_WP437	81/163	0.170358418	1	0.014947435	0.86872574	-1.331331993	2.63601E-10

Table B.30: Upregulated Panther genesets in pTRE-CPT1A clone 17 in response to *CPT1A* overexpression.

Term	Overlap	P-value	Adjusted P-value	Old P-value	Old Adjusted P-value	Z-score	Combined Score
Interferon-gamma signaling pathway_Homo sapiens_P00035	19/28	0.014974154	0.842985146	0.045082357	0.942152799	-1.454104809	0.248369741
p53 pathway feedback loops 2_ Homo sapiens_P04398	28/45	0.018846605	0.842985146	0.035472243	0.942152799	-1.535525583	0.262276893
Vasopressin synthesis_ Homo sapiens_P04395	8/10	0.030263436	0.842985146	0.102598617	0.942152799	-0.414769187	0.070845041
Ubiquitin proteasome pathway_ Homo sapiens_P00060	26/43	0.03653362	0.842985146	0.051722883	0.942152799	-1.074471106	0.183526049
DNA replication_Homo sapiens_ P00017	13/19	0.03902709	0.842985146	0.085879676	0.942152799	-0.207873651	0.035506055
FAS signaling pathway_Homo sapiens_ P00020	19/31	0.058948927	0.890199843	0.081752291	0.942152799	-0.692757605	0.080574151
p53 pathway_Homo sapiens_P00059	39/71	0.07418332	0.890199843	0.05273086	0.942152799	-0.717019375	0.08339602
Transcription regulation by bZIP transcription factor_Homo sapiens_ P00055	23/42	0.152219512	0.999985854	0.120096529	0.942152799	-0.084844636	1.20018E-06
PDGF signaling pathway_ Homo sapiens_P00047	55/112	0.262609674	0.999985854	0.091242135	0.942152799	-0.218250058	3.08729E-06
EGF receptor signaling pathway_ Homo sapiens_P00018	53/109	0.300505988	0.999985854	0.10608284	0.942152799	0.09503699	-1.34436E-06

Table B.31: Downregulated KEGG genesets in pTRE-CPT1A clone 17 in response to *CPT1A* overexpression.

Term	Overlap	P-value	Adjusted P-value	Old P-value	Old Adjusted P-value	Z-score	Combined Score
Ubiquitin mediated proteolysis_ Homo sapiens_hsa04120	89/137	4.01689E-06	0.00117695	2.17262E-05	0.006365782	-1.645025777	11.09541754
Valine, leucine and isoleucine degradation_Homo sapiens_hsa00280	33/48	0.001045435	0.114032247	0.004389122	0.336001534	-1.973149212	4.284247578
Lysosome_Homo sapiens_hsa04142	73/123	0.001556754	0.114032247	0.000807335	0.118274636	-1.699249096	3.689535378
Protein export_Homo sapiens_hsa03060	18/23	0.001502051	0.114032247	0.013439873	0.366851759	-1.479036126	3.211392682
Propanoate metabolism_Homo sapiens_ hsa00640	23/32	0.002440072	0.119156838	0.011168218	0.366851759	-1.505727714	3.203156686
Glycosylphosphatidylinositol(GPI)-anchor biosynthesis_Homo sapiens_hsa00563	19/25	0.002036014	0.119156838	0.013772592	0.366851759	-1.275723187	2.713864676
Fanconi anemia pathway_Homo sapiens_ hsa03460	34/53	0.00516358	0.216132715	0.008259153	0.366851759	-1.53066026	2.344761261
Sphingolipid metabolism_Homo sapiens_ hsa00600	30/47	0.009301728	0.340675795	0.013212076	0.366851759	-1.627989953	1.753058655
FoxO signaling pathway_Homo sapiens_ hsa04068	72/133	0.030583504	0.814633342	0.005032849	0.336001534	-1.572113954	0.322310329
Ubiquinone and other terpenoid-quinone biosynthesis_Homo sapiens_hsa00130	09-Nov	0.016589164	0.540069436	0.061384329	0.72793414	-0.271127945	0.167030421

Table B.32: Downregulated Reactome genesets in pTRE-CPT1A clone 17 in response to *CPT1A* overexpression.

Term	Overlap	P-value	Adjusted P-value	Old P-value	Old Adjusted P-value	Z-score	Combined Score
Homologous DNA Pairing and Strand Exchange_Homo sapiens_R-HSA-5693579	33/42	1.35786E-05	0.012268241	0.002214407	0.256360162	-2.150062576	9.461869426
Presynaptic phase of homologous DNA pairing and strand exchange_Homo sapiens_R-HSA-5693616	31/39	1.63033E-05	0.012268241	0.002626843	0.28238563	-2.116898092	9.315921104
Mitotic Prometaphase_Homo sapiens_ R-HSA-68877	70/107	2.94451E-05	0.014771646	0.000589317	0.159346453	-2.032383599	8.566589857
Resolution of Sister Chromatid Cohesion_ Homo sapiens_R-HSA-2500257	65/99	4.73832E-05	0.017827915	0.000848069	0.159346453	-2.064423139	8.313410887
Generic Transcription Pathway_Homo sapiens_ R-HSA-212436	419/812	0.000321913	0.069211402	7.80122E-07	0.001174084	-2.21539766	5.916418073
Nuclear Pore Complex (NPC) Disassembly_ Homo sapiens_R-HSA-3301854	26/34	0.00025457	0.067761606	0.007901028	0.503811279	-2.161900365	5.819315901
Resolution of D-loop Structures through Synthesis-Dependent Strand Annealing (SDSA)_Homo sapiens_R-HSA-5693554	21/26	0.000270146	0.067761606	0.010797081	0.541653561	-2.023745338	5.447435791
NS1 Mediated Effects on Host Pathways_ Homo sapiens_R-HSA-168276	28/39	0.000860423	0.161866993	0.010681099	0.541653561	-2.128454739	3.875874173
Branched-chain amino acid catabolism_ Homo sapiens_R-HSA-70895	18/23	0.001502051	0.251176373	0.021472843	0.719285486	-2.049153276	2.831109969
Transport of Ribonucleoproteins into the Host Nucleus_Homo sapiens_R-HSA-168271	22/30	0.001991403	0.272390972	0.018959846	0.711796498	-1.97866224	2.573283581

Table B.33: Downregulated WikiPathways genesets in pTRE-CPT1A clone 17 in response to *CPT1A* overexpression.

Term	Overlap	P-value	Adjusted P-value	Old P-value	Old Adjusted P-value	Z-score	Combined Score
Integrated Breast Cancer Pathway_ Homo sapiens_WP1984	87/155	0.005632395	0.809187378	0.000975001	0.420225539	-2.127329909	0.450408439
Integrated Cancer Pathway_ Homo sapiens_WP1971	32/48	0.002707704	0.809187378	0.006865658	0.739774697	-2.009492422	0.425459324
Retinoblastoma (RB) in Cancer_ Homo sapiens_WP2446	54/90	0.00436095	0.809187378	0.003050389	0.657358867	-1.925101836	0.407591746
DNA Damage Response_ Homo sapiens_WP707	39/68	0.035150165	1	0.017754816	0.86872574	-1.900460742	3.76288E-10
miRNA regulation of DNA Damage Response_Mus musculus_WP2087	37/64	0.034208996	1	0.01891683	0.86872574	-1.861744519	3.68622E-10
TGF-beta Signaling Pathway_ Homo sapiens_WP366	71/132	0.037178195	1	0.005902796	0.739774697	-1.852717473	3.66835E-10
Sphingolipid Metabolism_ Homo sapiens_WP1422	14/20	0.02475276	1	0.048798684	0.86872574	-1.583707823	3.13571E-10
Apoptosis Modulation by HSP70_ Homo sapiens_WP384	13/19	0.03902709	1	0.062750749	0.86872574	-1.414082763	2.79986E-10
Amino Acid metabolism_ Mus musculus_WP662	48/92	0.125725356	1	0.029986198	0.86872574	-1.386201539	2.74466E-10
EGF/EGFR Signaling Pathway_ Homo sapiens_WP437	81/163	0.170358418	1	0.014947435	0.86872574	-1.331331993	2.63601E-10

Table B.34: Downregulated Panther genesets in pTRE-CPT1A clone 17 in response to *CPT1A* overexpression.

Term	Overlap	P-value	Adjusted P-value	Old P-value	Old Adjusted P-value	Z-score	Combined Score
p53 pathway feedback loops 2_ Homo sapiens_P04398	28/45	0.018846605	0.842985146	0.035472243	0.942152799	-1.535525583	0.262276893
Interferon-gamma signaling pathway_ Homo sapiens_P00035	19/28	0.014974154	0.842985146	0.045082357	0.942152799	-1.454104809	0.248369741
Ubiquitin proteasome pathway_ Homo sapiens_P00060	26/43	0.03653362	0.842985146	0.051722883	0.942152799	-1.074471106	0.183526049
p53 pathway_Homo sapiens_P00059	39/71	0.07418332	0.890199843	0.05273086	0.942152799	-0.717019375	0.08339602
FAS signaling pathway_ Homo sapiens_P00020	19/31	0.058948927	0.890199843	0.081752291	0.942152799	-0.692757605	0.080574151
Vasopressin synthesis_ Homo sapiens_P04395	8/10	0.030263436	0.842985146	0.102598617	0.942152799	-0.414769187	0.070845041
DNA replication_ Homo sapiens_P00017	13/19	0.03902709	0.842985146	0.085879676	0.942152799	-0.207873651	0.035506055
PDGF signaling pathway_ Homo sapiens_P00047	55/112	0.262609674	0.999985854	0.091242135	0.942152799	-0.218250058	3.08729E-06
Transcription regulation by bZIP transcription factor_Homo sapiens_P00055	23/42	0.152219512	0.999985854	0.120096529	0.942152799	-0.084844636	1.20018E-06
EGF receptor signaling pathway_ Homo sapiens_P00018	53/109	0.300505988	0.999985854	0.10608284	0.942152799	0.09503699	-1.34436E-06

Table B.35: Upregulated KEGG genesets in MCF7 shRNA1 clone in response to *CPT1A* knockdown, compared to non-silencing control.

Term	Overlap	P-value	Adjusted P-value	Old P-value	Old Adjusted P-value	Z-score	Combined Score
Ribosome_Homo sapiens_hsa03010	96/137	4.95032E-06	0.001450443	1.36084E-05	0.003987267	-1.746138049	11.41255979
Spliceosome_Homo sapiens_hsa03040	87/134	0.000863141	0.126450192	0.000229518	0.033624441	-1.77196951	3.664267773
Non-alcoholic fatty liver disease (NAFLD)_ Homo sapiens_hsa04932	86/151	0.088857304	1	0.004353338	0.31888203	-1.83402353	5.3371E-11
RNA polymerase_Homo sapiens_hsa03020	22/32	0.033692559	1	0.033331699	0.65107919	-1.81944086	5.29466E-11
Ribosome biogenesis in eukaryotes_ Homo sapiens_hsa03008	51/89	0.145710455	1	0.022244928	0.538657626	-1.804099388	5.25002E-11
Huntington's disease_Homo sapiens_ hsa05016	109/193	0.078943834	1	0.00178487	0.174322302	-1.801778075	5.24326E-11
Proteasome_Homo sapiens_hsa03050	29/44	0.034502412	1	0.023284581	0.538657626	-1.584085426	4.60977E-11
Chronic myeloid leukemia_Homo sapiens_ hsa05220	41/73	0.230260077	1	0.045619066	0.74257702	-1.544697267	4.49515E-11
Oxidative phosphorylation_Homo sapiens_ hsa00190	73/133	0.219421874	1	0.014971049	0.538657626	-1.542795911	4.48961E-11
Aminoacyl-tRNA biosynthesis_Homo sapiens_ hsa00970	37/66	0.250588619	1	0.056326156	0.849889713	-1.5388376	4.47809E-11

Table B.36: Upregulated Reactome genesets in MCF7 shRNA1 clone in response to *CPT1A* knockdown, compared to non-silencing control.

Term	Overlap	P-value	Adjusted P-value	Old P-value	Old Adjusted P-value	Z-score	Combined Score
rRNA processing_Homo sapiens_R-HSA-72312	131/180	2.27506E-09	3.45354E-06	5.26191E-07	0.000399379	-2.027505558	25.49813675
Major pathway of rRNA processing in the nucleolus_Homo sapiens_R-HSA-6791226	120/166	2.03308E-08	1.54311E-05	1.97863E-06	0.001001185	-2.037037884	22.56860138
Processing of Capped Intron-Containing Pre-mRNA_Homo sapiens_R-HSA-72203	129/193	6.85401E-06	0.002601099	1.37825E-05	0.005230441	-2.13325627	12.69676025
Formation of a pool of free 40S subunits_ Homo sapiens_R-HSA-72689	71/96	3.98195E-06	0.002014865	0.000142834	0.018418939	-1.941052342	12.04850649
Influenza Viral RNA Transcription and Replication_Homo sapiens_R-HSA-168273	89/128	1.76486E-05	0.002726863	0.000107584	0.01814589	-2.01559186	11.90127049
Influenza Infection_Homo sapiens_ R-HSA-168254	100/147	2.36978E-05	0.003214243	7.62964E-05	0.016738192	-2.001151063	11.48693394
mRNA Splicing - Major Pathway_Homo sapiens_ R-HSA-72163	93/134	1.29894E-05	0.002726863	7.99621E-05	0.016738192	-1.940469769	11.45770434
Peptide chain elongation_Homo sapiens_ R-HSA-156902	62/84	1.79635E-05	0.002726863	0.000379598	0.026045385	-1.884299625	11.12604192
Selenocysteine synthesis_Homo sapiens_ R-HSA-2408557	64/87	1.58412E-05	0.002726863	0.000328614	0.024941768	-1.879014764	11.09483691
Nonsense-Mediated Decay (NMD)_ Homo sapiens_R-HSA-927802	76/106	1.26674E-05	0.002726863	0.000169872	0.018418939	-1.870115837	11.04229227

Table B.37: Upregulated WikiPathways genesets in MCF7 shRNA1 clone in response to *CPT1A* knockdown, compared to non-silencing control.

Term	Overlap	P-value	Adjusted P-value	Old P-value	Old Adjusted P-value	Z-score	Combined Score
mRNA processing_Mus musculus_WP310	243/398	3.84669E-05	0.01665616	1.36293E-06	0.000590147	-2.13612911	8.747395616
Cytoplasmic Ribosomal Proteins_ Homo sapiens_WP477	63/89	0.000126924	0.01831931	0.001056719	0.152519803	-1.953073984	7.811904515
mRNA Processing_Homo sapiens_WP411	86/127	0.000110455	0.01831931	0.000405397	0.087768357	-1.941057273	7.763840078
Cytoplasmic Ribosomal Proteins_ Mus musculus_WP163	48/70	0.0023339	0.252644628	0.006058257	0.524645064	-1.940461432	2.669631364
Estrogen signalling_Mus musculus_WP1244	50/75	0.004704345	0.407396275	0.007567885	0.546149015	-1.900182655	1.706304963
PluriNetWork_Mus musculus_WP1763	160/284	0.044704656	1	0.001428018	0.154582935	-1.846398794	2.9766E-11
TNF-alpha NF-kB Signaling Pathway_ Mus musculus_WP246	101/179	0.090133597	1	0.009746518	0.60289176	-1.820647406	2.93508E-11
Eukaryotic Transcription Initiation_ Mus musculus_WP567	28/41	0.019822993	1	0.03218215	0.972118652	-1.793666737	2.89159E-11
RANKL/RANK Signaling Pathway_ Homo sapiens_WP2018	35/55	0.042263909	1	0.035290413	0.972118652	-1.775492764	2.86229E-11
TOR Signaling_Homo sapiens_WP1471	25/36	0.02024715	1	0.036687478	0.972118652	-1.768534897	2.85107E-11

Table B.38: Upregulated Panther genesets in MCF7 shRNA1 clone in response to *CPT1A* knockdown, compared to non-silencing control.

Term	Overlap	P-value	Adjusted P-value	Old P-value	Old Adjusted P-value	Z-score	Combined Score
Ubiquitin proteasome pathway_ Homo sapiens_P00060	29/43	0.02274452	0.999998914	0.041532694	0.835048813	-1.439435008	1.56307E-06
Alpha adrenergic receptor signaling pathway_ Homo sapiens_P00002	15/23	0.126762421	0.999998914	0.140788295	0.835048813	-1.036031797	1.12502E-06
p53 pathway_Homo sapiens_P00059	39/71	0.303044048	0.999998914	0.131116039	0.835048813	-0.920706371	9.99785E-07
Oxytocin receptor mediated signaling pathway_Homo sapiens_P04391	22/39	0.310711232	0.999998914	0.190410543	0.835048813	-0.851255657	9.2437E-07
Thyrotropin-releasing hormone receptor signaling pathway_Homo sapiens_P04394	23/41	0.317610873	0.999998914	0.188897352	0.835048813	-0.828333458	8.99479E-07
p53 pathway by glucose deprivation_ Homo sapiens_P04397	15/21	0.049011697	0.999998914	0.094254695	0.835048813	-0.795947666	8.64311E-07
Parkinson disease_Homo sapiens_P00049	44/81	0.323850574	0.999998914	0.125440002	0.835048813	-0.612006508	6.64571E-07
p53 pathway feedback loops 2_ Homo sapiens_P04398	24/45	0.444080264	0.999998914	0.236001463	0.835048813	-0.199277098	2.16393E-07
mRNA splicing_Homo sapiens_P00058	5/5	0.035047544	0.999998914	0.152895645	0.835048813	-0.11767251	1.27779E-07
Apoptosis signaling pathway_ Homo sapiens_P00006	53/102	0.475645266	0.999998914	0.151536452	0.835048813	0.141395881	-1.5354E-07

Table B.39: Downregulated KEGG genesets in MCF7 shRNA1 clone in response to *CPT1A* knockdown, compared to non-silencing control.

Term	Overlap	P-value	Adjusted P-value	Old P-value	Old Adjusted P-value	Z-score	Combined Score
Ribosome_Homo sapiens_hsa03010	96/137	4.95032E-06	0.001450443	1.36084E-05	0.003987267	-1.746138049	11.41255979
Spliceosome_Homo sapiens_hsa03040	87/134	0.000863141	0.126450192	0.000229518	0.033624441	-1.77196951	3.664267773
Non-alcoholic fatty liver disease (NAFLD)_ Homo sapiens_hsa04932	86/151	0.088857304	1	0.004353338	0.31888203	-1.83402353	5.3371E-11
RNA polymerase_Homo sapiens_hsa03020	22/32	0.033692559	1	0.033331699	0.65107919	-1.81944086	5.29466E-11
Ribosome biogenesis in eukaryotes_ Homo sapiens_hsa03008	51/89	0.145710455	1	0.022244928	0.538657626	-1.804099388	5.25002E-11
Huntington's disease_Homo sapiens_hsa05016	109/193	0.078943834	1	0.00178487	0.174322302	-1.801778075	5.24326E-11
Proteasome_Homo sapiens_hsa03050	29/44	0.034502412	1	0.023284581	0.538657626	-1.584085426	4.60977E-11
Chronic myeloid leukemia_ Homo sapiens_hsa05220	41/73	0.230260077	1	0.045619066	0.74257702	-1.544697267	4.49515E-11
Oxidative phosphorylation_ Homo sapiens_hsa00190	73/133	0.219421874	1	0.014971049	0.538657626	-1.542795911	4.48961E-11
Aminoacyl-tRNA biosynthesis_ Homo sapiens_hsa00970	37/66	0.250588619	1	0.056326156	0.849889713	-1.5388376	4.47809E-11

Table B.40: Downregulated Reactome genesets in MCF7 shRNA1 clone in response to *CPT1A* knockdown, compared to non-silencing control.

Term	Overlap	P-value	Adjusted P-value	Old P-value	Old Adjusted P-value	Z-score	Combined Score
rRNA processing_Homo sapiens_R-HSA-72312	131/180	2.27506E-09	3.45354E-06	5.26191E-07	0.000399379	-2.027505558	25.49813675
Major pathway of rRNA processing in the nucleolus_Homo sapiens_R-HSA-6791226	120/166	2.03308E-08	1.54311E-05	1.97863E-06	0.001001185	-2.037037884	22.56860138
Processing of Capped Intron-Containing Pre-mRNA_Homo sapiens_R-HSA-72203	129/193	6.85401E-06	0.002601099	1.37825E-05	0.005230441	-2.13325627	12.69676025
Formation of a pool of free 40S subunits_ Homo sapiens_R-HSA-72689	71/96	3.98195E-06	0.002014865	0.000142834	0.018418939	-1.941052342	12.04850649
Influenza Viral RNA Transcription and Replication_Homo sapiens_R-HSA-168273	89/128	1.76486E-05	0.002726863	0.000107584	0.01814589	-2.01559186	11.90127049
Influenza Infection_Homo sapiens_ R-HSA-168254	100/147	2.36978E-05	0.003214243	7.62964E-05	0.016738192	-2.001151063	11.48693394
mRNA Splicing - Major Pathway_ Homo sapiens_R-HSA-72163	93/134	1.29894E-05	0.002726863	7.99621E-05	0.016738192	-1.940469769	11.45770434
Peptide chain elongation_Homo sapiens_ R-HSA-156902	62/84	1.79635E-05	0.002726863	0.000379598	0.026045385	-1.884299625	11.12604192
Selenocysteine synthesis_Homo sapiens_ R-HSA-2408557	64/87	1.58412E-05	0.002726863	0.000328614	0.024941768	-1.879014764	11.09483691
Nonsense-Mediated Decay (NMD)_ Homo sapiens_R-HSA-927802	76/106	1.26674E-05	0.002726863	0.000169872	0.018418939	-1.870115837	11.04229227

Table B.41: Downregulated WikiPathways genesets in MCF7 shRNA1 clone in response to *CPT1A* knockdown, compared to non-silencing control.

Term	Overlap	P-value	Adjusted P-value	Old P-value	Old Adjusted P-value	Z-score	Combined Score
mRNA processing_Mus musculus_ WP310	243/398	3.84669E-05	0.01665616	1.36293E-06	0.000590147	-2.13612911	8.747395616
Cytoplasmic Ribosomal Proteins_ Homo sapiens_WP477	63/89	0.000126924	0.01831931	0.001056719	0.152519803	-1.953073984	7.811904515
mRNA Processing_Homo sapiens_WP411	86/127	0.000110455	0.01831931	0.000405397	0.087768357	-1.941057273	7.763840078
Cytoplasmic Ribosomal Proteins_ Mus musculus_WP163	48/70	0.0023339	0.252644628	0.006058257	0.524645064	-1.940461432	2.669631364
Estrogen signalling_Mus musculus_WP1244	50/75	0.004704345	0.407396275	0.007567885	0.546149015	-1.900182655	1.706304963
PluriNetWork_Mus musculus_WP1763	160/284	0.044704656	1	0.001428018	0.154582935	-1.846398794	2.9766E-11
TNF-alpha NF-kB Signaling Pathway_ Mus musculus_WP246	101/179	0.090133597	1	0.009746518	0.60289176	-1.820647406	2.93508E-11
Eukaryotic Transcription Initiation_ Mus musculus_WP567	28/41	0.019822993	1	0.03218215	0.972118652	-1.793666737	2.89159E-11
RANKL/RANK Signaling Pathway_ Homo sapiens_WP2018	35/55	0.042263909	1	0.035290413	0.972118652	-1.775492764	2.86229E-11
TOR Signaling_Homo sapiens_WP1471	25/36	0.02024715	1	0.036687478	0.972118652	-1.768534897	2.85107E-11

Table B.42: Downregulated Panther genesets in MCF7 shRNA1 clone in response to *CPT1A* knockdown, compared to non-silencing control.

Term	Overlap	P-value	Adjusted P-value	Old P-value	Old Adjusted P-value	Z-score	Combined Score
Ubiquitin proteasome pathway_ Homo sapiens_P00060	29/43	0.02274452	0.999998914	0.041532694	0.835048813	-1.439435008	1.56307E-06
Alpha adrenergic receptor signaling pathway_Homo sapiens_P00002	15/23	0.126762421	0.999998914	0.140788295	0.835048813	-1.036031797	1.12502E-06
p53 pathway_Homo sapiens_P00059	39/71	0.303044048	0.999998914	0.131116039	0.835048813	-0.920706371	9.99785E-07
Oxytocin receptor mediated signaling pathway_Homo sapiens_P04391	22/39	0.310711232	0.999998914	0.190410543	0.835048813	-0.851255657	9.2437E-07
Thyrotropin-releasing hormone receptor signaling pathway_Homo sapiens_P04394	23/41	0.317610873	0.999998914	0.188897352	0.835048813	-0.828333458	8.99479E-07
p53 pathway by glucose deprivation_ Homo sapiens_P04397	15/21	0.049011697	0.999998914	0.094254695	0.835048813	-0.795947666	8.64311E-07
Parkinson disease_Homo sapiens_P00049	44/81	0.323850574	0.999998914	0.125440002	0.835048813	-0.612006508	6.64571E-07
p53 pathway feedback loops 2_ Homo sapiens_P04398	24/45	0.444080264	0.999998914	0.236001463	0.835048813	-0.199277098	2.16393E-07
mRNA splicing_Homo sapiens_P00058	5/5	0.035047544	0.999998914	0.152895645	0.835048813	-0.11767251	1.27779E-07
Apoptosis signaling pathway_ Homo sapiens_P00006	53/102	0.475645266	0.999998914	0.151536452	0.835048813	0.141395881	-1.5354E-07
5HT2 type receptor mediated signaling pathway_Homo sapiens_P04374	24/46	0.504681112	0.999998914	0.262239554	0.835048813	0.30674461	-3.33091E-07

Table B.43: Upregulated KEGG genesets in MCF7 shRNA2 clone in response to *CPT1A* knockdown, compared to non-silencing control.

Term	Overlap	P-value	Adjusted P-value	Old P-value	Old Adjusted P-value	Z-score	Combined Score
Ribosome_ Homo sapiens_hsa03010	126/137	6.91217E-28	2.01144E-25	1.73597E-12	5.05167E-10	-1.746138049	99.29549519
Spliceosome_ Homo sapiens_hsa03040	93/134	7.21871E-07	0.000105032	1.04478E-05	0.001013441	-1.77196951	16.23344317
RNA transport_ Homo sapiens_hsa03013	113/172	3.68639E-06	0.000343204	7.65662E-06	0.001013441	-1.818646653	14.50768105
Cell cycle_ Homo sapiens_hsa04110	85/124	4.71758E-06	0.000343204	3.41195E-05	0.002482194	-1.65735888	13.22105862
DNA replication_ Homo sapiens_hsa03030	28/36	0.000312529	0.018189207	0.004386834	0.208830265	-1.737606889	6.96246373
Parkinson's disease_ Homo sapiens_hsa05012	85/142	0.004169887	0.188152262	0.000885631	0.051543725	-1.648540408	2.75389292
Basal transcription factors_ Homo sapiens_hsa03022	31/45	0.004525999	0.188152262	0.009667627	0.281327937	-1.588514154	2.653618839
Nucleotide excision repair_ Homo sapiens_hsa03420	31/47	0.01185013	0.431048489	0.01468285	0.356059106	-1.562454789	1.314859908
Pyrimidine metabolism_ Homo sapiens_hsa00240	62/105	0.019106127	0.617764785	0.005152126	0.208830265	-1.571024109	0.756679837
Ribosome biogenesis in eukaryotes_ Homo sapiens_hsa03008	52/89	0.038113023	1	0.011322068	0.299520152	-1.709146788	2.16099E-10

Table B.44: Upregulated Reactome genesets in MCF7 shRNA2 clone in response to *CPT1A* knockdown, compared to non-silencing control.

Term	Overlap	P-value	Adjusted P-value	Old P-value	Old Adjusted P-value	Z-score
GTP hydrolysis and joining of the 60S ribosomal subunit_Homo sapiens_ R-HSA-72706	100/107	7.97753E-24	3.34581E-21	3.01917E-09	4.31302E-07	-2.009041336
Eukaryotic Translation Elongation_ Homo sapiens_R-HSA-156842	86/89	1.25722E-23	3.34581E-21	1.38372E-08	1.23314E-06	-1.999543502
Formation of a pool of free 40S subunits_ Homo sapiens_R-HSA-72689	92/96	2.4287E-24	3.34581E-21	5.70686E-09	5.76393E-07	-1.957868628
Peptide chain elongation_Homo sapiens_ R-HSA-156902	82/84	1.3589E-23	3.34581E-21	2.22101E-08	1.68241E-06	-1.929389474
3' -UTR-mediated translational regulation_ Homo sapiens_R-HSA-157279	99/106	1.54592E-23	3.34581E-21	3.70094E-09	4.31302E-07	-1.920146677
L13a-mediated translational silencing of Ceruloplasmin expression_Homo sapiens_ R-HSA-156827	99/106	1.54592E-23	3.34581E-21	3.70094E-09	4.31302E-07	-1.912399155
Viral mRNA Translation_Homo sapiens_ R-HSA-192823	82/84	1.3589E-23	3.34581E-21	2.22101E-08	1.68241E-06	-1.891750904
Translation_Homo sapiens_R-HSA-72766	130/151	2.76224E-22	3.80436E-20	5.03854E-10	1.52668E-07	-1.958454231
Eukaryotic Translation Initiation_ Homo sapiens_R-HSA-72613	104/114	1.60554E-22	2.43239E-20	3.4968E-09	4.31302E-07	-1.923012872
Cap-dependent Translation Initiation_ Homo sapiens_R-HSA-72737	104/114	1.60554E-22	2.43239E-20	3.4968E-09	4.31302E-07	-1.915641643

Table B.45: Upregulated WikiPathways genesets in MCF7 shRNA2 clone in response to *CPT1A* knockdown, compared to non-silencing control.

Term	Overlap	P-value	Adjusted P-value	Old P-value	Old Adjusted P-value	Z-score	Combined Score
Cytoplasmic Ribosomal Proteins_ Homo sapiens_WP477	83/89	8.18475E-20	3.51944E-17	4.54913E-08	1.95613E-05	-2.0113747	76.20222514
Cytoplasmic Ribosomal Proteins_ Mus musculus_WP163	67/70	6.16048E-18	1.3245E-15	4.82532E-07	6.9163E-05	-2.003293795	68.62831615
mRNA processing_Mus musculus_WP310	243/398	2.52258E-07	3.61569E-05	1.75486E-07	3.77294E-05	-2.085306546	21.32776806
G1 to S cell cycle control_ Mus musculus_WP413	45/60	2.53034E-05	0.002720119	0.001446587	0.119065727	-1.940011093	11.45979987
DNA Replication_Mus musculus_WP150	32/40	4.2154E-05	0.003094645	0.003396209	0.171748397	-1.969978797	11.38269947
DNA Replication_Homo sapiens_WP466	33/42	6.26473E-05	0.003581782	0.003594734	0.171748397	-1.897031669	10.68388286
mRNA Processing_Homo sapiens_WP411	84/127	4.31811E-05	0.003094645	0.000357236	0.038402881	-1.834512826	10.59996595
G1 to S cell cycle control_Homo sapiens_WP45	49/68	6.66378E-05	0.003581782	0.001661382	0.119065727	-1.840388461	10.36487426
Eukaryotic Transcription Initiation_ Mus musculus_WP567	32/41	0.000102539	0.004899086	0.004401732	0.189274472	-1.65644524	8.810146393
Eukaryotic Transcription Initiation_ Homo sapiens_WP405	33/44	0.000307395	0.013217998	0.005890253	0.230255351	-1.74801357	7.562214112

Table B.46: Upregulated Panther genesets in MCF7 shRNA2 clone in response to *CPT1A* knockdown, compared to non-silencing control.

Term	Overlap	P-value	Adjusted P-value	Old P-value	Old Adjusted P-value	Z-score
De novo purine biosynthesis_ Homo sapiens_P02738	21/26	0.000746254	0.081341683	0.014467927	0.788502013	-1.358444089
General transcription regulation_ Homo sapiens_P00023	21/28	0.00395651	0.215629787	0.024367679	0.885358993	-1.172366804
Parkinson disease_Homo sapiens_P00049	50/81	0.011280384	0.307390454	0.011833181	0.788502013	-1.225262519
DNA replication_Homo sapiens_P00017	15/19	0.00671703	0.244052075	0.040747569	0.938002313	-0.783523762
p53 pathway by glucose deprivation_ Homo sapiens_P04397	15/21	0.028789294	0.523005512	0.067355288	0.938002313	-0.20233436
Transcription regulation by bZIP transcription factor_ Homo sapiens_P00055	25/42	0.100797916	0.999970119	0.081674827	0.938002313	-0.569379066
p53 pathway_Homo sapiens_P00059	38/71	0.232919593	0.999970119	0.097854295	0.938002313	-0.513332379
p53 pathway feedback loops 2_ Homo sapiens_P04398	24/45	0.308331551	0.999970119	0.166980689	0.938002313	-0.199277098
Cytoskeletal regulation by Rho GTPase_ Homo sapiens_P00016	35/70	0.447181621	0.999970119	0.177949311	0.938002313	0.550919768
Ubiquitin proteasome pathway_ Homo sapiens_P00060	22/43	0.421474418	0.999970119	0.221645709	0.938002313	0.750348403

Table B.47: Downregulated KEGG genesets in MCF7 shRNA2 clone in response to *CPT1A* knockdown, compared to non-silencing control.

Term	Overlap	P-value	Adjusted P-value	Old P-value	Old Adjusted P-value	Z-score	Combined Score
Ribosome_Homo sapiens_hsa03010	126/137	6.91217E-28	2.01144E-25	1.73597E-12	5.05167E-10	-1.746138049	99.29549519
Spliceosome_Homo sapiens_hsa03040	93/134	7.21871E-07	0.000105032	1.04478E-05	0.001013441	-1.77196951	16.23344317
RNA transport_Homo sapiens_ hsa03013	113/172	3.68639E-06	0.000343204	7.65662E-06	0.001013441	-1.818646653	14.50768105
Cell cycle_Homo sapiens_ hsa04110	85/124	4.71758E-06	0.000343204	3.41195E-05	0.002482194	-1.65735888	13.22105862
DNA replication_Homo sapiens_ hsa03030	28/36	0.000312529	0.018189207	0.004386834	0.208830265	-1.737606889	6.96246373
Parkinson's disease_Homo sapiens_ hsa05012	85/142	0.004169887	0.188152262	0.000885631	0.051543725	-1.648540408	2.75389292
Basal transcription factors_ Homo sapiens_hsa03022	31/45	0.004525999	0.188152262	0.009667627	0.281327937	-1.588514154	2.653618839
Nucleotide excision repair_ Homo sapiens_hsa03420	31/47	0.01185013	0.431048489	0.01468285	0.356059106	-1.562454789	1.314859908
Pyrimidine metabolism_ Homo sapiens_hsa00240	62/105	0.019106127	0.617764785	0.005152126	0.208830265	-1.571024109	0.756679837
Ribosome biogenesis in eukaryotes_ Homo sapiens_hsa03008	52/89	0.038113023	1	0.011322068	0.299520152	-1.709146788	2.16099E-10

Table B.48: Downregulated Reactome genesets in MCF7 shRNA2 clone in response to *CPT1A* knockdown, compared to non-silencing control

Term	Overlap	P-value	Adjusted P-value	Old P-value	Old Adjusted P-value	Z-score	Combined Score
GTP hydrolysis and joining of the 60S ribosomal subunit_Homo sapiens_R-HSA-72706	100/107	7.97753E-24	3.34581E-21	3.01917E-09	4.31302E-07	-2.009041336	94.71942382
Eukaryotic Translation Elongation_Homo sapiens_R-HSA-156842	86/89	1.25722E-23	3.34581E-21	1.38372E-08	1.23314E-06	-1.999543502	94.27163347
Formation of a pool of free 40S subunits_Homo sapiens_R-HSA-72689	92/96	2.4287E-24	3.34581E-21	5.70686E-09	5.76393E-07	-1.957868628	92.30680578
Peptide chain elongation_Homo sapiens_R-HSA-156902	82/84	1.3589E-23	3.34581E-21	2.22101E-08	1.68241E-06	-1.929389474	90.96411111
L13a-mediated translational silencing of Ceruloplasmin expression_Homo sapiens_R-HSA-156827	99/106	1.54592E-23	3.34581E-21	3.70094E-09	4.31302E-07	-1.920612299	90.55029736
3' -UTR-mediated translational regulation_Homo sapiens_R-HSA-157279	99/106	1.54592E-23	3.34581E-21	3.70094E-09	4.31302E-07	-1.911927886	90.14085698
Viral mRNA Translation_Homo sapiens_R-HSA-192823	82/84	1.3589E-23	3.34581E-21	2.22101E-08	1.68241E-06	-1.891750904	89.18958133
Translation_Homo sapiens_R-HSA-72766	130/151	2.76224E-22	3.80436E-20	5.03854E-10	1.52668E-07	-1.958454231	87.57336671
Eukaryotic Translation Initiation_Homo sapiens_R-HSA-72613	104/114	1.60554E-22	2.43239E-20	3.4968E-09	4.31302E-07	-1.923012872	86.84869966
Cap-dependent Translation Initiation_Homo sapiens_R-HSA-72737	104/114	1.60554E-22	2.43239E-20	3.4968E-09	4.31302E-07	-1.915641643	86.51579411

Table B.49: Downregulated WikiPathways genesets in MCF7 shRNA2 clone in response to *CPT1A* knockdown, compared to non-silencing control

Term	Overlap	P-value	Adjusted P-value	Old P-value	Old Adjusted P-value	Z-score
Cytoplasmic Ribosomal Proteins_ Homo sapiens_WP477	83/89	8.18475E-20	3.51944E-17	4.54913E-08	1.95613E-05	-2.0113747
Cytoplasmic Ribosomal Proteins_ Mus musculus_WP163	67/70	6.16048E-18	1.3245E-15	4.82532E-07	6.9163E-05	-2.003293795
mRNA processing_ Mus musculus_WP310	243/398	2.52258E-07	3.61569E-05	1.75486E-07	3.77294E-05	-2.085306546
G1 to S cell cycle control_ Mus musculus_WP413	45/60	2.53034E-05	0.002720119	0.001446587	0.119065727	-1.940011093
DNA Replication_ Mus musculus_WP150	32/40	4.2154E-05	0.003094645	0.003396209	0.171748397	-1.969978797
DNA Replication_ Homo sapiens_WP466	33/42	6.26473E-05	0.003581782	0.003594734	0.171748397	-1.897031669
mRNA Processing_ Homo sapiens_WP411	84/127	4.31811E-05	0.003094645	0.000357236	0.038402881	-1.834512826
G1 to S cell cycle control_ Homo sapiens_WP45	49/68	6.66378E-05	0.003581782	0.001661382	0.119065727	-1.840388461
Eukaryotic Transcription Initiation_ Mus musculus_WP567	32/41	0.000102539	0.004899086	0.004401732	0.189274472	-1.65644524
Eukaryotic Transcription Initiation_ Homo sapiens_WP405	33/44	0.000307395	0.013217998	0.005890253	0.230255351	-1.74801357

Table B.50: Downregulated Panther genesets in MCF7 shRNA2 clone in response to *CPT1A* knockdown, compared to non-silencing control.

Term	Overlap	P-value	Adjusted P-value	Old P-value	Old Adjusted P-value	Z-score
De novo purine biosynthesis_ Homo sapiens_P02738	21/26	0.000746254	0.081341683	0.014467927	0.788502013	-1.358444089
General transcription regulation_ Homo sapiens_P00023	21/28	0.00395651	0.215629787	0.024367679	0.885358993	-1.172366804
Parkinson disease_ Homo sapiens_P00049	50/81	0.011280384	0.307390454	0.011833181	0.788502013	-1.225262519
DNA replication_ Homo sapiens_P00017	15/19	0.00671703	0.244052075	0.040747569	0.938002313	-0.783523762
p53 pathway by glucose deprivation_ Homo sapiens_P04397	15/21	0.028789294	0.523005512	0.067355288	0.938002313	-0.20233436
Transcription regulation by bZIP transcription factor_Homo sapiens_P00055	25/42	0.100797916	0.999970119	0.081674827	0.938002313	-0.569379066
p53 pathway_Homo sapiens_P00059	38/71	0.232919593	0.999970119	0.097854295	0.938002313	-0.513332379
p53 pathway feedback loops 2_ Homo sapiens_P04398	24/45	0.308331551	0.999970119	0.166980689	0.938002313	-0.199277098
Cytoskeletal regulation by Rho GTPase_ Homo sapiens_P00016	35/70	0.447181621	0.999970119	0.177949311	0.938002313	0.550919768
Ubiquitin proteasome pathway_ Homo sapiens_P00060	22/43	0.421474418	0.999970119	0.221645709	0.938002313	0.750348403

Table B.51: Upregulated KEGG genesets in combined MCF7 shRNA1/2 clones in response to *CPT1A* knockdown, compared to non-silencing control.

Term	Overlap	P-value	Adjusted P-value	Old P-value	Old Adjusted P-value	Z-score	Combined Score
Lysosome_Homo sapiens_hsa04142	88/123	2.24603E-07	6.58087E-05	3.10185E-05	0.009088432	-1.774614657	17.08733556
Amino sugar and nucleotide sugar metabolism_ Homo sapiens_hsa00520	36/48	0.000187944	0.02753385	0.003805048	0.185813188	-1.81131231	6.506848047
Phosphatidylinositol signaling system_ Homo sapiens_hsa04070	63/98	0.001373239	0.13411963	0.002682742	0.185813188	-1.810830966	3.638001271
AGE-RAGE signaling pathway in diabetic complications_ Homo sapiens_hsa04933	64/101	0.002149576	0.157456456	0.003186436	0.185813188	-1.97638418	3.653556298
Vibrio cholerae infection_Homo sapiens_ hsa05110	35/51	0.003232521	0.189425719	0.011139313	0.293053561	-1.793071285	2.983237258
Pancreatic cancer_Homo sapiens_hsa05212	43/66	0.005271749	0.257437075	0.010004555	0.293053561	-1.826072629	2.477943958
Peroxisome_Homo sapiens_hsa04146	52/83	0.007455075	0.312048134	0.008587533	0.279571907	-1.537014262	1.790003471
Inositol phosphate metabolism_Homo sapiens_ hsa00562	45/71	0.009181836	0.33628474	0.012002194	0.293053561	-1.710345558	1.863929521
Glycosphingolipid biosynthesis - ganglio series_ Homo sapiens_hsa00604	Dec-15	0.013806674	0.449483929	0.059285871	0.468820253	-0.760944033	0.608492837
Steroid biosynthesis_Homo sapiens_hsa00100	15/20	0.015732393	0.460959108	0.05167766	0.458834978	-0.683126195	0.529044309

Table B.52: Upregulated Reactome genesets in combined MCF7 shRNA1/2 clones in response to *CPT1A* knockdown, compared to non-silencing control.

Term	Overlap	P-value	Adjusted P-value	Old P-value	Old Adjusted P-value	Z-score	Combined Score
Asparagine N-linked glycosylation_ Homo sapiens_ R-HSA-446203	159/259	2.64668E-05	0.040070706	1.76172E-05	0.026672516	-2.121468661	6.824997503
Synthesis of substrates in N-glycan biosythesis_ Homo sapiens_R-HSA-446219	46/63	7.66923E-05	0.058056094	0.001688897	0.426164972	-1.81102872	5.154813632
Biosynthesis of the N-glycan precursor (dolichol lipid-linked oligosaccharide, LLO) and transfer to a nascent protein_ Homo sapiens_R-HSA-446193	53/78	0.000467013	0.171322453	0.002436081	0.449360023	-1.768125582	3.119340958
XBP1(S) activates chaperone genes_ Homo sapiens_R-HSA-381038	38/53	0.000584691	0.171322453	0.005052062	0.640277931	-2.161209424	3.812822542
IRE1alpha activates chaperones_ Homo sapiens_R-HSA-381070	39/55	0.000710411	0.171322453	0.005182695	0.640277931	-2.167447676	3.823828115
Transferrin endocytosis and recycling_ Homo sapiens_R-HSA-917977	23/29	0.000736701	0.171322453	0.012012344	0.739952057	-2.442618736	4.309287046
PLC-gamma1 signalling_Homo sapiens_ R-HSA-167021	26/34	0.000905271	0.171322453	0.010747191	0.739952057	-2.139727618	3.774924171
EGFR interacts with phospholipase C-gamma_ Homo sapiens_R-HSA-212718	26/34	0.000905271	0.171322453	0.010747191	0.739952057	-2.063635305	3.640681519
PI Metabolism_Homo sapiens_ R-HSA-1483255	41/60	0.001686787	0.283755137	0.006630028	0.640277931	-1.873583396	2.360047348
DAG and IP3 signaling_Homo sapiens_ R-HSA-1489509	24/32	0.002270693	0.342169387	0.01622033	0.739952057	-2.025093153	2.171809897

Table B.53: Upregulated WikiPathways genesets in combined MCF7 shRNA1/2 clones in response to *CPT1A* knockdown, compared to non-silencing control.

Term	Overlap	P-value	Adjusted P-value	Old P-value	Old Adjusted P-value	Z-score	Combined Score
PodNet: protein-protein interactions in the podocyte_Mus musculus_WP2310	175/305	0.001446818	0.627918834	5.49766E-05	0.022844647	-2.162864775	1.006476939
Signaling Pathways in Glioblastoma_ Homo sapiens_WP2261	51/83	0.013482129	1	0.009771762	0.521287956	-2.237669845	1.18228E-10
Sphingolipid Metabolism_Homo sapiens_ WP1422	15/20	0.015732393	1	0.047859089	0.654261852	-1.583707823	8.36757E-11
EGF/EGFR Signaling Pathway_Homo sapiens_ WP437	93/163	0.020180071	1	0.003355621	0.398186745	-1.951731624	1.0312E-10
MicroRNAs in Cardiomyocyte Hypertrophy_ Mus musculus_WP1560	48/79	0.021232808	1	0.013740501	0.521287956	-1.884983292	9.95936E-11
B Cell Receptor Signaling Pathway_ Homo sapiens_WP23	57/97	0.030338356	1	0.01252088	0.521287956	-1.850270788	9.77596E-11
Alzheimers Disease_Mus musculus_WP2075	44/73	0.031640665	1	0.01947661	0.603774901	-1.728412911	9.13212E-11
Focal Adhesion_Mus musculus_WP85	103/185	0.034593957	1	0.003669924	0.398186745	-1.851387356	9.78186E-11
AGE/RAGE pathway_Homo sapiens_WP2324	40/66	0.035300789	1	0.023647899	0.654261852	-1.704540388	9.00599E-11
IL-6 signaling Pathway_Mus musculus_WP387	56/97	0.047326409	1	0.016834743	0.562021413	-1.698273366	8.97288E-11

Table B.54: Upregulated Panther genesets in combined MCF7 shRNA1/2 clones in response to *CPT1A* knockdown, compared to non-silencing control.

Term	Overlap	P-value	Adjusted P-value	Old P-value	Old Adjusted P-value	Z-score	Combined Score
VEGF signaling pathway_Homo sapiens_P00056	38/54	0.001048565	0.11534216	0.015208028	0.611135601	-1.793943603	3.874653156
EGF receptor signaling pathway_Homo sapiens_P00018	68/109	0.002833989	0.155869419	0.010995932	0.611135601	-1.66940221	3.102979127
Endothelin signaling pathway_Homo sapiens_P00019	48/75	0.005544637	0.203303369	0.022321367	0.613837593	-1.542643749	2.457517862
Histamine H1 receptor mediated signaling pathway_ Homo sapiens_P04385	19/26	0.010406202	0.280592934	0.059479348	0.883632738	-1.025293151	1.302994101
Integrin signalling pathway_Homo sapiens_P00034	90/156	0.015305069	0.280592934	0.016667335	0.611135601	-1.303494511	1.65654638
Angiogenesis_Homo sapiens_P00005	79/142	0.059305476	0.806294591	0.042141354	0.790809024	-1.08684955	0.234005344
CCKR signaling map ST_Homo sapiens_P06959	90/165	0.078562877	0.806294591	0.043135038	0.790809024	-0.944000829	0.203249142
Angiotensin II-stimulated signaling through G proteins and beta-arrestin_Homo sapiens_P05911	21/34	0.088814516	0.806294591	0.130314903	0.883632738	-0.298321917	0.06423053
PDGF signaling pathway_Homo sapiens_P00047	62/112	0.09576847	0.806294591	0.070794982	0.883632738	-0.599788747	0.129138179
5HT2 type receptor mediated signaling pathway_ Homo sapiens_P04374	27/46	0.114600182	0.806294591	0.131682467	0.883632738	-0.34297753	0.073845156

Table B.55: Downregulated KEGG genesets in combined MCF7 shRNA1/2 clones in response to *CPT1A* knockdown, compared to non-silencing control.

Term	Overlap	P-value	Adjusted P-value	Old P-value	Old Adjusted P-value	Z-score	Combined Score
Ribosome_Homo sapiens_hsa03010	119/137	6.62275E-21	1.9206E-18	4.94538E-11	1.43416E-08	-1.746138049	71.23177309
Spliceosome_Homo sapiens_hsa03040	93/134	1.06572E-06	0.000154529	7.38312E-06	0.001070552	-1.77196951	15.54925634
Cell cycle_Homo sapiens_hsa04110	78/124	0.001092335	0.098444481	0.000383934	0.02783518	-1.682638698	3.900798249
Ribosome biogenesis in eukaryotes_ Homo sapiens_hsa03008	58/89	0.001357855	0.098444481	0.001119012	0.054390246	-1.899051987	4.402501068
RNA transport_Homo sapiens_hsa03013	101/172	0.00569601	0.33036858	0.00037173	0.02783518	-1.770138112	1.960509985
Parkinson's disease_Homo sapiens_hsa05012	83/142	0.013292337	0.642462947	0.001312868	0.054390246	-1.648540408	0.729390331
Proteasome_Homo sapiens_hsa03050	29/44	0.016722931	0.660771892	0.016172561	0.360772507	-1.428779059	0.592009737
RNA polymerase_Homo sapiens_hsa03020	22/32	0.01822819	0.660771892	0.02481554	0.439585395	-1.455403339	0.603041417
Aminoacyl-tRNA biosynthesis_ Homo sapiens_hsa00970	40/66	0.036327753	1	0.014268045	0.344811081	-1.8367639	3.04467E-11
Non-alcoholic fatty liver disease (NAFLD)_ Homo sapiens_hsa04932	85/151	0.039398097	1	0.002574506	0.093325828	-1.704855833	2.82602E-11

Table B.56: Downregulated Reactome genesets in combined MCF7 shRNA1/2 clones in response to *CPT1A* knockdown, compared to non-silencing control.

Term	Overlap	P-value	Adjusted P-value	Old P-value	Old Adjusted P-value	Z-score	Combined Score
rRNA processing_Homo sapiens_ R-HSA-72312	156/180	9.24433E-27	1.39959E-23	5.32853E-12	4.0337E-09	-2.027505558	106.6939869
Major pathway of rRNA processing in the nucleolus_ Homo sapiens_R-HSA-6791226	143/166	4.57439E-24	3.46282E-21	5.53139E-11	2.79151E-08	-2.037037884	95.96934548
Formation of a pool of free 40S subunits_ Homo sapiens_ R-HSA-72689	91/96	8.87638E-23	4.47961E-20	8.63648E-09	1.42037E-06	-1.941052342	86.47808515
Eukaryotic Translation Elongation_Homo sapiens_ R-HSA-156842	85/89	5.18054E-22	1.96084E-19	2.11848E-08	2.00461E-06	-1.990699041	85.75084577
Peptide chain elongation_Homo sapiens_ R-HSA-156902	81/84	6.96612E-22	2.10934E-19	3.43376E-08	2.66682E-06	-1.929389474	82.9690374
Selenocysteine synthesis_Homo sapiens_ R-HSA-2408557	83/87	1.99879E-21	4.3231E-19	3.19524E-08	2.66682E-06	-1.896405961	80.18980111
3' -UTR-mediated translational regulation_ Homo sapiens_R-HSA-157279	97/106	4.55866E-21	7.66868E-19	9.26583E-09	1.42037E-06	-1.903709095	79.40745994
Eukaryotic Translation Termination_Homo sapiens_ R-HSA-72764	83/87	1.99879E-21	4.3231E-19	3.19524E-08	2.66682E-06	-1.871301154	79.12824073
L13a-mediated translational silencing of Ceruloplasmin expression_Homo sapiens_ R-HSA-156827	97/106	4.55866E-21	7.66868E-19	9.26583E-09	1.42037E-06	-1.895972865	79.08476656
GTP hydrolysis and joining of the 60S ribosomal subunit_ Homo sapiens_R-HSA-72706	97/107	2.53297E-20	3.19577E-18	1.26892E-08	1.42608E-06	-1.926919618	77.62538758

Table B.57: Downregulated WikiPathways genesets in combined MCF7 shRNA1/2 clones in response to *CPT1A* knockdown, compared to non-silencing control.

Term	Overlap	P-value	Adjusted P-value	Old P-value	Old Adjusted P-value	Z-score	Combined Score
Cytoplasmic Ribosomal Proteins_ Homo sapiens_WP477	82/89	1.78742E-18	7.70377E-16	1.21592E-07	2.6203E-05	-2.0113747	69.99513845
Cytoplasmic Ribosomal Proteins_ Mus musculus_WP163	66/70	1.73309E-16	3.7348E-14	1.20356E-06	0.000172912	-2.003293795	61.93883161
mRNA processing_Mus musculus_WP310	257/398	1.24745E-10	1.79217E-08	4.89349E-09	2.10909E-06	-2.085306546	37.19614645
mRNA Processing_Homo sapiens_WP411	92/127	5.00037E-08	5.3879E-06	2.61352E-05	0.002816073	-1.887785049	22.90139059
Eukaryotic Transcription Initiation_ Mus musculus_WP567	32/41	0.000121359	0.010461156	0.005140609	0.349353894	-1.839407237	8.387855786
Eukaryotic Transcription Initiation_ Homo sapiens_WP405	33/44	0.000361934	0.025998895	0.006870884	0.370168879	-1.921945268	7.014526011
Estrogen signalling_Mus musculus_WP1244	50/75	0.001358023	0.083615408	0.005673961	0.349353894	-1.843532654	4.574776925
Electron Transport Chain_Homo sapiens_WP111	65/103	0.002433063	0.131081283	0.004539666	0.349353894	-1.852053079	3.763256411
Electron Transport Chain_Mus musculus_WP295	57/93	0.010469932	0.410230973	0.011445818	0.411095628	-1.740970174	1.551265234
Parkin-Ubiquitin Proteasomal System pathway_ Homo sapiens_WP2359	44/70	0.012628775	0.442003101	0.018177901	0.602667343	-1.610054807	1.314510541

Table B.58: Downregulated Panther genesets in combined MCF7 shRNA1/2 clones in response to *CPT1A* knockdown, compared to non-silencing control.

Term	Overlap	P-value	Adjusted P-value	Old P-value	Old Adjusted P-value	Z-score	Combined Score
Parkinson disease_Homo sapiens_P00049	47/81	0.060971067	0.999997287	0.03533651	0.966152793	-1.225262519	3.32358E-06
p53 pathway by glucose deprivation_ Homo sapiens_P04397	16/21	0.010060774	0.999997287	0.046221371	0.966152793	-1.191689871	3.23252E-06
Ubiquitin proteasome pathway_ Homo sapiens_P00060	26/43	0.08453118	0.999997287	0.076099785	0.966152793	-0.831161838	2.25457E-06
p53 pathway_Homo sapiens_P00059	39/71	0.181576217	0.999997287	0.085281711	0.966152793	-0.717019375	1.94495E-06
De novo purine biosynthesis_ Homo sapiens_P02738	17/26	0.067279119	0.999997287	0.09189801	0.966152793	-0.63744213	1.72909E-06
De novo pyrimidine deoxyribonucleotide biosynthesis_Homo sapiens_P02739	08-Oct	0.046951944	0.999997287	0.12194085	0.966152793	-0.572919781	1.55407E-06
General transcription regulation_ Homo sapiens_P00023	17/28	0.142575263	0.999997287	0.131984363	0.966152793	-0.295620776	8.01885E-07
mRNA splicing_Homo sapiens_P00058	05-May	0.027774789	0.999997287	0.135392394	0.966152793	-0.11767251	3.19192E-07
Transcription regulation by bZIP transcription factor_Homo sapiens_P00055	22/42	0.379960786	0.999997287	0.211518388	0.966152793	-0.084844636	2.30145E-07
p53 pathway feedback loops 2_ Homo sapiens_P04398	23/45	0.437744233	0.999997287	0.23121077	0.966152793	-0.077799963	2.11036E-07

Table B.59: Datasets analysed for survival analysis in different cancer types.

Dataset ID	Number and brief annotation of samples	Platform
METABRIC	1981 breast tumours	Illumina HumanWG-6 v3.0
GSE20685	347 breast tumours	Affymetrix U133 Plus2
GSE21653	266 breast tumours	Affymetrix U133 Plus2
GSE22219	216 breast tumours	Illumina humanRef-8 v1.0
GSE25066	508 breast tumours	Affymetrix U133A
GSE41313	52 breast cancer cell lines	Affymetrix U133 PlusPM
GSE42568	104 breast cancers, 17 normal breast biopsies	Affymetrix U133 Plus2
GSE46563	94 breast cancers	Illumina HumanWG-6 v3.0
GSE45827	11 normal breast tissues, 130 breast cancers	Affymetrix U133 Plus2
GSE65904	177 melanomas	Illumina HumanHT-12 V4.0
TCGA breast cancer cohort (UCSC Cancer Browser)	776 breast tumours with complete clinical data	Illumina HiSeq 2000
TCGA clear cell renal cell carcinoma cohort (UCSC Cancer Browser)	588 kidney tumours with complete clinical data	Illumina HiSeq 2000
TCGA melanoma cohort (UCSC Cancer Browser)	396 melanomas with complete clinical data	Illumina HiSeq 2000

Table B.60: Datasets analysed for neoadjuvant treatment analysis.

Dataset ID	Number and brief annotation of samples	Platform
Neoadjuvant anti-oestrogen therapy		
GSE5462	51 pre- and post letrozole treatment biopsy samples	Affymetrix U133A
FAIMoS	102 pre- and post anastrozole treatment biopsy samples	Illumina HumanWG-6 v3.0
GSE27473	MCF7 basal vs ESR1 knockdown	Affymetrix U133 Plus2
Neoadjuvant chemotherapy		
GSE20194	278 breast tumours	Affymetrix U133A
GSE23988	61 breast tumours	Affymetrix U133A
GSE25066	508 breast tumours	Affymetrix U133A
GSE32646	115 breast tumours	Affymetrix U133 Plus2
GSE42822	91 breast tumours	Affymetrix U133A
Hess et. al. (UCSC Cancer Browser)	133 breast tumours	Affymetrix U133A

Table B.61: Datasets analysed for tumour-normal analysis.

Dataset ID	Number and brief annotation of samples	Platform
GSE10072	49 normal lung, 58 lung adenocarcinomas	Affymetrix U133A
GSE13507	10 normal bladder mucosa, 58 primary bladder tumour stroma, 163 primary bladder tumours, 23 recurrent bladder tumours	Illumina HumanWG-6 v2.0
GSE13911	31 normal adjacent gastric tissues, 39 gastric cancers	Affymetrix U133 Plus2
GSE15471	36 normal pancreatic, 36 pancreatic cancers	Affymetrix U133 Plus2
GSE17679	18 normal skeletal muscle, 88 Ewing sarcomas	Affymetrix U133 Plus2
GSE30784	45 normal oral tissues, 17 oral dysplasia, 167 oral cancers	Affymetrix U133 Plus2
GSE44076	50 healthy colorectal mucosa, 98 colorectal cancers	Affymetrix U219
GSE53757	72 normal renal tissue, 72 ccRCC tumours	Affymetrix U133 Plus2
GSE6631	49 normal head and neck mucosa, 58 head and neck cancers	Affymetrix U95v2
GSE6919	81 normal, 65 primary prostate tumours, 25 metastatic prostate tumours	Affymetrix U95v2
GSE9750	24 normal pancreas, 33 pancreatic cancers	Affymetrix U133A

Table B.62: Datasets analysed for EMT and cell differentiation analysis.

Dataset ID	Number and brief annotation of samples	Platform
GSE16194	Lung cancer cell lines panel with SNAIL1 overexpression	Affymetrix U133 Plus2
GSE16997	Mouse mammary stem, luminal progenitor and mature luminal cells	Illumina MouseWG-6 v3.0
GSE17708	A549 cells treated with TGFB	Affymetrix U133 Plus2
GSE19446	Four subpopulations of mammary cells based on cell surface markers	Illumina MouseWG-6 v2.0
GSE19679	II-18 lung cancer cell lines with SNAIL1 overexpression	Illumina HumanWG-6 v2.0
GSE20402	Mouse mammary stem and mature luminal cells	Illumina MouseWG-6 v2.0
GSE23952	Panc-1 cells treated wih TGFB	Affymetrix U133 Plus2
GSE28569	MCF10A cells treated with TGFB	Agilent G4112F
GSE29672	MCF7 cells transduced with SNAIL1 and SLUG transcription factors	Affymetrix U133 Plus2
GSE40374	M-BE bronchial epithelial cells treated with TGFB	Agilent G4112F
GSE40690	HMEC mammary cells transduced with SNAIL1, SLUG and SNAIL3 transcription factors	Illumina HumanHT-12 v4.0
GSE41113	HCT116 cells treated with increasing doses of sodium butyrate	Illumina HumanWG-6 v2.0
GSE41802	HCT116 cells with various IDH1/2 mutations	Affymetrix U133 Plus2
GSE424	CC-531 rat colon cancer cells treated with sodium butyrate	Affymetrix Rat Genome U34
GSE43495	HLME mammary cells transduced with SNAIL1, SLUG and TWIST transcription factors	Illumina HumanRef-8 v3.0
GSE4410	MCE310 mouse colon epithelia cells treated with sodium butyrate	Affymetrix Mouse Genome 430A
GSE47376	Mouse mammary stem, luminal progenitor and mature luminal cells	Affymetrix Mouse Genome 430 2.0
GSE48204	NMuMG mouse mammary gland cells treated with TGFB, or treated and then withdrawn	Affymetrix Mouse Genome 430 2.0
GSE49644	Lung cancer cell lines panel treated with TGFB	Affymetrix U133 Plus2
GSE58296	Mouse intestinal organoids treated with Tgfb ligand or Tgfbr inhibitor	Affymetrix Mouse Genome 430 2.0
GSE74377	MCF10A cells treated with TGFB	Illumina HiSeq 2500
GSE77594	Mouse bone marrow cells with IDH1 mutation or treated with 2-HG	Affymetrix Mouse Genome 430 2.0
GSE79642	Normal colon or adenoma organoids treated with TGFB	HT HG-U133 PlusPM
GSE8096	HMECS1 and HMEC184 differentiation time course	Affymetrix U133A

Table B.63: Datasets analysed for Wnt and MAPK signalling analysis.

Dataset ID	Number and brief annotation of samples	Platform
GSE18560	Ls174T cells with dominant-negative Tcf4 or beta catenin siRNA	Affymetrix U133 Plus2
GSE21576	Bcl9 wild type vs knockout mouse colon tissues	Affymetrix Mouse Genome 430 2.0
GSE12445	BL or 224 melanoma cells treated with siRNA against mutant NRAS	Affymetrix U133A
GSE13487	A375 melanoma cells treated with vemurafenib or with BRAF knockdown	Affymetrix U133 Plus2
GSE20051	SkMel-5 cells treated with BRAF inhibitor	Affymetrix U133A
GSE28467	Ls174T cells with dominant-negative Tcf4	Illumina MouseWG-6 v3.0
GSE35094	Ex vivo mouse intestinal organoid with Apc wildtype or knockout	Illumina MouseWG-6 v2.0
GSE35272	DLD1 cells transduced with DKK-1 expression vector	Affymetrix HuGene 1.0
GSE38007	Human melanoma cells with BRAF V600E, or BRAF V600E and MITF overexpression	Affymetrix U133A
GSE39904	SW480 cells with APC transgene or beta catenin siRNA	Affymetrix U133 Plus2
GSE39984	NRAS depletion vs AZD6244 in mouse melanoma	Affymetrix Mouse Genome 430 2.0
GSE42872	A375 melanoma cells treated with vemurafenib	Affymetrix HuGene 1.0
GSE43825	Mouse mammary hyperplasia and tumours tissue with constitutive beta-catenin activity	Affymetrix Mouse Genome 430 2.0
GSE44097	SW480 and DLD1 cells with beta catenin siRNA	Affymetrix U133 Plus2
GSE45757	Panels of pancreatic cancer cell lines treated with MEK1/2 inhibitor	Affymetrix U133A2
GSE45757	Panel of pancreatic cancer cell lines treated with MEK inhibitor	Affymetrix U133A
GSE46801	Human melanocytes transduced with empty vector or mutant BRAF	Affymetrix U133 Plus2
GSE50791	HT29 DMSO vs vemurafenib	Illumina HumanHT-12 v4.0
GSE55624	SW480 colorectal cancer cells treated with MEK inhibitor	Affymetrix U133 Plus2
GSE56896	Ls174T cells with dominant-negative TCF4 transgene	Affymetrix U133 Plus2
GSE60837	Healthy mouse colon with wildtype or Bcl9 knockout, Apc/Kras tumour with wildtype and Bcl9 knockout	Illumina HiSeq 2500
GSE61705	BS149 glioblastoma cells with MITF overexpression	Affymetrix HuGene 1.0
GSE62827	MELST with empty vector, NRAS Q61K, or KRAS V12	Illumina HumanHT-12 v4.0
GSE65461	Mouse small intestine from wild type or 5 day post Apc knock out	Affymetrix Mouse Genome 430 2.0
GSE67186	Colon polyps with basal and APC knockdown	Illumina HiSeq 2000
GSE67637 vemurafenib	Melmet5 melanoma cells treated with vehicle control or	Illumina HumanHT-12 v4.0
GSE71881	MaMel15 melanoma cells with siRNA against MITF	Illumina HumanHT-12 v4.0
GSE9580	Normal mouse intestinal epithelial and intestinal tumours from Apc +/1638N	Affymetrix Mouse Genome 430A

Table B.64: Datasets analysed for experimental analysis and RNA-Seq chapters.

Dataset ID	**Number and brief annotation of samples**	**Platform**
E-TABM-157	51 breast cancer cell lines	Affymetrix U133A
GSE41313	52 breast cancer cell lines	HT HG-U133 PlusPM
GSE57083	AstraZeneca: Cancer cell lines from many tissues, but only breast cancer cell lines were analysed	Affymetrix U133 Plus2
Cancer Cell Line Encyclopedia (source code available from cBioPortal)	Broad Institute/Novartis: Cancer cell lines from many tissues, but only breast cancer cell lines were analysed	Affymetrix U133 Plus2
GSE59735	NCI-H2347 cells treated with pioglitazone over a time course	Illumina HumanHT-12 v4.0
GSE75193	PC3 cells with PGC1A overexpression	Illumina HumanHT-12 v4.0

Appendix C

Supplementary Figures

Table C.1: Gene members of the MAPK, Wnt and EMT signatures analysed in this thesis.

MAPK signature

DUSP3, DUSP4, DUSP6, DUSP7, ELK1, MAPK1, MAPK11, MAPK14, MAPK3, MAPK7, MEF2A, PPP2CA, PPP2R1A, PPP2R1B, PPP2R5D, RPS6KA1, RPS6KA2, RPS6KA3, RPS6KA5

Wnt signature

CXCL5, ZIC2, CBX2, GLS2, BAG2, ZNF503, LEF1, NELF, HOXA11, CKLFSF7, LIMS1, SLC19A2, SCLY, HIRA, GPR172A, DOCK4, AMPD2, MAT2A, TPST2, PPIF, SLC5A19, SLC1A5, TIMM10, POLRMT, ITGB4BP, ZNF275, SFRS7, RBM12, UMPK

EMT signature

ADAM12, CDH2, CDH11, COL1A1, COL3A1, COL6A1, COL6A3, CTGF, CYP1B1, DLC1, FBLN1, FBLN5, FGF2, FGFR1, FN1, HAS2, LAMC2, LUM, MMP2, MYL9, NID2, NR2F1, NRP1, PLAT, PPA2B, PRKCA, RECK, SERPINE1, SERPINE2, SPOCK1, TGM2, TNFAIP6, TPM, VCAN, WNT5A, CDKN2C, EMP3, FBN1, IGFBP3, IL1R1, LTBP1, MME, PMP22, PTGER2, PTX3, SYNE1, TAGLN, TUBA1A, VIM, ZEB1, DCN, ABCA1, GALNT10, SLC22A4, C5ORF13. CDK14, EML1, FSTL1, LTBP2, MAP1B, RGS4, SYT11, TMEM158, SRGN, LOX

References

In:

Abdelmagid, S. A. et al. (2015). "Comprehensive profiling of plasma fatty acid concentrations in young healthy Canadian adults". In: *PLoS ONE* 10.2, e0116195.

Agathocleous, M. et al. (2012). "Metabolic differentiation in the embryonic retina". In: *Nat. Cell Biol.* 14.8, pp. 859–864.

Agrawal, N. et al. (2011). "Exome sequencing of head and neck squamous cell carcinoma reveals inactivating mutations in NOTCH1". In: *Science* 333.6046, pp. 1154–1157.

Ahler, E. et al. (2013). "Doxycycline alters metabolism and proliferation of human cell lines". In: *PLoS ONE* 8.5, e64561.

Ahluwalia, M. S. and H. A. Daw (2005). "Adjuvant docetaxel for node-positive breast cancer". In: *N. Engl. J. Med.* 353.9, pp. 954–955.

Ahmad, A. et al. (2011). "Phosphoglucose isomerase/autocrine motility factor mediates epithelial-mesenchymal transition regulated by miR-200 in breast cancer cells". In: *Cancer Res.* 71.9, pp. 3400–3409.

Akbani, R. et al. (2015). "Genomic Classification of Cutaneous Melanoma". In: *Cell* 161.7, pp. 1681–1696.

Al Saleh, S., F. Al Mulla, and Y. A. Luq (2011). "Estrogen receptor silencing induces epithelial to mesenchymal transition in human breast cancer cells". In: *PLoS ONE* 6.6, e20610.

Albain, K. S. et al. (2010). "Prognostic and predictive value of the 21-gene recurrence score assay in postmenopausal women with node-positive, oestrogen-receptor-positive breast cancer on chemotherapy: a retrospective analysis of a randomised trial". In: *Lancet Oncol.* 11.1, pp. 55–65.

Alberghina, L. and D. Gaglio (2014). "Redox control of glutamine utilization in cancer". In: *Cell Death Dis* 5, e1561.

Altman, B. J., Z. E. Stine, and C. V. Dang (2016). "From Krebs to clinic: glutamine metabolism to cancer therapy". In: *Nat. Rev. Cancer* 16.10, pp. 619–634.

Anastasiou, D. (2017). "Tumour microenvironment factors shaping the cancer metabolism landscape". In: *Br. J. Cancer* 116.3, pp. 277–286.

Ardlie, K. G. et al. (2015). "Human genomics. The Genotype-Tissue Expression (GTEx) pilot analysis: multitissue gene regulation in humans". In: *Science* 348.6235, pp. 648–660.

Azzolin, L. et al. (2012). "Role of TAZ as mediator of Wnt signaling". In: *Cell* 151.7, pp. 1443–1456.

Bacci, M. et al. (2016). "miR-155 Drives Metabolic Reprogramming of ER+ Breast Cancer Cells Following Long-Term Estrogen Deprivation and Predicts Clinical Response to Aromatase Inhibitors". In: *Cancer Res.* 76.6, pp. 1615–1626.

Bailey, P. et al. (2016). "Genomic analyses identify molecular subtypes of pancreatic cancer". In: *Nature* 531.7592, pp. 47–52.

Balaban, S. et al. (2017). "Adipocyte lipolysis links obesity to breast cancer growth: adipocyte-derived fatty acids drive breast cancer cell proliferation and migration". In: *Cancer Metab* 5, pp. 1–14.

Beck, C. W., B. Christen, and J. M. Slack (2003). "Molecular pathways needed for regeneration of spinal cord and muscle in a vertebrate". In: *Dev. Cell* 5.3, pp. 429–439.

Beck, C. W., J. C. Izpisua Belmonte, and B. Christen (2009). "Beyond early development: Xenopus as an emerging model for the study of regenerative mechanisms". In: *Dev. Dyn.* 238.6, pp. 1226–1248.

Bergstrom, J. et al. (1974). "Intracellular free amino acid concentration in human muscle tissue". In: *J Appl Physiol* 36.6, pp. 693–697.

Berkers, C. R. et al. (2013). "Metabolic regulation by p53 family members". In: *Cell Metab.* 18.5, pp. 617–633.

Bertos, N. R. and M. Park (2011). "Breast cancer - one term, many entities?" In: *J. Clin. Invest.* 121.10, pp. 3789–3796.

Bianchini, G. et al. (2013). "Proliferation and estrogen signaling can distinguish patients at risk for early versus late relapse among estrogen receptor positive breast cancers". In: *Breast Cancer Res.* 15.5, R86.

Birsoy, K. et al. (2015). "An Essential Role of the Mitochondrial Electron Transport Chain in Cell Proliferation Is to Enable Aspartate Synthesis". In: *Cell* 162.3, pp. 540–551.

Bland, J. M. and D. G. Altman (2004). "The logrank test". In: *BMJ* 328.7447, p. 1073.

Bloom, H. J. and W. W. Richardson (1957). "Histological grading and prognosis in breast cancer; a study of 1409 cases of which 359 have been followed for 15 years". In: *Br. J. Cancer* 11.3, pp. 359–377.

Bonnefoi, H. et al. (2014). "Pathological complete response after neoadjuvant chemotherapy is an independent predictive factor irrespective of simplified breast cancer in-

trinsic subtypes: a landmark and two-step approach analyses from the EORTC 10994/BIG 1-00 phase III trial". In: *Ann. Oncol.* 25.6, pp. 1128–1136.

Boroughs, L. K. and R. J. DeBerardinis (2015). "Metabolic pathways promoting cancer cell survival and growth". In: *Nat. Cell Biol.* 17.4, pp. 351–359.

Bosch, A. et al. (2010). "Triple-negative breast cancer: molecular features, pathogenesis, treatment and current lines of research". In: *Cancer Treat. Rev.* 36.3, pp. 206–215.

Brand, A. et al. (2016). "LDHA-Associated Lactic Acid Production Blunts Tumor Immunosurveillance by T and NK Cells". In: *Cell Metab.* 24.5, pp. 657–671.

Brannon, A. R. et al. (2014). "Comparative sequencing analysis reveals high genomic concordance between matched primary and metastatic colorectal cancer lesions". In: *Genome Biol.* 15.8, p. 454.

Brindle, K. (2008). "New approaches for imaging tumour responses to treatment". In: *Nat. Rev. Cancer* 8.2, pp. 94–107.

Bruce, C. R. et al. (2009). "Overexpression of carnitine palmitoyltransferase-1 in skeletal muscle is sufficient to enhance fatty acid oxidation and improve high-fat diet-induced insulin resistance". In: *Diabetes* 58.3, pp. 550–558.

Bryant, K. L. et al. (2014). "KRAS: feeding pancreatic cancer proliferation". In: *Trends Biochem. Sci.* 39.2, pp. 91–100.

Brzozowski, A. M. et al. (1997). "Molecular basis of agonism and antagonism in the oestrogen receptor". In: *Nature* 389.6652, pp. 753–758.

Burotto, M. et al. (2014). "The MAPK pathway across different malignancies: a new perspective". In: *Cancer* 120.22, pp. 3446–3456.

Buzzai, M. et al. (2005). "The glucose dependence of Akt-transformed cells can be reversed by pharmacologic activation of fatty acid beta-oxidation". In: *Oncogene* 24.26, pp. 4165–4173.

Camarda, R. et al. (2016). "Inhibition of fatty acid oxidation as a therapy for MYC-overexpressing triple-negative breast cancer". In: *Nat. Med.* 22.4, pp. 427–432.

Capell, B. C. et al. (2016). "MLL1 is essential for the senescence-associated secretory phenotype". In: *Genes Dev.* 30.3, pp. 321–336.

Carracedo, A., L. C. Cantley, and P. P. Pandolfi (2013). "Cancer metabolism: fatty acid oxidation in the limelight". In: *Nat. Rev. Cancer* 13.4, pp. 227–232.

Carracedo, A. et al. (2012). "A metabolic prosurvival role for PML in breast cancer". In: *J. Clin. Invest.* 122.9, pp. 3088–3100.

Carter, C. L., C. Allen, and D. E. Henson (1989). "Relation of tumor size, lymph node status, and survival in 24,740 breast cancer cases". In: *Cancer* 63.1, pp. 181–187.

Cerami, E. et al. (2012). "The cBio cancer genomics portal: an open platform for exploring multidimensional cancer genomics data". In: *Cancer Discov* 2.5, pp. 401–404.

Chandel, N. S. et al. (1997). "Cellular respiration during hypoxia. Role of cytochrome oxidase as the oxygen sensor in hepatocytes". In: *J. Biol. Chem.* 272.30, pp. 18808–18816.

Chaneton, B. et al. (2012). "Serine is a natural ligand and allosteric activator of pyruvate kinase M2". In: *Nature* 491.7424, pp. 458–462.

Chang, C. et al. (2013). "Id2 complexes with the SNAG domain of Snai1 inhibiting Snai1-mediated repression of integrin 4". In: *Mol. Cell. Biol.* 33.19, pp. 3795–3804.

Chang, J. T. and J. R. Nevins (2006). "GATHER: a systems approach to interpreting genomic signatures". In: *Bioinformatics* 22.23, pp. 2926–2933.

Chapman, P. B. et al. (2011). "Improved survival with vemurafenib in melanoma with BRAF V600E mutation". In: *N. Engl. J. Med.* 364.26, pp. 2507–2516.

Chaturvedi, A. et al. (2016). "Enantiomer-specific and paracrine leukemogenicity of mutant IDH metabolite 2-hydroxyglutarate". In: *Leukemia* 30.8, pp. 1708–1715.

Chen, E. Y. et al. (2013). "Enrichr: interactive and collaborative HTML5 gene list enrichment analysis tool". In: *BMC Bioinformatics* 14, p. 128.

Chen, H. C. et al. (2012). "Wnt signaling induces epithelial-mesenchymal transition with proliferation in ARPE-19 cells upon loss of contact inhibition". In: *Lab. Invest.* 92.5, pp. 676–687.

Chen, W. et al. (2016). "Targeting renal cell carcinoma with a HIF-2 antagonist". In: *Nature* 539.7627, pp. 112–117.

Cheong, J. H. et al. (2011). "Dual inhibition of tumor energy pathway by 2-deoxyglucose and metformin is effective against a broad spectrum of preclinical cancer models". In: *Mol. Cancer Ther.* 10.12, pp. 2350–2362.

Chiaradonna, F. et al. (2006). "Ras-dependent carbon metabolism and transformation in mouse fibroblasts". In: *Oncogene* 25.39, pp. 5391–5404.

Chicco, A. J. and G. C. Sparagna (2007). "Role of cardiolipin alterations in mitochondrial dysfunction and disease". In: *Am. J. Physiol., Cell Physiol.* 292.1, pp. 33–44.

Cho, H. et al. (2016). "On-target efficacy of a HIF-2 antagonist in preclinical kidney cancer models". In: *Nature* 539.7627, pp. 107–111.

Chung, S. et al. (2007). "Mitochondrial oxidative metabolism is required for the cardiac differentiation of stem cells". In: *Nat Clin Pract Cardiovasc Med* 4 Suppl 1, S60–67.

Cianfrocca, M. and L. J. Goldstein (2004). "Prognostic and predictive factors in early-stage breast cancer". In: *Oncologist* 9.6, pp. 606–616.

Cirenajwis, H. et al. (2015). "Molecular stratification of metastatic melanoma using gene expression profiling: Prediction of survival outcome and benefit from molecular targeted therapy". In: *Oncotarget* 6.14, pp. 12297–12309.

Claypool, S. M. and C. M. Koehler (2012). "The complexity of cardiolipin in health and disease". In: *Trends Biochem. Sci.* 37.1, pp. 32–41.

Contesso, G. et al. (1987). "The importance of histologic grade in long-term prognosis of breast cancer: a study of 1,010 patients, uniformly treated at the Institut Gustave-Roussy". In: *J. Clin. Oncol.* 5.9, pp. 1378–1386.

Creighton, C. J. et al. (2013). "Comprehensive molecular characterization of clear cell renal cell carcinoma". In: *Nature* 499.7456, pp. 43–49.

Croft, D. et al. (2014). "The Reactome pathway knowledgebase". In: *Nucleic Acids Res.* 42.Database issue, pp. D472–477.

Cross, D. and J. K. Burmester (2004). "The promise of molecular profiling for cancer identification and treatment". In: *Clin Med Res* 2.3, pp. 147–150.

Cruz, F. D. and I. Matushansky (2012). "Solid tumor differentiation therapy - is it possible?" In: *Oncotarget* 3.5, pp. 559–567.

Cui, R. et al. (2007). "Central role of p53 in the suntan response and pathologic hyperpigmentation". In: *Cell* 128.5, pp. 853–864.

Currie, E. et al. (2013). "Cellular fatty acid metabolism and cancer". In: *Cell Metab.* 18.2, pp. 153–161.

Curtis, C. et al. (2012). "The genomic and transcriptomic architecture of 2,000 breast tumours reveals novel subgroups". In: *Nature* 486.7403, pp. 346–352.

Cuzick, J. et al. (2010). "Effect of anastrozole and tamoxifen as adjuvant treatment for early-stage breast cancer: 10-year analysis of the ATAC trial". In: *Lancet Oncol.* 11.12, pp. 1135–1141.

Dalmau, N. et al. (2015). "Epithelial-to-mesenchymal transition involves triacylglycerol accumulation in DU145 prostate cancer cells". In: *Mol Biosyst* 11.12, pp. 3397–3406.

Davidson, S. M. et al. (2016). "Environment Impacts the Metabolic Dependencies of Ras-Driven Non-Small Cell Lung Cancer". In: *Cell Metab.* 23.3, pp. 517–528.

Davies, C. et al. (2011). "Relevance of breast cancer hormone receptors and other factors to the efficacy of adjuvant tamoxifen: patient-level meta-analysis of randomised trials". In: *Lancet* 378.9793, pp. 771–784.

Dawood, S. et al. (2010). "Prognosis of women with metastatic breast cancer by HER2 status and trastuzumab treatment: an institutional-based review". In: *J. Clin. Oncol.* 28.1, pp. 92–98.

Dawson, S. J. et al. (2013). "A new genome-driven integrated classification of breast cancer and its implications". In: *EMBO J.* 32.5, pp. 617–628.

De Craene, B. and G. Berx (2013). "Regulatory networks defining EMT during cancer initiation and progression". In: *Nat. Rev. Cancer* 13.2, pp. 97–110.

DeBerardinis, R. J. and T. Cheng (2010). "Q's next: the diverse functions of glutamine in metabolism, cell biology and cancer". In: *Oncogene* 29.3, pp. 313–324.

Deberardinis, R. J., J. J. Lum, and C. B. Thompson (2006). "Phosphatidylinositol 3-kinase-dependent modulation of carnitine palmitoyltransferase 1A expression regulates lipid metabolism during hematopoietic cell growth". In: *J. Biol. Chem.* 281.49, pp. 37372–37380.

DeBerardinis, R. J. et al. (2007). "Beyond aerobic glycolysis: transformed cells can engage in glutamine metabolism that exceeds the requirement for protein and nucleotide synthesis". In: *Proc. Natl. Acad. Sci. U.S.A.* 104.49, pp. 19345–19350.

DeBerardinis, R. J. et al. (2008). "The biology of cancer: metabolic reprogramming fuels cell growth and proliferation". In: *Cell Metab.* 7.1, pp. 11–20.

Deep, G. and I. R. Schlaepfer (2016). "Aberrant Lipid Metabolism Promotes Prostate Cancer: Role in Cell Survival under Hypoxia and Extracellular Vesicles Biogenesis". In: *Int J Mol Sci* 17.7.

DeGrado, T. R. et al. (2010). "Synthesis and preliminary evaluation of 18-(18)F-fluoro-4-thia-oleate as a PET probe of fatty acid oxidation". In: *J. Nucl. Med.* 51.8, pp. 1310–1317.

Derwinger, K. et al. (2010). "Tumour differentiation grade is associated with TNM staging and the risk of node metastasis in colorectal cancer". In: *Acta Oncol* 49.1, pp. 57–62.

Deshiere, A. et al. (2013). "Unbalanced expression of CK2 kinase subunits is sufficient to drive epithelial-to-mesenchymal transition by Snail1 induction". In: *Oncogene* 32.11, pp. 1373–1383.

Desmedt, C. et al. (2007). "Strong time dependence of the 76-gene prognostic signature for node-negative breast cancer patients in the TRANSBIG multicenter independent validation series". In: *Clin. Cancer Res.* 13.11, pp. 3207–3214.

Desmedt, C. et al. (2008). "Biological processes associated with breast cancer clinical outcome depend on the molecular subtypes". In: *Clin. Cancer Res.* 14.16, pp. 5158–5165.

Dey, N. et al. (2013). "Wnt signaling in triple negative breast cancer is associated with metastasis". In: *BMC Cancer* 13, p. 537.

Dhasarathy, A. et al. (2011). "The transcription factors Snail and Slug activate the transforming growth factor-beta signaling pathway in breast cancer". In: *PLoS ONE* 6.10, e26514.

Dhomen, N. et al. (2009). "Oncogenic Braf induces melanocyte senescence and melanoma in mice". In: *Cancer Cell* 15.4, pp. 294–303.

Dieci, M. V. et al. (2013). "Fibroblast growth factor receptor inhibitors as a cancer treatment: from a biologic rationale to medical perspectives". In: *Cancer Discov* 3.3, pp. 264–279.

Diest, P. J. van, E. van der Wall, and J. P. Baak (2004). "Prognostic value of proliferation in invasive breast cancer: a review". In: *J. Clin. Pathol.* 57.7, pp. 675–681.

Donato, J., R. Frazao, and C. F. Elias (2010). "The PI3K signaling pathway mediates the biological effects of leptin". In: *Arq Bras Endocrinol Metabol* 54.7, pp. 591–602.

Doria, M. L. et al. (2014). "Fatty acid and phospholipid biosynthetic pathways are regulated throughout mammary epithelial cell differentiation and correlate to breast cancer survival". In: *FASEB J.* 28.10, pp. 4247–4264.

Dorr, J. R. et al. (2013). "Synthetic lethal metabolic targeting of cellular senescence in cancer therapy". In: *Nature* 501.7467, pp. 421–425.

Dow, L. E. et al. (2015). "Apc Restoration Promotes Cellular Differentiation and Reestablishes Crypt Homeostasis in Colorectal Cancer". In: *Cell* 161.7, pp. 1539–1552.

Dowsett, M. et al. (2008). "Relationship between quantitative estrogen and progesterone receptor expression and human epidermal growth factor receptor 2 (HER-2) status with recurrence in the Arimidex, Tamoxifen, Alone or in Combination trial". In: *J. Clin. Oncol.* 26.7, pp. 1059–1065.

Dowsett, M. et al. (2010). "Meta-analysis of breast cancer outcomes in adjuvant trials of aromatase inhibitors versus tamoxifen". In: *J. Clin. Oncol.* 28.3, pp. 509–518.

Dowsett, M. et al. (2013). "Comparison of PAM50 risk of recurrence score with oncotype DX and IHC4 for predicting risk of distant recurrence after endocrine therapy". In: *J. Clin. Oncol.* 31.22, pp. 2783–2790.

Drummond, C. G., C. A. Nickerson, and C. B. Coyne (2016). "A Three-Dimensional Cell Culture Model To Study Enterovirus Infection of Polarized Intestinal Epithelial Cells". In: *mSphere* 1.1.

Du, S. et al. (2014). "Fructose-bisphosphate aldolase a is a potential metastasis-associated marker of lung squamous cell carcinoma and promotes lung cell tumorigenesis and migration". In: *PLoS ONE* 9.1, e85804.

Duchartre, Y., Y. M. Kim, and M. Kahn (2016). "The Wnt signaling pathway in cancer". In: *Crit. Rev. Oncol. Hematol.* 99, pp. 141–149.

Dueregger, A. et al. (2015). "Differential Utilization of Dietary Fatty Acids in Benign and Malignant Cells of the Prostate". In: *PLoS ONE* 10.8, e0135704.

Dutertre, M. and C. L. Smith (2000). "Molecular mechanisms of selective estrogen receptor modulator (SERM) action". In: *J. Pharmacol. Exp. Ther.* 295.2, pp. 431–437.

Duvel, K. et al. (2010). "Activation of a metabolic gene regulatory network downstream of mTOR complex 1". In: *Mol. Cell* 39.2, pp. 171–183.

Eales, K. L., K. E. Hollinshead, and D. A. Tennant (2016). "Hypoxia and metabolic adaptation of cancer cells". In: *Oncogenesis* 5, e190.

EBCTCG (1998). "Tamoxifen for early breast cancer: an overview of the randomised trials. Early Breast Cancer Trialists' Collaborative Group". In: *Lancet* 351.9114, pp. 1451–1467.

EBCTCGb (2005). "Effects of chemotherapy and hormonal therapy for early breast cancer on recurrence and 15-year survival: an overview of the randomised trials". In: *Lancet* 365.9472, pp. 1687–1717.

Edmond, V. et al. (2015). "Downregulation of ceramide synthase-6 during epithelial-to-mesenchymal transition reduces plasma membrane fluidity and cancer cell motility". In: *Oncogene* 34.8, pp. 996–1005.

Ellis, M. J. et al. (2001). "Letrozole is more effective neoadjuvant endocrine therapy than tamoxifen for ErbB-1- and/or ErbB-2-positive, estrogen receptor-positive primary breast cancer: evidence from a phase III randomized trial". In: *J. Clin. Oncol.* 19.18, pp. 3808–3816.

Elsheikh, S. et al. (2008). "CCND1 amplification and cyclin D1 expression in breast cancer and their relation with proteomic subgroups and patient outcome". In: *Breast Cancer Res. Treat.* 109.2, pp. 325–335.

Elstrom, R. L. et al. (2004). "Akt stimulates aerobic glycolysis in cancer cells". In: *Cancer Res.* 64.11, pp. 3892–3899.

Enjoji, M. et al. (2016). "Intracellular mechanisms underlying lipid accumulation (white opaque substance) in gastric epithelial neoplasms: A pilot study of expression profiles of lipid-metabolism-associated genes". In: *J. Gastroenterol. Hepatol.* 31.4, pp. 776–781.

Epstein, A. C. et al. (2001). "C. elegans EGL-9 and mammalian homologs define a family of dioxygenases that regulate HIF by prolyl hydroxylation". In: *Cell* 107.1, pp. 43–54.

Eroles, P. et al. (2012). "Molecular biology in breast cancer: intrinsic subtypes and signaling pathways". In: *Cancer Treat. Rev.* 38.6, pp. 698–707.

Esen, E. et al. (2013). "WNT-LRP5 signaling induces Warburg effect through mTORC2 activation during osteoblast differentiation". In: *Cell Metab.* 17.5, pp. 745–755.

Eskandarpour, M. et al. (2009). "Oncogenic NRAS has multiple effects on the malignant phenotype of human melanoma cells cultured in vitro". In: *Int. J. Cancer* 124.1, pp. 16–26.

Fabregat, A. et al. (2016). "The Reactome pathway Knowledgebase". In: *Nucleic Acids Res.* 44.D1, pp. D481–487.

Fan, J. et al. (2013). "Glutamine-driven oxidative phosphorylation is a major ATP source in transformed mammalian cells in both normoxia and hypoxia". In: *Mol. Syst. Biol.* 9, p. 712.

Faubert, B. et al. (2014). "Loss of the tumor suppressor LKB1 promotes metabolic reprogramming of cancer cells via HIF-1". In: *Proc. Natl. Acad. Sci. U.S.A.* 111.7, pp. 2554–2559.

Fessler, E. et al. (2016). "TGF signaling directs serrated adenomas to the mesenchymal colorectal cancer subtype". In: *EMBO Mol Med* 8.7, pp. 745–760.

Fischer, J. M. et al. (2016). "Single cell lineage tracing reveals a role for TgfR2 in intestinal stem cell dynamics and differentiation". In: *Proc. Natl. Acad. Sci. U.S.A.* 113.43, pp. 12192–12197.

Fiske, B. P. and M. G. Vander Heiden (2012). "Seeing the Warburg effect in the developing retina". In: *Nat. Cell Biol.* 14.8, pp. 790–791.

Flaherty, K. T. et al. (2012). "Combined BRAF and MEK inhibition in melanoma with BRAF V600 mutations". In: *N. Engl. J. Med.* 367.18, pp. 1694–1703.

Fletcher, M. et al. (2015). "l-Arginine depletion blunts antitumor T-cell responses by inducing myeloid-derived suppressor cells". In: *Cancer Res.* 75.2, pp. 275–283.

Flier, L. G. Van der et al. (2007). "The Intestinal Wnt/TCF Signature". In: *Gastroenterology* 132.2, pp. 628–632.

Folmes, C. D. et al. (2011). "Somatic oxidative bioenergetics transitions into pluripotency-dependent glycolysis to facilitate nuclear reprogramming". In: *Cell Metab.* 14.2, pp. 264–271.

Folmes, C. D. et al. (2012). "Metabolic plasticity in stem cell homeostasis and differentiation". In: *Cell Stem Cell* 11.5, pp. 596–606.

Fournier, M. V. et al. (2006). "Gene expression signature in organized and growth-arrested mammary acini predicts good outcome in breast cancer". In: *Cancer Res.* 66.14, pp. 7095–7102.

Fu, Q. F. et al. (2015). "Alpha-enolase promotes cell glycolysis, growth, migration, and invasion in non-small cell lung cancer through FAK-mediated PI3K/AKT pathway". In: *J Hematol Oncol* 8, p. 22.

Fukushima, H. et al. (2001). "Frequent alterations of the beta-catenin and TCF-4 genes, but not of the APC gene, in colon cancers with high-frequency microsatellite instability". In: *J. Exp. Clin. Cancer Res.* 20.4, pp. 553–559.

Gaglio, D. et al. (2009). "Glutamine deprivation induces abortive s-phase rescued by deoxyribonucleotides in k-ras transformed fibroblasts". In: *PLoS ONE* 4.3, e4715.

Gameiro, P. A. et al. (2013). "In vivo HIF-mediated reductive carboxylation is regulated by citrate levels and sensitizes VHL-deficient cells to glutamine deprivation". In: *Cell Metab.* 17.3, pp. 372–385.

Gao, J. et al. (2013). "Integrative analysis of complex cancer genomics and clinical profiles using the cBioPortal". In: *Sci Signal* 6.269, pl1.

Garcia-Cao, I. et al. (2012). "Systemic elevation of PTEN induces a tumor-suppressive metabolic state". In: *Cell* 149.1, pp. 49–62.

Garibyan, L. and D. E. Fisher (2010). "How sunlight causes melanoma". In: *Curr Oncol Rep* 12.5, pp. 319–326.

Garraway, L. A. et al. (2005). "Integrative genomic analyses identify MITF as a lineage survival oncogene amplified in malignant melanoma". In: *Nature* 436.7047, pp. 117–122.

Gaspar, C. et al. (2008). "Cross-species comparison of human and mouse intestinal polyps reveals conserved mechanisms in adenomatous polyposis coli (APC)-driven tumorigenesis". In: *Am. J. Pathol.* 172.5, pp. 1363–1380.

Gatza, M. L. et al. (2014). "An integrated genomics approach identifies drivers of proliferation in luminal-subtype human breast cancer". In: *Nat. Genet.* 46.10, pp. 1051–1059.

Gaude, E. and C. Frezza (2016). "Tissue-specific and convergent metabolic transformation of cancer correlates with metastatic potential and patient survival". In: *Nat Commun* 7, p. 13041.

Geisler, J. et al. (2002). "Influence of letrozole and anastrozole on total body aromatization and plasma estrogen levels in postmenopausal breast cancer patients evaluated in a randomized, cross-over study". In: *J. Clin. Oncol.* 20.3, pp. 751–757.

Germann, A. et al. (2003). "Expression profiling of CC531 colon carcinoma cells reveals similar regulation of beta-catenin target genes by both butyrate and aspirin". In: *Int. J. Cancer* 106.2, pp. 187–197.

Ghuwalewala, S. et al. (2016). "CD44(high)CD24(low) molecular signature determines the Cancer Stem Cell and EMT phenotype in Oral Squamous Cell Carcinoma". In: *Stem Cell Res* 16.2, pp. 405–417.

Gilchrist, K. W. et al. (1985). "Interobserver reproducibility of histopathological features in stage II breast cancer. An ECOG study". In: *Breast Cancer Res. Treat.* 5.1, pp. 3–10.

Goding, C. R. (2011). "Commentary. A picture of Mitf in melanoma immortality". In: *Oncogene* 30.20, pp. 2304–2306.

Goncalves, R. and R. Bose (2013). "Using multigene tests to select treatment for early-stage breast cancer". In: *J Natl Compr Canc Netw* 11.2, pp. 174–182.

Gonzalez, C. (2013). "Drosophila melanogaster: a model and a tool to investigate malignancy and identify new therapeutics". In: *Nat. Rev. Cancer* 13.3, pp. 172–183.

Gras, B. et al. (2014). "Snail family members unequally trigger EMT and thereby differ in their ability to promote the neoplastic transformation of mammary epithelial cells". In: *PLoS ONE* 9.3, e92254.

Grassian, A. R. et al. (2012). "Isocitrate dehydrogenase (IDH) mutations promote a reversible ZEB1/microRNA (miR)-200-dependent epithelial-mesenchymal transition (EMT)". In: *J. Biol. Chem.* 287.50, pp. 42180–42194.

Grese, T. A. et al. (1997). "Molecular determinants of tissue selectivity in estrogen receptor modulators". In: *Proc. Natl. Acad. Sci. U.S.A.* 94.25, pp. 14105–14110.

Griner, E. M. and M. G. Kazanietz (2007). "Protein kinase C and other diacylglycerol effectors in cancer". In: *Nat. Rev. Cancer* 7.4, pp. 281–294.

Groger, C. J. et al. (2012). "Meta-analysis of gene expression signatures defining the epithelial to mesenchymal transition during cancer progression". In: *PLoS ONE* 7.12, e51136.

Guan, F., K. Handa, and S. I. Hakomori (2009). "Specific glycosphingolipids mediate epithelial-to-mesenchymal transition of human and mouse epithelial cell lines". In: *Proc. Natl. Acad. Sci. U.S.A.* 106.18, pp. 7461–7466.

Guo, G. et al. (2013). "Whole-genome and whole-exome sequencing of bladder cancer identifies frequent alterations in genes involved in sister chromatid cohesion and segregation". In: *Nat. Genet.* 45.12, pp. 1459–1463.

Gupta, R. et al. (2016). "Interferon alpha-inducible protein 6 regulates NRASQ61K-induced melanomagenesis and growth". In: *Elife* 5.

Gustafsson, J. A. (1999). "Estrogen receptor beta–a new dimension in estrogen mechanism of action". In: *J. Endocrinol.* 163.3, pp. 379–383.

Gyorffy, B. et al. (2015). "Multigene prognostic tests in breast cancer: past, present, future". In: *Breast Cancer Res.* 17, p. 11.

Gysin, S., J. Paquette, and M. McMahon (2012). "Analysis of mRNA profiles after MEK1/2 inhibition in human pancreatic cancer cell lines reveals pathways involved in drug sensitivity". In: *Mol. Cancer Res.* 10.12, pp. 1607–1619.

Haibe-Kains, B. et al. (2008). "Comparison of prognostic gene expression signatures for breast cancer". In: *BMC Genomics* 9, p. 394.

Haider, S. et al. (2016). "Genomic alterations underlie a pan-cancer metabolic shift associated with tumour hypoxia". In: *Genome Biol.* 17.1, p. 140.

Hall, A. et al. (2013). "Dysfunctional oxidative phosphorylation makes malignant melanoma cells addicted to glycolysis driven by the (V600E)BRAF oncogene". In: *Oncotarget* 4.4, pp. 584–599.

Halldorsson, S. et al. (2017). "Metabolic re-wiring of isogenic breast epithelial cell lines following epithelial to mesenchymal transition". In: *Cancer Lett.* 396, pp. 117–129.

Hamabe, A. et al. (2014). "Role of pyruvate kinase M2 in transcriptional regulation leading to epithelial-mesenchymal transition". In: *Proc. Natl. Acad. Sci. U.S.A.* 111.43, pp. 15526–15531.

Hammerman, P. S. et al. (2012). "Comprehensive genomic characterization of squamous cell lung cancers". In: *Nature* 489.7417, pp. 519–525.

Hanahan, D. (2014). "Rethinking the war on cancer". In: *Lancet* 383.9916, pp. 558–563.

Hanahan, D. and R. A. Weinberg (2011). "Hallmarks of cancer: the next generation". In: *Cell* 144.5, pp. 646–674.

Haq, R. et al. (2013). "Oncogenic BRAF regulates oxidative metabolism via PGC1 and MITF". In: *Cancer Cell* 23.3, pp. 302–315.

Hardy, S. et al. (2003). "Saturated fatty acid-induced apoptosis in MDA-MB-231 breast cancer cells. A role for cardiolipin". In: *J. Biol. Chem.* 278.34, pp. 31861–31870.

Harris, H. (2005). "A long view of fashions in cancer research". In: *Bioessays* 27.8, pp. 833–838.

Hatzis, C. et al. (2011). "A genomic predictor of response and survival following taxane-anthracycline chemotherapy for invasive breast cancer". In: *JAMA* 305.18, pp. 1873–1881.

Hatzivassiliou, G. et al. (2005). "ATP citrate lyase inhibition can suppress tumor cell growth". In: *Cancer Cell* 8.4, pp. 311–321.

Hay, N. (2016). "Reprogramming glucose metabolism in cancer: can it be exploited for cancer therapy?" In: *Nat. Rev. Cancer* 16.10, pp. 635–649.

He, S., D. Nakada, and S. J. Morrison (2009). "Mechanisms of stem cell self-renewal". In: *Annu. Rev. Cell Dev. Biol.* 25, pp. 377–406.

Helleday, T., S. Eshtad, and S. Nik-Zainal (2014). "Mechanisms underlying mutational signatures in human cancers". In: *Nat. Rev. Genet.* 15.9, pp. 585–598.

Henique, C. et al. (2010). "Increased mitochondrial fatty acid oxidation is sufficient to protect skeletal muscle cells from palmitate-induced apoptosis". In: *J. Biol. Chem.* 285.47, pp. 36818–36827.

Henry, N. L. and D. F. Hayes (2007). "Can biology trump anatomy? Do all node-positive patients with breast cancer need chemotherapy?" In: *J. Clin. Oncol.* 25.18, pp. 2501–2503.

Herbst, A. et al. (2014). "Comprehensive analysis of -catenin target genes in colorectal carcinoma cell lines with deregulated Wnt/-catenin signaling". In: *BMC Genomics* 15, p. 74.

Herr, R. et al. (2015). "B-Raf inhibitors induce epithelial differentiation in BRAF-mutant colorectal cancer cells". In: *Cancer Res.* 75.1. [DOI:10.1158/0008-5472.CAN-13-3686] [PubMed:25381152], pp. 216–229.

Herschkowitz, J. I. et al. (2008). "The functional loss of the retinoblastoma tumour suppressor is a common event in basal-like and luminal B breast carcinomas". In: *Breast Cancer Res.* 10.5, R75.

Hess, K. R. et al. (2006). "Pharmacogenomic predictor of sensitivity to preoperative chemotherapy with paclitaxel and fluorouracil, doxorubicin, and cyclophosphamide in breast cancer". In: *J. Clin. Oncol.* 24.26, pp. 4236–4244.

Heuvel, A. P. van den et al. (2012). "Analysis of glutamine dependency in non-small cell lung cancer: GLS1 splice variant GAC is essential for cancer cell growth". In: *Cancer Biol. Ther.* 13.12, pp. 1185–1194.

Hilsenbeck, S. G. et al. (1998). "Time-dependence of hazard ratios for prognostic factors in primary breast cancer". In: *Breast Cancer Res. Treat.* 52.1-3, pp. 227–237.

Hilvo, M. et al. (2011). "Novel theranostic opportunities offered by characterization of altered membrane lipid metabolism in breast cancer progression". In: *Cancer Res.* 71.9, pp. 3236–3245.

Ho, P. C. et al. (2015). "Phosphoenolpyruvate Is a Metabolic Checkpoint of Anti-tumor T Cell Responses". In: *Cell* 162.6, pp. 1217–1228.

Hodis, E. et al. (2012). "A landscape of driver mutations in melanoma". In: *Cell* 150.2, pp. 251–263.

Hoeflich, K. P. et al. (2009). "Antitumor efficacy of the novel RAF inhibitor GDC-0879 is predicted by BRAFV600E mutational status and sustained extracellular signal-regulated kinase/mitogen-activated protein kinase pathway suppression". In: *Cancer Res.* 69.7, pp. 3042–3051.

Horton, J. D. (2002). "Sterol regulatory element-binding proteins: transcriptional activators of lipid synthesis". In: *Biochem. Soc. Trans.* 30.Pt 6, pp. 1091–1095.

Hosios, A. M. et al. (2016). "Amino Acids Rather than Glucose Account for the Majority of Cell Mass in Proliferating Mammalian Cells". In: *Dev. Cell* 36.5, pp. 540–549.

Houten, S. M. and R. J. Wanders (2010). "A general introduction to the biochemistry of mitochondrial fatty acid -oxidation". In: *J. Inherit. Metab. Dis.* 33.5, pp. 469–477.

Howard, S. et al. (2011). "A positive role of cadherin in Wnt/-catenin signalling during epithelial-mesenchymal transition". In: *PLoS ONE* 6.8, e23899.

Huang, D. et al. (2014). "HIF-1-mediated suppression of acyl-CoA dehydrogenases and fatty acid oxidation is critical for cancer progression". In: *Cell Rep* 8.6, pp. 1930–1942.

Hulka, B. S. and P. G. Moorman (2008). "Breast cancer: hormones and other risk factors". In: *Maturitas* 61.1-2, pp. 203–213.

Hume, D. A. et al. (1978). "Aerobic glycolysis and lymphocyte transformation". In: *Biochem. J.* 174.3, pp. 703–709.

Hung, C. M. et al. (2011). "Osthole suppresses hepatocyte growth factor (HGF)-induced epithelial-mesenchymal transition via repression of the c-Met/Akt/mTOR pathway in human breast cancer cells". In: *J. Agric. Food Chem.* 59.17, pp. 9683–9690.

Hunnewell, M. G. and N. S. Forbes (2010). "Active and inactive metabolic pathways in tumor spheroids: determination by GC-MS". In: *Biotechnol. Prog.* 26.3, pp. 789–796.

Hutton, J. E. et al. (2016). "Oncogenic KRAS and BRAF Drive Metabolic Reprogramming in Colorectal Cancer". In: *Mol. Cell Proteomics* 15.9, pp. 2924–2938.

Imani, S. et al. (2016). "Prognostic Value of EMT-inducing Transcription Factors (EMT-TFs) in Metastatic Breast Cancer: A Systematic Review and Meta-analysis". In: *Sci Rep* 6, p. 28587.

Ishibashi, S., R. Cliffe, and E. Amaya (2012). "Highly efficient bi-allelic mutation rates using TALENs in Xenopus tropicalis". In: *Biol Open* 1.12, pp. 1273–1276.

Jacque, N. et al. (2015). "Targeting glutaminolysis has antileukemic activity in acute myeloid leukemia and synergizes with BCL-2 inhibition". In: *Blood* 126.11, pp. 1346–1356.

Jatoi, I. et al. (1999). "Significance of axillary lymph node metastasis in primary breast cancer". In: *J. Clin. Oncol.* 17.8, pp. 2334–2340.

Jiang, L., R. Deberardinis, and D. A. Boothman (2015). "The cancer cell 'energy grid': TGF-1 signaling coordinates metabolism for migration". In: *Mol Cell Oncol* 2.3, e981994.

Jiang, L. et al. (2015). "Metabolic reprogramming during TGF1-induced epithelial-to-mesenchymal transition". In: *Oncogene* 34.30, pp. 3908–3916.

Jing, Q. et al. (2016). "FGFs: crucial factors that regulate tumour initiation and progression". In: *Cell Prolif.* 49.4, pp. 438–447.

Jogi, A. et al. (2012). "Cancer cell differentiation heterogeneity and aggressive behavior in solid tumors". In: *Ups. J. Med. Sci.* 117.2, pp. 217–224.

Johnston, S. R. and M. Dowsett (2003). "Aromatase inhibitors for breast cancer: lessons from the laboratory". In: *Nat. Rev. Cancer* 3.11, pp. 821–831.

Joseph, E. W. et al. (2010). "The RAF inhibitor PLX4032 inhibits ERK signaling and tumor cell proliferation in a V600E BRAF-selective manner". In: *Proc. Natl. Acad. Sci. U.S.A.* 107.33, pp. 14903–14908.

Kang, H. M. et al. (2015). "Defective fatty acid oxidation in renal tubular epithelial cells has a key role in kidney fibrosis development". In: *Nat. Med.* 21.1, pp. 37–46.

Kelloff, G. J. et al. (2005). "Progress and promise of FDG-PET imaging for cancer patient management and oncologic drug development". In: *Clin. Cancer Res.* 11.8, pp. 2785–2808.

Kelly, C. M. and A. U. Buzdar (2010). "Anastrozole". In: *Expert Opin Drug Saf* 9.6, pp. 995–1003.

Kelly, C. M. et al. (2012). "Agreement in risk prediction between the 21-gene recurrence score assay (Oncotype DX) and the PAM50 breast cancer intrinsic Classifier in early-stage estrogen receptor-positive breast cancer". In: *Oncologist* 17.4, pp. 492–498.

Kennecke, H. et al. (2010). "Metastatic behavior of breast cancer subtypes". In: *J. Clin. Oncol.* 28.20, pp. 3271–3277.

Khramtsov, A. I. et al. (2010). "Wnt/beta-catenin pathway activation is enriched in basal-like breast cancers and predicts poor outcome". In: *Am. J. Pathol.* 176.6, pp. 2911–2920.

Kiebish, M. A. et al. (2008). "Cardiolipin and electron transport chain abnormalities in mouse brain tumor mitochondria: lipidomic evidence supporting the Warburg theory of cancer". In: *J. Lipid Res.* 49.12, pp. 2545–2556.

Kilburn, D. G., M. D. Lilly, and F. C. Webb (1969). "The energetics of mammalian cell growth". In: *J. Cell. Sci.* 4.3, pp. 645–654.

Kinnaird, A. et al. (2016). "Metabolic Modulation of Clear-cell Renal Cell Carcinoma with Dichloroacetate, an Inhibitor of Pyruvate Dehydrogenase Kinase". In: *Eur. Urol.* 69.4, pp. 734–744.

Koboldt, D. C. et al. (2012). "Comprehensive molecular portraits of human breast tumours". In: *Nature* 490.7418. [PubMed Central:PMC3465532] [DOI:10.1038/nature11412] [PubMed:23000897], pp. 61–70.

Koppenol, W. H. et al. (2011). "Otto Warburg's contributions to current concepts of cancer metabolism". In: *Nat. Rev. Cancer* 11.5, pp. 325–337.

Koscielny, S. et al. (1984). "Breast cancer: relationship between the size of the primary tumour and the probability of metastatic dissemination". In: *Br. J. Cancer* 49.6, pp. 709–715.

Kuleshov, M. V. et al. (2016). "Enrichr: a comprehensive gene set enrichment analysis web server 2016 update". In: *Nucleic Acids Res.* 44.W1, W90–97.

Kumar, R. et al. (2011). "The dynamic structure of the estrogen receptor". In: *J Amino Acids* 2011, p. 812540.

Kwong, L. N. et al. (2012). "Oncogenic NRAS signaling differentially regulates survival and proliferation in melanoma". In: *Nat. Med.* 18.10, pp. 1503–1510.

LaGory, E. L. et al. (2015). "Suppression of PGC-1 Is Critical for Reprogramming Oxidative Metabolism in Renal Cell Carcinoma". In: *Cell Rep* 12.1, pp. 116–127.

Lamouille, S., J. Xu, and R. Derynck (2014). "Molecular mechanisms of epithelial-mesenchymal transition". In: *Nat. Rev. Mol. Cell Biol.* 15.3, pp. 178–196.

Le, A. et al. (2012). "Glucose-independent glutamine metabolism via TCA cycling for proliferation and survival in B cells". In: *Cell Metab.* 15.1, pp. 110–121.

Le, A. et al. (2014). "Tumorigenicity of hypoxic respiring cancer cells revealed by a hypoxia-cell cycle dual reporter". In: *Proc. Natl. Acad. Sci. U.S.A.* 111.34, pp. 12486–12491.

Le Doussal, V. et al. (1989). "Prognostic value of histologic grade nuclear components of Scarff-Bloom-Richardson (SBR). An improved score modification based on

a multivariate analysis of 1262 invasive ductal breast carcinomas". In: *Cancer* 64.9, pp. 1914–1921.

Leav, I. et al. (2001). "Comparative studies of the estrogen receptors beta and alpha and the androgen receptor in normal human prostate glands, dysplasia, and in primary and metastatic carcinoma". In: *Am. J. Pathol.* 159.1, pp. 79–92.

Lee, S. Y. et al. (2015). "Dlx-2 is implicated in TGF-- and Wnt-induced epithelial-mesenchymal, glycolytic switch, and mitochondrial repression by Snail activation". In: *Int. J. Oncol.* 46.4, pp. 1768–1780.

Lee, S. Y. et al. (2016). "Dlx-2 and glutaminase upregulate epithelial-mesenchymal transition and glycolytic switch". In: *Oncotarget* 7.7, pp. 7925–7939.

Leoncikas, V. et al. (2016). "Generation of 2,000 breast cancer metabolic landscapes reveals a poor prognosis group with active serotonin production". In: *Sci Rep* 6, p. 19771.

Lewis, D. Y., D. Soloviev, and K. M. Brindle (2015). "Imaging tumor metabolism using positron emission tomography". In: *Cancer J* 21.2, pp. 129–136.

Li, B. et al. (2014). "Fructose-1,6-bisphosphatase opposes renal carcinoma progression". In: *Nature* 513.7517, pp. 251–255.

Li, F. et al. (2005). "Myc stimulates nuclearly encoded mitochondrial genes and mitochondrial biogenesis". In: *Mol. Cell. Biol.* 25.14, pp. 6225–6234.

Li, J. et al. (2016). "Downregulation of FBP1 Promotes Tumor Metastasis and Indicates Poor Prognosis in Gastric Cancer via Regulating Epithelial-Mesenchymal Transition". In: *PLoS ONE* 11.12, e0167857.

Li, Z. et al. (2017). "Pirfenidone suppresses MAPK signalling pathway to reverse epithelial-mesenchymal transition and renal fibrosis". In: *Nephrology (Carlton)* 22.8, pp. 589–597.

Liedtke, C. et al. (2009). "Genomic grade index is associated with response to chemotherapy in patients with breast cancer". In: *J. Clin. Oncol.* 27.19, pp. 3185–3191.

Lim, E. et al. (2010). "Transcriptome analyses of mouse and human mammary cell subpopulations reveal multiple conserved genes and pathways". In: *Breast Cancer Res.* 12.2, R21.

Lin, G. and J. M. Slack (2008). "Requirement for Wnt and FGF signaling in Xenopus tadpole tail regeneration". In: *Dev. Biol.* 316.2, pp. 323–335.

Liu, J. et al. (2013). "Targeting Wnt-driven cancer through the inhibition of Porcupine by LGK974". In: *Proc. Natl. Acad. Sci. U.S.A.* 110.50, pp. 20224–20229.

Liu, P. et al. (2009). "Targeting the phosphoinositide 3-kinase pathway in cancer". In: *Nat Rev Drug Discov* 8.8, pp. 627–644.

Liu, R. et al. (2015). "Why weight? Modelling sample and observational level variability improves power in RNA-seq analyses". In: *Nucleic Acids Res.* 43.15, e97.

Louie, S. M. et al. (2013). "Cancer cells incorporate and remodel exogenous palmitate into structural and oncogenic signaling lipids". In: *Biochim. Biophys. Acta* 1831.10, pp. 1566–1572.

Love, N. R. et al. (2011). "pTransgenesis: a cross-species, modular transgenesis resource". In: *Development* 138.24, pp. 5451–5458.

Love, N. R. et al. (2014). "Carbohydrate metabolism during vertebrate appendage regeneration: what is its role? How is it regulated?: A postulation that regenerating vertebrate appendages facilitate glycolytic and pentose phosphate pathways to fuel macromolecule biosynthesis". In: *Bioessays* 36.1, pp. 27–33.

Lunt, S. Y. and M. G. Vander Heiden (2011). "Aerobic glycolysis: meeting the metabolic requirements of cell proliferation". In: *Annu. Rev. Cell Dev. Biol.* 27, pp. 441–464.

Mani, S. A. et al. (2008). "The epithelial-mesenchymal transition generates cells with properties of stem cells". In: *Cell* 133.4, pp. 704–715.

Marjanovic, S., A. Wielburski, and B. D. Nelson (1988). "Effect of phorbol myristate acetate and concanavalin A on the glycolytic enzymes of human peripheral lymphocytes". In: *Biochim. Biophys. Acta* 970.1, pp. 1–6.

Marro, M. et al. (2014). "Molecular monitoring of epithelial-to-mesenchymal transition in breast cancer cells by means of Raman spectroscopy". In: *Biochim. Biophys. Acta* 1843.9, pp. 1785–1795.

Martin, M. et al. (2005). "Adjuvant docetaxel for node-positive breast cancer". In: *N. Engl. J. Med.* 352.22, pp. 2302–2313.

Massague, J. (2012). "TGF signalling in context". In: *Nat. Rev. Mol. Cell Biol.* 13.10, pp. 616–630.

Maupin, K. A. et al. (2010). "Glycogene expression alterations associated with pancreatic cancer epithelial-mesenchymal transition in complementary model systems". In: *PLoS ONE* 5.9, e13002.

Mayers, J. R. and M. G. Vander Heiden (2015). "Famine versus feast: understanding the metabolism of tumors in vivo". In: *Trends Biochem. Sci.* 40.3, pp. 130–140.

Mazouni, C. et al. (2007). "Inclusion of taxanes, particularly weekly paclitaxel, in preoperative chemotherapy improves pathologic complete response rate in estrogen receptor-positive breast cancers". In: *Ann. Oncol.* 18.5, pp. 874–880.

Mendoza, M. C., E. E. Er, and J. Blenis (2011). "The Ras-ERK and PI3K-mTOR pathways: cross-talk and compensation". In: *Trends Biochem. Sci.* 36.6, pp. 320–328.

Mertins, P. et al. (2016). "Proteogenomics connects somatic mutations to signalling in breast cancer". In: *Nature* 534.7605, pp. 55–62.

Metallo, C. M. et al. (2011). "Reductive glutamine metabolism by IDH1 mediates lipogenesis under hypoxia". In: *Nature* 481.7381, pp. 380–384.

Miller, J. A. et al. (2011). "Strategies for aggregating gene expression data: the collapseRows R function". In: *BMC Bioinformatics* 12, p. 322.

Minami, S. (1923). "Versuche an berlebendem Carcinomgewebe." In: *Biochem. Zeitschr.* 142, pp. 334–350.

Mitra, T. and S. S. Roy (2017). "Co-Activation of TGF and Wnt Signalling Pathways Abrogates EMT in Ovarian Cancer Cells". In: *Cell. Physiol. Biochem.* 41.4, pp. 1336–1345.

Mokry, M. et al. (2012). "Integrated genome-wide analysis of transcription factor occupancy, RNA polymerase II binding and steady-state RNA levels identify differentially regulated functional gene classes". In: *Nucleic Acids Res.* 40.1, pp. 148–158.

Moor, A. E. et al. (2015). "BCL9/9L--catenin Signaling is Associated With Poor Outcome in Colorectal Cancer". In: *EBioMedicine* 2.12, pp. 1932–1943.

Morrish, F. et al. (2010). "Myc-dependent mitochondrial generation of acetyl-CoA contributes to fatty acid biosynthesis and histone acetylation during cell cycle entry". In: *J. Biol. Chem.* 285.47, pp. 36267–36274.

Moullan, N. et al. (2015). "Tetracyclines Disturb Mitochondrial Function across Eukaryotic Models: A Call for Caution in Biomedical Research". In: *Cell Rep.*

Moumen, M. et al. (2013). "Myc is required for -catenin-mediated mammary stem cell amplification and tumorigenesis". In: *Mol. Cancer* 12.1, p. 132.

Moustakas, A. and C. H. Heldin (2007). "Signaling networks guiding epithelial-mesenchymal transitions during embryogenesis and cancer progression". In: *Cancer Sci.* 98.10, pp. 1512–1520.

Muller, J. et al. (2014). "Low MITF/AXL ratio predicts early resistance to multiple targeted drugs in melanoma". In: *Nat Commun* 5, p. 5712.

Munoz-Pinedo, C., N. El Mjiyad, and J. E. Ricci (2012). "Cancer metabolism: current perspectives and future directions". In: *Cell Death Dis* 3, e248.

Munyon, W. H. and D. J. Merchant (1959). "The relation between glucose utilization, lactic acid production and utilization and the growth cycle of L strain fibroblasts". In: *Exp. Cell Res.* 17.3, pp. 490–498.

Musgrove, E. A. et al. (2011). "Cyclin D as a therapeutic target in cancer". In: *Nat. Rev. Cancer* 11.8, pp. 558–572.

Muzny, D. M. et al. (2012a). "Comprehensive molecular characterization of human colon and rectal cancer". In: *Nature* 487.7407, pp. 330–337.

— (2012b). "Comprehensive molecular characterization of human colon and rectal cancer". In: *Nature* 487.7407, pp. 330–337.

Nagalla, S. et al. (2013). "Interactions between immunity, proliferation and molecular subtype in breast cancer prognosis". In: *Genome Biol.* 14.4, R34.

Nagarajan, A., P. Malvi, and N. Wajapeyee (2016). "Oncogene-directed alterations in cancer cell metabolism". In: *Trends Cancer* 2.7, pp. 365–377.

Nakazawa, M. S., B. Keith, and M. C. Simon (2016). "Oxygen availability and metabolic adaptations". In: *Nat. Rev. Cancer* 16.10, pp. 663–673.

Nassour, M. et al. (2012). "Slug controls stem/progenitor cell growth dynamics during mammary gland morphogenesis". In: *PLoS ONE* 7.12, e53498.

Neri, A. et al. (1988). "Analysis of RAS oncogene mutations in human lymphoid malignancies". In: *Proc. Natl. Acad. Sci. U.S.A.* 85.23, pp. 9268–9272.

Neve, R. M. et al. (2006). "A collection of breast cancer cell lines for the study of functionally distinct cancer subtypes". In: *Cancer Cell* 10.6, pp. 515–527.

Nickerson, M. L. et al. (2008). "Improved identification of von Hippel-Lindau gene alterations in clear cell renal tumors". In: *Clin. Cancer Res.* 14.15, pp. 4726–4734.

Nieto, M. A. et al. (2016). "EMT: 2016". In: *Cell* 166.1, pp. 21–45.

Nile, A. H. and R. N. Hannoush (2016). "Fatty acylation of Wnt proteins". In: *Nat. Chem. Biol.* 12.2, pp. 60–69.

Nowak, D., D. Stewart, and H. P. Koeffler (2009). "Differentiation therapy of leukemia: 3 decades of development". In: *Blood* 113.16, pp. 3655–3665.

Orchel, A. et al. (2005). "Butyrate-induced differentiation of colon cancer cells is PKC and JNK dependent". In: *Dig. Dis. Sci.* 50.3, pp. 490–498.

Ortega-Molina, A. and M. Serrano (2013). "PTEN in cancer, metabolism, and aging". In: *Trends Endocrinol. Metab.* 24.4, pp. 184–189.

Osthus, R. C. et al. (2000). "Deregulation of glucose transporter 1 and glycolytic gene expression by c-Myc". In: *J. Biol. Chem.* 275.29, pp. 21797–21800.

Padanad, M. S. et al. (2016). "Fatty Acid Oxidation Mediated by Acyl-CoA Synthetase Long Chain 3 Is Required for Mutant KRAS Lung Tumorigenesis". In: *Cell Rep* 16.6, pp. 1614–1628.

Paik, S. et al. (2004). "A multigene assay to predict recurrence of tamoxifen-treated, node-negative breast cancer". In: *N. Engl. J. Med.* 351.27, pp. 2817–2826.

Paik, S. et al. (2006). "Gene expression and benefit of chemotherapy in women with node-negative, estrogen receptor-positive breast cancer". In: *J. Clin. Oncol.* 24.23, pp. 3726–3734.

Pan, W. et al. (2016). "Whole exome sequencing identifies lncRNA GAS8-AS1 and LPAR4 as novel papillary thyroid carcinoma driver alternations". In: *Hum. Mol. Genet.* 25.9, pp. 1875–1884.

Park, G. B. et al. (2016). "GSK-3-mediated fatty acid synthesis enhances epithelial to mesenchymal transition of TLR4-activated colorectal cancer cells through regulation of TAp63". In: *Int. J. Oncol.* 49.5, pp. 2163–2172.

Park, J. B. et al. (2012). "Phospholipase signalling networks in cancer". In: *Nat. Rev. Cancer* 12.11, pp. 782–792.

Parker, J. S. et al. (2009). "Supervised risk predictor of breast cancer based on intrinsic subtypes". In: *J. Clin. Oncol.* 27.8, pp. 1160–1167.

Parmenter, T. J. et al. (2014). "Response of BRAF-mutant melanoma to BRAF inhibition is mediated by a network of transcriptional regulators of glycolysis". In: *Cancer Discov* 4.4, pp. 423–433.

Pascual, G. et al. (2017). "Targeting metastasis-initiating cells through the fatty acid receptor CD36". In: *Nature* 541.7635, pp. 41–45.

Pate, K. T. et al. (2014). "Wnt signaling directs a metabolic program of glycolysis and angiogenesis in colon cancer". In: *EMBO J.* 33.13, pp. 1454–1473.

Patel, D. et al. (2016). "Aspartate Rescues S-phase Arrest Caused by Suppression of Glutamine Utilization in KRas-driven Cancer Cells". In: *J. Biol. Chem.* 291.17, pp. 9322–9329.

Pawlikowski, J. S. et al. (2013). "Wnt signaling potentiates nevogenesis". In: *Proc. Natl. Acad. Sci. U.S.A.* 110.40, pp. 16009–16014.

Pelicano, H. et al. (2014). "Mitochondrial dysfunction in some triple-negative breast cancer cell lines: role of mTOR pathway and therapeutic potential". In: *Breast Cancer Res.* 16.5, p. 434.

Perou, C. M. et al. (2000). "Molecular portraits of human breast tumours". In: *Nature* 406.6797, pp. 747–752.

Pfeiffer, T., S. Schuster, and S. Bonhoeffer (2001). "Cooperation and competition in the evolution of ATP-producing pathways". In: *Science* 292.5516, pp. 504–507.

Phipson, B. et al. (2016). "Robust hyperparameter estimation protects against hypervariable genes and improves power to detect differential expression". In: *Ann Appl Stat* 10.2, pp. 946–963.

Pike, L. S. et al. (2011). "Inhibition of fatty acid oxidation by etomoxir impairs NADPH production and increases reactive oxygen species resulting in ATP depletion and cell death in human glioblastoma cells". In: *Biochim. Biophys. Acta* 1807.6, pp. 726–734.

Pinthus, J. H. et al. (2011). "Metabolic features of clear-cell renal cell carcinoma: mechanisms and clinical implications". In: *Can Urol Assoc J* 5.4, pp. 274–282.

Polakis, P. (2012). "Wnt signaling in cancer". In: *Cold Spring Harb Perspect Biol* 4.5.

Potts, M. B. and S. Cameron (2011). "Cell lineage and cell death: Caenorhabditis elegans and cancer research". In: *Nat. Rev. Cancer* 11.1, pp. 50–58.

Poumay, Y. and M. R. Pittelkow (1995). "Cell density and culture factors regulate keratinocyte commitment to differentiation and expression of suprabasal K1/K10 keratins". In: *J. Invest. Dermatol.* 104.2, pp. 271–276.

Prat, A. et al. (2012). "Concordance among gene expression-based predictors for ER-positive breast cancer treated with adjuvant tamoxifen". In: *Ann. Oncol.* 23.11, pp. 2866–2873.

Proffitt, K. D. et al. (2013). "Pharmacological inhibition of the Wnt acyltransferase PORCN prevents growth of WNT-driven mammary cancer". In: *Cancer Res.* 73.2, pp. 502–507.

Pyne, N. J. and S. Pyne (2010). "Sphingosine 1-phosphate and cancer". In: *Nat. Rev. Cancer* 10.7, pp. 489–503.

Quackenbush, J. (2002). "Microarray data normalization and transformation". In: *Nat. Genet.* 32 Suppl, pp. 496–501.

Raj, L. et al. (2011). "Selective killing of cancer cells by a small molecule targeting the stress response to ROS". In: *Nature* 475.7355, pp. 231–234.

Rangasamy, D., D. J. Tremethick, and I. K. Greaves (2008). "Gene knockdown by ecdysone-based inducible RNAi in stable mammalian cell lines". In: *Nat Protoc* 3.1, pp. 79–88.

Reed, K. R. et al. (2015). "Hunk/Mak-v is a negative regulator of intestinal cell proliferation". In: *BMC Cancer* 15, p. 110.

Ritchie, M. E. et al. (2015). "limma powers differential expression analyses for RNA-sequencing and microarray studies". In: *Nucleic Acids Res.* 43.7, e47.

Rizos, H. et al. (2014). "BRAF inhibitor resistance mechanisms in metastatic melanoma: spectrum and clinical impact". In: *Clin. Cancer Res.* 20.7, pp. 1965–1977.

Roberts, P. J. and C. J. Der (2007). "Targeting the Raf-MEK-ERK mitogen-activated protein kinase cascade for the treatment of cancer". In: *Oncogene* 26.22, pp. 3291–3310.

Roche, M. de la, J. Worm, and M. Bienz (2008). "The function of BCL9 in Wnt/beta-catenin signaling and colorectal cancer cells". In: *BMC Cancer* 8, p. 199.

Rohrig, F. and A. Schulze (2016). "The multifaceted roles of fatty acid synthesis in cancer". In: *Nat. Rev. Cancer* 16.11, pp. 732–749.

Rojas-Puentes, L. et al. (2016). "Epithelial-mesenchymal transition, proliferation, and angiogenesis in locally advanced cervical cancer treated with chemoradiotherapy". In: *Cancer Med* 5.8, pp. 1989–1999.

Rosen, P. P. et al. (1989). "Pathological prognostic factors in stage I (T1N0M0) and stage II (T1N1M0) breast carcinoma: a study of 644 patients with median follow-up of 18 years". In: *J. Clin. Oncol.* 7.9, pp. 1239–1251.

Rosen, P. P. et al. (1993). "Factors influencing prognosis in node-negative breast carcinoma: analysis of 767 T1N0M0/T2N0M0 patients with long-term follow-up". In: *J. Clin. Oncol.* 11.11, pp. 2090–2100.

RStudio Team (2015). *RStudio: Integrated Development Environment for R*. RStudio, Inc. Boston, MA. URL: http://www.rstudio.com/.

Rysman, E. et al. (2010). "De novo lipogenesis protects cancer cells from free radicals and chemotherapeutics by promoting membrane lipid saturation". In: *Cancer Res.* 70.20, pp. 8117–8126.

Sanchez-Martinez, R. et al. (2015a). "A link between lipid metabolism and epithelial-mesenchymal transition provides a target for colon cancer therapy". In: *Oncotarget* 6.36, pp. 38719–38736.

— (2015b). "A link between lipid metabolism and epithelial-mesenchymal transition provides a target for colon cancer therapy". In: *Oncotarget* 6.36, pp. 38719–38736.

Sanchez-Tillo, E. et al. (2011). "-catenin/TCF4 complex induces the epithelial-to-mesenchymal transition (EMT)-activator ZEB1 to regulate tumor invasiveness". In: *Proc. Natl. Acad. Sci. U.S.A.* 108.48, pp. 19204–19209.

Sartor, M. A. et al. (2010). "ConceptGen: a gene set enrichment and gene set relation mapping tool". In: *Bioinformatics* 26.4, pp. 456–463.

Schafer, Z. T. et al. (2009). "Antioxidant and oncogene rescue of metabolic defects caused by loss of matrix attachment". In: *Nature* 461.7260, pp. 109–113.

Schlaepfer, I. R. et al. (2014). "Lipid catabolism via CPT1 as a therapeutic target for prostate cancer". In: *Mol. Cancer Ther.* 13.10, pp. 2361–2371.

Schofield, C. J. and P. J. Ratcliffe (2004). "Oxygen sensing by HIF hydroxylases". In: *Nat. Rev. Mol. Cell Biol.* 5.5, pp. 343–354.

Scholer, J. et al. (2015). "The intracellular domain of teneurin-1 induces the activity of microphthalmia-associated transcription factor (MITF) by binding to transcriptional repressor HINT1". In: *J. Biol. Chem.* 290.13, pp. 8154–8165.

Schoumacher, M. et al. (2014). "Inhibiting Tankyrases sensitizes KRAS-mutant cancer cells to MEK inhibitors via FGFR2 feedback signaling". In: *Cancer Res.* 74.12, pp. 3294–3305.

Schug, Z. T. and E. Gottlieb (2009). "Cardiolipin acts as a mitochondrial signalling platform to launch apoptosis". In: *Biochim. Biophys. Acta* 1788.10, pp. 2022–2031.

Sciacovelli, M. et al. (2016). "Fumarate is an epigenetic modifier that elicits epithelial-to-mesenchymal transition". In: *Nature* 537.7621, pp. 544–547.

Scott, D. A. et al. (2011). "Comparative metabolic flux profiling of melanoma cell lines: beyond the Warburg effect". In: *J. Biol. Chem.* 286.49, pp. 42626–42634.

Seip, K. et al. (2016). "Fibroblast-induced switching to the mesenchymal-like phenotype and PI3K/mTOR signaling protects melanoma cells from BRAF inhibitors". In: *Oncotarget* 7.15, pp. 19997–20015.

Shackelford, D. B. et al. (2013). "LKB1 inactivation dictates therapeutic response of non-small cell lung cancer to the metabolism drug phenformin". In: *Cancer Cell* 23.2, pp. 143–158.

Shao, P. et al. (2016). "Histone demethylase PHF8 promotes epithelial to mesenchymal transition and breast tumorigenesis". In: *Nucleic Acids Res.*

Shechter, I. et al. (2003). "IDH1 gene transcription is sterol regulated and activated by SREBP-1a and SREBP-2 in human hepatoma HepG2 cells: evidence that IDH1 may regulate lipogenesis in hepatic cells". In: *J. Lipid Res.* 44.11, pp. 2169–2180.

Sheri, A. and M. Dowsett (2012). "Developments in Ki67 and other biomarkers for treatment decision making in breast cancer". In: *Ann. Oncol.* 23 Suppl 10, pp. x219–227.

Shim, H. et al. (1997). "c-Myc transactivation of LDH-A: implications for tumor metabolism and growth". In: *Proc. Natl. Acad. Sci. U.S.A.* 94.13, pp. 6658–6663.

Shimano, H. et al. (1999). "Sterol regulatory element-binding protein-1 as a key transcription factor for nutritional induction of lipogenic enzyme genes". In: *J. Biol. Chem.* 274.50, pp. 35832–35839.

Shirogane, Y. et al. (2010). "Epithelial-mesenchymal transition abolishes the susceptibility of polarized epithelial cell lines to measles virus". In: *J. Biol. Chem.* 285.27, pp. 20882–20890.

Shtutman, M. et al. (1999). "The cyclin D1 gene is a target of the beta-catenin/LEF-1 pathway". In: *Proc. Natl. Acad. Sci. U.S.A.* 96.10, pp. 5522–5527.

Siavoshian, S. et al. (2000). "Butyrate and trichostatin A effects on the proliferation/differentiation of human intestinal epithelial cells: induction of cyclin D3 and p21 expression". In: *Gut* 46.4, pp. 507–514.

Smith, I. E. and M. Dowsett (2003). "Aromatase inhibitors in breast cancer". In: *N. Engl. J. Med.* 348.24, pp. 2431–2442.

Solit, D. B. et al. (2006). "BRAF mutation predicts sensitivity to MEK inhibition". In: *Nature* 439.7074, pp. 358–362.

Sorlie, T. et al. (2001). "Gene expression patterns of breast carcinomas distinguish tumor subclasses with clinical implications". In: *Proc. Natl. Acad. Sci. U.S.A.* 98.19, pp. 10869–10874.

Sousa, U. L. Jambor de et al. (2005). "CPT1alpha over-expression increases long-chain fatty acid oxidation and reduces cell viability with incremental palmitic acid concentration in 293T cells". In: *Biochem. Biophys. Res. Commun.* 338.2, pp. 757–761.

Sprowl-Tanio, S. et al. (2016). "Lactate/pyruvate transporter MCT-1 is a direct Wnt target that confers sensitivity to 3-bromopyruvate in colon cancer". In: *Cancer Metab* 4, p. 20.

Srivastava, N. et al. (2014). “Inhibition of cancer cell proliferation by PPAR is mediated by a metabolic switch that increases reactive oxygen species levels”. In: *Cell Metab.* 20.4, pp. 650–661.

Stine, Z. E. et al. (2015). “MYC, Metabolism, and Cancer”. In: *Cancer Discov* 5.10, pp. 1024–1039.

Sullivan, L. B. et al. (2015). “Supporting Aspartate Biosynthesis Is an Essential Function of Respiration in Proliferating Cells”. In: *Cell* 162.3, pp. 552–563.

Sun, Y. et al. (2014). “Metabolic and transcriptional profiling reveals pyruvate dehydrogenase kinase 4 as a mediator of epithelial-mesenchymal transition and drug resistance in tumor cells”. In: *Cancer Metab* 2.1, p. 20.

Symmans, W. F. et al. (2010). “Genomic index of sensitivity to endocrine therapy for breast cancer”. In: *J. Clin. Oncol.* 28.27, pp. 4111–4119.

Szasz, A. M. et al. (2016). “Cross-validation of survival associated biomarkers in gastric cancer using transcriptomic data of 1,065 patients”. In: *Oncotarget* 7.31, pp. 49322–49333.

Tabuchi, Y. et al. (2006). “Genetic networks responsive to sodium butyrate in colonic epithelial cells”. In: *FEBS Lett.* 580.13, pp. 3035–3041.

Takada, K. et al. (2012). “Targeted disruption of the BCL9/-catenin complex inhibits oncogenic Wnt signaling”. In: *Sci Transl Med* 4.148, 148ra117.

Tam, W. L. et al. (2013). “Protein kinase C is a central signaling node and therapeutic target for breast cancer stem cells”. In: *Cancer Cell* 24.3, pp. 347–364.

Tanaka, M. et al. (2013). “Reduction of fatty acid oxidation and responses to hypoxia correlate with the progression of de-differentiation in HCC”. In: *Mol Med Rep* 7.2, pp. 365–370.

Tanaka, Y. et al. (1989). “Enhancement of butyrate-induced differentiation of HT-29 human colon carcinoma cells by 1,25-dihydroxyvitamin D3”. In: *Biochem. Pharmacol.* 38.21, pp. 3859–3865.

Tandon, P. et al. (2011). “Requirement for ribosomal protein S6 kinase 1 to mediate glycolysis and apoptosis resistance induced by Pten deficiency”. In: *Proc. Natl. Acad. Sci. U.S.A.* 108.6, pp. 2361–2365.

Taneja, P. et al. (2010). “Classical and Novel Prognostic Markers for Breast Cancer and their Clinical Significance”. In: *Clin Med Insights Oncol* 4, pp. 15–34.

Tang, S., H. Han, and V. B. Bajic (2004). “ERGDB: Estrogen Responsive Genes Database”. In: *Nucleic Acids Res.* 32.Database issue, pp. D533–536.

Terada, N. et al. (2010). “Identification of EP4 as a potential target for the treatment of castration-resistant prostate cancer using a novel xenograft model”. In: *Cancer Res.* 70.4, pp. 1606–1615.

Teslaa, T. and M. A. Teitell (2015). "Pluripotent stem cell energy metabolism: an update". In: *EMBO J.* 34.2, pp. 138–153.

Tetsu, O. and F. McCormick (1999). "Beta-catenin regulates expression of cyclin D1 in colon carcinoma cells". In: *Nature* 398.6726, pp. 422–426.

Thompson, C. B. (2014). "Wnt meets Warburg: another piece in the puzzle?" In: *EMBO J.* 33.13, pp. 1420–1422.

Thurlimann, B. et al. (2005). "A comparison of letrozole and tamoxifen in postmenopausal women with early breast cancer". In: *N. Engl. J. Med.* 353.26, pp. 2747–2757.

Tisza, M. J. et al. (2016). "Motility and stem cell properties induced by the epithelial-mesenchymal transition require destabilization of lipid rafts". In: *Oncotarget* 7.32, pp. 51553–51568.

Toda, K. et al. (2016). "Metabolic Alterations Caused by KRAS Mutations in Colorectal Cancer Contribute to Cell Adaptation to Glutamine Depletion by Upregulation of Asparagine Synthetase". In: *Neoplasia* 18.11, pp. 654–665.

Torrano, V. et al. (2016). "The metabolic co-regulator PGC1 suppresses prostate cancer metastasis". In: *Nat. Cell Biol.* 18.6, pp. 645–656.

Torre, L. A. et al. (2015). "Global cancer statistics, 2012". In: *CA Cancer J Clin* 65.2, pp. 87–108.

Torre, L. A. et al. (2016). "Global Cancer Incidence and Mortality Rates and Trends–An Update". In: *Cancer Epidemiol. Biomarkers Prev.* 25.1, pp. 16–27.

Turner, N. C. and J. S. Reis-Filho (2006). "Basal-like breast cancer and the BRCA1 phenotype". In: *Oncogene* 25.43, pp. 5846–5853.

Van Blerkom, J. (2009). "Mitochondria in early mammalian development". In: *Semin. Cell Dev. Biol.* 20.3, pp. 354–364.

Vayalil, P. K. and A. Landar (2015). "Mitochondrial oncobioenergetic index: A potential biomarker to predict progression from indolent to aggressive prostate cancer". In: *Oncotarget* 6.40, pp. 43065–43080.

Vazquez, A., E. K. Markert, and Z. N. Oltvai (2011). "Serine biosynthesis with one carbon catabolism and the glycine cleavage system represents a novel pathway for ATP generation". In: *PLoS ONE* 6.11, e25881.

Veer, L. J. van 't et al. (2002). "Gene expression profiling predicts clinical outcome of breast cancer". In: *Nature* 415.6871, pp. 530–536.

Venet, D., J. E. Dumont, and V. Detours (2011). "Most random gene expression signatures are significantly associated with breast cancer outcome". In: *PLoS Comput. Biol.* 7.10, e1002240.

Venneti, S. et al. (2015). "Glutamine-based PET imaging facilitates enhanced metabolic evaluation of gliomas in vivo". In: *Sci Transl Med* 7.274, 274ra17.

Vickers, P. J. et al. (1988). "A multidrug-resistant MCF-7 human breast cancer cell line which exhibits cross-resistance to antiestrogens and hormone-independent tumor growth in vivo". In: *Mol. Endocrinol.* 2.10, pp. 886–892.

Vijver, M. J. van de et al. (2002). "A gene-expression signature as a predictor of survival in breast cancer". In: *N. Engl. J. Med.* 347.25, pp. 1999–2009.

Visvader, J. E. and J. Stingl (2014). "Mammary stem cells and the differentiation hierarchy: current status and perspectives". In: *Genes Dev.* 28.11, pp. 1143–1158.

Vlodrop, I. J. van et al. (2017). "A Four-Gene Promoter Methylation Marker Panel Consisting of GREM1, NEURL, LAD1, and NEFH Predicts Survival of Clear Cell Renal Cell Cancer Patients". In: *Clin. Cancer Res.*

Wagle, N. et al. (2011). "Dissecting therapeutic resistance to RAF inhibition in melanoma by tumor genomic profiling". In: *J. Clin. Oncol.* 29.22, pp. 3085–3096.

Wan, J. C. et al. (2017). "Liquid biopsies come of age: towards implementation of circulating tumour DNA". In: *Nat. Rev. Cancer.*

Wang, D. and R.N. Dubois (2010). "Eicosanoids and cancer." In: *Nat. Rev. Cancer* 10.3, pp. 181–193.

Wang, T., C. Marquardt, and J. Foker (1976). "Aerobic glycolysis during lymphocyte proliferation". In: *Nature* 261.5562, pp. 702–705.

Wang, X. and M. McManus (2009). "Lentivirus production". In: *J Vis Exp* 32.

Ward, P. S. and C. B. Thompson (2012). "Metabolic reprogramming: a cancer hallmark even warburg did not anticipate". In: *Cancer Cell* 21.3, pp. 297–308.

Weigelt, B. and J. S. Reis-Filho (2009). "Histological and molecular types of breast cancer: is there a unifying taxonomy?" In: *Nat Rev Clin Oncol* 6.12, pp. 718–730.

Weinhouse, S. (1956). "On respiratory impairment in cancer cells." In: *Science* 124.3215, pp. 267–269.

Welbourne, T. C. (1979). "Ammonia production and glutamine incorporation into glutathione in the functioning rat kidney". In: *Can. J. Biochem.* 57.3, pp. 233–237.

Wellbrock, C. et al. (2008). "Oncogenic BRAF regulates melanoma proliferation through the lineage specific factor MITF". In: *PLoS ONE* 3.7, e2734.

Wellings, S. R., H. M. Jensen, and R. G. Marcum (1975). "An atlas of subgross pathology of the human breast with special reference to possible precancerous lesions". In: *J. Natl. Cancer Inst.* 55.2, pp. 231–273.

Wesolowski, R. and B. Ramaswamy (2011). "Gene expression profiling: changing face of breast cancer classification and management". In: *Gene Expr.* 15.3, pp. 105–115.

Wirapati, P. et al. (2008). "Meta-analysis of gene expression profiles in breast cancer: toward a unified understanding of breast cancer subtyping and prognosis signatures". In: *Breast Cancer Res.* 10.4, R65.

Wise, D. R. et al. (2008). "Myc regulates a transcriptional program that stimulates mitochondrial glutaminolysis and leads to glutamine addiction". In: *Proc. Natl. Acad. Sci. U.S.A.* 105.48, pp. 18782–18787.

Wise, D. R. et al. (2011). "Hypoxia promotes isocitrate dehydrogenase-dependent carboxylation of -ketoglutarate to citrate to support cell growth and viability". In: *Proc. Natl. Acad. Sci. U.S.A.* 108.49, pp. 19611–19616.

Wisniewski, J. R. et al. (2015). "Absolute Proteome Analysis of Colorectal Mucosa, Adenoma, and Cancer Reveals Drastic Changes in Fatty Acid Metabolism and Plasma Membrane Transporters". In: *J. Proteome Res.* 14.9, pp. 4005–4018.

Wittner, B. S. et al. (2008). "Analysis of the MammaPrint breast cancer assay in a predominantly postmenopausal cohort". In: *Clin. Cancer Res.* 14.10, pp. 2988–2993.

Wymann, M. P. and R. Schneiter (2008). "Lipid signalling in disease". In: *Nat. Rev. Mol. Cell Biol.* 9.2, pp. 162–176.

Xia, M. et al. (2009). "Identification of chemical compounds that induce HIF-1alpha activity". In: *Toxicol. Sci.* 112.1, pp. 153–163.

Xu, J., S. Lamouille, and R. Derynck (2009). "TGF-beta-induced epithelial to mesenchymal transition". In: *Cell Res.* 19.2, pp. 156–172.

Yanagawa, J. et al. (2009). "Snail promotes CXCR2 ligand-dependent tumor progression in non-small cell lung carcinoma". In: *Clin. Cancer Res.* 15.22, pp. 6820–6829.

Yanes, O. et al. (2010). "Metabolic oxidation regulates embryonic stem cell differentiation". In: *Nat. Chem. Biol.* 6.6, pp. 411–417.

Yang, L., S. Venneti, and D. Nagrath (2017). "Glutaminolysis: A Hallmark of Cancer Metabolism". In: *Annu Rev Biomed Eng.*

Yang, M. and K. H. Vousden (2016). "Serine and one-carbon metabolism in cancer". In: *Nat. Rev. Cancer* 16.10, pp. 650–662.

Yao, J. et al. (2012). "Identification of common prognostic gene expression signatures with biological meanings from microarray gene expression datasets". In: *PLoS ONE* 7.9, e45894.

Ye, X. and R. A. Weinberg (2015). "Epithelial-Mesenchymal Plasticity: A Central Regulator of Cancer Progression". In: *Trends Cell Biol.* 25.11, pp. 675–686.

Ying, H. et al. (2012). "Oncogenic Kras maintains pancreatic tumors through regulation of anabolic glucose metabolism". In: *Cell* 149.3, pp. 656–670.

Yuan, T. L. and L. C. Cantley (2008). "PI3K pathway alterations in cancer: variations on a theme". In: *Oncogene* 27.41, pp. 5497–5510.

Zaharieva, B. M. et al. (2003). "High-throughput tissue microarray analysis of 11q13 gene amplification (CCND1, FGF3, FGF4, EMS1) in urinary bladder cancer". In: *J. Pathol.* 201.4, pp. 603–608.

Zaidi, N., J. V. Swinnen, and K. Smans (2012). "ATP-citrate lyase: a key player in cancer metabolism". In: *Cancer Res.* 72.15, pp. 3709–3714.

Zeng, H. L. et al. (2015). "Yhhu981, a novel compound, stimulates fatty acid oxidation via the activation of AMPK and ameliorates lipid metabolism disorder in ob/ob mice". In: *Acta Pharmacol. Sin.* 36.3, pp. 343–352.

Zhang, B. et al. (2014). "Proteogenomic characterization of human colon and rectal cancer". In: *Nature* 513.7518, pp. 382–387.

Zhang, J. et al. (2011). "UCP2 regulates energy metabolism and differentiation potential of human pluripotent stem cells". In: *EMBO J.* 30.24, pp. 4860–4873.

Zhang, X. H. et al. (2013). "Metastasis dormancy in estrogen receptor-positive breast cancer". In: *Clin. Cancer Res.* 19.23, pp. 6389–6397.

Zheng, X. et al. (2016). "Metabolic reprogramming during neuronal differentiation from aerobic glycolysis to neuronal oxidative phosphorylation". In: *Elife* 5.

Zu, X. L. and M. Guppy (2004). "Cancer metabolism: facts, fantasy, and fiction". In: *Biochem. Biophys. Res. Commun.* 313.3, pp. 459–465.